AD-A111 436 GENERAL ELECTRIC CORPORATE RESEARCH AND DEVELOPMENT --ETC F/G 11/6
INVESTIGATION INTO THE ORIGIN OF MAGNETIC PROPERTIES OF AMORPHO--ETC(U)
OCT 81 F E LUBORSKY, J J BECKER N00014-76-C-0807
UNCLASSIFIED SRD-80-006 NL

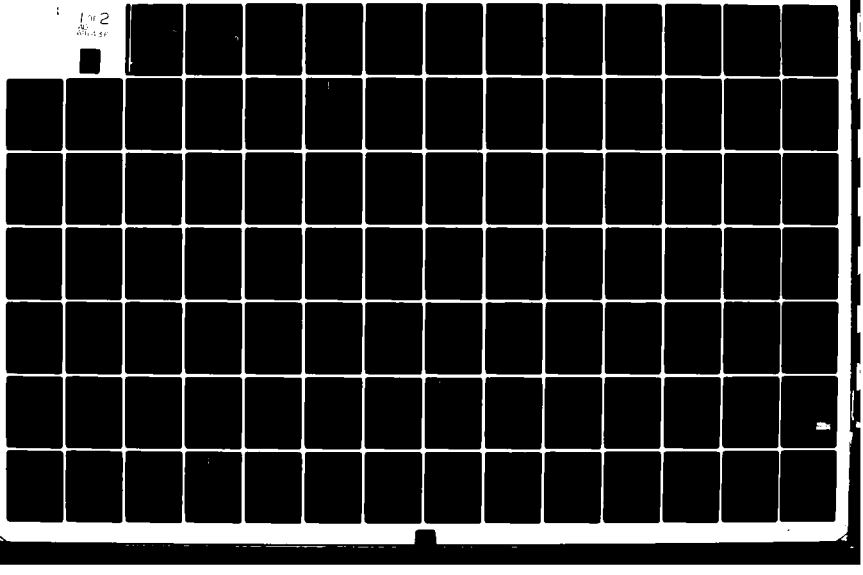

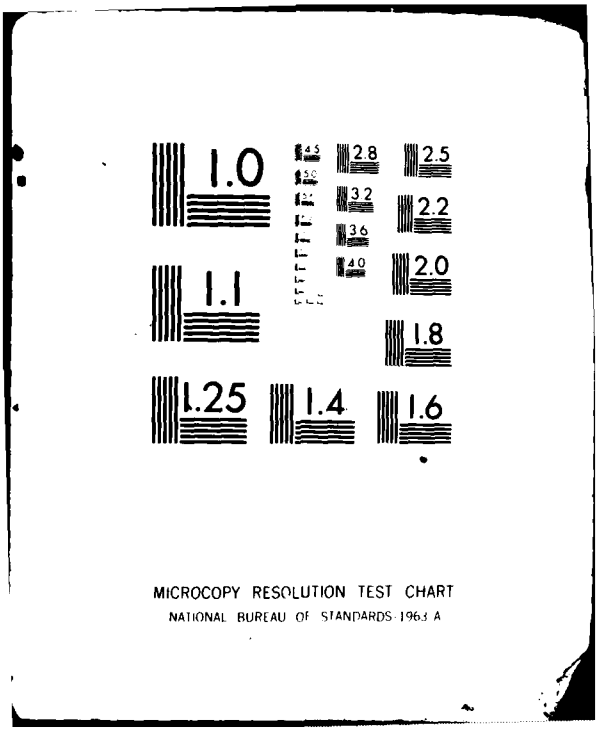
1.0
1.1
1.25
1.4
1.6
1.8
2.0
2.2
2.5
2.8
3.2
3.6
4.0
MICROCOPY RESOLUTION TEST CHART
NATIONAL BUREAU OF STANDARDS-1963 A

INVESTIGATION INTO THE ORIGIN OF MAGNETIC PROPERTIES OF AMORPHOUS METALLIC ALLOYS

Final Report
Contract N00014-76-C-0807

Prepared for:

Department of the Navy
Office of Naval Research
Arlington, Virginia 22217

Prepared by:

F.E. Luborsky and J.J. Becker
Properties Branch
Metallurgy Laboratory
General Electric Company
Corporate Research and Development
Schenectady, New York 12301

October 1981

UNCLASSIFIED

SECURITY CLASSIFICATION OF THIS PAGE *(When Data Entered)*

REPORT DOCUMENTATION PAGE	READ INSTRUCTIONS BEFORE COMPLETING FORM
1. REPORT NUMBER	2. GOVT ACCESSION NO. AD-A111 436	3. RECIPIENT'S CATALOG NUMBER
4. TITLE *(and Subtitle)* Final Report on Investigation into the Origin of ~~the~~ Magnetic Properties of Amorphous Metallic Alloys	5. TYPE OF REPORT & PERIOD COVERED Final Report October 1981
	6. PERFORMING ORG. REPORT NUMBER SRD-80-006
7. AUTHOR(s) F.E. Luborsky and J.J. Becker	8. CONTRACT OR GRANT NUMBER(s) N00014-76-C-0807
9. PERFORMING ORGANIZATION NAME AND ADDRESS General Electric Company Corporate Research and Development Center Schenectady, NY 12301	10. PROGRAM ELEMENT, PROJECT, TASK AREA & WORK UNIT NUMBERS
11. CONTROLLING OFFICE NAME AND ADDRESS Department of the Navy Office of Naval Research Arlington, VA 22217	12. REPORT DATE October 1981
	13. NUMBER OF PAGES 110
14. MONITORING AGENCY NAME & ADDRESS(if different from Controlling Office)	15. SECURITY CLASS. (of this report) Unclassified
	15a. DECLASSIFICATION/DOWNGRADING SCHEDULE

16. DISTRIBUTION STATEMENT *(of this Report)*

Approved for public release; distribution unlimited.

17. DISTRIBUTION STATEMENT *(of the abstract entered in Block 20, if different from Report)*

18. SUPPLEMENTARY NOTES

19. KEY WORDS *(Continue on reverse side if necessary and identify by block number)*

amorphous metals, magnetic properties, crystallization, magnetic ordering, stress relief, stress relaxation, transformers, cold rolling, embrittlement, resistivity, diffusion

20. ABSTRACT *(Continue on reverse side if necessary and identify by block number)*

Many amorphous alloy compositions were studied to determine the effect of composition on magnetic properties, crystallization, ordering, stress relaxation, embrittlement, and formation. The effects of annealing were also studied. In addition, the application of amorphous metals to large transformers was reported.

DD FORM 1 JAN 73 1473 EDITION OF 1 NOV 65 IS OBSOLETE UNCLASSIFIED

SECURITY CLASSIFICATION OF THIS PAGE *(When Data Entered)*

INTRODUCTION

The magnetic properties of amorphous iron based alloys have been found to have characteristics extremely desirable for low magnetic loss electromagnetic devices. The magnetic characteristics of these materials are strongly effected by composition variations as well as by processing and heat treatment techniques applied to the material after fabrication by melt spinning. Part of the collection of papers resulting from this contract deal with the effect of nickel as an alloying replacement for pure iron, and the effect of magnetic aging in $(Fe,Ni)_{80}B_{20}$ alloys. Metalloid alloying of carbon and phosphorous for boron also has a strong effect on the properties of these alloys. The variation of critical magnetic parameters with metalloid alloy additions has also been studied.

Alloy additions were shown to have a strong impact on the crystallization behavior of these alloys. Since crystallization represents the end of the useful life of these alloys as low loss magnetic materials, it is a vital concern in consideration of the range of applicability of amorphous metals in electromagnetic devices. A number of our papers cover this topic.

Because of the unique magnetic properties of amorphous metals, totally new magnetic material applications as well as significant improvements in device performance through direct material substitution are possible. These applications have been compared with the applications currently found for more conventional magnetic materials.

We were the first to publish the fact that magnetic properties of amorphous iron-boron alloys and other iron-base amorphous alloys exhibit extremely low alternating current magnetic losses making them very attractive for application in magnetic devices and in particular for distribution transformers. The key technical problems in applying amorphous metals to distribution transformers lie in (1) the development of higher saturation magnetization to allow amorphous metals to compete with higher magnetization crystalline magnetic materials and (2) the development of resistance to stress-induced anisotropy effects which lower the permeability of amorphous metals at low exciting fields. Our work in 1979-1981 has been directed towards these two major areas.

With the goal of trying to obtain higher saturation magnetization alloys than can be achieved with Fe-B, at equivalent cost, we have explored the properties of ternary and quaternary alloys of Fe-B-Si, Fe-B-C, Fe-B-Si-C, Fe-B-Al, Fe-B-Si-Al, Fe-B-Ga, and Fe-B-Ge. The results of these studies are described in detail in the attached references. No higher saturation magnetization alloys were found, but the Fe-B-Si-C alloys were found to possess much better characteristics than Fe-B and is now the preferred alloy. Much of our work with these alloys has been aimed at modeling the magnetic anisotropy to explain the induced anisotropy; on the effect of nickel on the magnetic properties; on stress relaxation effects which have implications for interpreting the structure of amorphous alloys; and on various aspects of the effects of stress on properties. These properties have been reported.

The effects of stress on the magnetic properties have been shown to be due to first, of course, the direct interaction of the stress with the magnetostriction, but secondly, it is also due to the development on annealing of a stress induced anisotropy. This stress induced anisotropy has been found to have a major influence on the properties of wound toroids.

A summary of our most significant results follows:

1. We found a ridge of constant saturation magnetization in the Fe-B-Si ternary alloys extending from $Fe_{80}B_{20}$ to $Fe_{82}B_{13}Si_5$. Silicon additions increased the ease of formation and stability, and lowered the losses without lowering saturation magnetization.

2. In the Fe-B-C ternary alloys a wider ridge of constant magnetization was found which extended out from $Fe_{80}B_{20}$ to $Fe_{83}B_{10}C_7$. However, the stability is decreased and losses increased.

3. The properties of Fe-B-Ga and Fe-B-Si-C-Al alloys were investigated. The results are similar to results obtained for the Fe-B-C, Fe-B-Si, and Fe-B-Ge alloys, but the range of alloys which could be prepared in the amorphous state was severely limited.

4. A composition of Fe-B-Si-C has been identified which produces the same high magnetization as the earlier identified Fe-B-C and Fe-B-Si alloys, but has significantly greater thermal stability and ease of casting resulting in thicker ribbons with optimum properties. The peak value of saturation magnetization occurs in the region $Fe_{82}B_{13}Si_{2.5}C_{2.5}$.

5. The maximum saturations achievable in the Fe-B, Fe-B-Si, Fe-B-C, Fe-B-Si-C, and Fe-B-Ge amorphous alloys are all within ± 2% of one another.

6. The maximum thickness of alloys which can be cast and still retain the good properties of the amorphous phase increases in the sequence $Fe_{80}B_{20}$, $Fe_{80}B_{16}Si_4$, $Fe_{80}B_{16}Si_2C_2$ from 42 μm to 52 μm to 57 μm, respectively. For this additional reason, the Fe-B-Si-C alloys are preferred.

7. To achieve minimum losses and other optimum magnetic properties, the thickness of the ribbon is critical. A thickness variation of ± 1 μm at an average thickness of 50 μm to 55 μm is desirable.

8. The saturation magnetization and Curie temperature for Fe-X alloys (X = B, Al, Ga, C, Si, Ge and P singly or in combination) when plotted as a function of total metalloid content shows an approximate trend in terms of charge transfer from the metalloid to the iron atoms. This common trend follows from the itinerant electron model.

9. The magnetization vs. temperature relations for Fe-B, Fe-B-C, Fe-B-Si and Fe-B-Ge alloys were found to obey the Bloch $T^{3/2}$ law below room temperature. The slope of the $T^{3/2}$ equation increased in the sequence -C, -Si, -Ge. This indicates that for the same low temperature magnetization, the Fe-B-C alloys would have the highest room temperature magnetization. The exchange stiffness constant (derived from the slope of the $T^{3/2}$ equation) correlated with the Curie temperature as expected, based on the itinerant electron model.

10. The magnetic anisotropy induced by annealing in a field K_u was deduced to be due principally to pair ordering with a small contribution from interstitial ordering in Fe-Ni-B alloys and Fe-Ni-B-P alloys. The kinetics of rotation of K_u were studied and found to be fast enough to cause some concern about their stability under certain conditions.

11. The embrittlement of Fe-B-P-B alloys was found to be due to migration of P. Phosphorus free alloys were found to be less susceptible to embrittlement.

12. Cold rolling amorphous alloys destroyed the local concentration fluctuations observed by small single x-ray diffraction. Annealing enhanced these concentration fluctuations.

13. Extrapolation of Arrhenius plots of crystallization kinetics predicted ultimate life times of at least 500 years at 175°C.

14. The losses of alloys in the series $(Fe_xNi_{1-x})_{80}B_{20}$ exhibited a peak at x = 75% corresponding to the peak in the induced anisotropy. Permeabilities exhibited a minimum at the same composition.

15. The behavior of the Curie temperature of binary metal-metalloid amorphous alloys has been adequately described using a phenomenological model. This theory, based on a localized band model, has been applied to a broad range of different amorphous metal alloys. Only one adjustable parameter has been required to fit the Curie temperature results over the entire range of binary amorphous metal compositions.

16. The potential application of iron based amorphous alloys in large transformers (e.g., distribution transformers) was analyzed. The losses and exciting power in large transformers were demonstrated to be reduced by a factor of three over conventional, high grade, Fe-3 1/4 Si oriented sheet steels. This could result in a savings of a 1/4 billion dollars per year in lower losses if all the distribution transformers were replaced by transformers made from amorphous alloys. An analysis of the sensitivity of the final transformer cost of the magnetic core material indicated that an increase of 50% in the core material cost would result in a 25% increase in finished transformer costs. This 25% increase would be returned by the savings in energy over the lifetime of the transformer.

17. The magnetic properties of toroids were found to improve with an increase in toroid diameter even after a stress relief anneal. This effect was attributed to a strain induced ordering. A world record in terms of low loss alloys was achieved with a 20 cm diameter toroid. Losses were decreased by more than a factor of 10 below the standard 1.4 cm diameter toroid, making the loss about 0.2 that of supermalloy at 100 Hz.

18. The substitution of C or Si for B was found to have no effect on the magnetostriction of Fe base amorphous alloys. This is consistent with the proportionality between magnetostriction and saturation magnetization.

19. Stress relaxation rate was found to increase with increase in Fe and decrease in ribbon thickness for Fe-B alloys. This has been interpreted as the result of the greater free volume in samples with more Fe and decrease in ribbon thickness due to the higher quench rate. We have examined stress relaxation over this composition range and find no discontinuity. In addition, no discontinuity is observed in the induced uniaxial anisotropy through the same range of compositions. This suggests that different atomic mechanisms may be more important for crystallization than for stress relaxation and induced anisotropy processes.

20. Increasing the melt temperature for casting the amorphous ribbon changed the ribbon geometry as predicted by the model based on the propagation of a thermal boundary layer. Changes in coercivity of the as-cast ribbon were removed by a stress relief anneal.

21. Changes in dc and 60 Hz coercivity, losses and exciting power were correlated with the size, shape and orientation of the air pockets developed on the surface of the tape during casting. It was concluded that these air pockets provide wall pinning sites which control the number and motion of walls present during magnetization reversal.

22. Crystallized amorphous iron alloys were shown to have potential as low cost permanent magnet materials. A $Fe_{40}Ni_{40}P_{20}$ alloy given a crystallization treatment of 15 minutes at 525°C developed a coercive force of 365 Oe, and saturation magnetization of about 8900 G. Other alloys have developed properties that would be excellent for hysteresis motor applications, especially since these alloys contain no cobalt or other strategic materials.

23. No change in resistivity was found for samples of various thicknesses. The resistivity is sensitive to the atomic structure and the preparation of ribbons with different thicknesses results in different quench rates and thus different atomic structures. The reasons for this disagreement is unknown.

24. The magnetic properties of ribbons which were chemically thinned were determined. The approach to saturation remained constant, but initially the coercivity changed rapidly, either up or down, with decreasing thickness, then increased linearly with reciprocal thickness. The results were interpreted in terms of surface and volume pinning.

25. The activation energy for the diffusion of Si into amorphous $Fe_{82}B_{12}Si_6$ was determined to be 2.2 eV. These results are very similar to previously reported results for the diffusion of B in amorphous alloys. It was concluded that an interstitial diffusion mechanism was taking place.

26. Several review papers were written summarizing the applications potential of amorphous alloys. These are included in the attached list of publications.

BIBLIOGRAPHY

1. Luborsky, F.E. "Kinetics of Reorientation of Magnetically Induced Anisotropy in Amorphous $Ni_{40}Fe_{40}P_{16}B_4$," *Proc. 21st Annu. Conf. on Magnetism and Magnetic Materials, AIP Conf. Proc. 29,* 1976, pp. 209-210. Reprint 7979.
2. Walter, J.L., F. Bacon, and F.E. Luborsky. "An Auger Analysis of the Embrittlement of the Amorphous Alloy $Ni_{40}Fe_{40}P_{14}B_6$," *Mater. Sci. Eng. 24,* 1976, pp. 239-245. Reprint 7988.
3. Luborsky, F.E. and J.L. Walter. "Stability of Amorphous Metallic Alloys," *J. Appl. Phys. 47,* 1976, pp. 3648-3650. Reprint 7998.
4. Luborsky, F.E., J.L. Walter, and D. LeGrand. "Cold Rolling and Annealing of Amorphous Ribbons," *IEEE Trans. Magn. Mag-12,* 1976, p. 930. Reprint 8011.
5. Luborsky, F.E. and J.L. Walter. "Magnetic Anneal Anistropy in Amorphous Alloys," *IEEE Trans. Magn. Mag-13,* 1977, p. 953. Reprint 8107.
6. Luborsky, F.E. and J.L. Walter. "Kinetics of Reorientation of the Induced Anisotropy in Amorphous $Fe_{40}Ni_{40}B_{20}$, *Mater. Sci. Eng. 28,* 1977, p. 77. Reprint 8124.
7. Becker, J.J., F.E. Luborsky, and J.L. Walter. "Magnetic Moments and Curie Temperature of $(Fe, Ni)_{80}(P,B)_{20}$ Amorphous Alloys," *IEEE Trans. Magn. Mag-13,* 1977, p. 988. Reprint 8151.
8. Luborsky, F.E. "Perspective on Application of Amorphous Alloys in Magnetic Devices," *Amorphous Magnetism II, Proc. Second Int. Symp. on Amorphous Magnetism, Rensselaer Polytechnic Institute, Troy, NY, August 25-27, 1976.* R.A. Levy and R. Hasegawa, Eds., New York: Plenum Press, 1977, pp. 345-368. Reprint 8161.
9. Luborsky, F.E. "Crystallization of Some Fe-Ni Metallic Glasses," *Mater. Sci. Eng. 28,* 1977, p. 139. Reprint 8123.
10. Becker, J.J. "Domain Observations in an Amorphous Iron-Nickel Alloy," *Proc. 21st Annu. Conf. on Magnetism and Magnetic Materials, AIP Conf. Proc. 29,* 1976, p. 204. Reprint 7975.
11. Luborsky, F.E. and J.L. Walter. "Magnetically Induced Anisotropy in Amorphous Alloys of Fe-Ni-P-B," *IEEE Trans. Magn. Mag-13,* 1977, p. 1635. Reprint 8231.
12. Walter, J.L., D.G. LeGrand, and F.E. Luborsky. "Small Angle X-ray Scattering from the Amorphous Alloy $Fe_{40}Ni_{40}P_{14}B_6$," *Mater. Sci. Eng. 29,* 1977, p. 161. Reprint 8171.
13. Luborsky, F.E. "Magnetism in Amorphous Alloys," *Nature 267,* 1977, p. 583.
14. Luborsky, F.E. "Magnetic Properties of Amorphous Alloys," *J. Magn. and Magn. Mater. 7,* 1978, p. 143. Reprint 8313.
15. Walter, J.L. and F.E. Luborsky. "The Ductile-Brittle Transition of Some Amorphous Alloys," *Mater. Sci. Eng. 33,* 1978, p. 91. Reprint 8336.
16. Luborsky, F.E., J.J. Becker, P.G. Frischmann, and L.A. Johnson. "Potential of Amorphous Alloys for Application in Magnetic Devices," *J. Appl. Phys. 49,* 1978, p. 1769. Reprint 8312.
17. Luborsky, F.E. "Applications of Amorphous Alloys," *IEEE Trans. Magn. Mag-14,* 1978, p. 1008. Reprint 8399.

18. Alben, B., J.J. Becker, and M.C. Chi. "Random Anisotropy in Amorphous Ferromagnets," *J. Appl. Phys. 49,* 1978, p. 1653. Reprint 8325.

19. Becker, J.J. "A New Mechanism for Magnetic Annealing in Amorphous Metals," *IEEE Trans. Magn. Mag-14,* 1978, p. 938. Reprint 8418.

20. Luborsky, F.E., H.H. Liebermann, J.J. Becker, and J.L. Walter. "The Magnetic Properties of Fe-B Amorphous Alloys," *Rapidly Quenched Metals III.* Ed. B. Cantor. London: The Metals Society, 1978. *2,* p. 188. Also GE Report 78CRD062.

21. Luborsky, F.E. and J.L. Walter. "Stress Relaxation in Amorphous Alloys," *Mater. Sci. Eng. 35,* 1978, p. 255. Reprint 8482.

22. Luborsky, F.E., J.J. Becker, and H.H. Liebermann. "Replacement of Boron by Carbon in Fe-B-C Amorphous Alloys," *Rapidly Quenched Metals III.* Ed. B. Cantor. London: The Metals Society, 1978. *21,* p. 249. Also GE Report 78CRD111.

23. Luborsky, F.E., P.G. Frischmann, and L.A. Johnson. "The Role of Amorphous Materials in the Magnetics Industry," *J. Magn. and Magn. Mater. 8,* 1978, p. 318. Reprint 8420.

24. Luborsky, F.E. and H.H. Liebermann. "Crystallization Kinetics of Fe-B Amorphous Alloys," *Appl. Phys. Lett. 33,* 1978, p. 233. Reprint 8426.

25. Luborsky, F.E., J.L. Walter, and H.H. Liebermann. "Engineering Magnetic Properties of Fe-NiB Amorphous Alloys," *IEEE Trans. Magn. Mag-15,* 1979, p. 909. Reprint 8510.

26. Luborsky, F.E., J.J. Becker, J.L. Walter, and H.H. Liebermann. "Formation and Magnetic Properties of Fe-B-Si Amorphous Alloys," *IEEE Trans. Magn. Mag-15,* 1979, p. 1146. Reprint 8624.

27. Luborsky, F.E. and J.J. Becker. "Strain Induced Anisotropy in Amorphous Alloys and the Effect of Toroid Diameter on Magnetic Properties," *IEEE Trans. Magn. Mag-15,* 1979, p. 1939. Reprint 8733.

28. Luborsky, F.E., P. Flanders, H.H. Liebermann, and J.L. Walter. "Effect of Metalloid on the Magnetostriction of Fe-B-C and Fe-B-Si Amorphous Alloys," *IEEE Trans. Magn. Mag-15,* 1979, p. 1961. Reprint 8746.

29. Luborsky, F.E. "Can a Solid Be Amorphous and Yet Be Ferromagnetic?" *Nav. Res. Rev. 32,* 1979, p. 4.

30. Luborsky, F.E. and H.H. Liebermann. "Stress Relaxation of Fe-B Amorphous Alloys," *J. Appl. Phys. 51 (1),* 1980, p. 796. Reprint 8730.*

31. Luborsky, F.E., J.J. Becker, J.L. Walter, and D.L. Martin. "The Fe-B-C Ternary Amorphous Alloys," *IEEE Trans Magn. Mag-16 (3),* 1980, pp. 521-525. Reprint 8872.*

32. Luborsky, F.E., E.P. Wohlfarth, J.L. Walter, and H.H. Liebermann. "The Effect of Temperature on Magnetic Saturation of Some Amorphous Alloys," *J. Magn. and Magn. Mater. 15-18,* 1980, p. 1351. Reprint 8800. Also GE Report 79CRD178.*

33. Luborsky, F.E., J.L. Walter, and E.P. Wohlfarth. "The Saturation Magnetization, Curie Temperature and Size Effect of Amorphous Iron Alloys," *J. Phys. F 10,* 1980, pp. 959-966.*

* Report found in Appendices.

34. Luborsky, F.E., P.G. Frischmann, and L.A. Johnson. "Amorphous Materials – A New Class of Soft Magnetic Alloys," *J. Magn. and Magn. Mater. 19,* 1980, pp. 130-137. Reprint 8832.*

35. Luborsky, F.E. and J.L. Walter. "The Preparation and Properties of Fe-B-Si-C Amorphous Alloys," *IEEE Trans. Magn. Mag-16 (4),* 1980, pp. 572-574. Reprint 8896.*

36. Luborsky, F.E. "Composition Dependence of the Curie Temperatures of Amorphous Alloys," *J. Appl. Phys. 51 (5),* 1980, pp. 2808-2810. Reprint 8835.*

37. Luborsky, F.E. and L.A. Johnson. "Applications of Magnetic Amorphous Alloys," *J. Phys. (Paris) 41,* 1980, pp. C8-820-826. Reprint 8997.*

38. Luborsky, F.E., H.H. Liebermann, and J.L. Walter. "Effect of Ribbon Thickness, Composition and Process Changes on the Properties of Rapidly Quenched Metal-Metalloid Alloys," *Proc. Conf. Metallic Glasses: Science and Technology.* Budapest: Organ. Comm., Central Res. Inst. Phys., *1,* 1980, pp. 203-214. (Dist. by Kultura Foreign Trade Co., Budapest, P.O. Box 149, Hungary, H-1389.) Also GE Report 80CRD126.*

39. Mogro-Campero, A. and F.E. Luborsky. "Effect of Ribbon Thickness on Resistivity of Amorphous Fe-B-Si," *J. Appl. Phys. 52 (5),* 1981, p. 515. Reprint 8969.

40. Allia, P., F.E. Luborsky, G.P. Soardo, and F. Vinai. "Torque Measurements of Induced Anisotropy in Amorphous $Fe_{80-x}B_{20+x}$ Alloys," *J. Appl. Phys. 52,* 1981, pp. 3553-3556. Reprint 9064.*

41. Becker, J.J. "Effects of Surface Treatment and Thinning on Magnetic Properties of Rapidly Quenched Amorphous Alloy Ribbons," *J. Appl. Phys. 52 (3),* 1981, pp. 1905-1907. Reprint 9024.*

42. Luborsky, F.E. and J.L. Walter. "The Fe-B-GE Amorphous Alloys," *IEEE Trans. Magn. Mag-17 (2),* 1981, pp. 1204-1207. Reprint 9088.*

43. Liebermann, H.H. and F.E. Luborsky." Embrittlement of Some Metallic Glasses by Sb, Se, and Te," *Acta Met. 29,* 1981, pp. 1413-1418. Also GE Report 81CRD061.*

44. Luborsky, F.E. and H.H. Liebermann. "Effect of Melt Temperature on Some Properties of $Fe_{80.5}B_{15}Si_4C_{0.5}$ and $Fe_{40}Ni_{40}B_{20}$ Amorphous Alloys," *Mater. Sci. Eng. 49,* 1981, p. 257. Also GE Report 81CRD060.*

45. Allia, P., F.E. Luborsky, R. Sato Turtelli, G.P. Soardo, and F. Vinai. "Magnetic Relaxation in Amorphous Ribbons Prepared with Different Quenching Rates," *IEEE Trans. Magn. Mag-17,* 1981, xxx.

46. Luborsky, F.E., S.C. Huang, and H.C. Fiedler. "Effect of Surface Features of Amorphous Alloys on Magnetic Behavior," *IEEE Trans. Magn. Mag-17,* November 1981. Also GE Report 81CRD062.*

47. Luborsky, F.E., J.L. Walter, and H.H. Liebermann. "Properties of Amorphous Alloys of Fe-B-Ga and Fe-B-Si-C-Al," *IEEE Trans. Magn. Mag-17,* 1981, xxx. Also GE Report 81CRD123.*

48. Taub, A.I. and F.E. Luborsky, "Creep, Stress Relaxation and Structural Change of Amorphous Alloys," *Acta Met. 29,* June 1981, pp. 1939-1948. Also GE Report 81CRD112.*

* Report found in Appendices.

49. Luborsky, F.E. and F. Bacon. " Diffusion of Silicon into Amorphous Fe-B-Si," *Proc. Fourth Int. Conf. Rapidly Quenched Metals* (Japan), 1981. Also GE Report 81CRD193.*

50. Huang, S.C., P.G. Frishmann, F.E. Luborsky, J.D. Livingston, and A. Mogro-Campero. *Effects of Ribbon Thickness and Annealing Temperature on the AC Magnetic Properties of the* $Fe_{81.5}B_{14.5}Si_3C_1$ *Alloy.* Holland: North Holland Publ. Co. Also GE Report 81CRD213.*

* Report found in Appendices.

APPENDICES

Stress relaxation of iron-boron amorphous alloys

F. E. Luborsky and H. H. Liebermann
General Electric Corporate Research and Development, Schenectady, New York 12301

(Received 10 July 1979; accepted for publication 14 August 1979)

The stress relaxation of Fe_xB_{100-x} alloys for $72 \leq x \leq 88$ at.% was measured after annealing for 2 h at 225°C on ribbons having thicknesses between 15 and 33 μm. Stress relaxation increases with x and with decrease in thickness. There was no evidence for any discontinuity in stress relaxation versus x as was previously found for the activation energy for crystallization versus x. This implies that different atomic processes are involved in stress relaxation and in crystallization.

PACS numbers: 61.40.Df, 81.40.Ef, 81.20.Pe

In a previous paper[1] we reported on the kinetics of crystallization of the series Fe_xB_{100-x}. It was noted that the activation energy ΔE and the preexponential constant A, both changed slope at about 81 at.% Fe. This compositional dependence of ΔE and A was attributed to the decreased filling of the holes by B in the Bernal structure as the Fe content increased. The holes are filled for compositions up to 81 at.% Fe thus resulting in the development of crystal nuclei by a self-diffusion mechanism during annealing resulting in only a small dependence of ΔE and A on composition. For compositions greater than 81 at.% Fe diffusion is aided by the increasing concentration of holes resulting in a large dependence of ΔE and A on composition. It may be expected that other processes that depend on atomic diffusion would also show a change in slope of their diffusion related parameters, for example, in stress relaxation or in magnetic annealing.

In this note we examine the stress-relaxation behavior. The same samples of amorphous alloys, in the series Fe_xB_{100-x}, were used as reported previously.[1-3] Stress relaxation during annealing for the fixed period of 2 h at 225°C was determined as previously described[2] by measuring the radius of curvature of a small hoop, annealing, and then measuring the radius of curvature of the relaxed hoop. A fractional stress relaxation has been defined[2] as $F = 1 - (\sigma/\sigma_0) = [(r_0/r_a) - (r_0/r_1)]/[1 - (r_0/r_1)]$ where the ribbon samples with an initial radius of curvature, r_1, are subjected to a strain by placing them in a restraining ring with radius, r_0, which imparts a strain σ_0. After annealing the sample has a residual strain σ. It is then removed from the ring and allowed to relax. Its new radius is then r_a. The results are shown in Fig. 1. Sample thicknesses were measured with a micrometer to $\pm 1.3\,\mu$m. The micrometer thickness was used rather than average thickness since it was thought that the maximum thickness might be the controlling factor. The average thicknesses were in general about 20% lower than the thickness determined with the micrometer. However, the same trend with composition was observed for the micrometer thickness shown in Fig. 1, as was observed for the average thicknesses. Note that two different sample types were used, vacuum cast and air cast. The result of casting in air appears to enhance the stress relaxation. This may be the result of the faster quench rate due to the higher heat transfer provided by the air surrounding the ribbon in contrast to the vacuum, or it may be the result of the rougher surface causing the micrometer thickness to be increased compared to the average thickness.

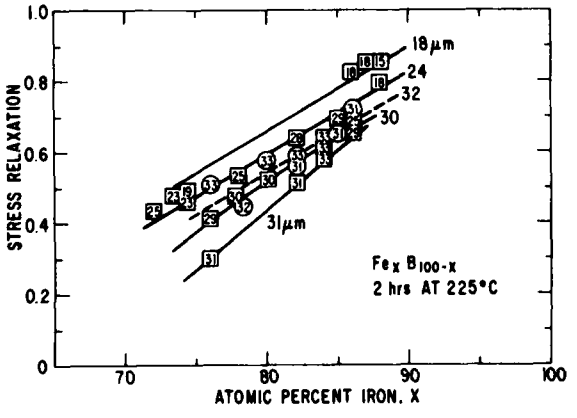

FIG. 1. Stress relaxation of Fe-B alloys as a function of iron content after annealing for 2 h at 225°C. □ made in vacuum; ○ made in air. Thicknesses in micrometers as measured by a micrometer are written in each symbol.

There is no evidence for any discontinuous behavior around 81% Fe. This implies that the atomic processes involved in stress relaxation are different than those involved in crystallization.

ACKNOWLEDGMENT

The partial support of the Office of Naval Research is gratefully acknowledged.

[1] F.E. Luborsky, H.H. Liebermann, and J.J. Becker, Appl. Phys. Lett. 33, 233 (1978).
[2] F.E. Luborsky and J.L. Walter, Mater. Sci. Eng. 35, 255 (1978).
[3] F.E. Luborsky, H.H. Liebermann, J.J. Becker, and J.L. Walter, *Rapidly Quenched Metals III*, edited by B. Cantor (The Metals Society, London, 1978), Vol. 2, p. 188.

 0021-8979/80/010796-01$01.10

The Fe-B-C Ternary Amorphous Alloys

FRED E. LUBORSKY, FELLOW, IEEE, JOSEPH J. BECKER, SENIOR MEMBER, IEEE, JOHN L. WALTER, AND D. L. MARTIN

Abstract—The properties of amorphous Fe-B-C alloys have been studied. The replacement of boron by carbon reduces the thermal stability of alloys containing more than approximately 80-percent iron, increases the Curie temperature slightly, and decreases the slope of the magnetization-temperature curve. Thus, although the low-temperature saturation magnetization decreases on replacement of B by C, as expected, the room-temperature magnetization exhibits a broad ridge of constant saturation magnetization per gram extending from approximately $Fe_{80}B_{20}$ to approximately $Fe_{83}B_{11}C_6$. This ridge follows one of the low-temperature magnetization contours. The density of the alloys in the series $Fe_{84}B_{16-x}C_x$ was measured and compared to calculated densities. The increase in density agrees with the calculated values and results in a slight increase in saturation magnetization per unit volume with increase in carbon. The coercivity, both as-cast and after stress relief annealing, increases on replacement of B by C. This is not understood.

INTRODUCTION

THIS WORK is part of a study to examine the properties of amorphous alloys and in particular alloys containing Fe with different glass-forming metalloids. Ternary Fe-B-C amorphous alloys have recently been reported [1]-[6]. Hatta *et al.* [1]-[4] claim values of $4\pi M_s$ above 16.5 kG, measured at room temperature, for various alloys of $Fe_{100-x-y}B_xC_y$ where the iron content is 84 at % or higher, and the carbon is above about 3-4 at %. Values of saturation magnetization above 17.5 kG were reported [3] for $Fe_{86}B_7C_7$ after annealing. These values are to be compared to 15.9-16.2 kG obtained [7] as the peak value of saturation magentization in the binary Fe-B amorphous alloys. This peak occurs at ~$Fe_{80}B_{20}$ [7]. However, over the same alloy series of $Fe_{84}B_{16-x}C_x$ and $Fe_{86}B_{14-x}C_x$, studied by Hatta *et al.*, we found [8] no values greater than the saturation magnetization per unit weight for $Fe_{80}B_{20}$ before annealing. It has been found [3] that the replacement of boron by carbon reduces the low-temperature moment of the iron and of the alloy. This is expected, based on the simple band theory involving charge transfer, since carbon has more electrons available than boron to fill the *d*-band of the alloy. Thus, Hatta *et al.* attribute the increase in $4\pi M_s$ at room temperature to 1) an increase in density [2] with addition of carbon, 2) a decrease in the slope of the reduced magnetization versus temperature curves at low temperatures [4], and 3) a structural change which occurs on annealing [9]. The decrease in the low-temperature magnetic moment has also been reported by Mitera *et al.* [5] and by Kazama *et al.* [6] for alloys of $Fe_{80}B_{20-x}C_x$. This report describes the formation, magnetic properties, thermal stability, and density of selected amorphous alloys in the ternary Fe-B-C system.

Manuscript received June 25, 1979; revised November 27, 1979.
The authors are with the General Electric Corporate Research and Development Center, Schenectady, NY 12301.

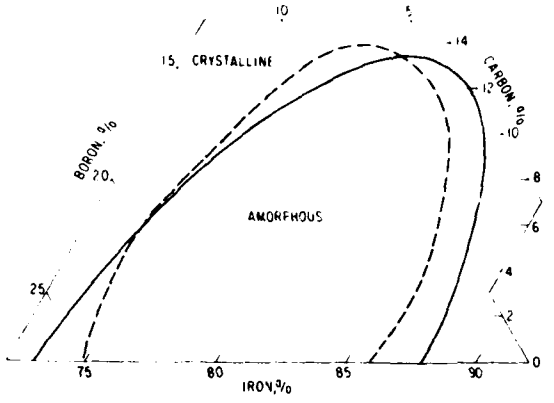

Fig. 1. Composition range for formation of amorphous Fe-B-C alloys. Solid line from this work; dashed line from Fujimori and Marumoto.

EXPERIMENTAL METHODS

Amorphous ribbons were prepared [10], [11] by melt quenching onto the surface of a rotating wheel. Curie temperatures, T_c, were determined using a thermogravimetric recording balance fitted with a permanent magnet to produce a field gradient in a field of 225 Oe. Samples were heated at 20°/min. Values of saturation magnetization σ_s were determined using a vibrating sample magnetometer at fields up to 20 kOe. Results reported were obtained by extrapolating to infinite field using a $1/H^2$ function. Coercive fields, H_c, were determined on 10 cm long ribbons using an integrating fluxmeter connected to a small sense coil in the center of a long solenoid. Annealing was carried out in a 30-Oe field.

FORMATION

The composition range over which the alloys may be quenched entirely into the amorphous phase is shown in Fig. 1. This boundary, of course, will depend on the particular system parameters controlling the quench rate, e.g., melt temperature, ribbon thickness, wheel material, and atmosphere. For the amorphous Fe-B-C alloys prepared in this work the ribbon thickness was 20-30 μm, the wheel material was copper, and casting was done in air. Melt temperatures were not measured. The results reported by Fujimori and Masumoto [12] are essentially the same, although no preparation conditions were reported.

0018-9464/80/0500-0521$00.75

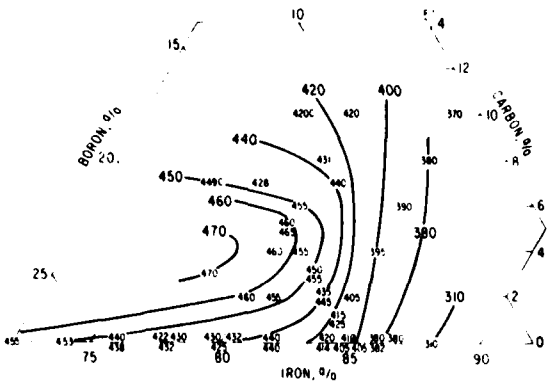

(a)

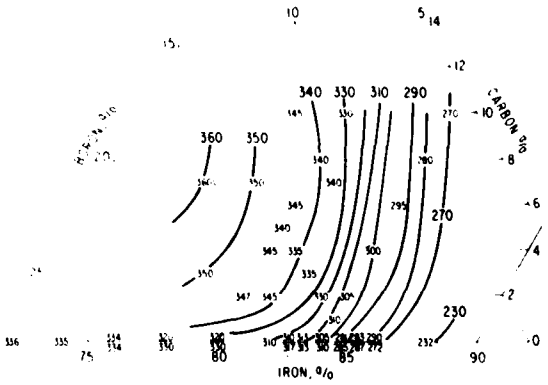

(b)

Fig. 2. Crystallization temperatures in °C for amorphous Fe-B-C alloys obtained at (a) heating rate of 20°/min and (b) 2-h anneal at increasing temperatures. The symbol *c* following the numbers denotes the detection of partial crystallinity.

Thermal Stability

The metallurgical change which occurs when crystallization begins was detected magnetically by two methods. The first method uses the magnetization-temperature curve. The magnetization falls with increasing temperature, typically to $M = 0$ at T_c. When crystallization starts, iron or compounds with high T_c values appear causing an increase in M. The beginning of this increase in M is denoted as the beginning of crystallization. The M-T curves were taken at the fixed rate of increase of temperature of 20°/min. The results are shown in Fig. 2(a). In the second method we looked for the beginning of the increase in H_c, as measured at room temperature, after successive 2-h anneals at increasing temperatures. This increase in H_c is associated with the appearance of crystalline phases. The temperature intervals were 25-30°C. The results shown in Fig. 2(b) do not quite parallel the results in Fig. 2(a). Crystallization does start at lower temperatures for the alloys in Fig. 2(b), as expected, because of the much slower heating of the incremental step anneals. It is clear that for alloys with greater than approximately 82-percent Fe, that replacement of B by C decreases the stability, or resistance to crystallization. For alloys containing less than approximately 82-percent Fe the stability first increases and then decreases as B is replaced by C.

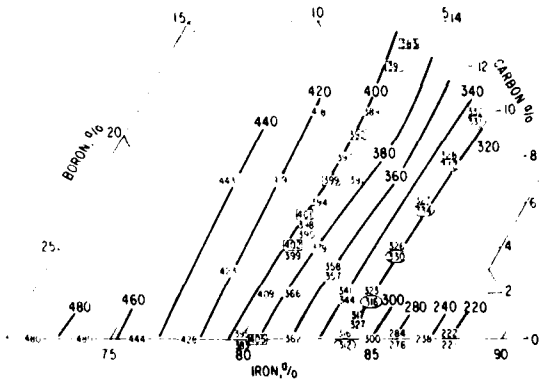

Fig. 3. Curie temperatures in °C for amorphous Fe-B-C alloys. Circled results reported by Hatta *et al.*, [1]. Results in squares from Kazama *et al.*, [6]. *c* = partially crystalline.

It is not clear why this behavior occurs nor why it is different than in the Fe-B-Si amorphous alloys [13]. In the Fe-B-Si alloys the stability increases, over the entire composition range, on replacing B by Si.

Magnetic Properties

Curie Temperature

The Curie temperatures of the Fe-B-C alloys are shown in Fig. 3. They show a slight increase in T_c with replacement of B by C for iron contents above about 79 percent. For iron below about 79 percent the T_c decreases slightly on replacement of B by C.

Saturation Magnetization

The low-temperature (77K) saturation magnetization in emu/g, shown in Fig. 4(a), exhibits the expected decrease in magnetization with the initial replacement of B by C. This decrease is the result of the greater number of electrons available from the carbon as compared to boron. These additional electrons fill the *d*-band of the alloy to a greater degree than would be the case for alloys containing only boron, reducing the magnetization. For larger additions of C it appears that σ_s no longer decreases. This is not understandable using the simple charge transfer model. These results have been recalculated in terms of Bohr magnetons per iron atom and are shown in Fig. 4(b). In the limit of pure iron, these results approach 2.2, the value for crystalline iron.

The room temperature σ_s values are shown in Fig. 5. As in the case for the Fe-B-Si alloys [13], the σ_s exhibits a ridge of maximum σ_s of constant value out to approximately 6-7-percent C. The decrease at higher iron contents is caused by the rapid decrease in σ_s as the T_c drops. The ridge, extending out to higher iron contents, is consistent with the shape of the low-temperature contours of σ_s. The present results indicate that there is no increase in σ_s with replacement of B by C, whereas Hatta *et al.* [1]-[4] observed an increase in σ_s. The difference between our results and, the results of Hatta *et al.* may be due to a difference in measuring technique. In our measurements we report σ_s at infinite field using a $1/H^2$ extrapolation from fields of up to 20 kOe. In [1]-[4] σ_s is re-

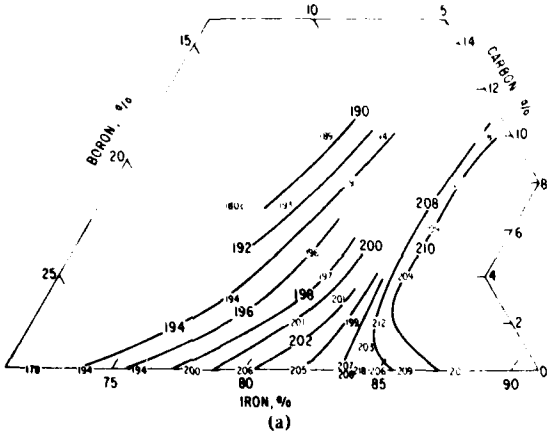

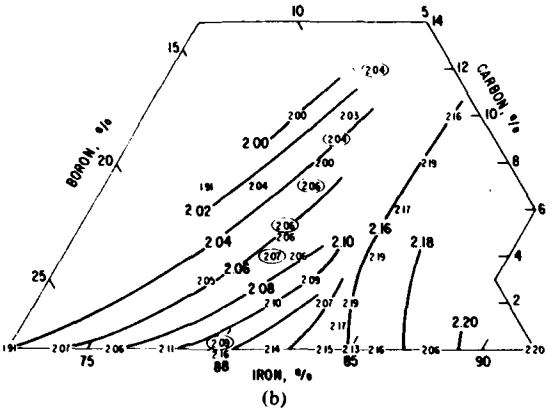

Fig. 4. Saturation magnetization measured at 77 K for amorphous Fe-B-C alloys: (a) in emu/g and (b) in Bohr magnetons per iron atoms. Circled results from Kazama *et al.*

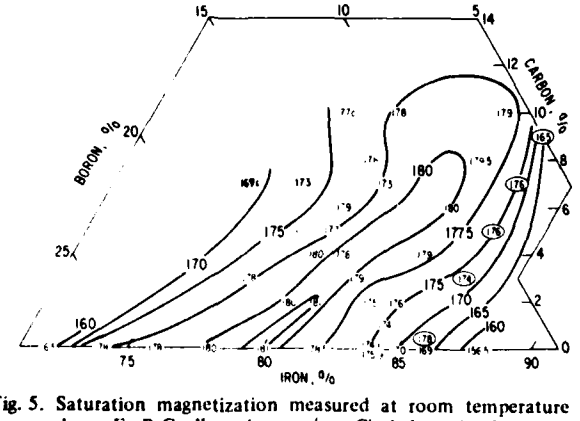

Fig. 5. Saturation magnetization measured at room temperature for amorphous Fe-B-C alloys in emu/g. Circled results from samples prepared by Hatta and measured by us. c = partially crystalline.

ported at 1 kOe. Since the susceptibility is significantly dependent on composition, as pointed out in [4], we would expect somewhat different results from these two different techniques for measuring σ_s. We have also observed [14] a decrease in the slope of the low-temperature reduced magnetization-temperature curve. This will also contribute to the increased room temperature σ_s.

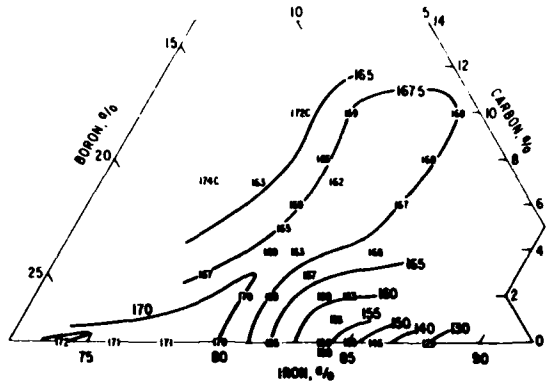

Fig. 6. Saturation magnetization measured at 100°C for amorphous Fe-B-C alloys in emu/g. c = partially crystalline.

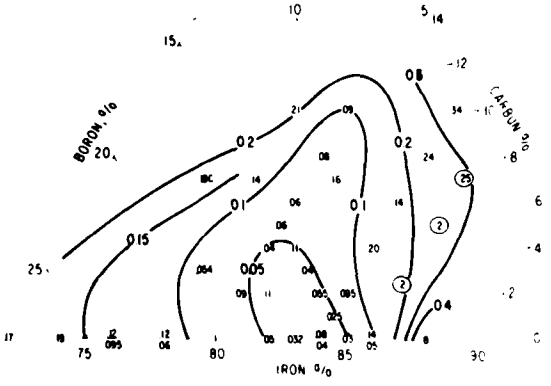

Fig. 7. Coercivity in Oe for as-cast Fe-B-C amorphous alloys. Circled results from samples prepared by Hatta and measured by us. c = partially crystalline.

The saturation magnetization has been obtained at 100°C and is shown in Fig. 6. This was derived from the magnetization-temperature curve used to determine T_c by normalizing the value at room temperature to the vibrating sample magnetometer measurement at room temperature. As expected, the ridge of maximum σ_s has been moved to lower iron contents and to a lower value since the measurements were made at 100°C, i.e., closer to T_c.

Coercivity

The coercivity of the as-cast amorphous alloys is shown in Fig. 7, and the results after annealing to a minimum in H_c are shown in Fig. 8. There appears to be much more scatter in these H_c results than in T_c, σ_s, or stability. This increased scatter is undoubtedly due to the random contributions to H_c from surface irregularities, internal strains, and defects. In any case, the H_c is seen to increase on replacement of B by C both in the as-cast and annealed state. This is tne reverse of the behavior in Fe-B-Si alloys on replacement of B by Si [13].

Density

The results of our density measurements and those of Hasegawa and Ray [16] are compared to calculated values in Fig. 9. The curves were derived by first calculating the packing frac-

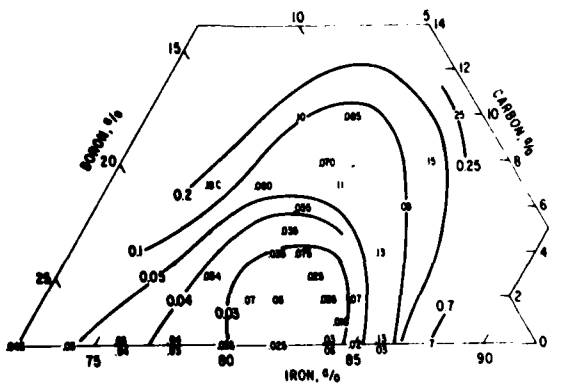

Fig. 8. Coercivity in Oe for Fe-B-C amorphous alloys annealed to minimum coercivity. c = partially crystalline.

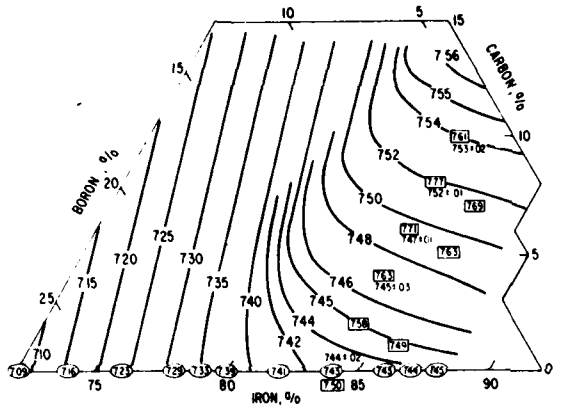

Fig. 9. Densities of Fe-B-C amorphous alloys in as-cast state in g/cm^3. Lines calculated as described in the text. Densities with squares around them from Hatta *et al.*, with circles around them from Hasegawa and Ray, and with nothing around them from this work.

tion versus the iron content of the Fe-B alloy series using the measured densities of Hasegawa and Ray [16]. Then the density of various Fe-B-C alloys was calculated by using these packing fractions for each iron content together with the tetrahedral covalent radii of boron (0.88) and carbon (0.77) as previously described [17], [18].

In this study, the density of a series of $Fe_{84}B_{16-x}C_x$ alloys up to 10 at % carbon was measured by the buoyancy method by comparing the weight in air to the weight in diethylphthalate (density of 1.1162 g/cm^3 at 22°C). The density variation of the diethylphthalate with temperature was calculated from that given by $\ln\rho = -0.000796\,T + 0.12741$ [15]. The samples were cut from ribbons about 1.5-mm wide to give a total sample weight of about 0.22 g. Ten independent density measurements were made on each alloy sample, the results were averaged, and the 99-percent confidence limit of the mean was determined. Because of the large number of strips needed for each specimen, a special wire holder with a tiny cobalt-samarium magnet fastened to one end was used to hold the strips during weighing in the diethylphthalate.

Our density measurements for the $Fe_{84}B_{16-x}C_x$ series are given in Fig. 9 by the bare numbers and compared in Fig. 10

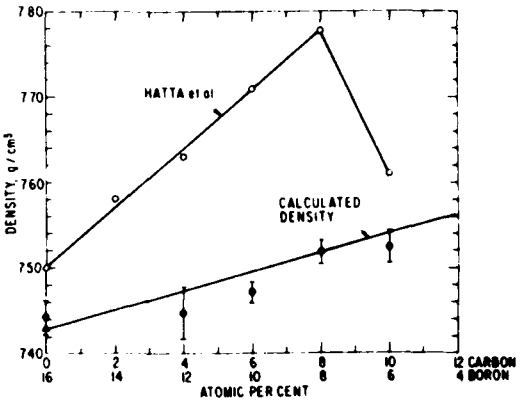

Fig. 10. Comparison of our measured density values with calculated values and those reported by Hatta *et al.* [2]. The error bars represent the 99-percent confidence interval of the mean.

with the calculated values and those reported by Hatta *et al.* [2]. There is a good agreement between our measured density values and the calculated values. Our density values are one to three percent lower than those reported by Hatta *et al.* [2].

The $4\pi M_s$ magnetization values of several alloys have been calculated from the density measurements and the saturization magnetization in emu/g from Fig. 5. The $4\pi M_s$ value of the $Fe_{80}B_{20}$ alloy was calculated to be 16.8 kG and that for the $Fe_{84}B_{10}C_6$ alloy to be 17.0 kG. As shown by Hatta *et al.* [1]-[4], these values will increase on annealing.

Comparison of Fe-B-C and Fe-B-Si Behavior

The region in which the Fe-B-C alloys can be prepared in the amorphous state is qualitatively the same as for the Fe-B-Si alloys, although the contour for the transition between the amorphous and crystalline states is tilted to the higher Fe contents for the Fe-B-C alloys. This difference is probably due to differences in the reduced glass temperature, T_g/T_m, where T_m is the melting point. Davies [19], for example, has shown that a good correlation exists between the critical cooling rate required for glass formation and T_g/T_m.

The crystallization of Fe-B-C exhibits a decrease in the temperature for the onset of crystallization T_x at Fe contents above about 84 percent as C replaces B, but at low Fe contents T_x first increases before decreasing as C replaces B. In the Fe-B-Si alloys, however, the T_x increases as Si replaces B over almost the entire region studied. These differences are probably due to differences in electronic concentrations and in atom sizes [20].

The changes in the Curie temperature T_c with composition are just about the same in the Fe-B-C and Fe-B-Si alloys. This indicates that the near neighbor environment of the Fe atoms is very similar in the two systems. However, Kazama *et al.* [6] reported that the $Fe_{80}B_{20-x}C_x$ had lower T_c values than $Fe_{80}B_{20-x}Si_x$.

The saturation magnetization at low temperatures shows very similar behavior in the Fe-B-C and Fe-B-Si amorphous alloys. The Fe-B-Si alloys exhibit slightly higher σ_s as Si replaces B than is observed for C replacing B. This is as expected [6], since the atomic size of Si is greater than C even though

both have the same outer electron configuration and affect the d-band in a similar way.

The saturation magnetization at room temperature is also qualitatively the same in both the Fe-B-C and Fe-B-Si systems as expected from the similarity in T_c and σ_s at low temperature. The difference in behavior of σ_s in the two alloy systems is in the width and length of the ridge of constant maximum σ_s. It is much broader in the Fe-B-C system and extends to lower boron contents than in the Fe-B-Si alloys. This appears to be due to the flatter σ_s versus T curves in the Fe-B-C alloys than in the Fe-B-Si alloys [14], indicating a difference in the long wavelength spin-wave spectrum.

Although the behavior of all of the previous properties are qualitatively similar in the Fe-B-C and Fe-B-Si alloys, the behavior of the coercivity is drastically different. In the case of replacement of B by C, H_c increases, while on replacement of B by Si H_c decreases. It is not due to differences in magnetostriction, since measurements [21] on $Fe_{80}B_{20-x}C_x$ and $Fe_{80}B_{20-x}Si_x$ showed no change in magnetostriction for either series of alloys. This behavior is not understood.

Conclusion

In the ternary Fe-B-C amorphous alloys, the T_c at a constant iron content is almost independent of the boron/carbon ratio. At low temperatures the σ_s decreases on replacement of B by C at constant iron, and the moment increases whith increase in Fe. However, at room temperature the moment first increases at low Fe contents but then decreases for Fe contents above about 82 percent. This is due to the decrease in T_c. The coercivity is always higher for the ternary Fe-B-C alloys than for the binary Fe-B alloys. In the region around the ridge of maximum σ_s the crystallization temperature first increases slightly and then decreases as boron is replaced by carbon. Addition of carbon increases the density of the Fe-B alloys by just the amount calculated.

Acknowledgment

The authors are grateful for the work of N. Marotta in obtaining the Curie temperatures and to J. Gillespie in performing magnetic measurements. The partial support of the Office of Naval Research is also acknowledged.

References

[1] S. Hatta, T. Egami, and C. D. Graham, Jr., *IEEE Trans. Magn.*, vol. MAG-14, p. 1013, 1978.
[2] —, *Rapidly Quenched Metals III*, Ed. B. Cantor, London: The Metals Society, 1978, vol. 2, p. 183.
[3] —, *Appl. Phys. Lett.*, vol. 34, p. 113, 1979.
[4] S. Hatta and T. Egami, *J. Appl. Phys.*, vol. 50, p. 1589, 1979.
[5] M. Mitera, M. Naka, T. Masumoto, N. Kazama, and K. Watanabe, *Phys. Stat. Sol.*, vol. (a) 49, p. K163, 1978.
[6] N. S. Kazama, M. Mitera, and T. Masumoto, *Rapidly Quenched Metals III*, B. Cantor, Ed. London: The Metals Society, 1978, vol. 2, p. 164.
[7] F. E. Luborsky, H. H. Liebermann, J. J. Becker, and J. L. Walter, *Rapidly Quenched Metals III*, B. Cantor, Ed. London: The Metals Society, 1978, vol. 2, p. 188.
[8] F. E. Luborsky, J. J. Becker, and H. H. Liebermann, *Rapidly Quenched Metals III*, B. Cantor, Ed. London: The Metals Society, 1978, vol. 2, p. 249.
[9] T. Egami, *J. Appl. Phys.*, vol. 50.
[10] H. H. Liebermann and C. D. Graham, Jr., *IEEE Trans. Magn.*, vol. MAG-12, p. 921, 1976.
[11] J. L. Walter, *Rapidly Quenched Metals III*, B. Cantor, Ed. London: The Metals Society, 1978, vol. 1, p. 30.
[12] H. Fujimori and T. Masumoto, *Suppl. to Sci. Rep. Res. Inst.*, Tohoku Univ., vol. A27, p. 181, 1978.
[13] F. E. Luborsky, J. J. Becker, J. L. Walter, and H. H. Liebermann, *IEEE Trans. Magn.*, vol. MAG-15, p. 1146, 1979.
[14] —, *J. Magnetism Magnet. Mater.*, to appear.
[15] H. C. Rogers, R. C. Leech, and L. F. Coffin, Final Rep., Contract NOw-65-0097-f, Naval Air Systems Command, Nov. 1965.
[16] R. Hasegawa and R. Ray, *J. Appl. Phys.*, vol. 49, p. 4174, 1978.
[17] G. S. Cargill, III, *Solid State Phys.*, vol. 30, p. 227, 1975.
[18] F. E. Luborsky, Ferromagnetic Materials, E. P. Wohlfarth, Ed. Amsterdam: North Holland, 1979, vol. 1, chapt. 6, pp. 451–529.
[19] H. A. Davies, *Physics and Chem. Glasses*, vol. 17, p. 159, 1976.
[20] I. W. Donald and H. A. Davies, *Rapidly Quenched Metals III*, B. Cantor, Ed. London: The Metals Society, 1978, vol. 1, p. 273.
[21] F. E. Luborsky, P. J. Flanders, H. H. Liebermann, and J. L. Walter, *IEEE Trans. Magn.*, vol. MAG-15, pp. 909–911, 1979.

GENERAL ELECTRIC

General Electric Company
Corporate Research and Development
Schenectady, New York

TECHNICAL INFORMATION SERIES

AUTHOR(S)
Luborsky, FE — Walter, JL
Wohlfarth, EP — Liebermann, HH

NO. 79CRD178
DATE October 1979
GE CLASS 1
NO. PAGES 4

TITLE
The Effect of Temperature on Magnetic Saturation of Some Amorphous Alloys

ORIGINATING COMPONENT
Metallurgy Laboratory
CORPORATE RESEARCH AND DEVELOPMENT SCHENECTADY, N.Y.

SUMMARY

The magnetization vs. temperature relation for the amorphous alloys $Fe_{100-x}B_x$, $Fe_{84}B_{16-x}C_x$, $Fe_{80}B_{20-x}Si_x$, $Fe_{80}B_{20-x}Ge_x$ and $Fe_{40}Ni_{40}B_{20-x}P_x$ are reported. Plots of the resulting spin wave stiffness constant D versus the Curie temperature T_c give roughly linear relationships extrapolating to zero D at finite T_c values. These results are discussed on the basis of the itinerant electron model. Neutron scattering values of D are also exhibited for comparison with those obtained here.

SUBJECT
magnetic saturation of amorphous alloys

KEY WORDS
amorphous alloys, magnetic saturation, temperature dependence of saturation

INFORMATION PREPARED FOR _____

Additional Hard Copies Available From
Corporate Research & Development Distribution
P.O. Box 43 Bldg. 5, Schenectady, N.Y., 12301

Microfiche Copies Available From
Technical Information Exchange
P.O. Box 43 Bldg. 5, Schenectady, N.Y., 12301

THE EFFECT OF TEMPERATURE ON MAGNETIC SATURATION OF SOME AMORPHOUS ALLOYS

F.E. Luborsky, E.P. Wohlfarth, J.L. Walter, and H.H. Liebermann

INTRODUCTION

Spin wave excitations in ferromagnets have a quadratic dispersion relation for their energy $E(K) = DK^2 + \ldots$ where K is the wave vector and D the spin wave, or exchange, stiffness constant. It was just a few years ago that spin wave resonances were first observed in amorphous ferromagnets.[1] At that time, whether or not spin waves could exist in the amorphous structure with only short range order was interesting from the theoretical point of view. In such amorphous structures the wave vector is not well defined and no simply defined Brillouin zone exists. Kaneyoshi[2] showed that the long wave length spin waves can be clearly and stably defined in an amorphous ferromagnet using the viewpoint that the amorphous magnets have a topologically disordered structure of the type given by the random close packing of atomic spheres.

From a more practical viewpoint, Hatta and Egami[3] reported that the high room temperature saturation magnetization of Fe-B-C alloys is, in large part, the result of the decrease in the slope of the magnetization vs. temperature curve as the content is increased. They reported values of β in the low temperature spin wave approximation

$$M(T)/M(O) = 1 - \beta(T/T_c)^{3/2} \qquad (1)$$

of 0.43 for $Fe_{84}B_9C_7$ compared to 0.65 for $Fe_{86}B_{14}$ and 0.55 for $Fe_{84}B_{10}C_6$ compared to 0.63 for $Fe_{84}B_{16}$. Hatta and Egami[3] and Fukamichi et al.[4] both reported some limited results for β of some $Fe_{100-x}B_x$ alloys. However, Kazama et al.[5] reported an increase in D with x for the entire series and showed that D varied linearly with T_c. They infer from these results the character of the Fe-Fe exchange interactions.

Thus it was of interest to examine the low temperature behavior of other amorphous alloy systems such as the Fe-B binary alloys as well as Fe-B alloys containing C, Si, Ge and Fe-Ni-B-P and to try to establish some degree of systematics of the spin wave stiffness, as dependent on the alloy composition.

EXPERIMENTAL PROCEDURE

Magnetizations at room temperature and below were determined in a vibrating sample magnetometer to a maximum field of 20 kOe on specimens about 0.5 cm long and about 0.1 cm wide. Results were extrapolated to infinite field using a $1/H^2$ law. Magnetization, M(T), above room temperature was determined using a force balance made up of a Dupont 951 thermogravimetric recording balance with a Dupont 990 thermal analyzer control unit. The furnace was noninductively wound and fitted with a large permanent magnet to produce a field gradient together with a field of 225 Oe along the length of 1-cm-long ribbons. The samples were heated at 20 deg/min. The Curie temperature, T_c, was determined as the intersection of M(T) with the temperature axis. The magnetization at 0 K, M(O), was determined by extrapolating to 0 K from 77 K and above on a $T^{3/2}$ scale.

TEMPERATURE DEPENDENCE OF M_s

The M(T) vs. T curves for the Fe-B amorphous alloys as the boron content increases are shown in Figure 1. We have calculated the values of β from the data between 77 and 300 K, using Eqn. (1). The use of magnetization results up to room temperatue may be justified on the basis of past experience[3,6-8] which showed that Eqn. (1) is valid for amorphous alloys to much higher temperatures than for crystalline alloys, in fact up to $T/T_c \cong 0.5$; i.e., near room temperature.

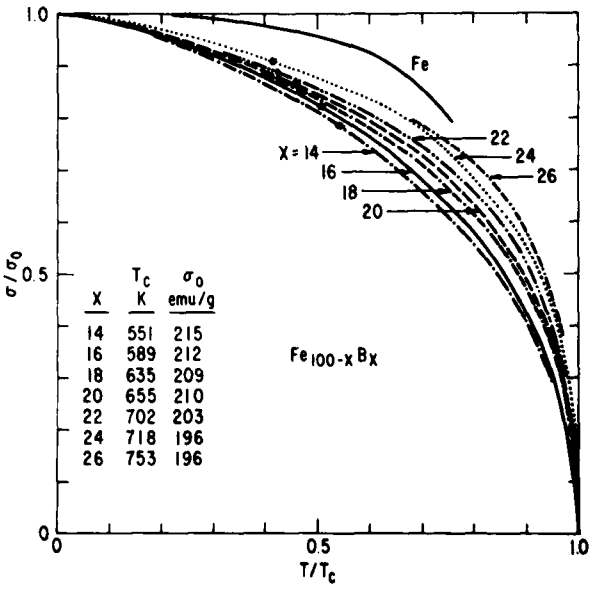

Figure 1. Reduced magnetization-temperature curves for $Fe_{100-x}B_x$ alloys compared to crystalline Fe. The * indicates room temperature.

Manuscript received July 13, 1979

There may be other contributions to M(T) for these materials, however, arising from itinerant ferromagnetism ($\sim T^2$), from thermal expansion effects and from the amorphicity itself, when compared to equivalent crystalline alloys. The values of β are shown in Figure 2. This trend is consistent with previously reported results[3,4] for the Fe-B alloys. Note that the values of β for the two extreme compositions are off the trend line. This is due to the fact that these two samples showed evidence for the presence of some slight crystallinity.[9]

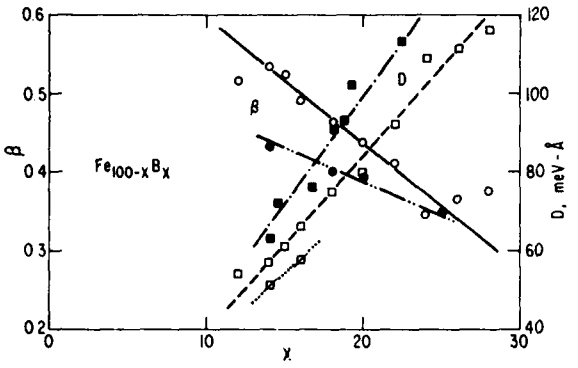

Figure 2. Slope of the spin wave equation β and the exchange stiffness constant D for $Fe_{100-x}B_x$ alloys. ■ from ref. 5; □ from ref. 3; O from ref. 11.

The magnetization vs. temperature curves for various Fe-B-X alloys were also determined. Where more than one sample was tested, the maximum deviation from the curve was ±3% at $T/T_c \cong 0.7$. The results for β are shown in Figure 3(a) for Fe-B-C, Fe-B-Si, Fe-B-Ge and Fe-Ni-B-P alloys. In contrast to the decrease in β by C, Si and Ge, the replacement of B by P in the $Fe_{40}Ni_{40}B_{20-x}P_x$ alloys results in an increase in β.

DISCUSSION

The Exchange Stiffness

The value of β can be expressed in terms of D by the equation[10]

$$\beta = (g\mu_\beta/M_o)\,(k/4\pi D)^{3/2}F_{3/2}(T) \qquad (2)$$

where g = 2.1, M_o = magnetization at 0 K, and $F_{3/2}(T)$ = Bose-Einstein integral function = 2.61. The values of D calculated from (2) are displayed in Figures 2 and 3(b). Note in Figure 2 that our values for D appear to fall between the previously reported values,[3,5] and the β values are close to values derived from Mossbauer hyperfine field measurements.[11] The values of M_o were obtained from the measured values (emu/g) using the densities of the various alloys. This density was calculated by first calculating the packing fraction vs. Fe content for the Fe-B alloy series using the measured densities of Hasegawa and Ray.[12] Then the densities of the various ternary alloys were calculated using these packing fractions for each Fe content together with the tetrahedral covalent radii of B, Si, Ge, and P as previously described.[10] Excellent agreement was obtained between these calculated densities and some measured densities in the Fe-B-C system[13] and for some few measured densities in the Fe-B-Si system.

The correlation between D and T_c found by Kazama et al.[5] for the Fe-B alloys was confirmed in this work as shown by closed symbols in Figure 4, and appears to hold also for most of the other Fe-B-X alloys as well as Fe-Ni-B-P. The values of D obtained here from M(T) data may be supplemented by values obtained from neutron scattering measurements[6-8,14-19] shown in Figure 4 by open symbols. It appears that the two sets of data agree reasonably well for the Fe-Ni-B-P alloys but not for the Fe-B-X alloys. Differing D values from magnetization and neutron sources also occur for crystalline materials such as nickel;[20] this effect is not fully understood. Figure 4 also shows a few values of D from neutron scattering for amorphous Co-X.

The general trend of these D vs. T_c plots seems rather clear. There are roughly three sets of data, giving an approximately linear dependence and corresponding to:

1. Fe-B and Fe-B-X,
2. Fe-Ni-B-P and
3. Co-X

in increasing order of D. For [1.] extrapolation of the curve to zero D occurs at T_c about 380 K, for [2.] at about 200 K and for [3.] at about 0 K. It may be noted that the value of T_c for "amorphous iron," obtained by extrapolating the data for $Fe_{100-x}B_x$ as $x \rightarrow 0$, is about 300 K.[9]

The correlation between D and T_c has been discussed for the itinerant electron model by Katsuki and Wohlfarth.[21] They obtained linear relationships between these two quantities for *weak* itinerant ferromagnets with slopes determined by the effective intra-atomic coulomb interaction and extrapolating to zero D at zero T_c. The observed data in Figure 4 also give such linear relationships but with the same slopes and with most of the results not extrapolating to zero. It has been suggested[22] that amorphous Fe-B alloys may be regarded as *strong* or almost strong itinerant ferromagnets. For these the D vs T_c curves of Ref. 21 are no longer strictly linear and the values of D *decrease* with increasing T_c so as to extrapolate to zero D at a finite T_c. In this case also the experimental data are thus only partially explained by the calculations of Ref. 21. These early calculations, however, were based on a very simple band structure and it can only be claimed that they already contain the germs of an explanation of the present complicated observations. If the extrapolation of the data to zero D at finite T_c is thus a real effect in the sense of this calculation; i.e., in the sense of spin wave mode softening, it may give

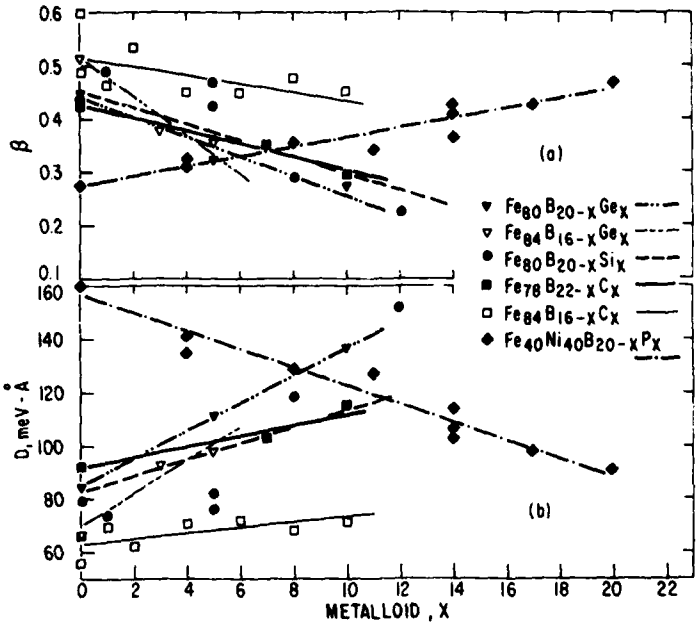

Figure 3. **(a) Slope of the low temperature spin wave equation as a function of metalloid content for various amorphous alloys. (b) The exchange stiffness constant for the same alloys as in (a).**

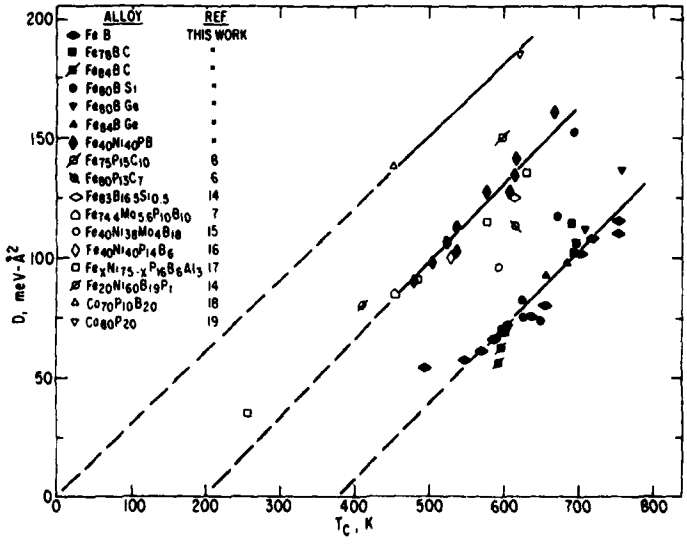

Figure 4. **The exchange stiffness constant D as a function of Curie temperature for various alloys. Solid and broken lines drawn through poi nts to guide the eye. Closed symbols, data from present measurements; open symbols, data from neutron measurements.**

a valuable hint as to the nature of magnetism in amorphous materials.

ACKNOWLEDGMENTS

The ribbons were prepared by W. Rollins. The measurements of magnetization were made by H. Patchen under the direction of I.S. Jacobs and by J.J. Becker. The high temperature measurements were made by N. Marotta. The densities were calculated by J. Gillespie and measured by D.L. Martin. The partial support of the Office of Naval Research is gratefully acknowledged. E.P. Wohlfarth thanks the General Electric Company for the award of a Visiting Fellowship.

REFERENCES

1. T. Kaneyoshi, *J. Phys.* C5 (1972) 5304.
2. T. Kaneyoshi, *J. Phys. Soc. of Japan* 45 (1978) 1835.
3. S. Hatta and T. Egami, *J. Appl. Phys.* 50 (1979) 1589.
4. K. Fukamichi, M. Kikuchi, S. Arakawa and T. Masumoto, *Solid State Comm.* 23 (1977) 955; K. Fukamichi, H. Hiroyoshi, M. Kikuchi and T. Masumoto, *J. Magnetism Magn. Mat.* 10 (1979) 294.
5. N.S. Kazama, M. Mitera and T. Masumoto, in *Rapidly Quenched Metals III*, Vol. 2, B. Cantor, ed. (The Metals Soc., London, 1978) p. 164.
6. N. Kazama, T. Masumoto and H. Watanabe, *J. Phys. Soc. Japan* 37 (1974) 1171.
7. J.D. Axe, G. Shirane, T. Mizoguchi and K. Yamauchi, *Phys. Rev.* B15 (1977) 2763.
8. C.L. Chien and R. Hasegawa, *Phys. Rev.* B16 (1977) 2115.
9. F.E. Luborsky, H.H. Liebermann, J.J. Becker and J.L. Walter, *Rapidly Quenched Metals III*, Vol. 2, B. Cantor, ed. (The Metals Soc., London, 1978), p. 188.
10. F.E. Luborsky, in *Ferromagnetic Materials*, E.P. Wohlfarth, ed. (North-Holland Publ. Co., 1979).
11. C.L. Chien, D. Musser, E.M. Gyorgy, R.C. Sherwood, H.S. Chen, F.E. Luborsky and J.L. Walter, *Phys. Rev.*, to appear.
12. R. Hasegawa and R. Ray, *J. Appl. Phys.* 49 (1978) 4174.
13. F.E. Luborsky, J.J. Becker, J.L. Walter and D.L. Martin, *IEEE Trans. Magnetics*, to appear.
14. J.J. Rhyne, J.W. Lynn, F.E. Luborsky and J.L. Walter, *J. Appl. Phys.* 50 (1979) 1583.
15. R. Krichnan, S. Prasad and K. Branski, *Proc. Joint Intermag-MMM Conf.*, 1979.
16. J.W. Lynn and J.J. Rhyne, to appear.
17. J.A. Tarvin, G. Shirane, R.J. Birgeneau and H.S. Chen, *Phys. Rev.* 17 (1978) 241, and *AIP Conf. Proc.* 34 (1976) 313.
18. J.R. McColl, D. Murphy, G.S. Cargill and T. Mizoguchi, *AIP Conf. Proc.* 29 (1976) 172.
19. H.A. Mook, N. Wakabayashi and D. Pan, *Phys. Rev. Lett.* 34 (1975) 104.
20. E.P. Wohlfarth, in *Ferromagnetic Materials*, E.P. Wohlfarth, ed. (North-Holland Publ. Co., 1979).
21. A. Katsuki and E.P. Wohlfarth, *Proc. Roy. Soc.* A295 (1966) 182.
22. E.P. Wohlfarth, *J. Magnetism Magn. Mat.* 10 (1979) 120.

J. Phys. F: Metal Phys., 10(1980)959–66. Printed in Great Britain

The saturation magnetisation, Curie temperature and size effect of amorphous iron alloys

F E Luborsky, J L Walter and E P Wohlfarth†
General Electric Corporate Research and Development, PO Box 8, Schenectady, New York 12301, USA

Received 20 August 1979, in final form 21 November 1979

Abstract. Measurements of the saturation magnetisation, Curie temperature and size effects are reported for the amorphous iron alloys Fe–X, where X is one of, or a combination of, B, Al, Ga, C, Si, Ge and P. The saturation magnetisation when plotted as a function of the total metalloid content shows an approximate trend in terms of charge transfer from the metalloid to iron atoms. The Curie temperature data show an approximate coincidence when plotted against X except for Fe–B–Al and Fe–B–Ge. This common curve follows semiquantitatively from results obtained here on the basis of the itinerant electron model. The relative change of volume $d\ln V/dx$ was found to vary systematically with the effective valency of the added metalloid.

1. Introduction

Amorphous alloys containing transition metals, such as iron, and metalloids, such as boron, silicon and phosphorus, have been much studied in the last few years because of their low coercive force and ready manufacture. These properties make them potentially suitable for applications as economic soft magnetic materials. Among material properties to this end are the saturation magnetisation and Curie temperature. These are clearly also important properties to be considered in making a physical interpretation of their magnitudes and their systematic variation in terms of the physics of these amorphous alloys. Hence, several series of measurements have already been published, for example by Mitera *et al* (1978) and Kazama *et al* (1978) who restricted themselves, as we do, to iron alloys. However, the papers so far published do not clearly establish any systematic trends for variations of the metalloid content. Hence, we report here a new series of measurements of the saturation magnetisation and Curie temperature of amorphous alloys of iron with the following metalloids: B, Al, Ga, C, Si, Ge, P, taken singly or severally. The results were plotted in relation to the *total* metalloid content in iron and a number of significant trends became thereby apparent. In order to interpret these results it was found to be necessary to have available values of the relative size effect $d\ln V/dx$, where V is the atomic volume and x the concentration of the metalloid. Values of the size variations were also reported by Kazama *et al* (1978) but the new data reported here again establish a significant trend not previously noted.

† On leave from Department of Mathematics, Imperial College, London SW7, England, UK until 30 September 1979.

0305-4608/80/050959 + 08 $01.50

An interpretation of these data is intrinsically very difficult due to the following features of amorphous magnetic alloys.

(i) The alloys have properties best described by the itinerant electron model: these properties were summarised and the application of the model briefly described by Wohlfarth (1978a). This model lacks the immediate appeal and the simplicity of the direct exchange aspects of the localised model of ferromagnetism. Furthermore, the itinerant model has many controversial features (see, for example, Edwards 1979) which make its application even for simple systems like metallic nickel anything but straightforward. Nevertheless, the above cited review of amorphous magnetism established clearly that this model has of necessity to be used for interpreting the properties of the present alloys.

(ii) To discuss the electronic properties of alloys in general it is necessary to have available a usable and soundly based energy band model of alloy behaviour. The rigid band model which served such a useful purpose for many years has been found to be inadequate in many cases. Furthermore, a description in terms of the coherent potential approximation, local environment effects, etc has so far only been applied in a preliminary way to amorphous alloys (Alben *et al* 1976). Hence, a very simple minded viewpoint is adopted here so as to give at least a semiquantitative interpretation of the data. Alloying with metalloids is envisaged to cause a charge transfer to the iron atoms and the local environment effect is taken into account by relating the width of the energy band of the iron d electrons to the number of nearest-neighbour iron atoms. Finally, the size effect also influences this width.

Although both these difficulties arise together in interpreting the present series of measurements the results of the present analysis seem to have established a more systematic trend on this basis, however imperfect, than in earlier related work. It is hoped that further experimental and theoretical work on these fascinating materials will be engendered thereby.

2. Experimental details and results

The iron alloys were prepared in the amorphous state by rapid quenching and were in the form of ribbons 1–2 mm wide. The *total* metalloid content varied between 12 and 31 at%. Magnetisations at room temperature and below were determined in a vibrating-sample magnetometer to a maximum field of 20 kOe on specimens about 0·5 cm long and about 0·1 cm wide. Results were extrapolated to infinite field using a $1/H^2$ law. Magnetisation, $M(T)$, above room temperature was determined using a force balance made up of a Dupont 951 thermogravimetric recording balance with a Dupont 990 thermal analyser control unit. The furnace was non-inductively wound and fitted with a large permanent magnet to produce a field gradient together with a field of 225 Oe along the length of 1 cm long ribbons. The samples were heated at 20 deg min^{-1}. The Curie temperature, T_c, was determined as the intersection of $M(T)$ with the temperature axis. The magnetisation at 0 K, $M(0)$, was determined by extrapolating to 0 K from 77 K and above on a $T^{3/2}$ scale.

The density ρ of some of the specimens was measured by the buoyancy method by comparing the weight in air to the weight in diethylphthalate (density of 1·1162 g cm^{-3} at 22 C). The density variation of the diethylphthalate with temperature was calculated from that given by $\ln \rho = -0{\cdot}000796\,T + 0{\cdot}12741$ (Rogers *et al*

1965). The samples were cut from ribbons about 1·5 mm wide to give a total sample weight of about 0·22 g. Ten independent density measurements were made on each alloy sample, the results were averaged and the 99% confidence limit of the mean was determined. Because of the large number of strips needed for each specimen, a special wire holder with a tiny cobalt–samarium magnet fastened to one end was used to hold the strips during weighing in the diethylphthalate. These results, and results from the literature, were used to calculate the average volume per atom, $1/\rho_0$, for each alloy using the tetrahedral covalent radii for the metalloids (boron = 0·88; carbon = 0·77; etc) as previously described (Luborsky 1980). For Fe–Si and Fe–P the x-ray data given by Mangin *et al* (1977) and by Logan (1975), respectively, were used to calculate the average volume. These measurements made it possible to estimate the relative size effect $d\ln V/dx$, where V is the atomic volume.

The results of these measurements of magnetisation and T_c were mostly plotted on ternary diagrams and contours of constant magnetisation and constant T_c were drawn (Luborsky *et al* 1979a, b). Values of magnetisation and T_c were then read off these smooth contours at selected values of constant boron. These results are shown in figures 1 and 2 plotted as a function of the *total* metalloid content, x, expressed in at%. Note that for any one of the ternary alloys there is often more than one curve. These different curves correspond to differing results for different boron contents.

The results are complicated but show the following approximate trends.

(i) For Fe–B the decrease in the magnetic moment per iron atom tends to be the least; the slope of the curve giving this decrease at 20%B is roughly 0·011 μ_B per Fe atom per at%B.

(ii) For alloys of Fe–B–X with X = C, Si and Ge the decrease is larger, with a value of this slope at 20% total metalloid content equal to roughly 0·019 μ_B per Fe atom per at% metalloid.

(iii) Finally with X = P the decrease is larger still but there are not enough data to estimate this slope beyond pointing out this trend.

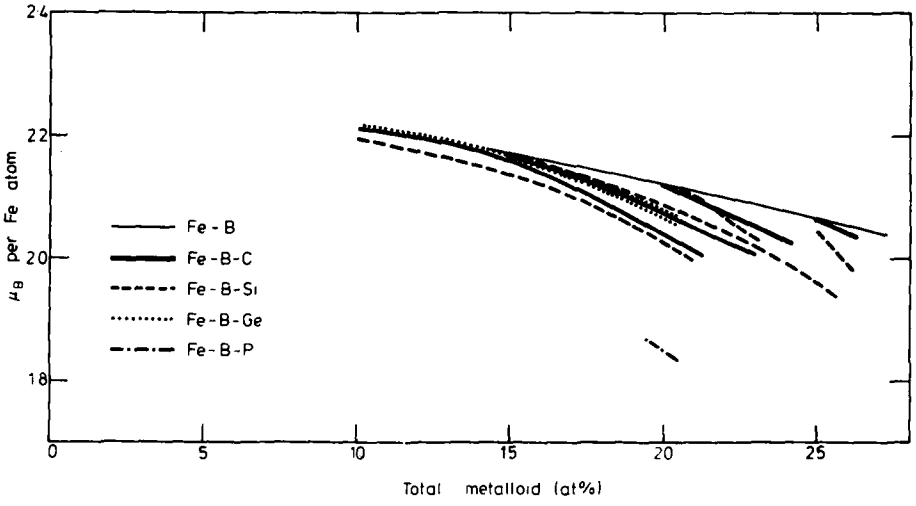

Figure 1. Saturation magnetisation at 0 K in μ_B per Fe atom for amorphous iron alloys, plotted as a function of the total metalloid content x, given in at%.

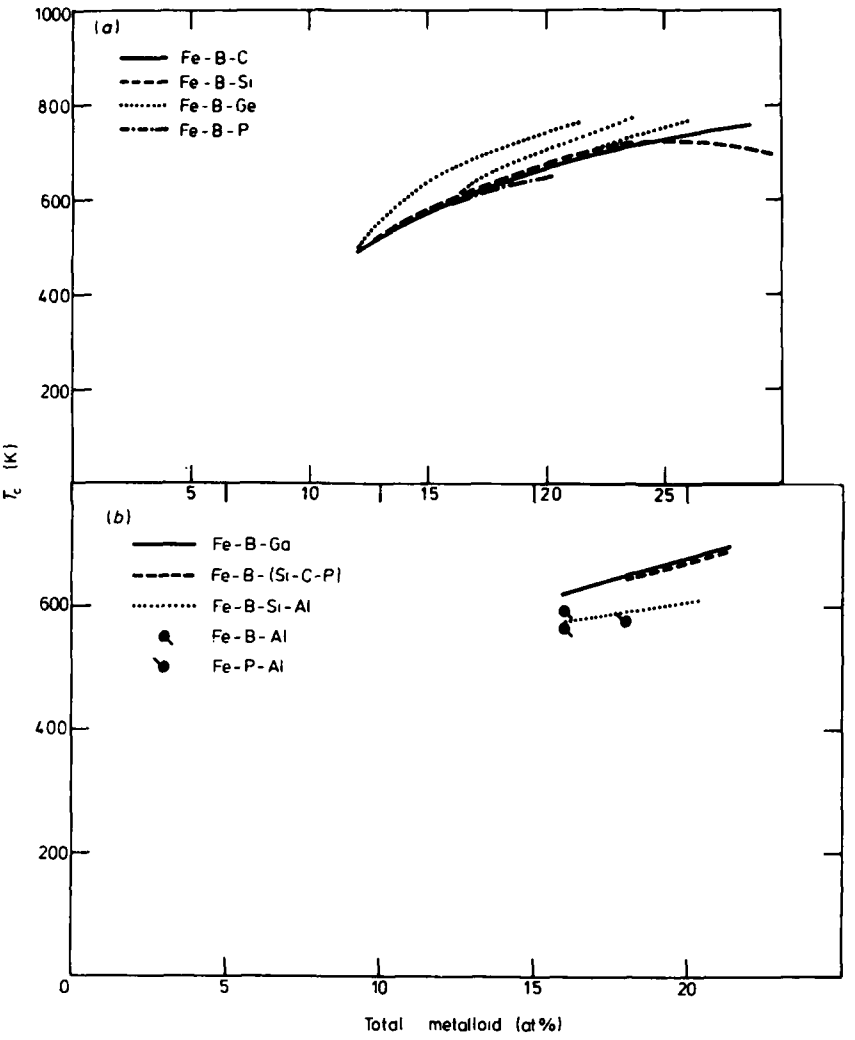

Figure 2. Curie temperature in K for amorphous iron alloys plotted as a function of the total metalloid content x, given in at%.

It means, however, that the sensitivity of the magnetic moment per iron atom to metalloid additions in these amorphous alloys is determined on the whole by just the effective valency n of the added metalloid, defining this from the outer electrons as 1 for B, 2 for C, Si and Ge and 3 for P. This trend thus implies that the magnetisation is determined by the resulting charge transfer from the metalloid to Fe, as had frequently been suggested (Luborsky 1980).

In figure 2 the Curie temperatures are shown, also plotted as a function of the total metalloid content. The trend shown by these data is surprisingly simple and is established here in this clear form for the first time.

(i) With two exceptions, all the data for Fe–B and Fe–B–X, with X singly or in

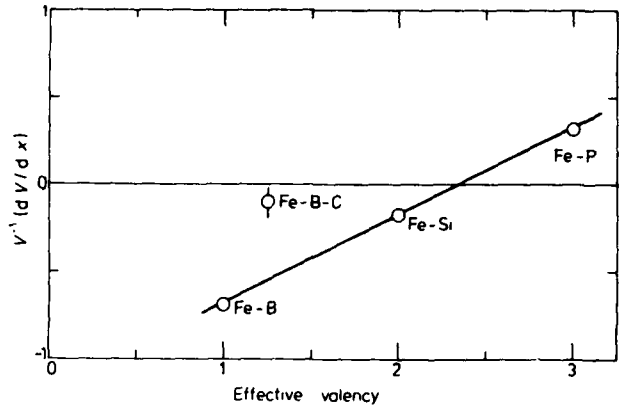

Figure 3. Relative size effect $d\ln V/dx$ as a function of the effective valency n for amorphous iron alloys; x is here fractional.

combination equal to Ga; C, Si; P (in increasing order of effective valency), lie on a single curve, showing pronounced curvature, in the range of metalloid contents 12–25% (above 25% the data for Fe–B–Si deviate downwards from this common curve so as to even pass through a slight maximum). An estimation of T_c for pure 'amorphous iron' is extremely difficult on this basis; a slightly more reliable estimate is given below.

(ii) For Fe–B–Ge the Curie points lie significantly above this common curve.

(iii) For Fe–B–Al they lie significantly below.

The differences between the T_c for the three different aluminium containing alloys is not considered to be significant. These results imply that the Curie temperatures of these amorphous alloys are much less sensitive to charge transfer effects than is the saturation magnetisation. As will be shown now, there is a size effect in these materials which, however, affects neither the saturation magnetisation nor the Curie temperature in any detectably systematic way.

It should be noted that our results do not completely agree with the results obtained by Kazama *et al* (1978). These authors reported that the T_c of Fe–B–C, Fe–B–Si and Fe–B–Ge formed an ordered set with T_c for C < Si < Ge; we report T_c for C ≃ Si < Ge. In addition the results for μ_B per Fe atom were also reported by Kazama to vary with C < Si < Ge. We find, however, that Si < Ge < C. The reasons for these differences are not known; however, the differences between C, Si and Ge are all small.

In figure 3 appears the dependence of the relative size effect $d\ln V/dx$ (x is here fractional) as a function of the effective valency n for Fe–B ($n = 1$), Fe–B–C ($n = 1{\cdot}25$), Fe–Si ($n = 2$) and Fe–P ($n = 3$). The systematic trend shown involving a sign change between $n = 2$ and 3 is here also established for the first time. It is not clear why the Fe–B–C value deviates from the others.

3. Discussion

The discussion adopted here is, for the reasons stated above, no more than semiquantitative. The change of the Curie temperature T_c with composition x is given

by

$$\frac{dT_c}{dx} = \left(\frac{\partial T_c}{\partial x}\right)_V - \left(\frac{\partial T_c}{\partial P}\right)_x \frac{1}{KV}\frac{dV}{dx} + \left(\frac{\partial T_c}{\partial z}\right)_x \frac{dz}{dx}. \tag{1}$$

Here the first term gives the change in T_c with metalloid content at constant volume, arising from the charge transfer which, as described above, affects the saturation magnetisation. The second term gives the influence on T_c of the size effect $d\ln V/dx$. It is convenient to introduce here the concept of the pressure dependence of T_c through the compressibility $K = -d\ln V/dP$ since this establishes a relation with (i) the Invar properties of amorphous ferromagnets (Wohlfarth 1978a), (ii) the influence of carbon on T_c of crystalline Fe–Ni Invar alloys which was also discussed in terms of a pressure effect (Cadeville and Wohlfarth 1974). In these analyses account was taken of the change in W, the width of the iron d band, with the atomic volume which can be changed by pressure or by carbon or other additions. The variation normally adopted is $W \sim V^{-5.3}$ (Heine 1967). In calculating T_c as a function of W a formula given by Kanamori (1963) is normally used which gives the intra-atomic interaction I between the electrons in terms of W and the assumption is made that the density of states at the Fermi energy scales inversely as W when this is varied as here. A fuller review of the pressure phenomena is given, for example, by Kortekaas and Franse (1976) which leads to the relationship

$$(\partial T_c/\partial P)_x = \tfrac{5}{3}K\,[T_c - \tfrac{1}{2}(I/I_b)\,(T_F^2/T_c)] \tag{2}$$

where I_b is the bare (i.e. Hartree–Fock) interaction used by Kanamori (1963) and T_F the effective degeneracy temperature related to the features of the density-of-states curve at the Fermi energy. As discussed by Wohlfarth (1978a) not much change is expected in these features when contrasting crystalline and amorphous alloys of the present type, so that the established theory of Invar behaviour can be applied here.

The third term in equation (1) relates T_c to the number of nearest-neighbour iron atoms z. This also influences the width of the d band of these atoms since in a very much simplified tight-binding approach

$$W = wz(x)t(x). \tag{3}$$

Here w is a constant, z depends on the metalloid content x in the following simple way (Wohlfarth 1978b)

$$z(x) = z(0)(1 - x)^2 \tag{4}$$

and the hopping integral t varies with x through the volume or pressure effect discussed above. In the paper just quoted the amorphous state was proposed to be characterised by local fluctuations in the magnetisation engendered by those in the concentration and in the interatomic distance. Using equations (3) and (4) and the same analysis as used to derive equation (2) it is easily shown that

$$(dT_c/dx) = A + [2(1 - x) + \tfrac{5}{3}\,d\ln V/dx]\,[\tfrac{1}{2}(I/I_b)(T_F^2/T_c) - T_c] \tag{5}$$

where $A = (\partial T_c/\partial x)_V$ represents the effect on T_c of the charge transfer. Although this formula is very simple it has a considerable physical content and can be used to analyse the present data semiquantitatively.

(i) The magnetisation data shown in figure 1 point to a marked influence of the charge transfer. This seems natural on the basis of any alloy theory as arising from a

shift of the Fermi energy on alloying. However, as shown in figure 2, the Curie temperature data do *not* show any systematic influence of this charge transfer effect, so that the term A in equation (5) must be small. This would follow from a much less direct influence of the shift of the Fermi energy on T_c if the density of states at this energy and the interaction I do not vary very sensitively during this shift. A similar effect was noted by Cadeville and Wohlfarth (1974) for Fe Ni C crystalline alloys.

(ii) For $x = 0{\cdot}2$, for example, the square bracket in equation (5) has the values $1{\cdot}6 - 1{\cdot}1 = 0{\cdot}5$, $1{\cdot}6 - 0{\cdot}2 = 1{\cdot}4$, $1{\cdot}6 - 0{\cdot}3 = 1{\cdot}3$ and $1{\cdot}6 + 0{\cdot}5 = 2{\cdot}1$ for Fe B, Fe-B-C, Fe Si and Fe P, respectively. Hence the influence of the size effect on T_c is only relatively important. As seen in figure 2, the observations, in fact, show a single T_c against x curve except for the Fe-B-Ge and Fe B Al alloys. Neither this surprising coincidence nor the deviations can be fully understood on the present basis, although the size effect on T_c has just been shown to be less than decisive and the charge transfer effect was shown above to be even more unimportant.

(iii) The value of dT_c/dx at $x = 0{\cdot}2$, for example, is about 1400 K per fractional metalloid addition for the common curve shown in figure 2. Using a typical value of $I/I_b = 0{\cdot}5$ this gives for T_f the approximate value 2200 K. This value is very close to those derived from other materials, e.g., on the basis of pressure data for some crystalline rare-earth-cobalt compounds (Wohlfarth 1979a) and is very reasonable (Lipton and Jacobs 1970). With a value of T_f equal to 2200 K the positive term in the second square bracket of equation (5) is only just over twice the negative term. From the theory of Invar behaviour in itinerant electron ferromagnets (Wohlfarth 1979b) this implies that these amorphous alloys are 'almost strong'. This is to be expected, since (i) the saturation magnetisation does not parallel the Curie temperature as shown in figures 1 and 2, (ii) both of these quantities are relatively high. In fact, this specification for amorphous Fe–B alloys was already proposed in this publication (Wohlfarth 1979b).

The data of figure 2 give a marked non-linear variation of T_c with x and this is also given by the relation (5). Not too much reliance can be placed on this agreement, but the implied plot of the *square* of T_c against x does, in fact, give a more nearly linear variation over a broad range of x for the common curve. If this is (dangerously) extrapolated to $x = 0$ it leads to a very rough estimate of T_c for 'amorphous iron' of 140 K. The observed curve is thus in semiquantitative agreement with the formula (5) derived above. On the other hand, the size effect data of figure 3 show a clear correlation between the lattice expansion and the effective valency. This is expected on the basis of the differences between the amorphous structures of FeB, FeSi and FeP as the atom size increases in going along the series.

Fukamichi *et al* (1979) have reported measurements of the Curie temperature of binary Fe–P alloys which are not included in figure 2. The data show strong deviations from the common curve in that T_c varies very little between 13 and 18%P. This additional result must mean that, because of the large change of effective valency (see figure 3) the charge transfer term A in equation (5), small for the other alloys, becomes important when phosphorus is alloyed.

Acknowledgments

We wish to thank W E Rollins for preparing the samples, N A Marotta for measuring the Curie temperatures and J J Becker and H Patchen (under the direction of

I S Jacobs) for measuring the magnetisation. E P Wohlfarth is grateful to the General Electric Company for the award of a Visiting Fellowship. The partial support of the Office of Naval Research is also gratefully acknowledged.

References

Allen R C, Budnick J I and Cargill G S III 1976 *Metallic Glasses* ed H J Leamy and J Gilman (Metals Park, Ohio: American Soc. Metals) chap 12
Cadeville M C and Wohlfarth E P 1974 *Phys. Stat. Solidi* a **26** K157
Edwards D M 1980 *J. Magn. Magn. Mater.* to be published
Fukamichi K, Masumoto T and Kikuchi M 1979 *IEEE Trans. Mag.* **15** 1404
Heine V 1967 *Phys. Rev.* **153** 673
Kanamori J 1963 *Prog. Theor. Phys.* **30** 275
Kazama N S, Mitera M and Masumoto T 1978 *Rapidly Quenched Metals III* vol 2 (London: The Metals Society) p 164
Kortekaas T F M and Franse J J M 1976 *J. Phys. F: Metal Phys.* **6** 1161
Lipton D and Jacobs R L 1970 *J. Phys. C: Solid St. Phys., Metal Phys. Suppl.* **3** 389
Logan J 1975 *Phys. Stat. Solidi* a **32** 361
Luborsky F E 1980 *Ferromagnetic Materials* vol 1 (Amsterdam: North-Holland) to be published
Luborsky F E, Becker J J, Walter J L and Liebermann H H 1979a *IEEE Trans. Mag.* **15** 1146
Luborsky F E, Becker J J, Walter J L and Martin D L 1979b *IEEE Trans. Mag.* **15** to appear
Mangin Ph, Marchal G, Rodmacq B and Janot C 1977 *Phil. Mag.* **36** 643
Mitera M, Naka M, Masumoto T, Kazama N and Watanabe K 1978 *Phys. Stat. Solidi* a **49** K163
Rogers H C, Leech R C and Coffin L F 1965 *Naval Air Systems Command Final Report, Contract* NOw-65-0097-f
Wohlfarth E P 1978a *IEEE Trans. Mag.* **14** 933
1978b *Phys. Lett.* **69A** 222
1979a *J. Phys. F: Metal Phys.* **9** L123
1979b *J. Magn. Magn. Mater.* **10** 120

Journal of Magnetism and Magnetic Materials 19 (1980) 130–137

SESSION 4: AMORPHOUS MATERIALS

AMORPHOUS MATERIALS – A NEW CLASS OF SOFT MAGNETIC ALLOYS

F.E. LUBORSKY, P.G. FRISCHMANN and L.A. JOHNSON
General Electric Corporate Research and Development Schenectady, NY 12301, USA

The key events in the development of amorphous alloys are briefly summarized within the context of applying them as soft magnetic alloys. Some of their pertinent magnetic properties, such as saturation magnetization, losses, exciting current, permeability and stress sensitivity are reviewed and compared with conventional alloys. New results on iron-rich alloys will be presented. We have recently discovered that increasing the diameter of the toroid prepared from narrow tapes produces a remarkable improvement in the magnetic properties attributable to the decreasing contribution of stress induced ordering. The losses become significantly less than the best results reported for the Permalloys and are much less than 1/10 the losses of Fe–3.2% Si.

1. Introduction

In the first papers [1,2] on the potential application of amorphous alloys as soft magnetic materials attention was directed mainly towards their static magnetic properties such as coercivity, H_c, remanence, B_r, saturation magnetization, $4\pi M_s$, Curie temperature, T_c, and the effect of annealing and stress on these properties. In later papers [3–9] losses and permeabilities were discussed in the general context of potential applications. Various devices were studied and their requirements were reviewed [5–9]. In this paper we will review briefly the material properties of importance to various classes of devices and then discuss recent results aimed at developing the understanding of the relation between these device-oriented parameters and fundamental parameters.

2. Comparisons of material properties

In electronic type applications, where various nickel–iron alloys are presently used, available amorphous alloys have lower losses, higher B_r and $4\pi M_s$ and equivalent or lower H_c values. However, amorphous alloys tend to have lower T_c, lower magnetic stability, lower initial permeabilities and higher stress sensitivities.

In power devices, such as in large distribution transformers, where Fe–3$\frac{1}{4}$% Si is presently used, the amorphous alloys have considerably lower losses, lower H_c and higher permeabilities. However, the $4\pi M_s$ is lower than Fe–Si by about 15%. This is considered to be a major drawback, adding to the overall cost of the final transformer.

3. Saturation magnetization

In recent years there has been a considerable effort [10–20] directed towards exploring methods of raising $4\pi M_s$ of low cost amorphous alloys. This has taken the direction, of necessity, towards trying to modify the basic Fe–B amorphous alloy by replacing some of the B with other metalloids and by annealing. Additions of Co or Ni are considered to be too costly. It has been claimed [14] that replacement of boron by carbon to make $Fe_{86}B_7C_7$ raises $4\pi M_s$ from 16.1 kG for the $Fe_{81}B_{19}$, which is the peak value in the Fe–B alloys, to 17.4 kG. This is further raised to 17.8 kG by annealing at 270°C for approximately 2 h. However, these reported values depend on the density used and the densities reported by Hatta et al. [14] are higher by about 3% than the densities reported by Luborsky et al. [17]. The ternary corner of the Fe–B–C diagram for iso-magnetization curves measured at room temperature in emu g^{-1} is shown in fig. 1 [17]. By measuring the $4\pi M_s$ in emu g^{-1} the problem with measuring the density to convert to Gauss is avoided. These curves show that a ridge of

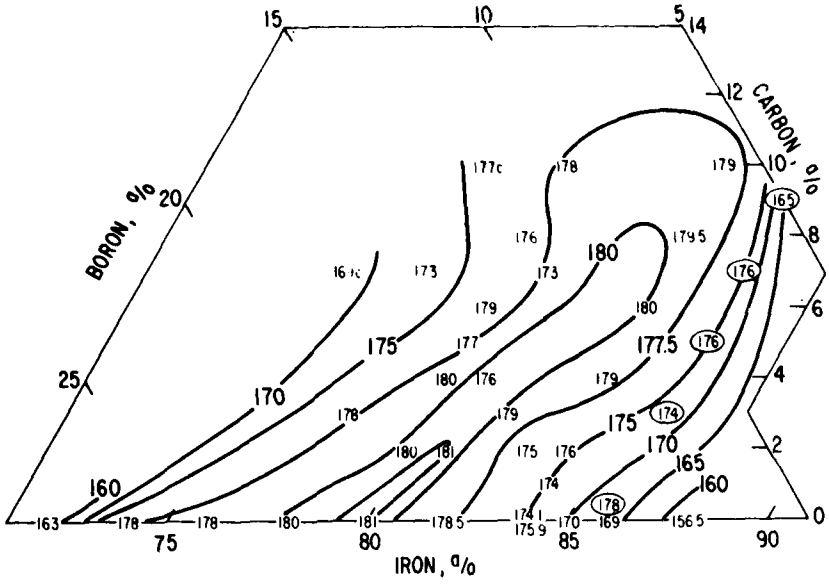

Fig. 1. Saturation magnetizations in emu g^{-1} at room temperature in the ternary Fe–B–C amorphous alloys.

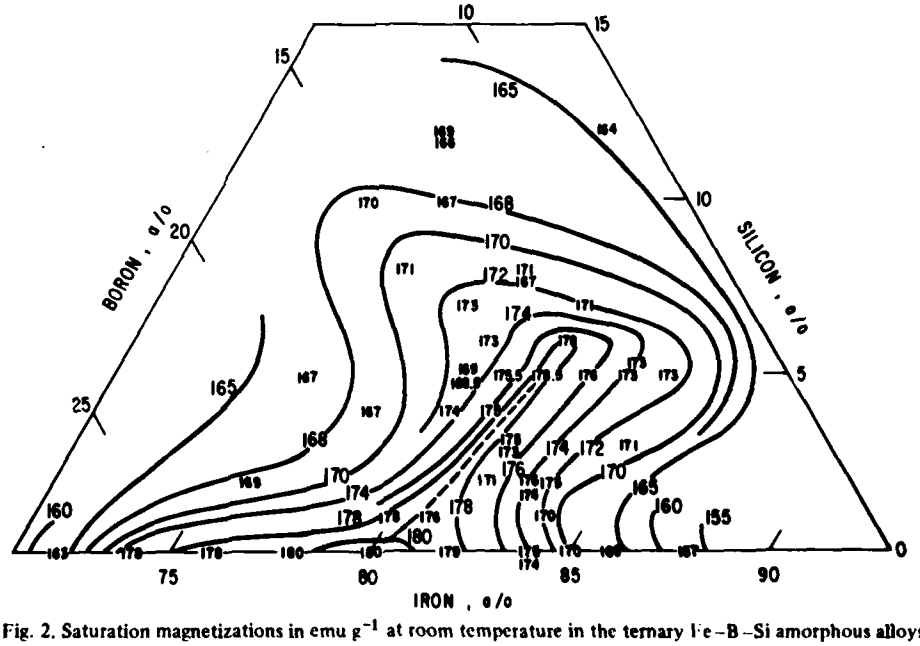

Fig. 2. Saturation magnetizations in emu g^{-1} at room temperature in the ternary Fe–B–Si amorphous alloys.

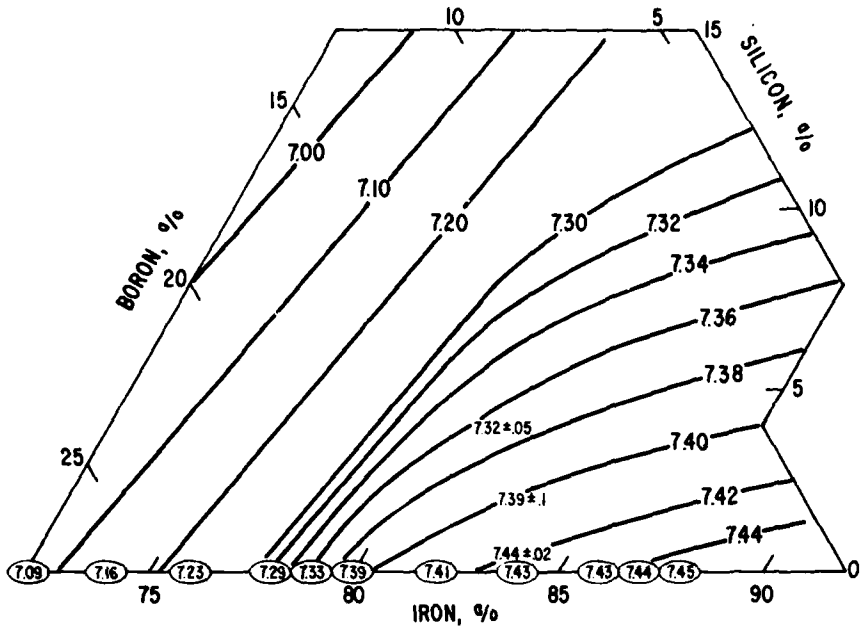

Fig. 3. Density in g cm^{-3} at room temperature in the ternary Fe–B–Si amorphous alloys. Curves calculated. Circled numbers from Hasegawa and Ray, J. Appl. Phys. 49 (1978) 4174. Small numbers measured by Martin, unpublished.

constant $4\pi M_s$ in emu g^{-1} extends out from $Fe_{80}B_{20}$ to $Fe_{83}B_9C_8$. Since the density increases from 7.38_5 to 7.51_5 g cm^{-3} [17], about 1.8%, this means that $4\pi M_s$ in Gauss measured at room temperature increases by about 1.8% also, or from 16.1 kG to 16.4 kG. Similar iso-magnetization curves have also been generated for the Fe–B–Si alloys as shown in fig. 2 [15]. The ridge of constant $4\pi M_s$ in this case is much narrower than for the Fe–B–C alloys and extends from $Fe_{80}B_{20}$ to only $Fe_{82}B_{12}Si_6$. The densities for the Fe–B–Si alloys have not been reported before. They are calculated here as described previously [17] and compared with a few measured values as shown in fig. 3. The agreement between calculated and measured values, as also observed for the Fe–B–C alloys, is excellent. Thus, the density decreases in going from $Fe_{80}B_{20}$ to $Fe_{83}B_{12}Si_6$, i.e., from 16.1–16.0 kG. More recently we have been examining the properties of Fe–B–Si–C alloys and have found the T_c, M_s and H_c behavior to be more or less additive functions of the individual Fe–B–Si and Fe–B–C parameters. However, the ease of preparation and the resultant stability of the quaternary alloys appears to be better than for either of the constituent ternary alloys.

Preliminary results on Fe–B–Ge ternary amorphous alloys indicate that replacement of B by Ge indeed raises T_c considerably as previously reported [21,22] and that σ_s at room temperature has a similar ridge of constant value. However, the density increases from 7.38_5 to 7.7 or 4% corresponding to an increase in room temperature $4\pi M_s$ from 16.1–16.7 kG, before annealing, compared with 16.4 in the Fe–B–C system.

The effect of elevated temperatures must also be considered since most transformers operate at temperatures as high as 100°C. In the case of Fe–Si because its T_c is so high (~755°C), $4\pi M_s$ is virtually unchanged at 100°C from its value at 25°C. However, the amorphous alloys with their relatively low T_c (~370°C) are found to have a reduction of $4\pi M_s$ equal to 6% for $Fe_{81.5}B_{13.5}C_5$ and equal to 7% for $Fe_{81.5}B_{13.5}Si_5$. In the case of Fe–B–Ge alloys T_c is increased substantially and thus the effect of temperature should be smaller.

4. Losses

A major improvement in losses was reported [23] recently resulting from studies on the effect of strain-induced anisotropy as a result of the winding stresses introduced in toroids. It was found, for example, that in narrow amorphous alloy tapes the properties improved remarkably as the diameter of the toroid increased. Thus, a 20 cm diameter toroid had roughly $\frac{1}{10}$ the losses of a 1.4 cm diameter toroid. These losses represent the lowest losses at 60 Hz of any alloy so far reported. In fig. 4 these losses are compared with losses of all the other amorphous alloys reported so far, from zero magnetostrictive alloys, given by the dotted curve labelled 0, to the high magnetization alloys labelled E, all measured on small diameter toroids. Other alloys reported [3] have losses which all fall between 0 and E as indicated by the cross hatched area. The losses of the commercially available Fe–B–Si–C amorphous alloy (METGLAS^R 2605SC) are indicated by the curve labelled L. Also, for comparison, shown in fig. 4, are results on various grades of Fe–3.2% Si alloys. The thin tapes, 25–100 μm thick, are used in small electronic devices and have poor losses because of the poor orientation developed in these thicknesses. The 280–355 μm thick Fe–Si have good orientation and, up until the past few years, were used exclusively in high quality distribution and power transformers as well as in other specialized devices. The newer Hi-B variety, originally developed in Japan [24] achieves even lower losses by improved grain orientation, improved tension effect of the coating, reduced sheet thickness and grain size and by reduction in inclusions and internal stresses. These Hi-B alloys are now being used in modern high quality distribution and power transformers.

The new results on losses of the 20 cm diameter toroid are now less than the losses reported for any of the best commercial Ni–Fe alloys. These results are compared at 50 kHz, in fig. 5, with previous results on high magnetization $Fe_{80}B_{20}$ and also with commercially available Fe–B–Si–C (METGLAS^R

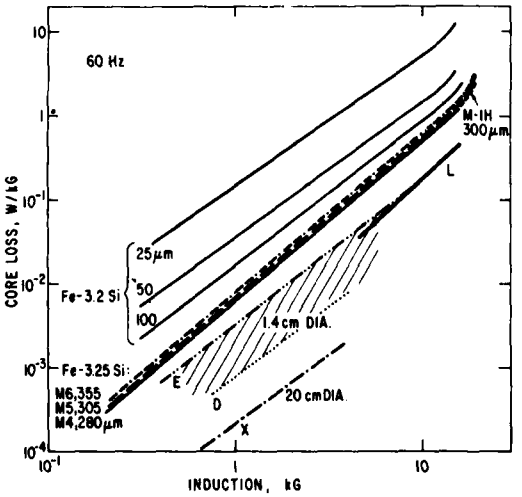

Fig. 4. Core losses versus induction for Fe–3¼% Si alloys and for amorphous alloys all measured at 60 Hz. The 25, 50 and 100 μm Fe–Si tapes from Arnold Bulletin 5C-107A, March 1963. M4, M5, M6, Fe–Si sheet from Armco Catalog, 1974. M-1H Fe–Si from Nippon Steel Cat. EXE 320, 1976. E = $Fe_{80}B_{20}$ 1.4 cm diameter narrow tape [3]; cross-hatched area enclosed all other curves for amorphous alloys [3]; X = $Fe_{83}B_{15}Si_2$ 20 cm diameter narrow tape [23]; L = $Fe_{81}B_{13.5}Si_{3.5}C_2$ METGLAS^R 2605SC from Allied Chem. Co. Bulletin 6/79.

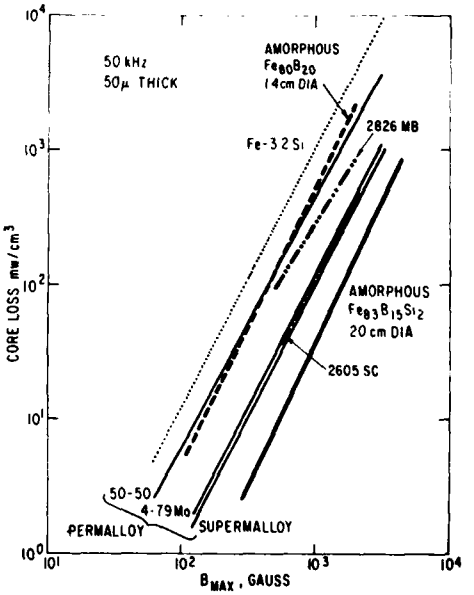

Fig. 5. Core losses versus induction measured at 50 kHz for 50 μm thick Permalloys and 30 μm thick amorphous $Fe_{83}B_{15}Si_2$ of narrow ribbon measured as a 20 cm diameter toroid [23]. $Fe_{80}B_{20}$ from [3], METGLAS^R 2605SC and 2826 MB from Allied Chem. Co. Bulletin 6/79.

2605SC). This improvement in losses for the 20 cm diameter toroid holds at all frequencies. Thus, as far as losses are concerned, the amorphous alloys are clearly better than any of the best commercial alloys. Furthermore, they have the considerably higher $4\pi M_s$ of 16 kG compared with 8 kG for 4–79 Mo Permalloy and Supermalloy and have the same 16 kG as the 50–50 Permalloy but are lower than the 20 kG of the Fe–3.2% Si.

5. Permeability

The permeabilities at ΔB = 100 G, i.e., near the initial permeability range, are shown in fig. 6 for some commercial Fe–Si and Ni–Fe alloys and for some amorphous alloys. The cross-hatched area corresponds to the range of results previously reported [3] for amorphous alloys from zero magnetostriction, with the highest μ_z, to high magnetization $Fe_{80}B_{20}$ alloys with lower μ_z. The new results on the 20 cm diameter toroid and some results from Allied Chemical Company data sheets for their Fe–B–Si–C alloy (METGLAS^R 2605SC) are also shown. The permeability at 60 Hz of 30 000 for METGLAS^R 2826MB is probably among the highest yet reported for amorphous alloys except for zero magnetostrictive alloys [25]. However, these values are still considerably below the 4–79 Mo–Permalloy and the

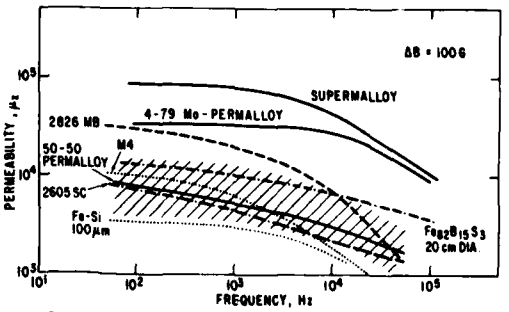

Fig. 6. Impedance permeability measured at ΔB = 100 G versus frequency for various Permalloys from Arnold Cat. TC-101B, 1972; Fe–3½% Si grade M4 305 μm thick from Armco Cat. 1974; METGLAS^R 2605SC and 2826MB amorphous alloys from Allied Chem. Co. Bulletin 6/79; and $Fe_{82}B_{15}Si_3$ amorphous alloy 20 cm diameter toroid from narrow tape [23].

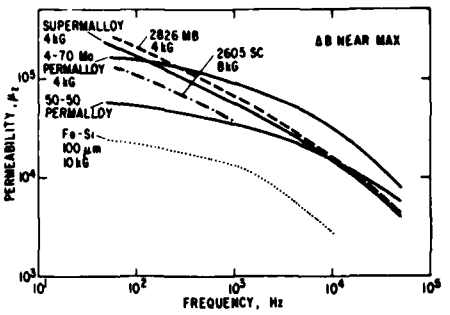

Fig. 7. Impedance permeability measured near its peak value as a function of frequency for various Permalloys and Fe–Si thin tape from Magnetic Metals Cat. C1-171-20M and for METGLAS^R alloys from Allied Chem. Co. Bulletin 6/79.

Supermalloy. It is not clear why higher values of μ_z have not yet been achieved.

In fig. 7 are shown results which are similar to the results in fig. 6 but for permeabilities near their maximum value. A similar sequence is shown but with the amorphous alloys reaching higher values of μ_z (max) than for the corresponding Permalloy, i.e., METGLAS^R 2826MB should be compared with Supermalloy and 4–79 Mo–Permalloy of similar $4\pi M_s$ and METGLAS^R 2605SC should be compared with to 50–50 Permalloy also of similar $4\pi M_s$. It is believed that the more rapid fall-off with frequency for the amorphous alloys compared with the Permalloys is the result of their rougher surface. Values of μ(max) for dc fields of greater than 2×10^6 have been reported [26] for various $(Fe_{1-x}Ni_x)$–Si–B alloys. This is well above any of the values expected from fig. 7 at low frequencies.

6. Excitation power

Very little has been reported on the very important parameter in amorphous alloys of excitation power for evaluating distribution transformer performance. This was first reported in 1978 [6] for small 1.4 cm diameter toroids of $Fe_{80}B_{20}$ and $Fe_{40}Ni_{40}P_{14}B_6$. New results are reported in fig. 8 from our own measurements and from the Allied Chemical Company compared with results on Fe–Si. The amorphous alloys are clearly superior to 50 μm Fe–Si tapes. We can compare the amorphous alloys to Hi-B or M-4

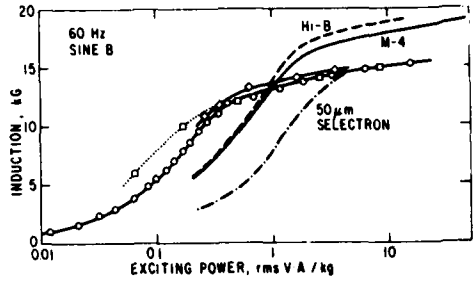

Fig. 8. Induction versus exciting power measured at 60 Hz for various Fe–3¼% Si alloys, M4 280 μm thick from Armco Cat. 1974, Hi-B 300 μm thick from Nippon Steel Corp. Cat. EXE 320, 1975; Selectron from Arnold Bulletin SC-107A 1963; □ METGLAS^R 2605SC amorphous alloy from Allied Chem. Co. bulletin 6/79; ◇ METGLAS^R 2605SC amorphous alloy toroid prepared in this work with 13.9 cm outside diameter 7.9 cm inside diameter and 2.5 cm height unbonded, ○ the same core after impregnation bonding.

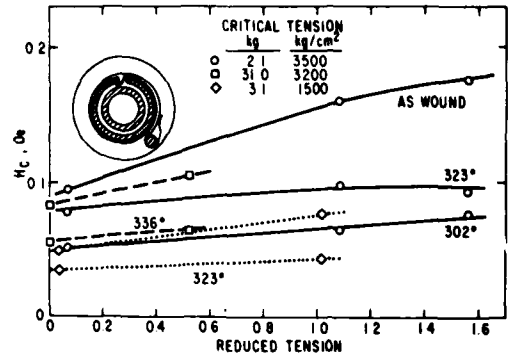

Fig. 9. Coercivity of toroids wound under tension. The reduced tension is the ratio of the winding tension to the critical tension required to reduce the maximum compressive stress to zero. Open symbols as-wound, solid and crossed symbols after 2 h anneal in a circumferential field at the temperature indicated. ○ $Fe_{82}B_{15}Si_3$, 2 mm wide; ○ METGLAS^R 2605B, 2.5 cm wide; ◇ $Fe_{81.5}B_{14.5}Si_4$, 1 cm wide.

Fe–Si in different ways. First, the induction developed at the same exciting power occurs at 1 VA kG^{-1} and gives B = 13.5 kG. Secondly, by comparing the B achieved at the knee of each curve. For amorphous alloys the knee occurs at ~0.45 VA kG^{-1} compared with ~1.5 VA kG^{-1}, i.e., a factor of three smaller, but $B \simeq$12.5 kG compared with 17 kG, i.e., ≃25% lower than the Fe–Si. We may also compare the ratio of the value of B at the knee with the value of B at saturation. For amorphous alloys this ratio is 12.6/16.1 = 0.78 while the value for Fe–Si is 17.0/20 = 0.85. Thus, we expect some further improvements in the amorphous alloys.

7. Stress sensitivity

In the oriented Fe–Si alloys any anisotropy caused by stress must compete with the rather large crystal anisotropy of 3.5×10^5 erg cm^{-3}. In the iron-rich stress-relieved amorphous alloys the only anisotropy present is probably a field-induced anisotropy which may be of the order of 1×10^3 erg cm^{-3} [27]. Thus, even for alloys with the same magnetostriction, and the oriented Fe–Si and amorphous Fe–B–Si have similar magnetostrictions, the effect of a given stress will be much larger on the amorphous alloy. Furthermore, the application of a coating which imparts a stress to the Fe–Si reduces the effective magnetostriction. Such coatings have not as yet been developed for the amorphous alloys.

There have been various reports on the effect of tensile stresses on the properties of amorphous alloys [1,23]. These tensile stresses interact with the positive magnetostriction to decrease H_c and increase B_H/B_s. On winding a toroid it is desirable to wind with high tension to increase the packing fraction. It was first thought that this high tension in the toroid would indeed enhance the properties as was observed on applying tension to straight ribbons. However, just the reverse was observed [23] as indicated by the increase in H_c shown in fig. 9 on winding toroids. A similar decrease in B_H/B_S was also reported. This deterioration was demonstrated [23] to be due to the simultaneous application of face pressure which develops as tension is applied during winding the toroid. We now report, in fig. 10, on the effect of applying only face pressure to the amorphous alloy. Face pressure was developed by applying a static load on the face of a stack of about 75 rings chemically etched out of 2.5 cm wide tape. The load was applied between three segments of windings onto a thick glass ring to distribute the load evenly. The windings were connected to a standard hysteresigraph. The face stress sensitivity of the as-cast rings, both in B and in H_c, are much less than after annealing in a field with a 4 kG cm^{-2} load and both of these show much less stress sensitivity than the rings annealed in a field but

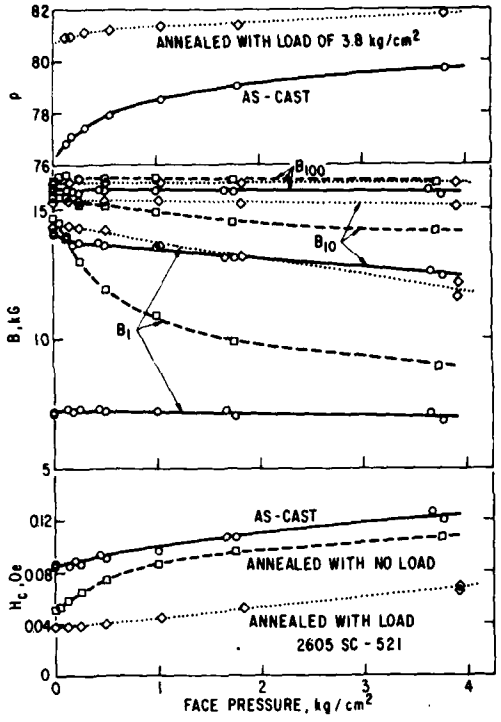

Fig. 10. The effect of face pressure on magnetic properties and packing fraction of rings before and after annealing of METGLAS^{R} 2605SC.

with no load. This is the sequence expected since the as-cast samples have the highest anisotropy and the samples annealed with no load have the lowest anisotropy. The application of face pressure will produce a random planar contribution to the easy axis which in the case of the annealed specimen, for example, does not change the easy axis–planar anisotropy although there will be a change in the out-of-plane anisotropy. Thus, there should be no change in the magnetization curve. This view, of course, ignores the possible effects of frictional constraints on the ideal expansion of the compressed ring samples which could contribute to a compressive stress component along the ribbon length. This could contribute to the observed behavior. Furthermore, surface irregularities not only will cause stress enhancement, but would yield stress components in various unwanted directions.

Using the same fixture the packing fraction was measured as a function of face pressure by noting the compression of the stack of rings. The results are also shown in fig. 10. The large dependence of packing on pressure for the as-cast rings is expected due to the random variations in flatness exhibited by the rings. Annealing with a load, of course, flattened and compressed the stack, resulting in higher packing and less dependence of packing on pressure.

8. Summary and conclusions

In the past year or two the saturation magnetization has been increased from 16 kG to approximately 17 kG by substituting some boron by carbon. Further improvements may occur by substituting with germanium. Losses have also improved substantially now achieving levels well below the best Permalloys, but the permeabilities reported have only increased a small amount. More attention must now be paid to the exciting power required to reach various induction values. Finally, the extreme stress sensitivity of the amorphous alloys must be considered in fabricating and using these alloys.

Acknowledgement

The authors wish to thank the Office of Naval Research for their support.

References

[1] T. Egami, P.J. Flanders and C.D. Graham, Jr., AIP Conf. Proc. No. 24 (1975) 697.
[2] E.M. Gyorgy, H.J. Leamy, R.C. Sherwood and H.S. Chen, AIP Conf. Proc. No. 29 (1976) 198.
[3] F.E. Luborsky, in: Amorphous Magnetism II, eds, R.A. Levy and R. Hasegawa (Plenum Press, New York, 1977) p. 345.
[4] F.E. Luborsky, P.G. Frischmann and L.A. Johnson, J. Magn. Magn. Mat. 8 (1978) 318.
[5] F.E. Luborsky, J.J. Becker, P.G. Frischmann and L.A. Johnson, J. Appl. Phys. 49 (1978) 1769.
[6] F.E. Luborsky, IEEE Trans. Magnetics 14 (1978) 1008.
[7] K.J. Overshott, Electron. Power Mag. (1979) 347.
[8] R. Hasegawa and R.C. O'Handley, J. Appl. Phys. 50 (1979) 1551.
[9] W. Wolf, R. Mohs and U. König, J. Magn. Magn. Mat. 19 (1980) 177.

[10] K. Hoselitz, in: Rapidly Quenched Metals III, Vol. 2, ed. B. Cantor (The Metals Soc., London, 1978) p. 245.
[11] S. Hatta, T. Egami and C.D. Graham, Jr., in: Rapidly Quenched Metals III, Vol 2, ed. B. Cantor (The Metals Soc., London, 1978) p. 183.
[12] F.E. Luborsky, J.J. Becker and H.H. Liebermann, in: Rapidly Quenched Metals III, Vol. 2, ed. B. Cantor (The Metals Soc., London, 1978) p. 249.
[13] S. Hatta, T. Egami and C.D. Graham, Jr., IEEE Trans. Magnetics 14 (1978) 1013.
[14] S. Hatta, T. Egami and C.D. Graham, Jr., Appl. Phys. Lett. 34 (1979) 113.
[15] F.E. Luborsky, J.J. Becker, J.L. Walter and H.H. Liebermann, IEEE Trans. Magnetics 15 (1979) 1146.
[16] R.C. O'Handley, C.-P. Chou and N. DeCristofaro, J. Appl. Phys., to be published.
[17] F.E. Luborsky, J.J. Becker, J.L. Walter and D.L. Martin, IEEE Trans. Magnetics 15 (1979).
[18] M. Mitera, T. Masumoto and N.S. Kazama, J. Appl. Phys. 50 (1979) 7609.
[19] K. Hoselitz, Phys. Stat. Sol. (a)53 (1979) K23.
[20] K. Hoselitz, J. Mag. Mag. Mat. 20 (1980) to be published.
[21] M. Mitera, M. Naka, T. Masumoto, N. Kazama and K. Watanabe, Phys. Stat. Sol. (a)49 (1978) K163.
[22] N.S. Kazama, M. Mitera and T. Masumoto, in: Rapidly Quenched Metals III, Vol. 2 ed. B. Cantor (The Metals Soc., London, 1978) p. 164.
[23] F.E. Luborsky and J.J. Becker, IEEE Trans. Magnetics 15 (1979).
[24] S. Taguchi, Trans. ISIJ 17 (1977) 604.
[25] S. Ohnuma and T. Masumoto, in: Rapidly Quenched Metals III, ed. B. Cantor Vol. 2 (The Metals Soc., London, 1978) p. 197.
[26] T. Masumoto, K. Watanabe, M. Mitera and S. Ohnuma, in: Amorphous Magnetism II, eds. R.A. Levy and R. Hasegawa (Plenum Press, New York, 1977) p. 369.
[27] F.E. Luborsky and J.L. Walter, IEEE Trans. Magnetics 13 (1977) 953.

Preparation and Properties of Fe-B-Si-C Amorphous Alloys

FRED E. LUBORSKY, FELLOW, IEEE, AND JOHN L. WALTER

Abstract—The crystallization temperatures, magnetic properties, and density of amorphous alloys of $Fe_xB_ySi_zC_z$ are reported for $72 < x < 88$, $16 < y < 28$, and $0 < 2z < 12$. The peak value of $4\pi M_s$ is 17 kG in the as-cast state and occurs in the region of $Fe_{82}B_{13}Si_{2.5}C_{2.5}$. The crystallization temperatures, Curie temperatures, saturation magnetization, and density all appear to be average values of the ternary Fe-B-Si and Fe-B-C properties.

INTRODUCTION

THIS WORK represents a report on our continuing effort to explore the effect of various metalloids on the crystallization temperature, Curie temperature, and saturation magnetization of iron-metalloid amorphous alloys. In previous papers [1]-[5] we reported on the preparation and properties of Fe-B, Fe-B-Si, and Fe-B-C amorphous alloys. In particular, we were looking for the maximum obtainable saturation magnetization. Table I gives a summary of these maximum values in each alloy system studied. In the as-cast condition $\sigma_s = 180 \pm 2$ emu/g and $4\pi M_s = 16.85 \pm 0.35$ kG for all alloy systems, with Fe-B-C and Fe-B-Si-C being the highest. Until now only the binary Fe-B and various ternary alloys have been reported. In this paper we report on the properties of amorphous alloys of $Fe_xB_ySi_zC_z$.

Manuscript received December 5, 1979; revised January 25, 1980. This work was supported in part by the Office of Naval Research.

The authors are with the General Electric Corporate Research and Development Center, Schenectady, NY 12301.

EXPERIMENTAL

Amorphous ribbons were prepared [6], [7] by melt quenching onto the surface of a rotating wheel. We determined Curie temperatures T_c using a thermogravimetric recording balance fitted with a permanent magnet to produce a field gradient in a field of 225 Oe. Samples were heated at 20°C/min. The saturation magnetizations σ_s were determined using a vibrating sample magnetometer at fields up to 20 kOe on samples about 5-mm long. Results were extrapolated to infinite field using a $1/H^2$ function. We calculated the densities d as described

0018-9464/80/0700-0572$00.75

TABLE I
MAXIMUM SATURATION MAGNETIZATION OBTAINED IN VARIOUS AMORPHOUS ALLOY SYSTEMS

Alloy System	Maximum Saturation Magnetization at Room Temperature: as-cast σ_s emu/g	as-cast $4\pi M_s$ kG	annealed σ_s emu/g	annealed $4\pi M_s$ kG	Reference
Fe-B	180	16.7	184	17.0	[1]
Fe-B-C	180	16.9	184	17.3	[2], [4]
Fe-B-Si	170	16.5	183	16.9	[3]
Fe-B-Ge	179	17.2	183	17.6	[5]
Fe-B-Ga	(178)*	–	–	–	[5]
Fe-B-Si-C	182	17.0	186	17.3	this work

*Value in parenthesis is preliminary.

previously [4], [8], by first calculating the packing fraction versus iron content for the Fe-B alloys using the measured densities of Hasegawa and Ray [9]. Then we calculated the density of the alloy using these packing fractions for each iron content together with the tetrahedral covalent radii of boron (0.88 Å), carbon (0.77 Å), and silicon (1.17 Å). This technique gave excellent agreement with measured densities in the Fe-B-C [4] and the Fe-B-Si [8] amorphous alloys. The density was used to convert σ_s to $4\pi M_s$ using $4\pi M_s = 4\pi\sigma_s d$.

RESULTS AND DISCUSSION

Fig. 1(a) and (b) shows the crystallization temperatures T_x obtained by two different methods. The first method uses the magnetization curve obtained as a function of temperature while heating at 20°C/min. The magnetization M first falls with increase in temperature to $M = 0$ at T_c. When crystallization starts, iron or iron compounds with high values of T_c appear causing an increase in M. The beginning of this increase in M is taken as the beginning of crystallization. In the second method the samples were heated for 2 h at each of a series of increasing temperatures at 25–30°C intervals. At low annealing temperatures the coercivity H_c first decreases due to stress relaxation. With the appearance of crystalline iron or iron compounds H_c increases drastically. The beginning of this increase in H_c is taken as the beginning of crystallization. It is clear that T_x for the 2-h anneals at constant temperature is much lower than T_x for the 20°C/min anneals, as expected. However, the shapes of the contours of constant T_x are similar. These contours correspond roughly to the average of the values of the contours for Fe-B-C [4] and Fe-B-Si [3] alloys. There does not appear to be any enhancement of thermal stability by the addition of the fourth atom, although in many cases it has been found [10] that the addition of more elements to an amorphous alloy improves the thermal stability.

Fig. 2 shows the Curie temperatures for the $Fe_xB_ySi_zC_z$ amorphous alloys. There was almost no difference in T_c between Fe-B-C [4] and Fe-B-Si [3] alloys, and thus there is no essential difference between the T_c of the Fe-B-Si-C alloys and the Fe-B-Si or Fe-B-C alloys.

Fig. 3(a) shows the saturation magnetization measured at room temperature, and Fig. 3(b) shows σ_s measured at 100°C.

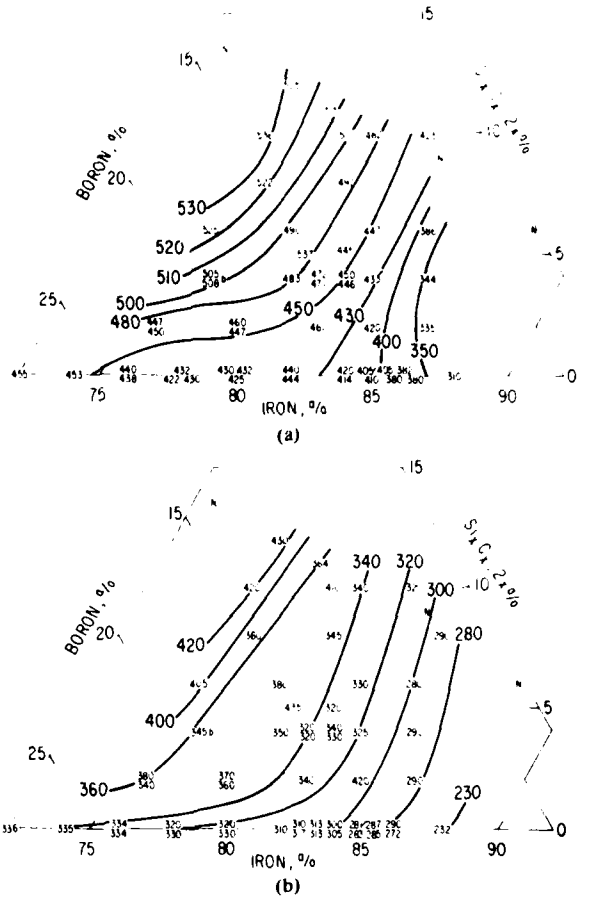

Fig. 1. The temperature in °C for the initiation of crystallization of Fe-B-Si-C amorphous alloys as determined from (a) magnetization measurements using a heating rate of 20°C/min and from (b) coercivity measurements using 2-h sequential anneals. "*b*" indicates a slightly brittle sample. "*N*" indicates the alloy could not be cast into ribbon.

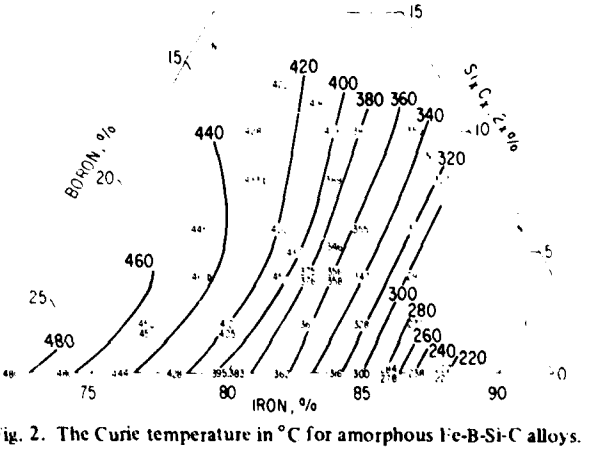

Fig. 2. The Curie temperature in °C for amorphous Fe-B-Si-C alloys.

As expected these results are also essentially the average of the values for Fe-B-C [4] and Fe-B-Si [3]. As in the case of the individual ternary alloys, a ridge of roughly constant σ_s at room temperatures extends out from approximately $Fe_{80}B_{20}$

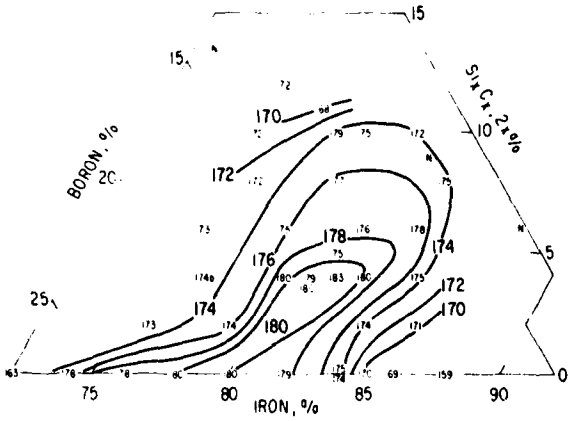

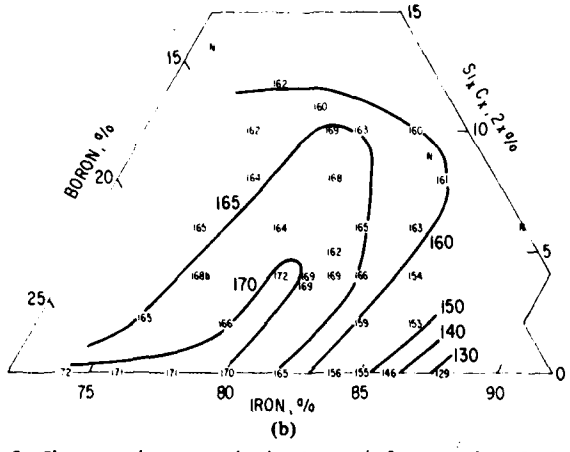

Fig. 3. The saturation magnetization in emu/g for amorphous Fe-B-Si-C alloys measured at (a) room temperature and at (b) 100°C.

to $Fe_{82}B_{13}Si_{2.5}C_{2.5}$. This shows a slight peak. In Table I we have compared the maximum value of σ_s obtained along the ridge of the Fe-B-Si-C studied in this work to other maximum values. Note that the maximum values are all within ±1.5 percent of 16.95 kG. In Table I we have also reported the maximum values of σ_s after annealing. These all increase by about two percent as was reported previously [11].

The values of $4\pi M_s$ are of greater practical interest. To obtain these the densities of the quaternary amorphous alloys were calculated as described in the experimental section with the results shown in Fig. 4. These were then combined with the results in Fig. 3(a) to give the $4\pi M_s$ contours shown in Fig. 5. The shapes of the contours are modified slightly showing the peak at approximately $Fe_{82}B_{13}Si_{2.5}C_{2.5}$.

Summary

This paper reports the crystallization temperature, Curie temperature, saturation magnetization, and calculated density for the quaternary Fe-B-Si-C alloys. All properties appear to be simply the average of the properties of the individual ternary Fe-B-C and Fe-B-Si alloys. This includes the stability, although it was expected that the quaternary alloys would be more stable than the ternary alloys. A peak $4\pi M_s$ of 17.0 kG was obtained for $Fe_{82}B_{13}Si_{2.5}C_{2.5}$.

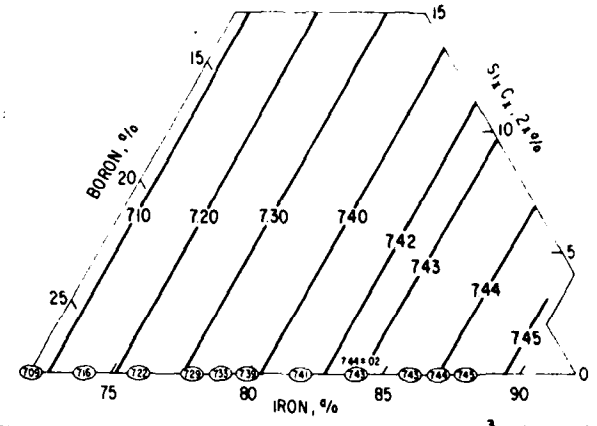

Fig. 4. Densities of Fe-B-Si-C amorphous alloys in g/cm^3 calculated as described in the text. Circled numbers from Hasegawa and Ray [9]. Uncircled numbers from this work.

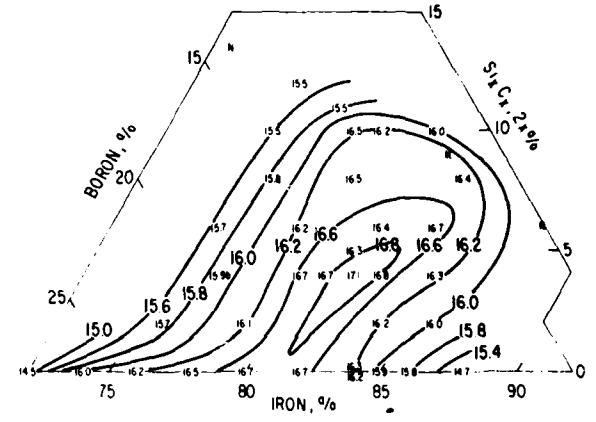

Fig. 5. The saturation magnetization in kG for amorphous Fe-B-Si-C alloys at room temperature, calculated from Figs. 3 and 4.

Acknowledgment

We thank J. Gillespie for his careful magnetic measurements, H. Patchen for his measurements of σ_s, and N. Marotta for her measurements of T_c.

References

[1] F. E. Luborsky, H. H. Liebermann, J. J. Becker, and J. L. Walter, *Rapidly Quenched Metals* III, B. Cantor, Ed. London: The Metals Soc.,1978, vol. 2, p. 188.
[2] F. E. Luborsky, J. J. Becker, and H. H. Liebermann, *Rapidly Quenched Metals III*, B. Cantor, Ed. London: The Metals Soc., 1978, vol. 2, p. 249.
[3] F. E. Luborsky, J. J. Becker, J. L. Walter and H. H. Liebermann, *IEEE Trans. Magn.*, vol. MAG-15, p. 1146, 1979.
[4] F. E. Luborsky, J. J. Becker, J. L. Walter and D. L. Martin, *IEEE Trans. Magn.*, vol. MAG-16, pp. 521-525, May 1980.
[5] F. E. Luborsky, to appear.
[6] H. H. Liebermann and C. D. Graham, Jr., *IEEE Trans. Magn.*, vol. MAG-12, p. 921, 1976.
[7] J. L. Walter, *Rapidly Quenched Metals III*, B. Cantor, Ed. London: The Metals Soc., 1978, vol. 1, p. 30.
[8] F. E. Luborsky, P. G. Frischmann, and L. A. Johnson, *J. Magnetism Magn. Mat.*, to appear.
[9] R. Hasegawa and R. Ray, *J. Appl. Phys.*, vol. 49, p. 4174, 1978.
[10] F. E. Luborsky, *Materials Sci. Eng.*, vol. 28, p. 139, 1977.
[11] S. Hatta, T. Egami, and C. D. Graham, Jr., *IEEE Trans. Magn.*, vol. MAG-14, p. 1013, 1978.

Composition dependence of the Curie temperatures of amorphous alloys

F. E. Luborsky
General Electric Corporate Research and Development, Schenectady, New York 12301

(Received 6 December 1979; accepted for publication 28 January 1980)

The Curie temperatures of 25 amorphous alloy systems involving a binary metal together with metalloids have been fitted to phenomenological equations based on a localized band model involving only one adjustable parameter to describe the variation of Curie temperature with metal composition.

PACS numbers: 77.80.Bh, 75.50.Kj, 75.10.Lp

INTRODUCTION

As has recently been shown,[1] a band theoretical interpretation of the variation of the Curie temperature of amorphous ferromagnetic alloys is reasonably successful. The interpretation is only semiquantitiave due to the following properties of the band theory of magnetism: (a) The theory is intrinsically difficult and controversial even for pure metals like nickel. (b) No usable theory of alloys has been developed to cover the case of amorphous materials.

Persuasive reasons have been given,[2] as to why the band theory should, nevertheless, be used as a physical basis for the properties of these complicated alloys. Nevertheless, the localized model of ferromagnetism involving nearest neighbor exchange integrals has an attractive simplicity so that its application to this problem may be useful at this stage. As in the case of the band model, a description of alloy behavior is a necessary additional ingredient also for the localized model and it is provided for this model by the work of Kouvel[3] and Wu and Foo.[4] We therefore propose to use this localized model in an analysis of the Curie temperature of a very wide range of amorphous alloys. The analysis is useful in specifying the observed data with only a very few parameters. In addition, it may eventually be found that these parameters have a deeper significance than is implied by the localized model in the simple form used here.

THE LOCALIZED BAND MODELS

Kouvel[3] has derived the dependence of the Curie temperatures of binary ferromagnetic alloys on their concentration. He used a phenomenological model based on the molecular field theory suitably modified so that the individual atomic moments are allowed to vary in magnitude with their local environment. Only nearest negihbor interactions were considered. He then derived the equation for the T_c of a disordered alloy:

$$T_c = \tfrac{1}{2}(T'_{AA} + T'_{BB}) + [\tfrac{1}{4}(T'_{AA} - T'_{BB})^2 + T'_{AB}T'_{BA}]^{1/2}, \tag{1}$$

where the primes are interaction temperatures each of which are functions of composition and are defined in terms of the spin quantum numbers, the moments at 0 K, the probability that any atom has A or B neighbors, and the exchange coefficients. If the variation in magnitude of the individual atomic moments with composition is small the calculation of T_c was simplified giving

$$\begin{aligned} T'_{AA} &= T_{AA}(1-x), \quad T'_{AB} = T_{AB}x, \\ T'_{BA} &= T_{BA}(1-x), \quad T'_{BB} = T_{BB}x, \end{aligned} \tag{2}$$

for the alloy $A_{1-x}B_x$, where the interaction temperatures T_{AA}, T_{AB}, T_{BA}, and T_{BB} are defined as for the T's. Substituting Eq. (2) into Eq. (1), we get

$$T_c = \tfrac{1}{2}[T_{AA}(1-x) + T_{BB}x] + \{\tfrac{1}{4}[T_{AA}(1-x) - T_{BB}x]^2 + T^2_{AB}x(1-x)\}^{1/2}. \tag{3}$$

Both Kouvel[3] and Ray and Chandra[5] have used Eq. (3) to fit experimental T_c results on disordered crystalline Ni-Fe, Fe-Mn, and Ni-Mn alloys with good results. The values of T_{AA}, T_{BB}, and T_{AB} were obtained by fitting the T_c vs x results. Negative values of the interaction temperature indicate antiferromagnetic interactions.

Foo and Wu[4] have taken a different approach to calculating T_c vs x. The disordered composition dependent exchange interaction is treated in a coherent potential approximation (CPA). In the weak scattering limit the CPA reduces to the result of the mean field theory. However, in the strong scattering limit, the CPA predicts such effects as a critical concentration for the appearance of ferromagnetism which is beyond the scope of the mean field theory. They derive a cubic equation for T_c, namely,

$$\begin{aligned} \alpha^2 T_c^3 &+ [\alpha(J_{AA} + J_{BB} + J_{AB}) - \alpha(1+\alpha)\langle J\rangle]T_c^2 \\ &+ [(1+\alpha)J_{AA}J_{BB}J_{AB}\langle 1/J\rangle \\ &- \alpha(J_{AA}J_{BB} + J_{AB}J_{AA} + J_{AB}J_{BB})]T_c \\ &- J_{AA}J_{BB}J_{AB} = 0, \end{aligned} \tag{4}$$

where

$$\alpha = (z/2) - 1, \tag{5}$$

z is the number of nearest neighbors, the $\langle\ \rangle$ denotes a composition average, and the J's are the exchange interactions. Following Chein *et al.*,[6] if we assume that the value of $J_{BB} = 0$ for the Ni-Ni exchange, then Eq. (4) reduces to a quadratic, using $J\alpha T$, $\langle J\rangle = x^2T_{AA} + 2x(1-x)T_{AB} + (1-x)^2T_{BB}$, and $\langle 1/J\rangle = (x^2/T_{AA}) + [2x(1-x)/T_{AB}] + [(1-x)^2/T_{BB}]$; namely,

$$\begin{aligned} \alpha^2 T_c^2 &+ \{\alpha(T_{AA} + T_{AB}) - \alpha(1+\alpha) \\ &\times [x^2T_{AA} + 2x(1-x)T_{AB}]\}T_c \\ &+ [(1+\alpha)(1-x)^2 - \alpha]T_{AA}T_{AB} = 0. \end{aligned} \tag{6}$$

At the critical concentration $T_c = 0$ K and

 0021-8979/80/052808-03$01.10

TABLE I. Amorphous alloys and fitting parameters.[a]

(*B-A*) alloy	Electrons available per mole[b]	T_{BB} (°K)	T_{AB} (°K)	T_{AA} (°K)	X_c	Z	Reference
$(Fe\text{-}Co)_{77}B_{11}SiO_{10}$	0.33	717	1002	697	...	...	7
$(Fe\text{-}Co)_{78}B_{12}Si_{10}$	0.32	693	908	718	...	...	8
$(Fe\text{-}Co)_{75}B_{10}Si_{15}$	0.40	675[c]	866	675	...	...	9
$(Fe\text{-}Co)_{80}B_{10}P_{10}$	0.40	640	1075	765	...	...	12
$(Fe\text{-}Co)_{75}P_{16}B_6Al_3$	0.63	600	804	635	...	...	10,15
$(Fe\text{-}Co)_{80}P_{13}C_7$	0.53	595	838	650	...	...	9
$(Fe\text{-}Ni)_{78}B_{14}Si_8$	0.30	721[d]	875	...	0.015	...	11
$(Fe\text{-}Ni)_{78}B_{12}Si_{10}$	0.32	721	875	...	0.015	...	11
$(Fe\text{-}Ni)_{80}P_{10}B_{10}$	0.40	653	861	...	0.010	...	12
$(Fe\text{-}Ni)_{80}B_{20}$	0.20	652	1025	...	0.02	...	13
$(Fe\text{-}Ni)_{79}P_{13}B_8$	0.47	627	825	...	0.070	15	14
$(Fe\text{-}Ni)_{80}P_{14}B_6$	0.48	615	775	...	0.050	20	6,13,15
$(Fe\text{-}Ni)_{80}P_{12}B_8$	0.44	608	800	...	0.010	...	14
$(Fe\text{-}Ni)_{75}P_{16}B_6Al_3$	0.63	600	600	...	0.045	23	10,15
$(Fe\text{-}Ni)_{80}P_{13}C_7$	0.53	585	700	...	0.02	...	16
$(Co\text{-}V)_{80}P_{10}B_{10}$		765	675	...	0.78	2.1	12
$(Co\text{-}Cr)_{80}P_{10}B_{10}$		765	750	...	0.77	2.1	12
$(Co\text{-}Mn)_{80}P_{10}B_{10}$		765	1050	...	0.64	2.3	12
$(Fe\text{-}Mo)_{80}B_{20}$		685	137	...	0.87	2.05	19
$(Co\text{-}Ni)_{78}P_{14}B_8$		675[c]	525	...	0.22	5.0	17
$(Co\text{-}Ni)_{75}P_{16}B_6Al_3$		630	550	...	0.38	3.2	10,15
$(Fe\text{-}Mo)_{75}P_{16}B_6Al_3$		645	140	...	0.70	2.2	18
$(Fe\text{-}V)_{80}P_{10}B_{10}$		640	250	...	0.64	2.3	12
$(Fe\text{-}Cr)_{80}P_{10}B_{10}$		640	250	...	0.62	2.35	12
$(Fe\text{-}Mn)_{80}P_{10}B_{10}$		640	300	...	0.59	2.4	12

[a]FeCo results calculated from Ray and Chandra; remainder calculated from Foo and Wu.
[b]Assuming B = 1, Si and C = 2, P and Al = 3 electrons participating.
[c]Extrapolated.
[d]Interpolated following curve for $(Fe\text{-}Ni)_{78}B_{12}Si_{10}$.

$$X_c = 1 - [(z-2)/z]^{1/2}. \tag{7}$$

In contrast to Kouvel's results this result does not assume that the variation of the individual moments with composition is small.

We will now use Eqs. (3) and (6) to fit the available experimental Curie temperature results.

EXPERIMENTAL RESULTS OF T_c FITTED TO THE MODELS

The various amosphous alloy systems to be fitted by Eqs. (3) and (6) are listed in Table I. For the Fe-Co alloys the values of T_{AA} and T_{BB} are obtained from the experimental data.[7-10] Thus, only the value of T_{AB} has to be adjusted to

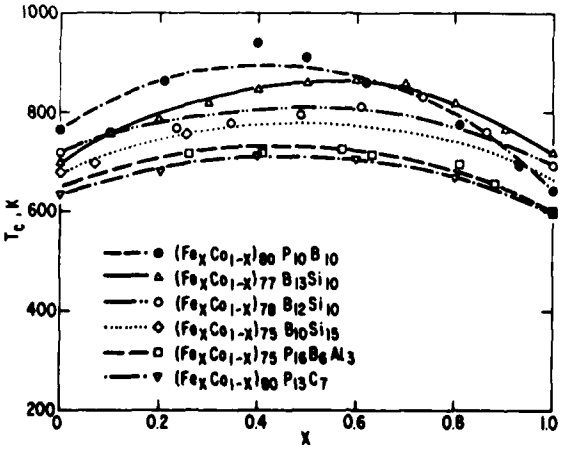

FIG. 1. Curie temperatures of Fe-Co base amorphous alloys as a function of iron content. Curves calculated using Eqs. (3).

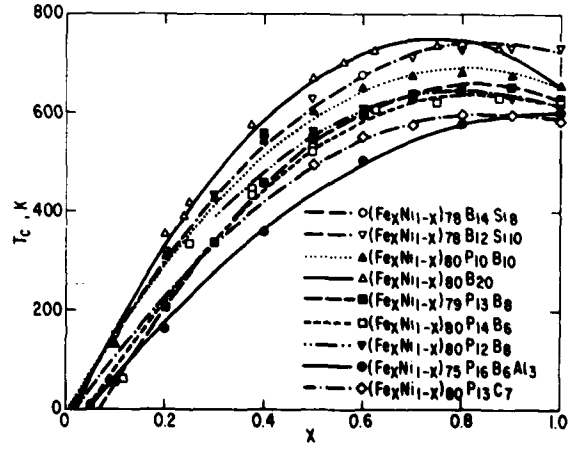

FIG. 2. Curie temperatures of Fe-Ni base amorphous alloys as a function of iron content. Curves calculated using Eq. (6).

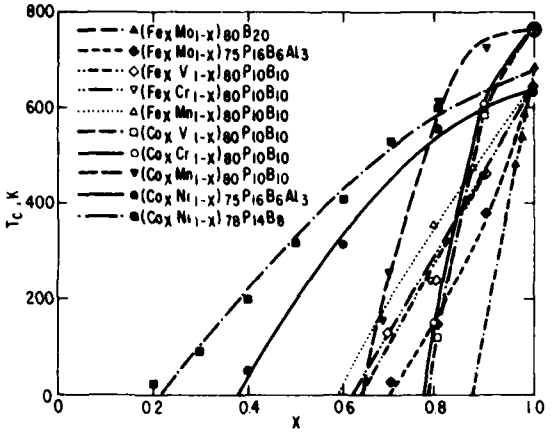

FIG. 3. Curie temperatures of other Co and Fe base amorphous alloys as a function of Co or Fe content. Curves caluculated using Eq. (6).

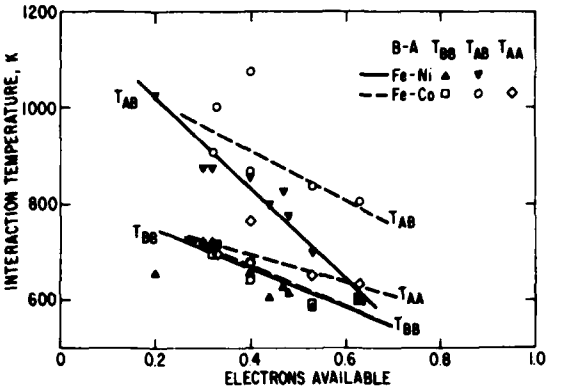

FIG. 4. Interaction temperatures as a function of electrons available from the glass formers.

give the best fit to the experimental results using Eq. (3) since the variation in moments is small. These values are given in Table I and the calculated curves are shown in Fig. 1 together with the experimental data points. In the case of the remainder of the alloys, the values of T_{AA} and X_c are obtained from the experimental results.[11-19]. Then Z and α are calculated from Eqs. (5) and (7). The calculated values of T_{AB} are then obtained from Eq. (6) since now the variation in moments with composition is large. These results are listed in Table I and the calculated curves are shown in Figs. 2 and 3 together with the experimental data. In all cases the calculated curve fits the experimental results over the entire range. A reasonable correlation is obtained, as expected, between the interaction temperatures and the number of electrons available from the metalloids, as shown in Fig. 4. In any case, the use of Eq. (3) or (6) and the fitting parameters given in Table I provide a concise description of the behavior of T_c in these alloy systems.

SUMMARY

The bahavior of the Curie temperature of binary metal-metalloid amorphous alloys can be adequately described using the phenomenological models based on the localized band model. Only one adjustable parameter, the interaction temperature T_{AB} between the binary metal atoms, is required to fit the T_c results over the entire range of binary metal compositions.

ACKNOLWLEDGMENTS

We thank E.P. Wohlfarth for his critical review of this manuscript during his stay in our laboratory as a Visiting Fellow. The partial support of The Office of Naval Research is gratefully acknowledged. J. Gillespie ran the fitting routines.

[1]F.E. Luborsky, J.L. Walter, and E.P. Wohlfarth, J. Phys. F 10, (1980).
[2]E.P. Wohlfarth, IEEE Trans. Magn. MAG-14, 933 (1978).
[3]J.S. Kouvel, *Magnetism and Metallurgy*, edited by A.E. Berkowitz and E. Kneller (Academic, New York, 1969), Vol. 2, p. 523.
[4]E-Ni Foo and Der-Hsueh Wu, Phys. Rev. B 5, 98 (1972).
[5]J. Ray and G. Chandra, Phys. Status. Soildi. A 34, K169 (1976).
[6]C.L. Chien, D.P. Musser, F.E. Luborsky, J.J. Becker, and J.L. Walter, Solid State Commun. 24, 231 (1977).
[7]M. Goto, H. Tange, and T. Tokunaga, Jpn. J. Appl. Phys. 17, 1877 (1978).
[8]H. Fujimori, H. Morita, Y. Obi, and S. Ohta, *Amorphous Magnetism II*, edited by R.A. Levy and R. Hasegawa (Plenum, New York, 1977).
[9]H. Fujimori, M. Kikuchi, Y. Obi, and T. Masumoto, Sci. Rep. Res. Inst. Tohoku Univ. Ser. A 26, 36 (1976).
[10]E.M. Gyorgy, H.J. Leamy, R.C. Sherwood, and H.S. Chen, AIP Conf. Proc. 29, 198 (1976).
[11]T. Masumoto, K. Watanabe, M. Mitera, and S. Ohnuma, *Amorphous Magnetism II*, edited by R.A. Levy and R. Hasegawa (Plenum, New York, 1977), p. 369.
[12]T. Mizoguchi, K. Yamauchi, and H. Miyajima, *Amorphous Magnetism*, edited by F.O. Hooper and A.M. deGraaf (Plenum, New York, 1973), p. 325; *Proceedings of the International Conference on Magnetism* (NAUKA, Moscow, 1974), Vol. II, p. 50.
[13]J.J. Becker, F.E. Luborsky, and J.L. Walter, IEEE Trans. Magn. MAG-13, 988 (1977).
[14]J. Durand, *Amorphous Magnetism II*, edited by R.A. Levy and R. Hasegawa (Plenum, New York, 1977), p. 305.
[15]R.C. Sherwood, E.M. Gyorgy, H.S. Chen, S.D. Ferris, G. Norman, and H.J. Leamy, AIP Conf. Proc. 24, 745 (1975).
[16]R. Hasegawa and J.A. Derman, Phys. Lett. 42A, 407 (1973).
[17]A. Amamou, IEEE Trans. Magn. MAG-12, 948 (1976).
[18]C.L. Chien and H.S. Chen, J. Appl. Phys. 50, 1574 (1979).
[19]C.L. Chien and R. Hasegawa, J. Appl. Phys. 49, 1721 (1978).

APPLICATIONS OF MAGNETIC AMORPHOUS ALLOYS

F.E. Luborsky and L.A. Johnson

General Electric Corporate Research & Development, P.O. Box 8, Schenectady, NY 12301, U.S.A.

Abstract.- Device applications are divided into two general categories ; power devices such as distribution transformers and electronic devices such as miniature transformers and sensing elements. In the case of power devices the recent thrust has been towards developing alloys with maximum M_s at minimum cost since losses are not a problem. Losses are now at least three to ten times lower than for the best Fe-Si alloys with a similar decrease in exciting power. The status, and possible future, of these material developments are summarized. In the case of electronic size devices the results reported in the literature are reviewed. These include the use of amorphous alloys in such devices as multivibrators, electronically controlled delay lines and surface acoustic wave devices, filter elements, electronic current transformers, magnetic shielding material, recording heads, leakage current alarms, d.c. current transformers and in switched mode power supplies.

INTRODUCTION

There have been a number of reviews written on the properties and the potential applications of amorphous alloys [1-13]. However, we have not as yet observed any product announcements using amorphous alloys in a magnetic device although at least three companies offer amorphous alloys for sale [14-16] and one of them [14] offers magnetic shielding material. As evidenced by the large patent literature [17-25] and journal articles [26-38] on magnetic devices using amorphous alloys, there is great activity in this area. The activity is spurred on by the unique and high quality magnetic and mechanical properties exhibited by these amorphous alloys. They are unique in that (1) they combine high magnetostriction with high modulus which is useful in force transducer applications; (2) they have exceptionally high values of ΔE, the change in Young's modulus with field and the magnetomechanical coupling factor, both useful in electronically controllable delay lines; (3) they have exceptional hardness and wear resistance combined with high permeability which makes them good for application in recording heads; and finally (4) they have very low losses and high permeabilities both very desirable properties in both small and large transformer and motor applications. In the first three types of applications the cost of the material is normally not an overriding factor in its possible application, but in the large transformer and motor applications the cost/performance ratio is critical.

We will now describe some of these applications in more detail and the materials and device developments which are going on to promote the possible use of amorphous alloys.

POWER DEVICE APPLICATIONS

Iron losses in transformers and in motors cost the United States over $\$1.8 \times 10^9$ annually. In distribution transformers alone iron losses amount to $\$740 \times 10^6$ annually while in motors iron losses amount to $\$1100 \times 10^6$ annually. Based on our test results on losses in model transformers we estimate that we could save over 60% of these costs per year if all of the presently used distribution transformer cores were replaced with amorphous metal cores. Thus, the incentive is tremendous to develop a cost competitive motor and transformer made with an amorphous alloy.

(a) Distribution Transformers

The requirements for distribution transformers are:

(1) reliability greater than 25 years. (2) Losses less than Fe-3.2 Si. (3) Cost competitive with existing transformers. (4) At 110% of rated voltage the exciting current should increase by less than 10 times. (5) The exciting current should be no more than 3% of the rated full load current. (6) Noise must meet NEMA standards. We will now discuss some of these requirements.

There have been a number of studies concerned with the irreversible end-of-life of amorphous alloys, defined as the beginning of crystallization [4,10]. These have shown, for example, that the $Fe_{80}B_{20}$ alloy will require 500 years at 175°C or 25 years at 200°C to start to crystallize assuming an Arrhenius extrapolation from higher temperatures. This is more than sufficient for this application. The lower temperature, reversible stability is of more recent concern and is related to the development of induced anisotropy and its rotation [4,10]. Recently, DeCristofaro et. al. have related improved thermal stability, in the range of 125-150°C, to the achieving of eutectic compositions in the Fe-B-Si-C alloys [39]. Other authors have been studying the magnetic after effect and its origins [40]. There are still insufficient results to say whether these reversible changes will be a problem.

There is no problem in achieving losses 2 to 10 times lower than in Fe-3.2 Si and there have been many reports comparing these losses [2,4,6-8,10,12]. Another comparison is shown in Fig. 1 based on ribbon thickness. This shows that if Fe-3.2 Si could be made as thin as the amorphous alloys, without a decrease in the excellent preferred orientation, the properties would fall in the range of the amorphous alloys. However, even if this could be done, if the same processing was used, the cost of the additional rolling would limit the competitiveness of this material.

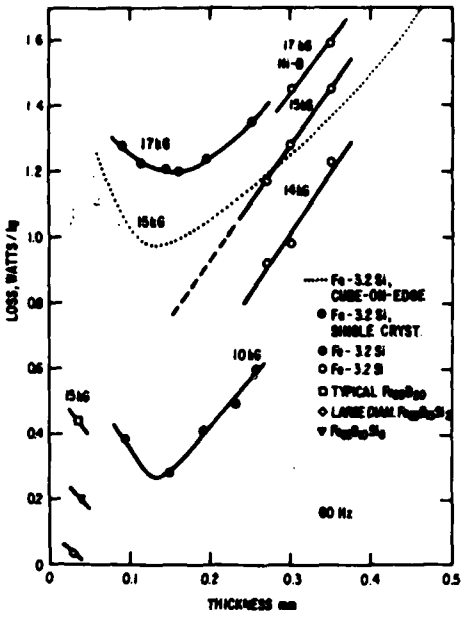

Fig. 1. Loss as a function of thickness for Fe-3.2Si and amorphous alloys vs sheet thickness. O, Fe-Si data on maximum loss from Nippon Steel Corp. Cat. EXE 320, Nov. 1976; ● from Hill and Overshott, J. Magn. Mag. Mat'ls, to appear. □ $Fe_{80}B_{20}$ data from ref. 4. ◇ $Fe_{83}B_{15}Si_2$ data from ref. 12. ▽, $Fe_{82}B_{10}Si_8$ from ref. 41. ◒ from R.F. Miller and S.D. Washko, IEEE Trans. Magnetics, to appear. .... from M.F. Littman, J. Appl. Phys. 38 1104 (1967).

The cost competitiveness of amorphous alloy transformers is more difficult to evaluate since this involves not only the first cost but also the costs over the operating life of the transformer. The basic raw materials costs for $Fe_{81.5}B_{14.5}Si_4$ is projected to be about \$0.52/Kg assuming boron costs contribute \$0.39/Kg. This should be compared to the present day selling price of oriented Fe-3.2 Si of about \$1.43/Kg. Our preliminary

analysis of processing costs for amorphous alloys produced in large volume suggests the total cost, including materials and profit, would not exceed $1.43/Kg. Since the losses are reduced, the total owning costs would be reduced. In fact buyers for large utilities are now paying a premium for lower loss Fe-Si core transformers. The average premium corresponds to $2-4/watt incremental lower losses at no load conditions and $1-2/watt incremental lower losses at full load. Thus, utilities are evaluating transformer costs on the basis of total owning costs throughout the lifetime of the transformer rather than on the basis of just its initial cost. It is not yet clear what kind of premium would be paid for the 2 to 5 times lower losses as exhibited by the amorphous alloys.

The requirement that the exciting current should increase by less than 10 times for a 10% overvoltage means that the core material must be operating sufficiently below saturation to accommodate this increase. We have observed that the exciting current is the most sensitive parameter to changes in stress on the core. Exciting currents have been achieved on 14 cm o.d., 8 cm i.d. and 2.5 cm high model transformer cores which are a factor of 3 times smaller than normally achieved in Fe-3.2 Si [12].

(b) Motors

The requirements for large motors normally specify a 20 year operating life, a specified torque and speed and a low first cost. However, as with transformers, sophisticated users are now starting to pay a small $0.5-1/watt premium for lower losses. To minimize cost, at a specified torque and speed, high saturation magnetization is required. Methods for forming laminations or solid structures all at low final cost without too severe deterioration in flux available are also important. Normally, because motors operate with the major part of the applied mmf in the air gap, excitation requirements are not too severe. Values up to 10 Oe are quite acceptable.

One of the problems with the use of amorphous alloys in distribution transformers or large motors is that their saturation flux is less than that of Fe-3.2 Si. Much effort has been reported [41-54] aimed at finding alloys with greater values of $4\pi M_s$ without addition of expensive alloying elements such as cobalt. The status of some of this work is summarized in Table I. All of these systems have been thoroughly explored to find the composition giving the maximum $4\pi M_s$ at room temperature.

TABLE I

Maximum Saturation Magnetization Obtained in Various Amorphous Alloy Systems

	Maximum Saturation Magnetization at R.T.				
	as-cast		annealed		
Alloy System	σ_s emu/g	$4\pi M_s$ kG	σ_s emu/g	$4\pi M_s$ kG	Reference
Fe-B	180	16.7	184	17.0	45
Fe-B-C	180	16.9	184	17.3	43
Fe-B-Si	179	16.5	183	16.9	44
Fe-B-Ge	179	17.2	183	17.6	to appear
Fe-B-Ga	(178)	-	-	-	to appear
Fe-B-Si-C	182	17.0	186	17.3	42

value in parenthesis is preliminary.

Note that all of the maximum values for the different alloy systems are the same, namely 17.3 kG ±0.3 kG = ±1.7% after annealing. This is to be compared to Fe-3.2 Si which has $4\pi M_s$ = 20 kG. Thus, it now appears that these values of $4\pi M_s$ are as high as will be found. The optimum choice for the alloy composition for this type of application includes consideration of ease of preparation, stability, losses and permeability in addition to maximizing $4\pi M_s$. The ease of preparation really considers the minimum quench rate, and thus the maximum thickness, which the alloy can be cast to form the

amorphous state. The thicker the ribbon the higher the packing fraction achievable in wound or stacked cores and structures, and thus the greater the flux carrying ability. For example, for ribbon thicknesses of about 35 μm a packing fraction of about 0.8 is normally obtained. Doubling this thickness to 70 μm will result in a packing fraction of 0.9, equivalent to an increase in $4\pi M_s$ of more than 10%. Thus, another direction of exploration involves learning how to cast thicker amorphous ribbons. One approach, just reported [55], demonstrated the increase in maximum thickness obtainable as the alloy complexity increased. On a 15 cm diameter casting surface the maximum thickness which could be cast and still have it come out amorphous was 42 μm for $Fe_{80}B_{20}$, 52 μm for $Fe_{80}B_{16}Si_4$ and 57 μm for $Fe_{80}B_{16}Si_2C_2$. It was further shown that by increasing the distance the ribbon stuck to the wheel during casting, and thus the better the cooling, the thicker the maximum thickness it was possible to cast.

It should be noted that in recent years, because of the premium on lower loss transformers, designers are decreasing the operating flux level by using more core material in order to decrease the losses in conventional Fe-3.2 Si. Thus, the gap between the flux available from amorphous alloys and from Fe-3.2 Si is decreasing.

ELECTRONIC DEVICE APPLICATIONS

In most of these types of devices the amount of magnetic material used in each device is small. Thus, the cost of the material is normally not a significant fraction of the total cost of the device. In these types of applications the performance characteristics dominate and therefore expensive alloys or alloying additions are permissible.

Until 1976, there were no devices described in the literature using amorphous alloys. In 1976, two different applications of amorphous metals were reported. The first of these applications was the use of the ribbon for shielding [26]. Large sheets were made by simple weaving and then coating with a polymer. Cylindrical shields made from these woven fabrics were measured at 60 Hz and compared to an equal weight shield wrapped from polycrystalline 80Ni20Fe foil. Neither were annealed. Shielding ratios of the woven glass compared favorably with the polycrystalline foils. The woven glass, however, has the advantage of flexibility without altering shielding performance and is less sensitive to mechanical strain.

The second application reported in 1976 was for accoustical delay lines [27,34]. Delay lines are important components in radar, computer and all signal processing equipment. Their quality is determined by their magnetomechanical and ΔE behavior where ΔE is the change in Young's modulus E with applied field H where E is directly related to the sound velocity. The ΔE effect was extremely large in a variety of amorphous alloys tested for the delay lines. $Fe_{80}P_{13}C_7$ had a peak ΔE of 0.8 at 5 Oe; $Fe_{78}Si_{10}B_{12}$ had a peak value of 1.9 [56], the largest ever reported. In these same works, the magnetomechanical coupling factor k was also measured. The value of k is the most important dynamic transducer parameter and gives a measure of the elastic energy generated by magnetic excitation. The very large values of 0.53 for annealed $Fe_{80}P_{13}C_7$ and 0.75 for $Fe_{78}Si_{10}B_{12}$ were found. Delay times of ∿2 μs/cm were obtained in zero field; maximum changes of ∿12% were obtained in a field of 8 Oe at 100 kHz.

Other applications have been reported in 1977. An electronic current transformer was described [29]. This used an amorphous metal tape core made from $Fe_{40}Ni_{40}P_{14}B_6$ operating into a virtually zero ohm load by using feedback from an operational amplifier. Due to the very low flux density created by virtually short circuiting the transformer, the non-linear effects and

core losses are reduced substantially. A transformer core of reduced size may be used by utilizing such an electronic transformer. Test results have shown that the amorphous metal core using the active load has performance equal to 80Ni20Fe with respect to magnitude error. However, the phase shift is somewhat poorer than for NiFe of the same size. The amorphous core is significantly superior to the FeSi core in both magnitude and phase shift error. The results demonstrated the suitability of this amorphous core material for use as a current transformer with the active load.

Another application reported in 1977 was the use of amorphous cores as tensile-stress transducers in a multivibrator configuration [28,31]. This makes use of the remarkable sensitivity in magnetic properties with tensile stress of amorphous alloys. A differential type of multivibrator was constructed using two cores wound from $Fe_{40}Ni_{40}P_{14}B_6$. Tension or compression could be applied to the windings of one of the cores. It was made with two types of transducing behavior: (1) an analog type with no zero output but good linearity and sensitivity and no hysteresis and (2) a threshhold type with zero output for tensile stress under a critical stress and maximum output for stress over this critical stress. Conventional crystalline permalloy would be very poor for use in this application because of its soft mechanical behavior.

Also reported in 1977 was the use of amorphous ribbon in transversal filters [57]. These are essentially delay lines and make use of the magnetostrictive waves on the amorphous ribbon. They are commonly used in communication and telephone lines. Arbitrary transfer functions were easily realized by adjusting voltages and polarities.

The alloys of low magnetostriction and high permeability for use as cores in recording heads were reported in 1977 through 1979 [21,23,25]. Alloying of Fe-B-Si with Mn, Mo, V and Al was found to reduce the magnetostriction substantially without a correspondingly large decrease in saturation magnetization. Ruthenium additions were also found to act in a similar manner. Still, the zero magnetostrictive high cobalt containing amorphous alloys are preferred for this application.

A leakage current alarm, sensitive enough to detect 1 mA, was described [32] in 1978.

By using a toroidal amorphous core with high permeability and a rectangular hysteresis loop combined with a common iron core of low permeability d.c. current transformers, phasemeters, analog to digital converters or small power wattmeters were made [32].

A novel overcurrent alarm with temperature memory was described [32]. This made use of the fact that amorphous alloys of low Curie temperature will transform to their crystalline state as a function of time and temperature. This changes B_m and H_c. Thus, watching the changes in the induced voltage waveform provides a history of the time-temperature excursions.

In 1979 work was reported on the use of $Fe_{40}Ni_{40}(MoSiB)_{20}$ and $Co_{57}Fe_5Ni_{10}(SiB)_{28}$ in switched mode power supplies operating at frequencies of 20 kHz-50 kHz. Materials for this application must have low a.c. losses, sufficiently high $4\pi M_s$, and a Curie temperature of at least 250°C. It was concluded that either of these two alloys would behave satisfactorily giving greater outputs per unit volume than either crystalline Permalloy or MnZn ferrites.

In 1980, magnetostrictive thin films of amorphous Fe_xSi_{1-x} deposited on the surface of acoustic wave devices (SAW) were shown to offer a means of electronic tuning [58]. Best results were obtained with $Fe_{69}Si_{31}$ annealed in air for 30 min. at about 200°C. The relative change in surface wave velocity, $\Delta V/V$,

reached values as high as 0.05% in saturating fields as low as ∿50 Oe.

SUMMARY AND CONCLUSIONS

Although no magnetic device using amorphous alloys is presently sold in commercial quantities the outstanding performance of a variety of such devices gives us confidence in their eventual successful application.

REFERENCES

1. D.E. Polk, B.C. Giessen and F.S. Gardner, Materials Sci. Eng. 23 309 (1976).
2. F.E. Luborsky, Amorphous Magnetism II, ed. R. A. Levy and R. Hasegawa, Plenum Press NY 1977, p. 345.
3. T. Masumoto and H. Fujimori, Kagaku-to-Kohgyo 30 723 (1977), in Japanese.
4. F.E. Luborsky, Kirk-Othmer: Encyclopedia of Chemical Technology, Vol. 2, Third Edition. John Wiley & Sons, NY 1978, p. 537-569.
5. T. Masumoto, Machine Design 5 52 (1978), in Japanese.
6. F.E. Luborsky, J.J. Becker, P.G. Frischmann and L.A. Johnson, J. App. Phys. 49 1769 (1978).
7. F.E. Luborsky, IEEE Trans. Magnetics MAG-14 1008 (1978).
8. F.E. Luborsky, P.G. Frischmann and L.A. Johnson, J. Magnetism Magn. Mat. 8, 318 (1978).
9. K.J. Overshott, Electronics and Power, p. 347, May 1979.
10. F.E. Luborsky, Ferromagnetic Materials, ed. E.P. Wohlfarth, North-Holland Publ. Co., Amsterdam, Vol. 1, 1980. Chap. 6, p. 451.
11. H. Warlimont, Physics in Tech. 11 28 (1980).
12. F.E. Luborsky, P.G. Frischmann and L.A. Johnson, J. Magnetism Magn. XX XXX (1980).
13. W. Wolf, R. Mohs and U. Konig, J. Magnetism Magn. Mat. XX XXX (1980).
14. Allied Chemical Corp., Morristown, NJ 07960, USA.
15. Vacuumschmelze, Hanau 1, Germany.
16. Marko Materials Inc., 222C Arsenal St., Watertown, Mass. 02172, USA.
17. B.S. Berry and W.C. Pritchet, U.S. Patent 3,820,040, June 25, 1974.
18. M. Dutoit, U.S. Patent 3,838,365, Sept. 24, 1974.
19. L.I. Mendelsohn, U.S. Patent 4,030,892, June 21, 1977.
20. L.I. Mendelsohn, U.S. Patent 4,126,287, Nov. 21, 1978.
21. K. Aso, S. Uedaira, S. Ito, H. Tamura and Y. Makino, UK Patent Appl. BG2005303A., April 19, 1979.
22. V. Honsinger, U.S. Patent 4,155,397, May 22, 1979.
23. Tohoku Univ., Jap. Patent 52114-421, Sept. 26, 1977.
24. Matsushita Elec., Jap. Patent 53133-505, Nov. 21, 1978.
25. Sony Corp., German Patent 2839-626, March 22, 1979, K. Aso, A. Uchira, H. Murata, M. Ito and Y. Makino, Jap. Patent 5.54-56916, May 8, 1979.
26. L.I. Mendelsohn, E.A. Nesbitt and G.R. Bretts, IEEE Trans. Magnetics MAG-12 924 (1976).
27. K. Arai, N. Tsuya, N. Yamada and T. Masumoto, IEEE Trans. Magnetics MAG-12 936 (1976).
28. K. Mohri and S. Korekoda, Memoirs Kyoshu Inst. Tech., Eng 7 25 (1977).
29. M. Milkovic, F.E. Luborsky, D. Chen and R.E. Tompkins, IEEE Trans. Magn. MAG-13 1224 (1977).
30. M. Kikuchi, K. Fukamichi and T. Masumoto, Sci. Repts. Res. Inst. Tohoku Univ A26 232 (1977).

31. K. Mohri and S. Korekoda, IEEE Trans. Magnetics, MAG-14 1072 (1978).
32. K. Murakami, Sci. Rep. Res. Inst. Tohoku Univ. A 221 (1978).
33. Y. Makino, K. Aso, S. Uedaira, S. Ito and M. Hayakawa Sony Tech. Review, MR78-18, p. 39.
34. N. Tsuya, K. I. Arai and T. Ohsaka, IEEE Trans. Magnetics MAG-14 946 (1978).
35. D.C. Webb, D.W. Forester, A.K. Ganguly and C. Vittoria, IEEE Trans. Magnetics MAG-15 1410 (1979).
36. K. Mohri and E. Sudoh, IEEE Trans. Magnetics MAG-15 1806 (1979).
37. Design News, p. 24 Feb. 18, 1980.
38. W. Kunz and D. Gratzer, J. Magnetism and Magn. Mat., XX XXX 1980).
39. N. DeCristofaro, A. Freilich and D. Nathasingh, presented at the Materials Research Soc., 1979 Annual Mtg., Cambridge, Mass., Nov. 26-30, 1979.
40. See J. Magnetism Magn. Mat'ls. 1980.
41 R.C. O'Handley, C.P. Chou and N. DeCristofaro, J. Appl. Phys. 50 (1979) 3603.
42. F.E. Luborsky and J.L. Walter, IEEE Trans. Magnetics, MAG-16 XXX (1980).
43. F.E. Luborsky, J.J. Becker and J.L. Walter, IEEE Trans. Magnetics, MAG-16 XXX (1980).
44. F.E. Luborsky, J.J. Becker, J.L. Walter and H.H. Liebermann, IEEE Trans. Magnetics MAG-15 1146 (1979).
45. F.E. Luborsky, H.H. Liebermann, J.J. Becker & J.L. Walter, Rapidly Quenched Metals III, ed. B. Cantor, The Metals Soc., London 1978 Vol. 2, p. 188.
46. S. Hatta, T. Egami and C.D. Graham, Jr., Appl. Phys. Lett. 34 113 (1979).
47. S. Hatta, T. Egami and C.D. Graham, Jr., Rapidly Quenched Metals III, ed. B. Cantor, The Metals Soc., London Vol. 2, p. 183.
48. M. Mitera, M. Naka, T. Masumoto, N. Kazama and K. Watanabe, Phys. Stat. Sol. (a) 49 K163 (1978).
49. M. Mitera, T. Masumoto and N.S. Kazama, J. Appl. Phys. 50 7609 (1979).
50. N.S. Kazama, T. Masumoto and M. Mitera, J. Magnetism Magn. Mat. XX XXX (1980).
51. C. Hargitai and A. Lovas, Proc. Conf. Soft Magn. Mat.-3, Bratislava, Czech. Sept. 1977.
52. K. Hoselitz, Phys. Stat. Sol. (a)44 K191 (1977).
53. K. Hoselitz, Rapidly Quenched Metals III, ed. B. Cantor, The Metals Soc., London 1978, Vol. 2, p. 245.
54. K. Hoselitz, J. Magnetism Magn. Mat. XX XXX (1980).
55. F.E. Luborsky, H.H. Liebermann and J.L. Walter, Proc. Conf. on Metallic Glasses, Budapest, Hungary, 30 June-4 July, 1980.
56. N. Tsuya, K.I. Arai and M. Yamada, Physica 86--88B 775 (1977).
57. K. Shirae and K. Mashino, 1977 INTERMAG, paper 30-11.
58. E.M. Simpson and W.P. Robbins, 1980 INTERMAG, paper 19-9.

GENERAL ELECTRIC

General Electric Company
Corporate Research and Development
Schenectady, New York

TECHNICAL INFORMATION SERIES

AUTHOR Luborsky, FE
Liebermann, HH
Walter, JL

SUBJECT amorphous alloys

NO 80CRD126

DATE June 1980

TITLE **The Effect of Ribbon Thickness, Composition and Process Changes on the Properties of Rapidly Quenched Metal-Metalloid Alloys**

GE CLASS 1

NO PAGES 6

ORIGINATING COMPONENT Metallurgy Laboratory

CORPORATE RESEARCH AND DEVELOPMENT SCHENECTADY, N.Y.

SUMMARY

Alloys of Fe-Ni-B, Fe-B, Fe-B-Si, and Fe-B-Si-C were prepared in the form of ribbons by melt-spinning. The ribbon thickness was varied from 15 μm to 300 μm by changing the substrate wheel speed. Coercivity, H_c, of the as-quenched ribbons all decreased with increase in thickness until the average quench rate was inadequate to produce completely amorphous alloys. The H_c then increased with ribbon thickness. The low-field magnetization at 1 Oe, M_1, increased with increasing ribbon thickness reaching a maximum at the same thickness as for the minimum H_c. The M_1 then decreased with further increase in thickness as the ribbon became increasingly crystalline. The thickness, t_c, at which the quench rate was sufficiently slow as to initiate crystallinity depended on the alloy composition and wheel diameter. The value of t_c decreased with increasing wheel diameter for the same linear speeds.

After stress relief annealing, the H_c for Fe-Ni-B became independent of thickness in the amorphous region while the Fe-B, Fe-B-Si, and Fe-B-Si-C alloys remained strongly dependent on thickness. It is believed that for the Fe-Ni-B alloy, the H_c does not depend on surface pinning but rather depends on the interactions of strains with magnetostrictive fluctuations. In the highly magnetostrictive iron-rich alloys, even after stress relief annealing, residual strains may be sufficient to cause a significant contribution to H_c, resulting in the retention of the thickness dependence in these alloys. The stress relaxation rate for all of the alloys decreased with increasing thickness, while the embrittlement rate and changes in magnetic properties increased with increasing thickness on annealing completely amorphous samples. This confirms the view that the free volume of the amorphous structure, and thus that the rate of the atomic rearrangements involved in the stress relaxation and in embrittlement, depends on the quench rate. For further increases in thickness, as the samples became increasingly crystalline the stress relaxation and strain for fracture approached a constant, low value. The stress relaxation tended to increase in the sequence Fe-B, Fe-B-Si, to Fe-B-Si-C.

KEY WORDS

amorphous alloys, magnetic properties, preparation of amorphous alloys, glassy metals

INFORMATION PREPARED FOR _____

_____

Additional Hard or Microfiche Copies Available From

Technical Information Exchange
Bldg. 81 Room A133, Schenectady, N.Y., 12345

THE EFFECT OF RIBBON THICKNESS, COMPOSITION AND PROCESS CHANGES ON THE PROPERTIES OF RAPIDLY QUENCHED METAL-METALLOID ALLOYS

F. E. Luborsky, H. H. Liebermann, and J. L. Walter

INTRODUCTION

There are a number of reports[1-7] describing the effect of process variables, such as orifice geometry, ejection pressure, wheel speed, atmosphere, and melt temperature, on the geometry of the resultant amorphous ribbons. Only a few are cited above. Other reports[8-10] describe the effect of changing quench rate on the kinetics of embrittlement and stress relaxation. There have been very few reports describing the effect of process variables on the extrinsic magnetic properties of amorphous alloys such as coercivity, H_c, magnetization, M, losses, W, and permeability, μ. Takayama and Oi[11] showed that, over a limited range of wheel speeds, H_c, decreased and M_r and μ_{max} increased with increasing speed for $Fe_{40}Ni_{40}B_{20}$ amorphous alloy. H_c increased, M_r remained relatively constant, and μ_{max} decreased with increasing temperature for the same alloy over a range of melt temperature from 1000 to 1500 °C. The crystallization temperatures, Curie temperatures, saturation magnetization, M_s, and hardness did not vary for this range of wheel speed and melt temperature. The changes reported were discussed in terms of the effect of the cooling rate on the amorphous structure. More recently, Novak et al.[12] examined the effect of a wider range of wheel speeds on the H_c of the alloy $Fe_{83.4}B_{16.6}$. They found a minimum in H_c with wheel speed. They further reported that H_c decreased with increasing melt temperature in contrast to the results of Takayama and Oi.[11] Finally, Lovas et al.[13] reported on the hardness and H_c for a series of Fe-B alloys. They showed that the glassy state could be obtained under the widest range of processing conditions when casting an alloy near the eutectic composition and that the physical properties are almost independent of the process conditions while both the mechanical and magnetic properties change drastically with process conditions.

In this report, we will present detailed results on the dependence of melt-spun ribbon properties on process parameters for various glass-forming alloy systems. Considered are the effect of wheel speed on ribbon thickness and resultant magnetic properties, stress relaxation and embrittlement, and the response of all these properties to annealing.

EXPERIMENTAL METHODS

Amorphous alloys were prepared by melt spinning[2] using two different pieces of equipment; one by H.H. Liebermann and the other by J.L. Walter. All preparation parameters were kept constant except for the substrate wheel speed and diameter. The ribbon thickness was found to be inversely proportional to wheel speed and the ribbon width was found to be independent of wheel speed. The thicknesses reported here were all measured with a micrometer to ±1.3 μm and were found to be about 20% greater than the average thickness determined by calculation from the ribbon weight divided by length, width, and density. The two different equipments, both using 0.051-cm-diameter orifices were found to give the same thickness for the same linear wheel velocity. The various alloys examined in this work were found to all give the same thickness within ±20% for the same linear wheel velocity. Magnetic measurements of dc hysteresis loops were made on straight samples placed in a long magnetizing coil and sensed with a small pickup coil in the center connected to an integrating fluxmeter. The H_c and B at 1 Oe, B_1, were measured from the loops. Stress relaxation was measured[9] by comparing the radius of curvature of the ribbon during annealing with the radius after release. This annealing was done for 2 hr at 225 and 300 °C. Embrittlement was determined by calculating the fracture strain ratio[14] from the radius at which the sample fractures on simple bending. The shiny side was always on the outside of the bend. Crystallization temperatures were determined using a differential scanning calorimeter (Perkin-Elmer DSC-2).

RESULTS FOR $Fe_{81.5}B_{14.5}Si_4$

In Figures 1-4 are shown the results for ribbons having the nominal composition $Fe_{81.5}B_{14.5}Si_4$. These curves are typical of all of the alloys tested. As the wheel speed increases the thickness decreases. At very low wheel speeds, the thick ribbons are at least partially crystalline and thus have high H_c (Figure 1), low B_1 (Figure 2), a low rate of stress relaxation (Figure 3), and are brittle (Figure 4). With increasing speed and decreasing ribbon thickness, the degree of crystallinity decreases, H_c decreases, B_1 increases, stress relaxation increases slightly, and brittleness decreases. At a critical speed, the samples become sufficiently thin that the quench rate through the thickness of the sample is great enough to produce a completely amorphous ribbon. At this critical thickness, t_c, in the as-cast state the sample is completely ductile on bending, H_c is a minimum, B_1 is maximum, and the stress relaxation starts rising rapidly. With further increase in wheel speed, as the samples become still thinner, the average quench rate through the ribbon thickness increases further. For these com-

Manuscript received April 25, 1980

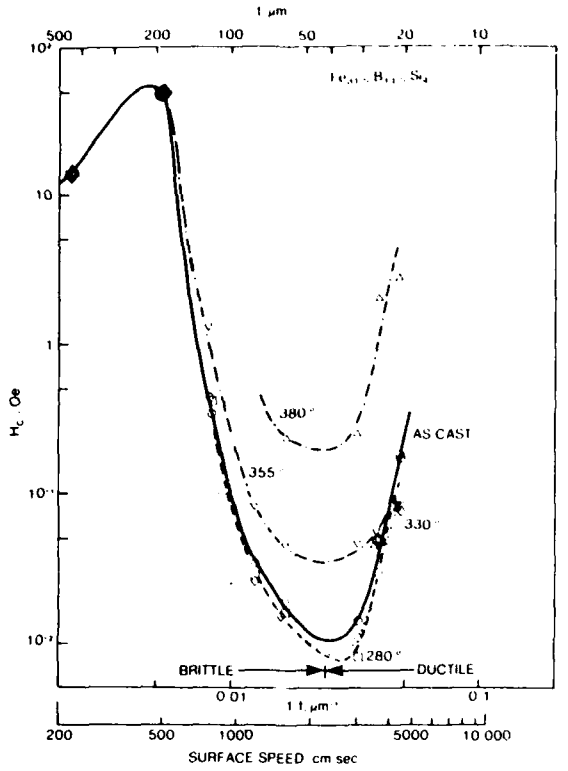

Figure 1. Coercivity vs inverse ribbon thickness for Fe-B-Si in various states of anneal.

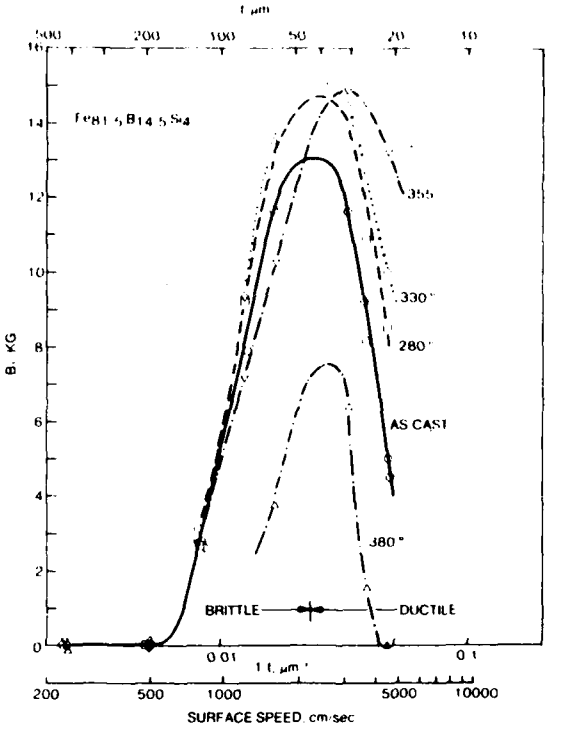

Figure 2. Magnetization at 1 Oe vs inverse ribbon thickness for Fe-B-Si in various states of anneal.

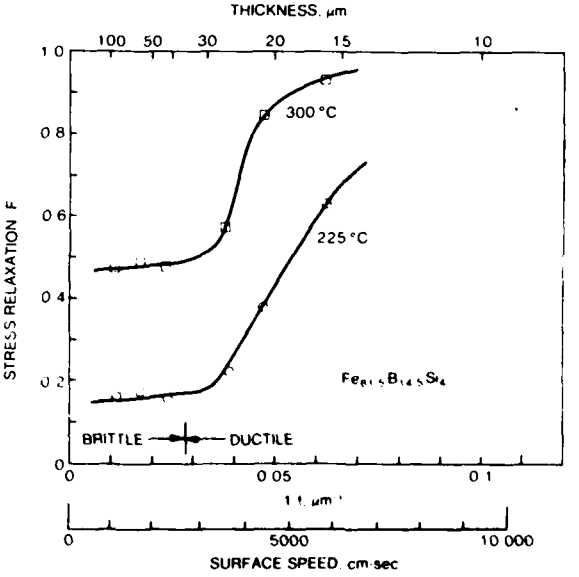

Figure 3. Stress relaxation vs inverse ribbon thickness for Fe-B-Si annealed for 2 hours at 225 and 300 °C.

pletely amorphous samples which are thinner than t_c, in the as-cast state, the H_c increases with decrease in thickness, B_1 decreases, the stress relaxation increases substantially, and the samples remain completely ductile. Annealing the thick, highly crystalline ribbons, H_c does not change suggesting that they are mostly, if not completely, crystalline. As the percentage of amorphous phase increases with decreasing thickness, the H_c decreases with increasing anneal temperatures. When the anneal temperature exceeds the crystallization temperature, T_x, the H_c then starts to increase; the increase in H_c starts first with the thicker amorphous ribbons. The B_1 of this alloy, on annealing, increases until T_x is reached and then decreases. The stress relaxation increases with increase in anneal temperature while the fracture strain ratio decreases with increasing anneal temperature.

The crystallization temperatures, T_x, were determined using the DSC scanning at 40 °/ min. The initiation of crystallization occurred at 492 ± 5 °C, the position of the first peak occurred at 524 ± 3 °C, and the position of the second peak occurred at 563 ± 2 °C. These crystallization temperatures were all independent of ribbon thickness. The T_x was also determined from the changes in H_c and B_1 on isochronal annealing from ribbon thicknesses near the minimum in H_c and near the maximum in B_1. These results are listed in Table 1.

RESULTS FOR OTHER ALLOYS

A number of other alloys were tested in the same way as just described for $Fe_{81.5}B_{14.5}Si_4$. The results for

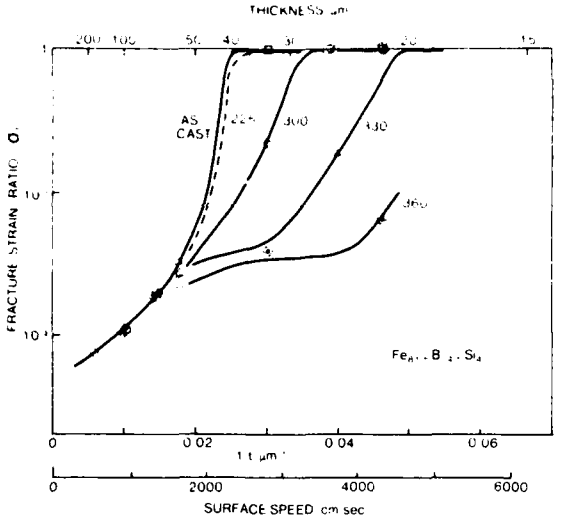

Figure 4. Fracture strain ratio vs inverse ribbon thickness for Fe-B-Si in various states of anneal.

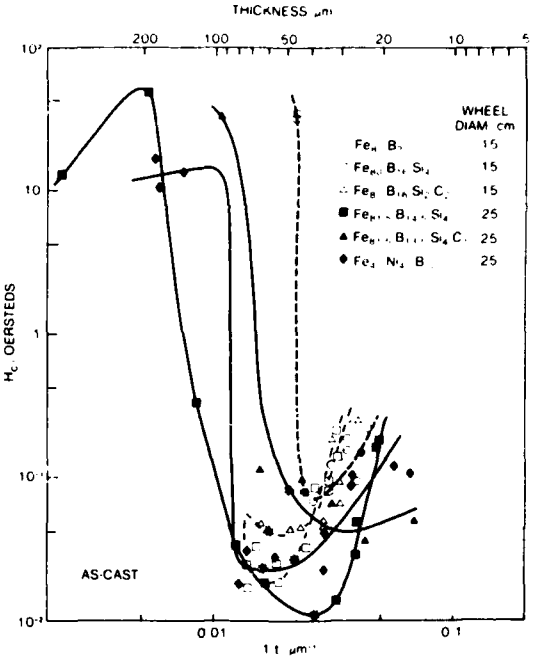

Figure 5. Coercivity vs inverse ribbon thickness for various alloys all as-cast. The * indicates the boundary between brittle and ductile samples.

Table 1

CRITICAL THICKNESS FOR PREVENTING CRYSTALLIZATION AND CRYSTALLIZATION TEMPERATURES OBTAINED FROM ISOCHRONAL ANNEALING

		t_c (μm)			T_x(°C, ± 10, for 2 hr)	
Alloy	Wheel Diam (cm)	(from H_c)	(from B_1/B_{100})	Avg	(from H_c)	(from B_1/B_{100})
$Fe_{81.5}B_{14.5}Si_4$	2.5	53 ± 7	53 ± 5	53	—	—
$Fe_{80}B_{20}$	15	42 ± 3	42 ± 3	42	325	320
$Fe_{80}B_{16}Si_4$	15	54 ± 10	50 ± 10	52	345	360
$Fe_{80}B_{16}Si_2C_2$	15	63 ± 10	50 ± 10	57	375	385
$Fe_{81.5}B_{14.5}Si_4$	25	36 ± 5	33 ± 5	35	340	350
$Fe_{81.5}B_{13.5}Si_4C_1$	25	50 ± 15	52 ± 7	51	345	345
$Fe_{40}Ni_{40}B_{20}$	25	65 ± 20	60 ± 10	63	355	360

the as-cast H_c and B_1 are shown in Figures 5 and 6. The open symbols refer to alloys made on the 15-cm-diameter wheel; the solid symbols refer to slightly different alloy compositions prepared on the 25-cm-diameter wheel. The results of casting on the 2.5-cm-diameter wheel are not shown. Note that the general shape of all the curves are the same. Only the values of H_c at the minimum, or B_1 at the maximum, and the position of the minimum or maximum, i.e., t_c, varies. The values of t_c derived from these curves are listed in Table 1.

The effect of annealing these same alloys on H_c and B_1 is shown in Figures 7 and 8. Only the curve representing the alloy near the optimum, anneal temperature T_a

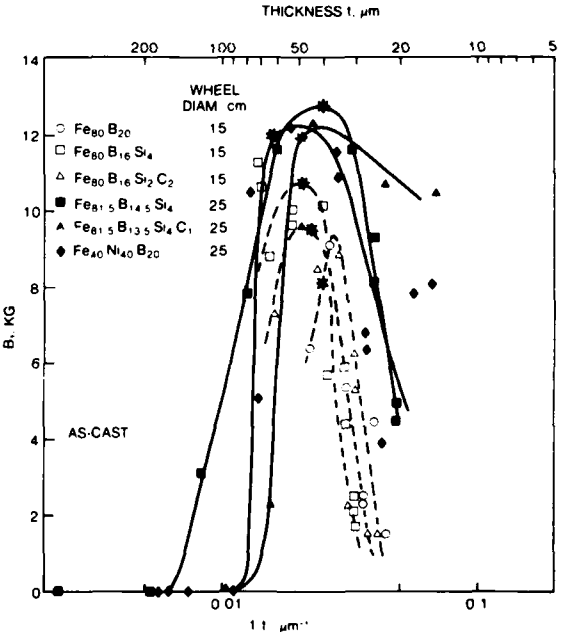

Figure 6. Magnetization at 1 Oe vs inverse ribbon thickness for various alloys all as-cast.

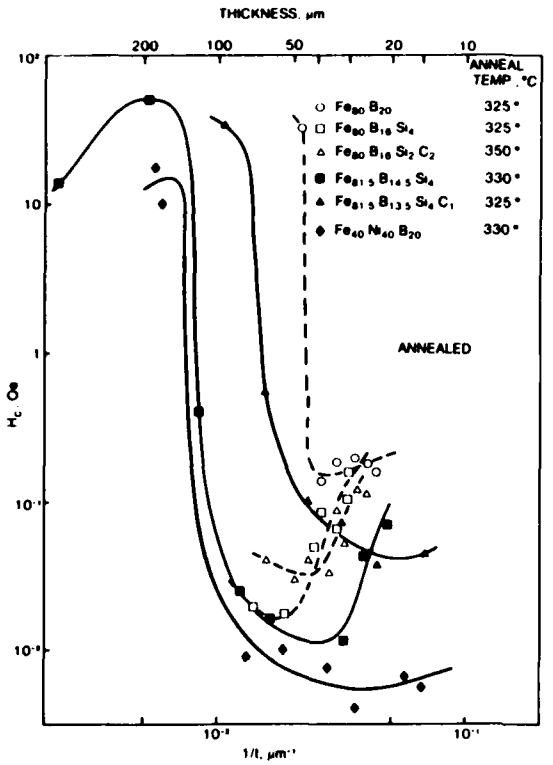

Figure 7. Coercivity vs inverse ribbon thickness for various alloys all annealed to give near minimum H_c. This optimum anneal temperature is shown.

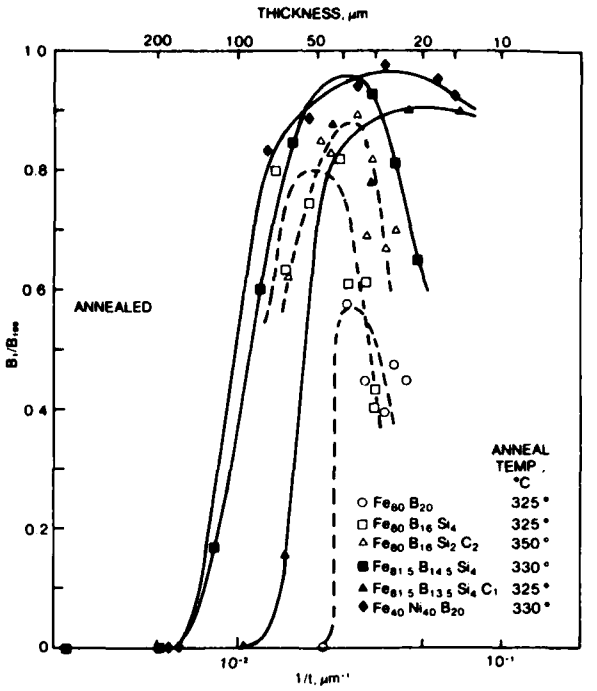

Figure 8. Magnetization at 1 Oe vs inverse ribbon thickness for various alloys annealed as in Figure 7.

for each alloy is shown. One of the points to note is the relatively flat H_c and B_1 curve with decreasing ribbon thickness in the amorphous region for $Fe_{40}Ni_{40}B_{20}$. The $Fe_{80}B_{20}$ alloy was the least stable; the Fe-B-Si-C alloys were the most stable toward changes on annealing, but all of the alloys exhibited more stable H_c and B_1 values on annealing as the ribbon thickness decreased. The values of T_x determined from the beginning of the increase in H_c, or decrease in B_1, on annealing of samples with thicknesses near the minimum in H_c are shown in Table 1.

The stress relaxation for the various alloys at two anneal temperatures are summarized in Table 2. The result of embrittlement on annealing these various alloys is shown by plotting the thickness at which embrittlement is first detectable vs anneal temperature. The thickness at which embrittlement is detected was obtained by interpolating to $\sigma_f = 1$ from results as shown in Figure 4 for the various alloys. These results are shown in Figure 9 and are summarized in Table 2.

DISCUSSION

The decrease in H_c and increase in B_1, as the thickness decreases for the crystalline ribbons, are due to the decreasing fraction of crystallized material and probably also the decrease in size of the crystallites. The values of H_c at the minimum, or B_1 at the maximum, do not appear to correlate with the differences in alloy composition or wheel size. They are undoubtedly strongly influenced by changes in the surface finish of the ribbons due to changes in wheel finish or subtle changes in process parameters from one series of runs to the next. In the amorphous region, the increase in H_c and decrease in B_1 with further decrease in ribbon thickness is probably due to the effect of fluctuations in magnetostrictive-strain anisotropy, where fluctuations in strain have been shown[15] to be a function of thickness. It is not due to surface geometric pinning sites since the $Fe_{40}Ni_{40}B_{20}$ alloy tested had a similar increase in H_c for the decreasing thickness of ribbon in the amorphous range but this increase in H_c disappeared after annealing. Annealing does not remove geometric pinning sites. However, the Fe-Ni-B alloy has only about 1/3 the magnetostriction of the Fe-B-Si alloy. Thus, any fluctuation of strain in Fe-Ni-B would produce only about 1/3 the anisotropy which would occur in Fe-B-Si.

The increase in t_c observed with increasing complexity of the alloy, shown in Table 1, increases in the sequence Fe-B, Fe-B-Si, Fe-B-Si-C. Thus, thicker amorphous alloys may be prepared as the number of alloying constituents increases. This trend with alloy complexity is consistent with the results on the crystallization of amorphous alloys[16] where it was also shown that the activation energy for crystallization scaled with the alloy complexity. Ths trend was also seen here in the effect of annealing on the various alloys. Anneal

Table 2

THICKNESS FOR STRESS RELAXATION AND EMBRITTLEMENT

Alloy	Wheel Diam (cm)	Stress Relaxation Thickness (μm) 2 hr at 225 °C for $F = 0.35$	Stress Relaxation Thickness (μm) 2 hr at 300 °C for $F = 0.8$	Thickness for Embrittlement (μm) As-Cast	Thickness for Embrittlement (μm) 2 hr at 275 °C	Thickness for Embrittlement (μm) 2 hr at 300 °C
$Fe_{81.5}B_{14.5}Si_4$	2.5	39	39	—	—	—
$Fe_{80}B_{20}$	15	27	27	28	26	22
$Fe_{80}B_{16}Si_4$	15	28	28	42	31	—
$Fe_{80}B_{16}Si_2C_2$	15	29	29	43	20	—
$Fe_{81.5}B_{14.5}Si_4$	25	22	23	43	36	28
$Fe_{81.5}B_{13.5}Si_4C_1$	25	30	29	42	38	19
$Fe_{40}Ni_{40}B_{20}$	25	36	36	50	44	42

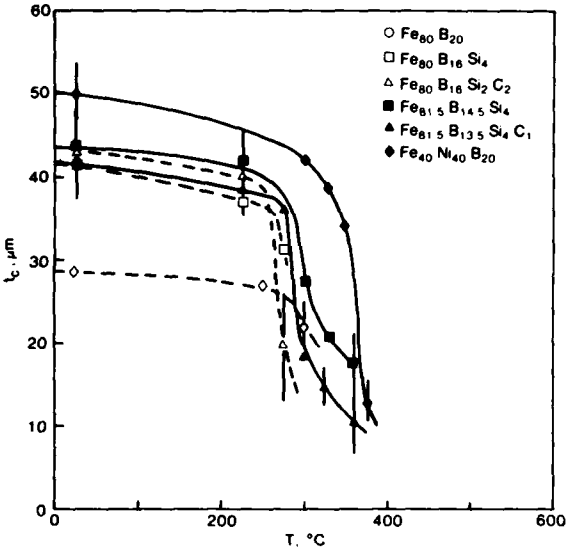

Figure 9. Critical thickness for embrittlement vs anneal temperature for various alloys.

temperatures to reach the minimum H_c increased in the sequence Fe-B, Fe-B-Si, Fe-B-Si-C as shown by the values of T_x in Table 1. The large effect of the casting wheel diameter on t_c, seen by comparing the very similar alloys $Fe_{80}B_{16}Si_4$ and $Fe_{81.5}B_{14.5}Si_4$, may be attributed to the observed[17] general decrease in sticking distance with increase in wheel diameter for the 3-4 g melts used. The decrease in sticking distance means that the ribbon leaves the substrate wheel at a higher temperature leading to a lower average quench rate and thus more rapid crystallization.

In the case of the stress relaxation results in Table 2, it appears that the greater the rate of stress relaxation the greater the complexity of the alloy. However, the differences in thickness for a given relaxation are quite small and may not be significant. In the case of the results on embrittlement, shown in Table 2, there also appears to be a weak correlation between the thickness for embrittlement and the alloy complexity.

The increase in stress relaxation for thickness less than t_c confirms the now accepted view[8,18] that the "amorphous" phase represents a continuum of structures with increasing free volume as the quench rate increases. This increase in free volume means that the atomic rearrangements responsible for the stress relaxation can occur faster. In the case of the change in fracture strain ratio with annealing and ribbon thickness, we see a similar trend. For samples thinner than t_c, higher annealing temperatures are required to embrittle a sample of some given thickness. Thus again, we picture the rate of the atomic rearrangments responsible for embrittlement as dependent on the average quench rate of the ribbon. Finally, with decreasing thickness we observed an increase in stability of the magnetic properties on annealing associated with the beginning of crystallization. The difference between the stress relaxation, F, and embrittlement, σ_f, and magnetic properties is that with decreasing ribbon thickness, F increases; i.e., the rate increases while σ_f and the magnetic properties resist changes more. The difference implies that the different atomic mechanisms involved in the processes respond differently to the change in free volume.

SUMMARY AND CONCLUSIONS

The magnetic properties of various amorphous alloys have been shown to be very sensitive to ribbon thickness as controlled by the substrate wheel speed. This thickness dependence is attributed to the formation of crystallites in samples made at low wheel speeds and is probably due to fluctuation in strains at higher

wheel speeds. The thickness for achieving the optimum magnetic properties depends on alloy composition; the binary alloys achieve optimum properties for the thinnest ribbons, ternary alloys for thicker ribbons, and quaternary alloys for the thickest ribbons. The wheel diameter, which influences the average sticking distance of the ribbon on the casting wheel, also influences the quenching rate and thus the thickness at which the optimum occurs. On annealing, the rate of change in the stress relaxation, the fracture strain, and the magnetic properties all depend on the ribbon thickness. For thicknesses in the amorphous region this dependence demonstrates the changes in the amorphous structure and the increasing free volume of the amorphous phase with increasing quench rate.

ACKNOWLEDGMENTS

The authors wish to acknowledge the work of J. Gillespie in carrying out the magnetic measurements and the preparation of some of the ribbons by W. R. Rollins. The partial support of the Office of Naval Research is gratefully acknowledged.

REFERENCES

1. J-C. Hubert, F. Mollard, and B. Lux, *Z. Metallkd. 64,* 835 (1973).
2. H.H. Liebermann and C.D. Graham, Jr., *IEEE Trans. Magn. MAG-12,* 921 (1976).
3. J.L. Walter, *Rapidly Quenched Metals III,* Ed. B. Cantor, The Metals Soc., London 1978, Vol. 1, p. 30.
4. H.H. Liebermann, *Mater. Sci. Eng. 43,* XXX (1980).
5. S. Kavesh, in *Metallic Glasses,* Eds. H.S. Leamy and J.J. Gilman, American Soc. Metals, Metals Park, Ohio 1977, p. 76.
6. S. Takayama and T. Oi, *J. Appl. Phys. 50,* 4962 (1979).
7. H. Hillmann and H.R. Hilzinger, *Rapidly Quenched Metals III,* Ed. by B. Cantor, The Metals Soc., London 1978, Vol. 1, p. 22.
8. G.C. Chi, H.S. Chen, and C.E. Miller, *J. Appl. Phys. 49,* 1715 (1978).
9. F.E. Luborsky and J.L. Walter, *Mater. Sci. Eng. 35,* 255 (1978).
10. F.E. Luborsky and H.H. Liebermann, *J. Appl. Phys. 50,* 796 (1980).
11. S. Takayama and T. Oi, *J. Appl. Phys. 50, 1595 (1979).*
12. L. Novak, L. Potocky, A. Lovas, E. Kisdi-Koszo, and J. Takacs, *J. Magn. & Magn. Mater.,* to appear. Presented as paper 4.08, Conference on Soft Magnetic Materials 4, Munster, West Germany, September 1979.
13. A. Lovas, C. Hargitac, E. Kisdi-Koszo, J. Takacs, J. Kiraly, and G. Sos, *J. Magn. & Magn. Mater.,* to appear. Presented as paper 4.14, Conference on Soft Magnetic Materials 4, Munster, West Germany, September, 1979.
14. J.L. Walter and F.E. Luborsky, *Mater. Sci. Eng. 33,* 91 (1978).
15. J.D. Livingston, *Phys. Status Solidi A 56,* 637 (1979).
16. F.E. Luborsky, *Mater. Sci. Eng. 28,* 139 (1979).
17. H.H. Liebermann, *J. Mater. Sci.,* submitted.
18. R.W. Cahn, *Contemp. Phys. 21,* 43 (1980).

Torque measurements of induced anisotropy in amorphous $Fe_{80-x}B_{20+x}$ alloys

P. Allia
Istituto Elettrotecnico Nazionale Galileo Ferraris, Gruppo Nazionale Struttura della Materia del CNR - 10125 Torino, Italy

F. E. Luborsky
General Electric Research and Development Center, Schenectady, New York 12301

G. P. Soardo and F. Vinai
Istituto Elettrotecnico Nazionale Galileo Ferraris, Gruppo Nazionale Struttura della Materia del CNR - 10125 Torino, Italy

(Received 15 August 1980; accepted for publication 11 December 1980)

Torque magnetometer measurements were used to obtain the anisotropy energy k_u induced by magnetic annealing (up to 6 h at temperatures from 50 to 70 °C below crystallization) on special patchwork samples of amorphous $Fe_{80-x}B_{20+x}$ ribbons ($-6 \leqslant x \leqslant +6$). The dependence of k_u on annealing time and temperature tends to show that the directional ordering processes are characterized by a very wide distribution of activation energies. At a constant temperature and time k_u is independent of composition, as was also found in results on stress relaxation but not in results on crystallization. Thus different atomic processes control k_u than control crystallization.

PACS numbers: 75.30.GW,75.50.Kj,75.60.Nt,81.40.Rs,

INTRODUCTION

In previous papers we reported a discontinuity in the activation energy for crystallization as a function of B content[1] near 82*a/o* Fe in $Fe_x B_{100-x}$, but we reported a lack of discontinuity in stress relaxation as a function of B content[2]. These results implied that different atomic processes were involved in the rate controlling steps in crystallization and in stress relaxation. In this work we report on the behavior of the induced anisotropy, k_u as the boron content is varied in Fe-B amorphous alloys.

EXPERIMENTAL

Measurements of the anisotropy energy k_u induced by magnetic annealing were performed as a function of time and temperature of annealing on amorphous samples having the composition $Fe_{80-x}B_{20+x}$, with x varying between -6 and +6. These samples were prepared and their properties described previously.[1-4] The induced anisotropy energy was determined by means of high-sensitivity torque magnetometer on convenient samples, from the difference between the torque curves traced after identical annealing treatments, in which the magnetic field was applied along two mutually perpendicular directions. As known, this technique requires the use of circular samples to eliminate the effect of the shape anisotropy, which would strongly reduce the sensitivity of the measurements. The amorphous materials were actually prepared in ribbon form, having a width of about 2 mm, too small to cut out reasonable size circular samples for the torque magnetometer. Therefore special samples were prepared made up of several small ribbon pieces, randomly distributed onto quartz disks (15 mm diameter) and then encased into a Ceramfix matrix. By proper selection of some of these patchwork samples, the residual shape anisotropy could be reduced to values comparable or lower than the expected induced anisotropy, which was then determined with good precision[5].

The crossed magnetic annealing treatments were performed in the very same torque magnetometer, by maintaining the samples at temperatures some 50 °C lower than the corresponding crystallization values T_x. These magnetic annealings were preceded by a stress relief treatment some 20 °C below T_x.

The investigation concerned the following amorphous alloys: $Fe_{74}B_{26}$, $Fe_{78}B_{22}$, $Fe_{82}B_{18}$, and $Fe_{86}B_{14}$. In all cases the following procedure was used: (i) Two stress relief treatments for 2 h, some 20 °C below T_x in the presence of saturating magnetic field, applied along mutually perpendicular directions; (ii) annealing under saturating magnetic field (about 10^6 A/m) applied along a direction i for a time t_a, rapid cooling to room temperature, tracing of torque curve, followed by an identical sequence, the field during annealing being along a direction perpendicular to i. The annealing temperature was chosen some 25 °C below the stress relief one. Three successive series of measurements were performed differing for the annealing t_a, which is chosen equal to 2, 4, and 6 h; (iii) the same procedure described in (ii) was repeated for each sample at a different annealing temperature, some 25 °C below the previously selected one.

The actual crystallization, stress relief, and magnetic annealing temperatures are summarized for the investigated amorphous compositions in Table I.

RESULTS AND DISCUSSION

All of the curves obtained as the difference between the torque measurements after the crossed annealings were found to be well described by a law of the type $k_u(T_a, t_a)\cos^2 w$ where w is the angle between the direction of the field applied during annealing and the one applied during the

 0021-8979/81/053553-04$01.10

TABLE I. Crystallization, stress relief, and magnetic annealing temperatures (in °C)

Amorphous alloy	T_x [a]	T_v [b]	T_{a1} [c]	T_{a2} [d]
$Fe_{86}B_{14}$	275	255	230	205
$Fe_{82}B_{18}$	325	305	280	255
$Fe_{78}B_{22}$	325	305	280	255
$Fe_{74}B_{26}$	350	330	305	280

[a] T_x is the crystallization temperature.
[b] T_v is the temperature of stress relief annealings.
[c] T_{a1} is the temperature of first crossed magnetic annealings.
[d] T_{a2} is the temperature of second crossed magnetic annealings.

torque measurement. This confirms that the results should not be affected by spurious effects such as the ones possibly resulting from magnetostrictive contributions induced by the Ceramfix matrix on the patchwork samples. It has further been checked that within the investigated temperature ranges, the observed effects are fully reversible.

The k_u values, for the annealing temperatures T_a listed in Table I, and as a function of annealing time t_a as reported for the different compositions in Figs. 1 and 2. The maximum induced anisotropy energy values, clearly obtained after 6 h annealings, are also reported in Table II. The order of magnitude of these k_u values is rather large and comparable to values found by Luborsky and Walter[6] for $Fe_{80}B_{20}$ but are larger by about a factor of 10 than those found in $Fe_{80-x}B_{20+x}$ $(-7<x+3)$ alloys by Kisdi-Koszo *et al.*[7] In these previous cases, however, the induced anisotropy was measured from the magnetization curves. In the case of Luborsky and Walter, they measured the susceptibility change on annealing in longitudinal and transverse fields. These were followed to equilibrium at each temperature. In the case of Kisdi-Koszo *et al.* the induced anisotropy was measured as the difference between the energy required for saturation of the sample before and after magnetic annealing. However, no anneal temperatue or time was reported. Both methods are considered to be less precise than the presently used torque magnetometer one.

For all examined compositions, the k_u vs t_a curves for different annealing temperatues do not tend to show a common saturation value, but are shifted by a constant k_u over the entire span of annealing items. This is indicative of the lack of a single activated process as generally observed in crystalline alloys. Indeed a rather good fit of the experimental curves is obtained making use of the following logarithmic dependence on annealing time:

$$k_u(T_a,t_a) = A(T_a) + B(T_a)\ln t_a. \quad (1)$$

This behavior is typical of activated processes characterized by a wide distribution of time constants, the upper and lower limits of which fall well beyond the time span used in the magnetic annealing experiments[8]. This distribution of time constants can be related to the presence of a wide spectrum of activation energies for elementary activated processes.[9]

However, from the present results it is difficult, if not impossible, to unequivocably identify the limits and actual form of this spectrum, and it is not fully clear whether the presently observed directional ordering phenomena can be suitably described in terms of a superposition of independent elementary events. Care should also be taken in interpreting the data of Table II as an indication of correlation between boron concentrations and k_u values, which would favor the hypothesis of monatomic directional ordering of metalloid atoms[10,11]. In fact the tendency of k_u to increase with increasing boron concentration may be simply related to the higher values of annealing temperatures used, owing to the increased crystallization temperature of the alloys richer in B. This is clearly shown by Fig 3, where the k_u (T_a,t_a) are

TABLE II. $k_u(T_a, t_a = 6\ \text{h})$ values

Amorphous alloy	k_u (erg/cm^3) $T_a = T_{a1}$	k_u (erg/cm^3) $t_a = T_{a2}$
$Fe_{86}B_{14}$	1.6×10^5	1.1×10^5
$Fe_{82}B_{18}$	2.0×10^5	1.6×10^5
$Fe_{78}B_{22}$	2.5×10^5	1.9×10^5
$Fe_{74}B_{26}$	2.7×10^5	2.2×10^5

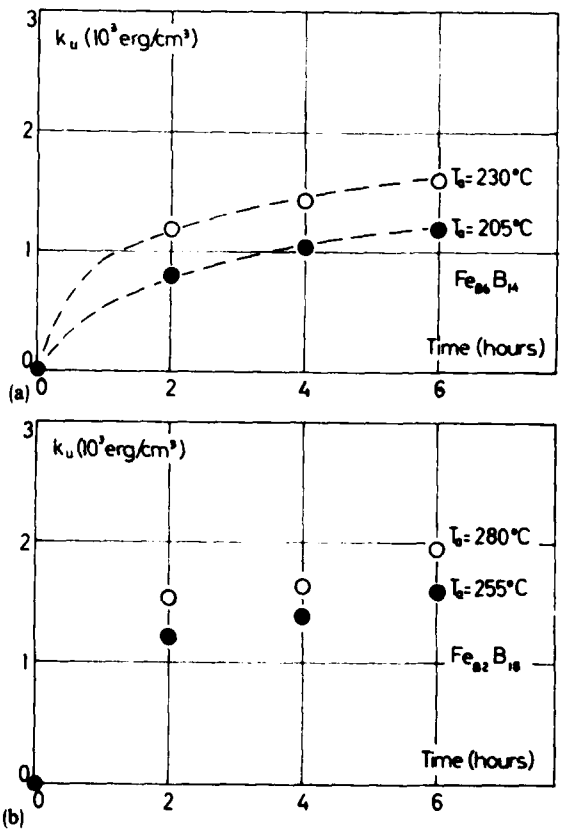

FIG. 1. k_u vs annealing time for $Fe_{86}B_{14}$ [a] and $Fe_{82}B_{18}$ [b]. Dashed lines in (a): $k_u(t_a,T_a)$ curves calculated from Eq. (1) by conveniently choosing the A and B constants.

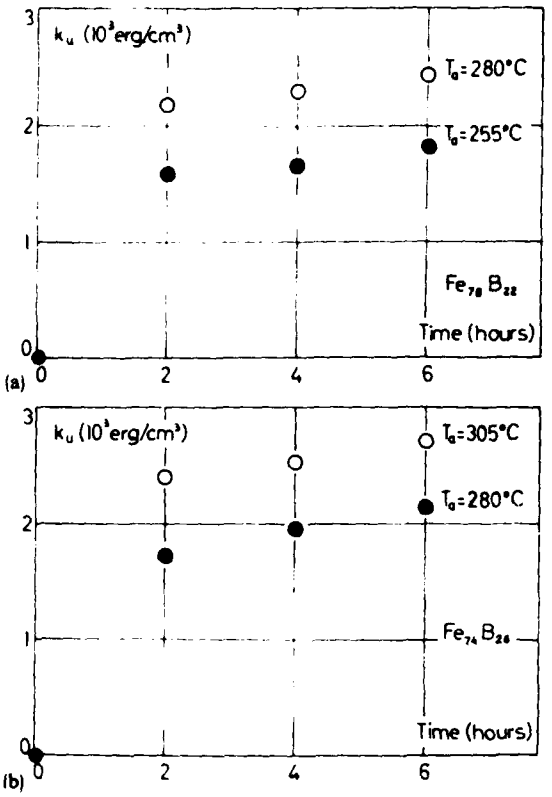

FIG. 2. The same as in Fig. 1 for $Fe_{78}B_{22}$ (a) and $Fe_{74}B_{26}$ (b).

reported as a function of annealing temperatures T_a for t_a = 6 h (open symbols) and t_a = 2 h (black symbols) for all examined compositions. As seen, the k_u vs T_a data are closely fitted by two nearly parallel straight lines for t_a = 6 and 2 h. It should be noted that the increase of k_u with temperature is the reverse of that found by Luborsky and Walter[6] for $Fe_{80}B_{20}$ using magnetization measurements. Furthermore, at a constant time, for example, at 6 h, the k_u values appear

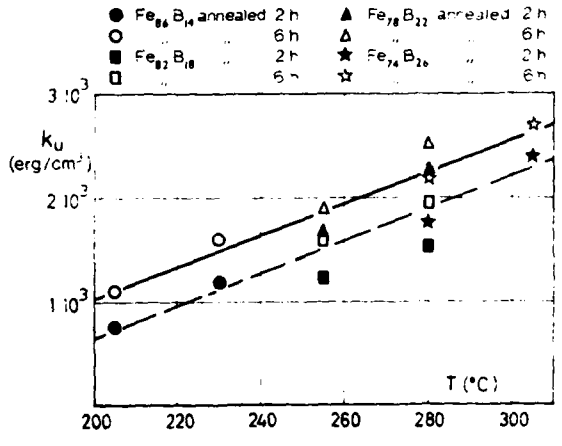

FIG. 3. k_u vs annealing temperature. Straight lines ($k_u = aT + b$) obtained by linear regression.

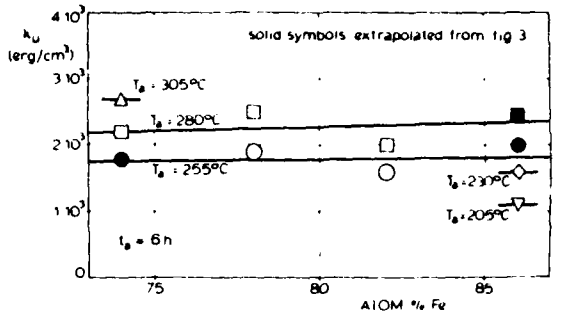

FIG. 4. k_u vs composition of Fe-B at various anneal temperatures for an anneal time of 6 h. Solid points are extrapolated from results in Fig. 3.

to be independent of composition at a given temperature as shown in Fig. 4. There does not appear to be any discontinuity in k_u near 80% Fe as found in the kinetics of crystallization[1] but in agreement with the results on stress relaxation[2]. Thus the atomic processes involved in the rearrangements leading to crystallization are different than those involved in the development of the induced anisotropy and in stress relaxation.

Both the behavior of Fig. 3 and behavior of the curves of k_u vs t_a for various temperatures seem to point to the presence of a quasiuniform distribution of activation energies related to a superposition of independent directional ordering processes. Because of this wide distribution of activation energy, the experiments cannot be considered strictly isothermal, and due account should be taken of the heating and cooling periods, which were only relatively fast, if any analysis is performed on the results, to possibly compute the actual shape of the energy distribution.

CONCLUSIONS

In conclusion the present results, on directional ordering in amorphous alloys of the type $Fe_{80-x}B_{20+x}$, obtained by means of the torque magnetometer technique applied to special patchwork samples, seem to be consistent with the hypothesis of an activated process characterized by a continuous distribution of energies. One final note concerns the fact that a logarithmic dependence on time of the induced anisotropy energy, as the one of Eq. (1), could possibly be related, as recently suggested by Egami[12], to a change with time of a single activation energy, rather than to a wide distribution of these energies. On the other hand, the present results show that the induced anisotropy effects in Fe-B amorphous alloys are largely reversible, at least after performing stress relief treatments, and this seems to disagree with the hypothesis of a change with time of the activation energy, which typically gives rise to irreversible phenomena. The hypothesis of the presence, in stress relieved samples, of a continuous static distribution of activation energies seems thus to be favored by these results, although further measurements are certainly needed to possibly clarify this point. The absence of any discontinuity in k_u near 80% Fe suggests that the atomic processes involved in the rearrangements

leading to k_u are different than those involved in crystallization but might possibly be the same as are involved in stress relaxation.

[1]F. E. Luborsky and H. H. Liebermann, Appl. Phys. Lett. **33**, 233 (1978).
[2]F. E. Luborsky and H. H. Liebermann, J. Appl. Phys. **51**, 796 (1980).
[3]F. E. Luborsky, H. H. Liebermann, J. J. Becker, and J. L. Walter, *Rapidly Quenched Metals III*, edited by B. Cantor (Metals Society, London, 1978), Vol. 2, p. 188
[4]C. L. Chien, D. Musser, E. M. Gyorgy, R. C. Sherwood, H. S. Chen, F. E. Luborsky, and J. L. Walter, Phys. Rev. B **20**, 283 (1979).
[5]P. Allia, G. P. Soardo, and F. Vinai, Solid State Commun. **24**, 517 (1977).
[6]F. E. Luborsky and J. L. Walter, IEEE Trans. Magn. MAG-**13**, 953 (1977).
[7]É. Kisdi-Koszó, L. Ptocký, and A. Novak, J. Mag. Mater. **15-18**, 1383 (1980).
[8]S. Chikazumi, *Physics of Magnetism* (Wiley, New York, 1964), p. 308.
[9]P. Allia, P. Mazzetti, G. P. Soardo, and F. Vinai, J. Mag. Mag. Mater. **15-18**, 1361 (1980).
[10]F. E. Luborsky and J. L. Walter, IEEE Trans. Magn. MAG-**13**, 1635 (1977).
[11]P. Allia and F. Vinai, IEEE Trans. Magn. MAG-**14**, 1050 (1978).
[12]T. Egami, J. Appl. Phys. **50**, 1564 (1979).

Effects of surface treatment and thinning on magnetic properties of rapidly quenched amorphous alloy ribbons[a)]

J. J. Becker

General Electric Research and Development Center, Schenectady, New York 12301

The magnetization curves and hysteresis loops of rapidly quenched transition-metal–glass-former amorphous ribbons of various compositions were measured as they were chemically thinned, down to about 10% of their original thickness. The specific saturation moment did not change showing that the ribbons are chemically homogeneous through their thickness. In general, the approach to saturation of as-cast ribbons remained remarkably constant. Although annealing experiments indicate that the approach to saturation is controlled by stresses, they are not distributed in such a way that they are affected by thinning of the sample. The coercive force initially changed rapidly, either up or down, with decreasing thickness, then increased linearly with reciprocal thickness. The results can be simply interpreted in terms of surface and volume pinning.

PACS numbers: 75.50.Kj, 75.60.Ej

INTRODUCTION

Surfaces often make an important contribution to the magnetization reversal behavior of magnetic materials, especially materials in the form of particles or films. Alteration of the surface can produce drastic changes in the structure-sensitive properties. Chemical polishing, for example, has been shown to produce order-of-magnitude increases in the coercive force of cobalt-rare-earth particles.(1)

The magnetic behavior of rapidly quenched amorphous ribbons can also be affected by surface treatment, as might be expected from their geometry. This paper describes some effects produced by chemical thinning of such ribbons.

EXPERIMENTAL

Amorphous ribbons of various compositions were prepared by the single-roller method(2) in air or vacuum or obtained from Allied Chemical Company. All the ribbons were approximately 0.1 to 0.2 cm wide and 0.004 cm thick. Magnetic measurements were made on single ribbons about 10 cm long in a pickup coil inside a magnetizing solenoid, connected to a duplicate coil and solenoid so that the induction due to H alone was cancelled. DC magnetization curves and hysteresis loops were drawn by varying the solenoid current and recording the output of an integrating fluxmeter connected to the pickup coils. Maximum fields of 100 Oe were applied.

The as-cast ribbons were immersed for various times in a chemical polishing solution consisting of 3 parts by volume HNO_3, 1 part H_2SO_4, 1 part H_3PO_4, and 5 parts CH_3COOH. After each treatment they were rinsed with acetone, air dried, weighed, and placed in a glass tube for magnetic measurement. The thickness was ultimately reduced to 10-20% of its original value. Since the ribbons are very thin compared to their width, the thickness is proportional to the weight, related to it by the known density. Microscopic examination indicated that the thickness remained reasonably uniform, the thinnest samples perhaps containing an occasional small hole.

RESULTS

The results of such a series of thickness reductions on a sample of $Fe_{80}B_{20}$ are summarized in Fig. 1. A number of observations can be made. The ratio of magnetization in 100 Oe to weight remains constant. The slight rise at large amounts of reduction appears to come about because with much etching the ends of the sample become thinned slightly more than the center, making the cross sectional area under the coil a bit larger than average. Thus the ribbons are chemically homogeneous throughout their thickness, as might be expected. More than that, the shape of the magnetization

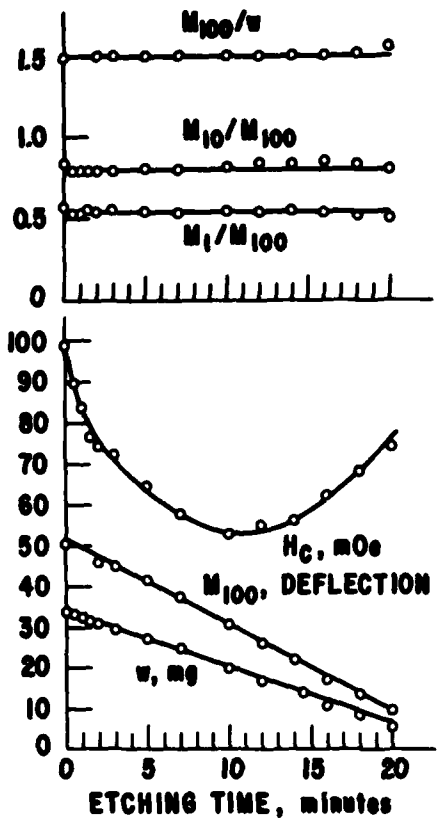

Fig. 1 Effects of chemical reduction of thickness on amorphous ribbon of $Fe_{80}B_{20}$ (METGLAS^R 2605). Dependence on etching time of, from the bottom: weight, fluxmeter deflection in 100 Oe, coercive force, ratios of fluxmeter deflections in 1, 10, and 100 Oe, and fluxmeter deflection divided by weight.

 0021-8979/81/031905-03$1.10

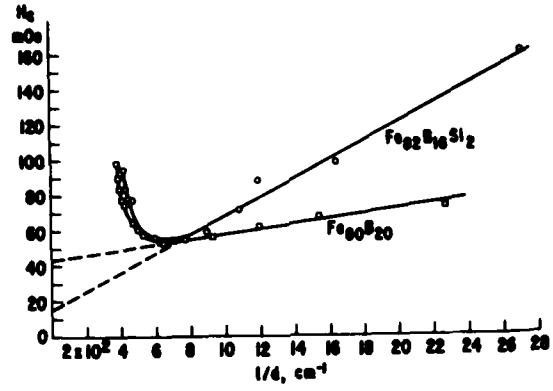

Fig. 2 Coercive force as a function of reciprocal thickness for $Fe_{82}B_{16}Si_2$ and $Fe_{80}B_{20}$ (METGLAS^R 2605).

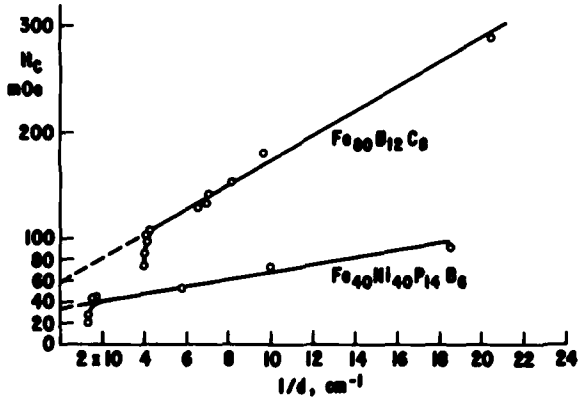

Fig. 3 Coercive force as a function of reciprocal thickness for $Fe_{80}B_{12}C_8$ and $Fe_{40}Ni_{40}P_{14}B_6$ (METGLAS^R 2826).

curves remains constant, as indicated by the constant values of M_1/M_{100} and M_{10}/M_{100}. This was generally true for as-cast ribbons of various compositions. It is well known that the approach to saturation is enhanced by a stress-relief anneal. For example, the values of M_1/M_{100} and M_{10}/M_{100} for an as-cast ribbon of $Fe_{81.5}B_{14.5}Si_4$ were 0.75 and 0.95, while after a 30-minute anneal at 375°C they were 0.97 and 0.99. Thus the difficulty in reaching saturation is usually attributed to systems of residual stresses in the as-cast ribbons. Remarkably enough, it appears that any such system of stresses is not affected by chemically thinning the sample until most of it is gone.

A contrasting behavior is shown by the coercive force H_c. In Fig. 1, H_c can be seen to decrease rapidly as thinning begins, reach a minimum, and then rise again. A number of materials behaved in this way. Others, however, showed only an increase in H_c. Both kinds of behavior are shown for four alloys in Figs. 2 and 3. Here the coercive force is plotted as a function of the reciprocal thickness. In all cases there is a rapid initial change, either up or down, followed by a linear increase with 1/d.

DISCUSSION

The behavior shown in Figs. 2 and 3 can be interpreted on the basis of some simple assumptions about domain boundaries in their materials. Fig. 4 represents the cross section of a ribbon, with a domain boundary traversing its thickness. There are pinning centers throughout the volume of the ribbons. Pinning also occurs at each surface. With a field H applied as shown, for a unit length along the ribbon, the force on the wall is $2M_sHd$. The total available pinning force is $2f_s + f_vd$, where f_s is the surface pinning force per unit length and f_v the volume pinning force per unit area of wall. Taking H_c as the field at which these forces balance,

$$H_c = \frac{f_s}{M_s}\left(\frac{1}{d}\right) + \frac{f_v}{2M_s}$$

Thus the slope of H_c vs 1/d is f_s/M_s and the intercept is $f_v/2M_s$. Here f_s represents the pinning effect of the surface after enough etching has taken place so that both surfaces are the same and remain so. Initially, the surfaces would be expected to have different pinning characteristics from this and from each other, since the surface that contacted the wheel is typically less smooth than the free surface. Thus, rather than f_s, the surface pinning forces are f_f and f_w for the free and wheel-contacting surfaces. Initially, for a rigid wall, H_c will increase if $f_f + f_w < 2f_s$ and decrease if

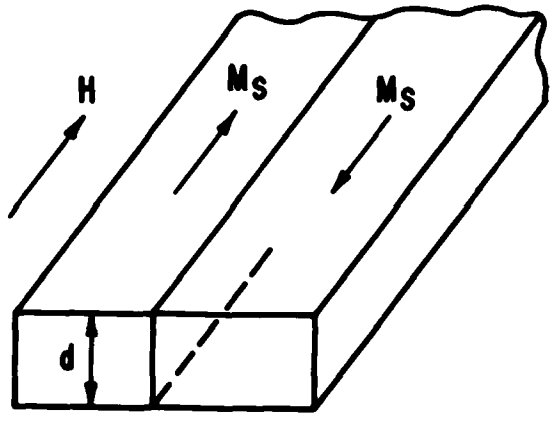

Fig. 4 End view of ribbon with domain wall intersecting top and bottom surfaces.

$f_f + f_w > 2f_s$. In the latter case one might expect f_w to be greater than f_f. Then the wheel side of the ribbon might be more susceptible to modification by etching. To illustrate this, some $Fe_{81.5}B_{14.5}Si_4$ ribbon was etched on one side only, the other being masked with a plastic tape. As Fig. 5 shows, practically all of the effect comes from decreasing the pinning strength on the wheel side of the ribbon.

Tsukahara et al(3) found changes in both domain structure and anisotropy on electrolytically thinning $Fe_{40}Ni_{40}P_{14}B_6$ ribbons. The large changes in H_c seen here seem consistent with their observations, but the relative lack of change in the approach to saturation is a little surprising.

Both f_s and f_v seem to show considerable variation

from one sample to another. One would expect variations in f_v with stress state, voids and inclusions, and degree of amorphousness or incipient crystallinity. The final surface pinning would depend on the interactions between the particular ribbon composition and structure and the particular etching reagent and conditions under which it is used. It would be informative to study the effects of applied stress and annealing on the kinds of results shown here.

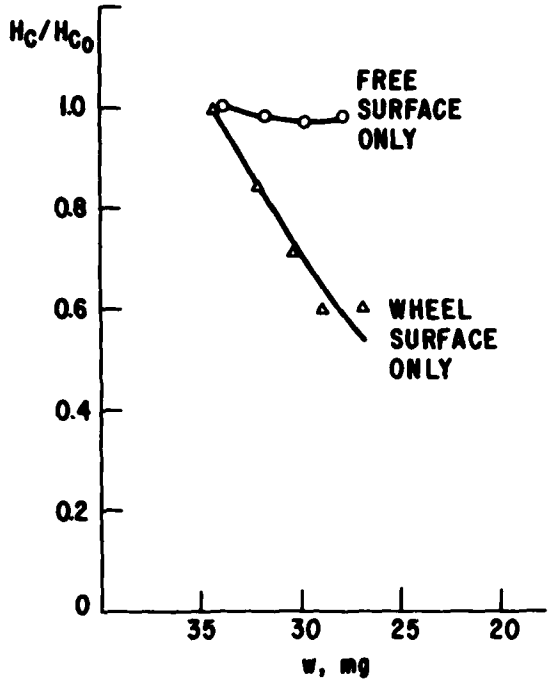

Fig. 5 Ratio of coercive force H_c to as-cast coercive force H_{c_0} for ribbon of $Fe_{81.5}B_{14.5}Si_4$ as a function of weight after etching from either the free surface only or the wheel surface only.

ACKNOWLEDGEMENT

The author would like to thank J. D. Livingston for helpful discussions and J. L. Walter and H. H. Liebermann for supplying samples.

REFERENCES

a) Supported in part by the Office of Naval Research.

1. J. J. Becker, IEEE Trans. Mag. MAG-5, 211 (1969).
2. H. H. Liebermann and C. D. Graham, Jr., IEEE Trans. Mag. MAG-12, 921 (1976).
3. S. Tsukahara, T. Satoh, and T. Tsushima, IEEE Trans. Mag. MAG-14, 1022 (1978).

The Fe-B-Ge Amorphous Alloys

FRED E. LUBORSKY, FELLOW, IEEE, AND JOHN L. WALTER

Abstract—The crystallization behavior, the saturation magnetization, and the Curie temperatures of Fe-B-Ge amorphous alloy ribbons are reported and compared to previously reported results for Fe-B, Fe-B-C, Fe-B-Si, Fe-B-Si-C, and Fe-B-Ga.

INTRODUCTION

THIS PAPER represents a continuation of studies on the effect of changing metalloid composition on the saturation magnetization M_s of amorphous alloys containing mostly iron plus metalloid. This is an effort aimed at trying to increase the M_s available in low cost (i.e., mostly iron containing amorphous alloys), while maintaining the three to ten times lower losses than obtained in high-quality Fe-3-1/4Si. In previous papers we reported on the properties of Fe-B [1], Fe-B-C [2], [3], Fe-B-Si [4], and Fe-B-Si-C [5]. Other workers have confirmed the general features reported in these papers. For example, the Fe-B [6]-[8], the Fe-B-Si [9]-[15], and the Fe-B-C systems have been reported on [16]-[18], and there have been a number of papers reporting on a variety of additions to the binary Fe-B or to the ternary Fe-B-C or Fe-B-Si alloys [19]-[23]. In the Fe-B system, the saturation magnetization in emu/g, σ_s, exhibited a broad peak at $Fe_{80}B_{20}$ of 180 emu/g at room temperature. In the ternary and quaternary alloys, the σ_s at room temperature exhibited a ridge of approximately constant maximum σ_s still equal to 180 emu/g extending out from $Fe_{80}B_{20}$ to $Fe_{82}B_{13}X_5$ where X = Si, C or Si + C. This value can be increased a few percent to 184 emu/g by annealing.

The properties of amorphous Fe-B-Ge alloys will be discussed and compared to the properties obtained in the other systems.

EXPERIMENTAL

Amorphous ribbons were prepared [24], [25] by melt quenching onto the surface of a rotating wheel. Curie temperatures T_c were determined using a thermogravimetric recording balance fitted with a permanent magnet to produce a field gradient in a field of 225 Oe. Samples were heated at 20 deg/min. The saturation magnetizations, σ_s in emu/g, were determined by using a vibrating sample magnetometer at fields up to 20 kOe on samples about 5-mm long. The results were extrapolated to infinite field using a $1/H^2$ function. The densities d were calculated as described previously [3], [26], by first calculating the packing fraction versus iron content for Fe-B alloys using the measured densities of Hasegawa and Ray [8]. Then the density of the alloy was calculated using these packing fractions for each iron content together with the tetrahedral covalent radii of boron (0.88 Å) and germanium (1.22 Å). This technique gave excellent agreement with measured densities in the Fe-B-C [3] and Fe-B-Si [26] amorphous alloys. The density was used to convert σ_s to $4\pi M_s$ using $4\pi M_s = 4\pi\sigma_s d$.

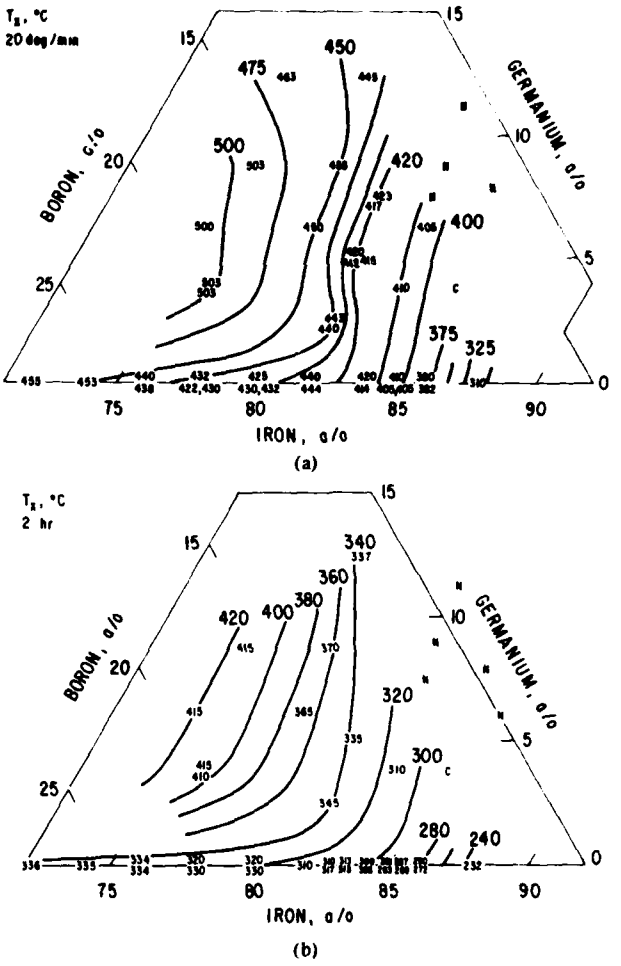

Fig. 1. Temperature in °C for start of crystallization for Fe-B-Ge amorphous alloys heated (a) at 20 deg/min and (b) for 2 h. N is not castable into usable ribbon; C is made ribbon but crystalline.

RESULTS AND DISCUSSION

The stability of Fe-B alloys with Ge, shown in Fig. 1, do not change very much, particularly above 80 percent Fe, on re-

Manuscript received August 18, 1980. This paper was supported in part by the Office of Naval Research.

The authors are with General Electric Corporate Research and Development, Building 81, Room E113, Schenectady, NY, 12345.

0018-9464/81/0300-1204$00.75

TABLE I
COMPARISON OF STABILITY OF VARIOUS ALLOYS[a]

Alloy Fe-B-X	r = Atomic radii of X (Å)	$\Delta r = r_X - r_B$ (Å)	X (percent)	Crystallization temperature, 77.5 percent Fe (20 deg/min)	80 percent Fe (20 deg/min)	84 percent Fe (20 deg/min)	Reference
Fe-B-C	0.77	-0.11	0	435	430	415	[3]
			5	470	461	395	
			7.5	445	440	383	
Fe-B-Si	1.17	0.29	5	500	500	410	[4]
			7.5	500	500	385	
Fe-B-Ge	1.22	0.34	5	475	440	395	this work
			7.5	471	432	–	
Fe-B-Si-C	–	–	5	507	483	390	[5]
			7.5	516	485	375	

[a]From smoothed data.

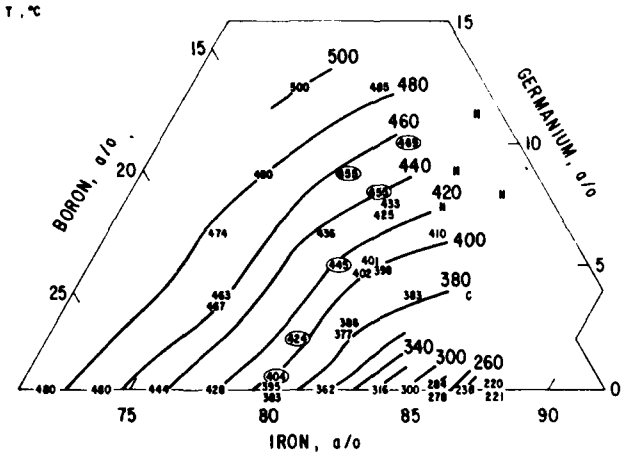

Fig. 2. Curie temperatures in °C for Fe-B-Ge amorphous alloys. Circled numbers from Kazama *et al.* [4].

TABLE II
CURIE TEMPERATURES[a]

Alloy	T_C at $Fe_{80}B_{15}X_5$ (°C)	T_C at $Fe_{81.5}B_{13.5}X_5$ (°C)	T_C at $Fe_{83}B_{12}X_5$ (°C)	Reference
Fe-B	389	363	338	[1]
Fe-B-C	396	371	344	[3]
Fe-B-Si	396	375	351	[4]
Fe-B-Ge	417	400	393	this work
Fe-B-Ga	(410)	(387)	(373)	to appear
Fe-B-Si-C	404	367	341	[5]

[a]From smoothed data.

placing B with Ge. The shape of these contours are similar to the contours for Fe-B-C [3], Fe-B-Si [4], and Fe-B-Si-C [5]. Detailed comparisons show that the C alloys are the least stable, and the Si alloys the most stable of the alloys. The stabilities of some selected compositions are compared in Table I. Since the electronic structure of these alloys are the same, whether C, Si, or Ge are substituted, the differences in stability must be due to differences in atomic sizes. Comparing the tetrahedral covalent radii, used in modeling the alloy density [27], C = 0.77 Å, Si = 1.17 Å, and Ge = 1.22 Å, compared to B = 0.88 Å. However, B and C are expected to be present as an interstitial, and Si and Ge as substitutional additives based on their atomic radii. Thus it is concluded that interstitial substitutions decrease stability, whereas substitutional additives improve stability, provided their atomic radii are not too much different from their host atoms.

The Curie temperature of Fe-B-Ge amorphous alloys, shown in Fig. 2, exhibits a pronounced increase when substituting B with Ge. This is in sharp contrast to the substitution of B by C [3] and by Si [4], which exhibits only a very slight increase in T_c (see Table II). Note the large effect of Fe content. For example, at 80 percent Fe, T_c goes from 390°C to 420°C in going from 0 percent Ge to 5 percent Ge, a change of 30°C. For C or Si, T_c = 395°C at 5 percent C or Si, which is essentially unchanged. This greater change for Ge additions may be attributed to the effect of the metalloid element size on the Fe-Fe coordination and interatomic distance based on the Bethe-Slater curve [19]. This lends support to the previous views based on the itinerant electron model [28]. This increase in T_c will decrease the temperature coefficient of M_s in going from low temperature to room temperature.

The saturation magnetizations measured at 77 K room temperature and at 100°C are shown in Fig. 3. The 77-K results, shown in Fig. 3(b), do not agree with the results from Kazama *et al.* [19]. They reported an increase in M_s in μ_B/Fe atom for $Fe_{80}B_{20-x}Ge_x$, as x increased as shown by the circled numbers in Fig. 3(b). A convoluted function has been found, first decreasing and then increasing as Ge replaces B. This abnormal behavior becomes a smooth normal function when plotted as emu/g, as shown in Fig. 3(a). The difference cannot be accounted for between our results and those of Kazama *et al.* However, our general trend of M_s with varying metalloid and metalloid content can be accounted for in terms of the itinerant electron model [28].

The room temperature results of M_s (Fig. 3(c)) can be compared to previously reported results on Fe-B-C [3], Fe-B-Si [4], and Fe-B-Si-C [5]. The general trends are all the same, that is, a ridge of approximately constant maximum σ_s extends out from near $Fe_{80}B_{20}$ to near $Fe_{82.5}B_{12.5}X_5$. The maximum values obtained in each alloy system, shown in Table III, are all essentially the same. The Fe-B-C exhibits quite a wide ridge; for example, at 5 percent C in going from one side of the ridge at 175 emu/g to the other side at 175 emu/g, the Fe content changes from 78 to 86 percent. The Fe-B-Si alloys

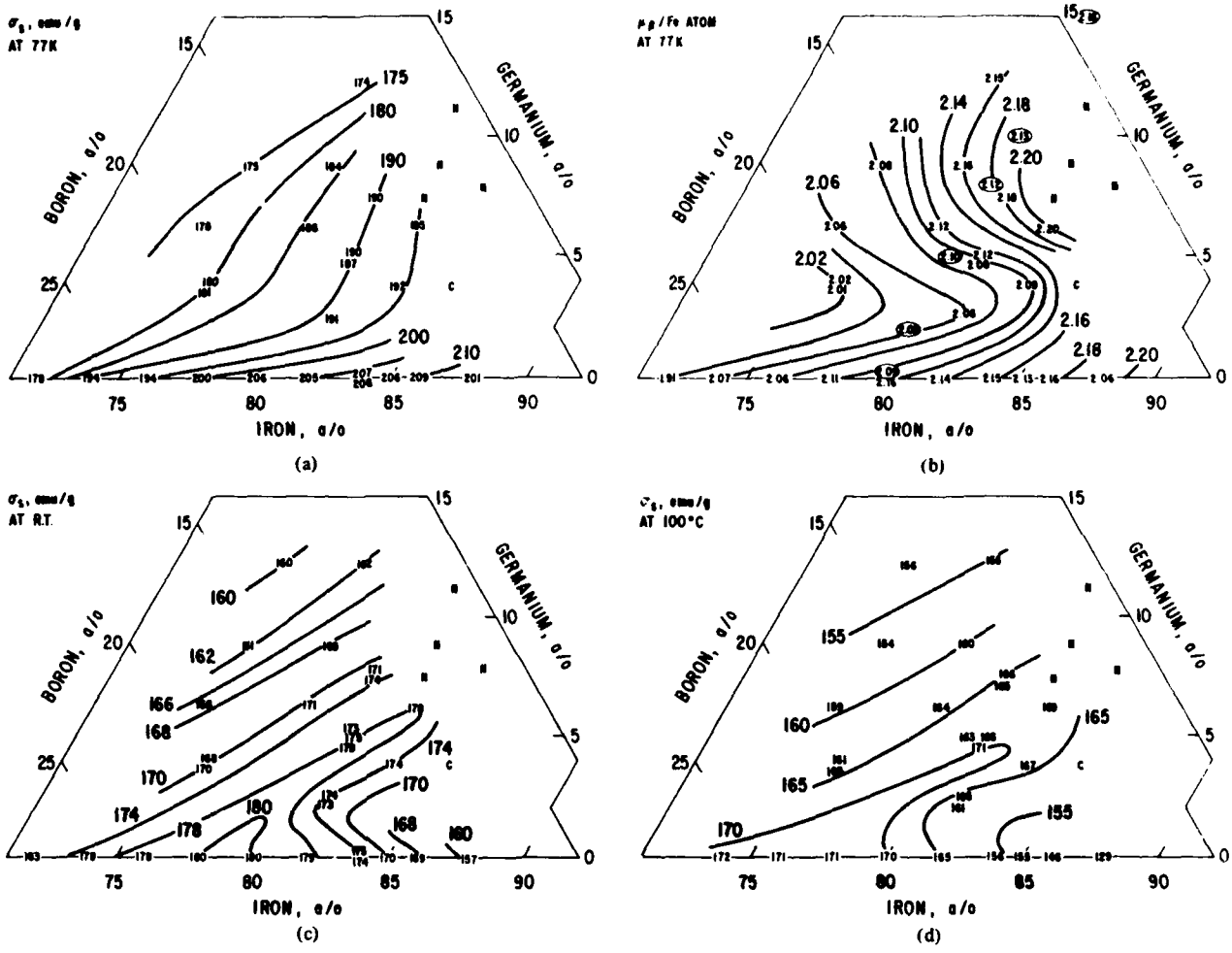

Fig. 3. Saturation magnetization for Fe-B-Ge amorphous alloys measured (a) at 77 K in emu/g; (b) at 77 K in Bohr magnetons/Fe atom, circled numbers reported by Kazama *et al.* [19] at 0 K; (c) at room temperature in emu/g; and (d) at 100°C in emu/g.

TABLE III
MAXIMUM SATURATION MAGNETIZATION OBTAINED IN VARIOUS AMORPHOUS ALLOY SYSTEMS[a]

Alloy System Fe-B-X	Maximum Saturation Magnetization at Room Temperature As-Cast σ_s (emu/g)	As-Cast $4\pi M_s$ (kG)	Annealed σ_s (emu/g)	Annealed $4\pi M_s$ (kG)	Width of ridge at 5 percent X for 175 emu/g (percent)	Composition at tip of the 178 emu/g contour	Reference
Fe-B	180	16.7	184	17.0	–	$Fe_{80}B_{20}$	[1]
Fe-B-C	180	16.9	184	17.3	8.0	$Fe_{82.5}B_6C_{11.5}$	[3]
Fe-B-Si	179	16.5	183	16.9	2.5	$Fe_{82}B_{12}Si_6$	[4]
Fe-B-Ge	179	17.2	183	17.6	4.5	$Fe_{82.5}B_{11}Ge_{6.5}$	this work
Fe-B-Ga	(178)	–	–	–	–	–	to appear
Fe-B-Si-C	182	17.0	186	17.3	6.5	$Fe_{82}B_{12.4}Si_{2.8}C_{2.8}$	[5]

[a]From smoothed data.

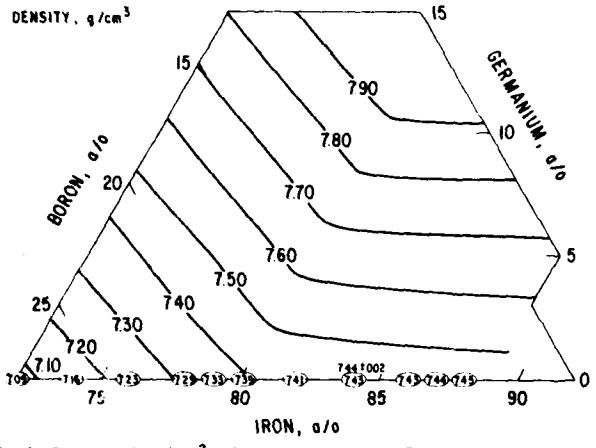

Fig. 4. Density, in g/cm³ of amorphous Fe-B-Ge alloys calculated as described in text.

exhibit a very narrow ridge of maximum σ_s. For the same change in σ_s, the Fe content changes from only 81 to 83.5 percent Fe. The Fe-B-Ge alloys exhibit an intermediate width ridge; the Fe content changes from 79 to 83.5 percent Fe for the same change in σ_s from 175 emu/g on one side of the ridge to the other side. These widths are summarized in Table III.

The results of M_s measured at 100°C are important for applications. These are shown in Fig. 3(d) and show the same trends as described above for M_s measured at room temperature.

The densities of Fe-B-Ge alloys are shown in Fig. 4. These were calculated as described previously. Using the maximum σ_s at room temperature of 179 emu/g at the density of 7.65 g/cm³ corresponding to $Fe_{82}B_{13}Ge_5$, gives $4\pi M_s = 17.2$ kG for the as-cast saturation magnetization. This is somewhat higher than any of the previously reported alloy systems as summarized in Table III. On annealing the M_s increases by about 2.5 percent; the same holds true for the previously reported alloys, as shown in Table III.

The coercivities and low-field magnetization appear to be independent of Ge additions, but because these samples were prepared at widely separated times, the casting conditions were somewhat different, leading to wide variations in H_c and B_1/B_{100} even for the same compositions. These wide variations are attributed to different surface features and to different quenched in stresses. The surface features, of course, remain after stress relief annealing, and the different stresses produce different stress-induced anisotropies after the stress relief annealing. For these reasons these results were not suitable for reporting at this time.

Conclusion

It has been shown that the stability of Fe-B-Ge alloys are quantitatively very similar to Fe-B-C alloys, and both are less stable in general than Fe-B-Si alloys. These changes do not follow the changes in atomic radii of the C, Si, or Ge, but may be due to whether they substitute interstitially or substitutionally. The Curie temperature rises rapidly on substituting Ge for B, in contrast to no change on substituting C or Si for B. This may be attributed to the effect of the large size of the Ge on the Fe-Fe coordination and interatomic distance. The maximum room temperature saturation magnetization believed to be achieved with Fe-B-Ge was 17.2 kG as-cast and 17.6 kG after annealing. This occurred at $Fe_{82}B_{13}Ge_5$, assuming a density of 7.65 g/cm³. These $4\pi M_s$ values are higher than obtained with Fe-B-C or Fe-B-Si alloys.

Acknowledgment

We are grateful to W. Rollins for the preparation of the ribbons, to J. Gillespie for many of the magnetic measurements, to H. Patchen for the saturation magnetization measurements, and to N. Marotta for the Curie temperature measurements.

References

[1] F. E. Luborsky, H. H. Liebermann, J. J. Becker, and J. L. Walter, in *Rapidly Quenched Metals III*, B. Cantor, Ed. London: The Metals Soc., 1978, vol. 2, p. 188.
[2] F. E. Luborsky, J. J. Becker, and H. H. Liebermann, in *Rapidly Quenched Metals III*, B. Cantor, Ed. London, The Metals Soc., 1978, vol. 2, p. 249.
[3] F. E. Luborsky, J. J. Becker, J. L. Walter, and D. L. Martin, *IEEE Trans. Magn.*, vol. MAG-16, p. 521, 1980.
[4] F. E. Luborsky, J. J. Becker, J. L. Walter, and H. H. Liebermann, *IEEE Trans. Magn.*, vol. MAG-15, p. 1146, 1979.
[5] F. E. Luborsky and J. L. Walter, *IEEE Trans. Magn.*, vol. MAG-16, p. 572, 1980.
[6] C. Hargitai and A. Lovas, in *Conf. Proc. Soft Magn. Mat. 3*, Bratislava, Czech., Sept. 1977.
[7] K. Fukamichi, M. Kikuchi, S. Arakawa, and T. Masumoto, *Solid-State Comm.*, vol. 23, p. 955, 1977.
[8] R. Hasegawa and R. Ray, *J. Appl. Phys.*, vol. 49, p. 4174, 1978.
[9] K. Narita, J. Yamasaki, and H. Fukunaga, *IEEE Trans. Magn.*, vol. MAG-14, p. 1016, 1978.
[10] K. Narita, H. Fukanaga and J. Yamasaki, *Japan. J. Appl. Phys.*, vol. 16, p. 2063, 1977.
[11] F.J.A. den Broeder and J. van der Borst, *J. Appl. Phys.*, vol. 50, p. 4279, 1979.
[12] K. Hoselitz, *Phys. Stat. Sol.*, vol. (a)44, p. K191, 1977.
[13] —, in *Rapidly Quenched Metals III*, B. Cantor, Ed. London: The Metals Soc., vol. 2, p. 245, 1978.
[14] —, *J. Magnetism Magn. Mat.*, vol. 20, p. 201, 1980.
[15] S. Hatta, T. Egami and C. D. Graham, Jr., in *Rapidly Quenched Metals III*, B. Cantor, Ed. London: The Metals Soc., vol. 2, p. 183, 1978.
[16] —, *IEEE Trans. Magn.*, vol. MAG-14, p. 1013, 1978.
[17] —, *Appl. Phys. Lett.*, vol. 34, p. 113, 1979.
[18] N. S. Kazama, M. Mitera, and T. Masumoto, in *Rapidly Quenched Metals III*, B. Cantor, Ed. London: The Metals Soc., vol. 2, p. 164, 1978.
[19] M. Mitera, M. Naka, T. Masumoto, N. S. Kazama, and K. Watanabe, *Phys. Stat. Sol.*, vol. (a)49, p. K163, 1978.
[20] M. Mitera, T. Masumoto, and N. S. Kazama, *J. Appl. Phys.*, vol. 50, p. 7609, 1979.
[21] R. C. O'Handley, C.-P. Chou, and N. DeCristofaro, *J. Appl. Phys.*, vol. 50, p. 3603, 1979.
[22] N. S. Kazama, T. Masumoto, and M. Mitera, *J. Magnetism Magn. Mat.*, vol. 15-18, p. 1331, 1980.
[23] J. L. Walter, in *Rapidly Quenched Metals III*, B. Cantor, Ed. London: The Metals Soc., 1978, vol. 1, p. 30.
[24] H. H. Liebermann and C. D. Graham, Jr., *IEEE Trans. Magn.*, vol. MAG-12, p. 921, 1976.
[25] F. E. Luborsky, P. G. Frischmann, and L. A. Johnson, *J. Magnetism Magn. Mat.*, vol. 19, p. 130, 1980.
[26] G. S. Cargill III, *Solid-State Phys.*, vol. 30, p. 227, 1975.
[27] F. E. Luborsky, J. L. Walter, and E. P. Wohlfarth, *J. Phys.-F.*, vol. 10, p. 959, 1980.

Acta Metallurgica Vol. 29, pp. 1413 to 1418, 1981
Printed in Great Britain

0001-6160/81/081413-06$02.00/0

EMBRITTLEMENT OF SOME METALLIC GLASSES BY Sb, Se, AND Te

H. H. LIEBERMANN and F. E. LUBORSKY

General Electric Corporate Research and Development
Schenectady, NY 12301 U.S.A.

(Received 9 February 1981)

Abstract—Some metallic glasses have been found to embrittle after annealing at low temperatures, much as do some steels. In phosphorus-bearing alloys, phosphorus has been found to segregate during annealing and result in sample embrittlement. The present report describes the effects of the steel-embrittling elements Sb, Se, and Te on metallic glasses in which the primary metallic constituents are Fe and/or Ni. Bend ductility and stress relaxation measurements of as-cast and annealed glassy alloy ribbons have been used to study embrittlement resulting from less than 0.2 at.% Sb, Se, and Te addition to the base alloys. XRD, DSC, and magnetic measurements have been used to further characterize the samples and to check for changes in magnetic properties which may accompany embrittlement. Results show that P is a very weak embrittler compared with Sb, Se, and Te. Furthermore, the embrittling power of these three elements varies in the sequence Te > Se ≫ Sb, the same sequence as found in steels. The effect of a given embrittler is enhanced when substituting Fe in place of Ni. No substantial changes in DSC or magnetic measurements have been found as a result of substituting the small amount of embrittler into the base alloys investigated.

Résumé—Nous avons trouvé que certains verres métalliques étaient fragilisés par un recuit à basse température, comme certains aciers. Dans les alliages pour paliers au phosphore, le phosphore ségrège au cours du recuit, ce qui conduit à une fragilisation de l'échantillon. Dans cet article, nous présentons les effets de l'addition de Sb, Se and Te, qui sont des éléments fragilisant des aciers, sur des verres métalliques dont les constituents métalliques principaux sont Fe et/ou Ni. Des mesures de ductilité en flexion et de relaxation de contrainte sur des rubans d'alliages vitreux bruts de coulée et recuits ont permis de mettre en évidence une fragilisation provenant de l'addition de moins de 0,2 at% de Sb, Se et Te aux alliages de base. Des mesures de diffraction X, de DSC et magnétiques ont ensuite permis de caractériser plus précisément les échantillons et d'observer une éventuelle variation des propriétés magnétiques qui pourrait accompagner la fragilisation. Nos résultats montrent que le P est beaucoup moins fragilisant que Sb, Se et Te. De plus, le pouvoir fragilisant de ces trois éléments varie selon la séquence Te > Se ≫ Sb, c'est á dire la même que dans les aciers. On augmente l'effect d'un élément fragilisant en remplaçant du Ni par du Fe. Nous n'avons pas vu de changement notable du DSC ou des propriétés magnétiques à la suite de la substitution d'une faible quantité d'élément fragilisant dans l'alliage de base.

Zusammenfassung—Einige metallische Gläser verspröden während der Auslagerung bei niedrigen Temperaturen wie gewisse Stähle. In phosphorhaltigen Legierungen wurde gefunden, daß Phosphor während der Auslagerung segregiert und dadurch die Versprödung verursacht. Die vorliegende Arbeit beschreibt den Einfluß der Stahl-versprödenden Elemente Sb, Se und Te auf metallische Gläser mit den metallischen Hauptkomponenten Fe und/oder Ni. Mit Messungen der Biegeduktilität und der Spannungsrelaxation an frisch hergestellten und ausgelagerten Bändern metallischer Gläser wurde die Versprödung untersucht, die von Sb-, Se- und Te-Zugaben in Mengen von weniger als 0,2 At.-% verursacht wird. Mit XRD-, DSC- und magnetischen Messungen wurden die Proben weiterhin untersucht, um mögliche, mit der Versprödung einhergehende Änderungen der magnetischen Eigenschaften aufzufinden. Die Ergebnisse zeigen, daß P im Vergleich zu Sb, Se und Te sehr schwach versprödend wirkt. Die Wirksamkeit dieser Elemente ändert sich in der Folge Te > Se ≫ Sb wie in den Stählen. Der Einfluß eines versprödenden Elementes wird verstärkt, wenn Ni durch Fe ersetzt wird. Es wurden keine bedeutenden Änderungen bei DSC- und magnetischen Messungen gefunden, die als Folge der Einführung des kleinen Anteils versprödender Elemente in die Basislegierung auftraten.

INTRODUCTION

The embrittlement of some metallic glasses may occur without the onset of crystallization during annealing at temperatures well below those required to cause crystallization. This embrittlement is analogous to that found in steels [1, 2], except that it is irreversible. Phosphorus is a metalloid used in the formation of some metallic glasses and the discovery of embrittlement in glassy alloys containing this element has prompted numerous investigations [3–8]. It has been suggested that P enrichment occurs on a highly localized scale in these alloys during annealing, resulting in sample embrittlement because of sharply reduced ductility in the segregated regions and the extent to which the ductile–brittle transition temperature is

suppressed varying directly with phosphorus content [7].

Elements such as Sb, Se and Te are much more potent embrittlers of steel than is P [9]. The current investigation deals with the nature of temper embrittlement in metallic glasses of nominal composition $Fe_{81.5}B_{14.5}Si_4$, $Fe_{40}Ni_{40}B_{20}$, and $Ni_{81.5}B_{14.5}Si_4$ containing 0.2 at.% or less of the embrittling agents Sb, Se or Te. The alloy compositions have been selected to be phosphorus-free so that properties measured will not be the result of P segregation. Furthermore, the nominal compositions chosen permit a comparison of embrittlement as Ni and Fe are interchanged in the base alloy.

Embrittlement of a metallic glass is not only dependent upon the addition of embrittling alloying elements but is also determined by processing conditions with which the sample is manufactured. For example, it has been found that glassy alloy embrittlement increases with decreased ribbon-substrate contact distance during chill block melt-spinning [10]. A similar correlation has been established between glassy ribbon stress relaxation and ribbon-substrate contact distance [11]. Increased tendency for embrittlement has also been demonstrated with increased as-cast ribbon thickness [12]. Whether by reduced ribbon-substrate contact distance or by excessive ribbon thickness, the increased embrittlement and reduced stress relaxation result from the 'self-anneal' of the ribbon when departing from the substrate surface without having undergone sufficient heat removal during melt-spinning.

EXPERIMENTAL

Master alloys of the compositions investigated were premelted using high purity constituent alloying elements in an alumina crucible atmosphere and poured into a split copper mold under Ar atmosphere. The resultant ingots were then crushed and pieces chill block melt-spun in vacuum [13]. A 125 mm diameter copper substrate wheel was used at 2, 4, 6, and 12 krpm to result in a set of ribbons having average thicknesses of from 8 μm to 45 μm for each alloy composition investigated. Ribbon-substrate sticking distance was not found to vary with the alloy compositions studied for a given geometric cross-section and substrate velocity. Although the embrittling elements studied are also surface active and reduce liquid iron and nickel surface tension [14], no significant change in ribbon geometry was noted when casting embrittler-bearing samples. This is presumably because of substantial melt puddle turbulence during casting and suggests a uniform distribution of the embrittler elements in the ribbons.

Ribbons of various thicknesses for each composition were examined by transmission Laue X-ray diffraction (Charles Supper precession camera with a GE XRD-4 power generator) to check for indications of crystallinity. These samples were also subjected to bend ductility testing in which a ribbon sample is gradually bent (shiny side out) to a decreasing radius of curvature between the platens of a micrometer drive and the platen separation at sample fracture converted to a relative maximum strain to fracture [4] using micrometer (maximum) ribbon thickness for calculation. The degree to which atomic motion is possible was monitored through stress relaxation measurements on all of the ribbons formed. Stress relief data were obtained by annealing ribbon segments in 1 cm i.d. toroidal cans for two hours at 498 K and measuring the degree of spring-back exhibited by each sample on removal from the can [15]. Ductile, glassy ribbons of about 25 μm average thickness were sealed in evacuated glass tubes and subjected to 1 h anneals at 373, 473, 573 and 673 K. The relative strain to fracture for these annealed ribbon samples was then remeasured and embrittlement assessed.

Differential scanning calorimetry (DSC) using a Perkin Elmer DSC II at 40 K min heating rate was used to compare crystallization temperatures of some ribbon samples with and without embrittler alloy additions. Magnetic coercivity measurements using an 800 Am^{-1} (10 Oe) drive field have also been used to examine the annealing response of $Fe_{40}Ni_{40}B_{20}$ base metallic glass containing small amounts of Sb and Se.

RESULTS AND DISCUSSION

Embrittlement

The embrittlement of all ribbons in the as-cast state has been measured by the relative maximum strain to fracture of U-shaped samples [4], a typical data set of which is shown in Fig. 1 for the $Fe_{40}Ni_{40}B_{20}$ base alloys. The sharp increase in fracture strain with decreasing ribbon thickness has been drawn to comply with this kind of variation typically exhibited by glassy alloys [7]. The dashed portion of the $Fe_{40}Ni_{40}B_{19.9}Te_{0.1}$ data curve is an extrapolation to a maximum relative strain of 1.0. Fracture strain data scatter is well-masked by the steepness of the curves drawn. From such plots, the maximum ductile sample thickness (t_d^m) for each composition is obtained by reading the thickness at which the maximum relative strain to fracture drops below unity. Note that the t_d^m values obtained are particular to the melt-spinning apparatus and conditions (such as ribbon-roller contact distance) used and may vary when using other equipments. A summary of t_d^m for all the glassy alloy compositions investigated is given in Table 1. From this data, it is seen that as-cast $Fe_{81.5}B_{14.5}Si_4$ ribbons show less embrittlement (can be made thicker yet ductile) than either $Fe_{40}Ni_{40}B_{20}$ or $Ni_{81.5}B_{14.5}Si_4$ ribbons. This is presumably because of the greater thermal stability of the Fe-based metallic glass, as shown by the DSC data in Table 4. The right-hand column in Table 1 lists the ratio of maximum as-cast ductile ribbon thickness for a given base composition (t_b^m) to the equivalent thickness for an embrittler-containing

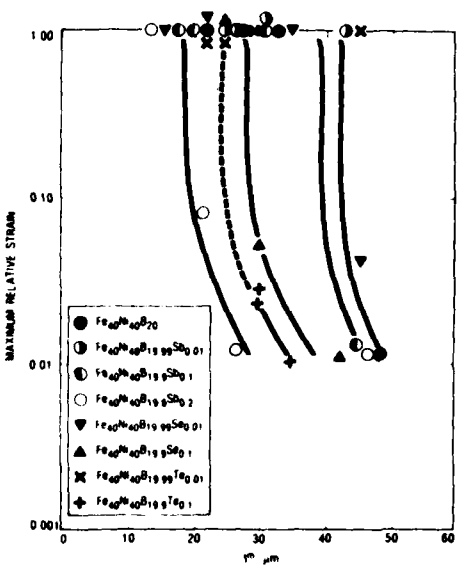

Fig. 1. Relative maximum strain to fracture data for as-cast samples as a function of glassy alloy ribbon micrometer (maximum) thickness for the $Fe_{40}Ni_{40}B_{20}$ base alloy and samples containing small amounts of the embrittlers Sb, Se or Te.

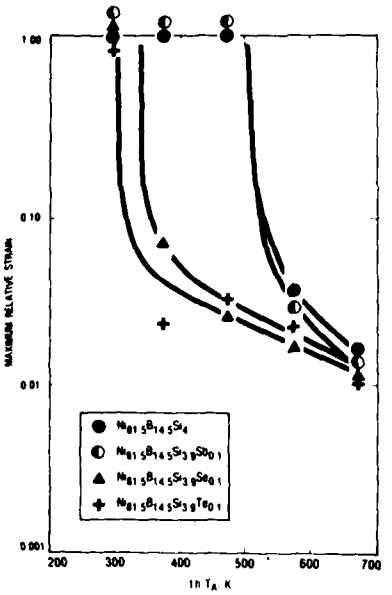

Fig. 2. Relative maximum strain to fracture data as a function of one hour isochronal annealing temperature for the $Ni_{81.5}B_{14.5}Si_4$ base alloy and sample containing 0.1 at.% of the embrittler Sb, Se, or Te.

alloy (t_c^m). This ratio eliminates the difference in thermal stability of the three base alloy compositions and gives an indication of relative embrittlement, with 1.00 corresponding to that of the embrittler-free base alloy. The sequence of elements in order of increased embrittling power in $Fe_{40}Ni_{40}B_{20}$ glassy alloy data shown in Fig. 1 is Sb, Se, Te for 0.1 at.% embrittler addition. The results also show that increased quantities of Sb in $Fe_{40}Ni_{40}B_{20}$ result in increased embrittlement. This increased embrittling strength with concentration of embrittler would presumably also be the case for the other base alloys as well. In the $Ni_{81.5}B_{14.5}Si_4$ glassy alloy system, there seems to be no embrittling effect due to Sb, Se or Te at the 0.1 at.% concentration in any of the as-cast ribbons.

Table 1. Maximum as-cast glassy alloy ribbon micrometer thickness at which completely ductile bending is possible (t_d^m), and ratio of ductile base alloy to ductile embrittler-containing alloy ribbon thickness (t_b^m/t_c^m).

Composition	t_d^m, μm	t_b^m/t_c^m
$Fe_{81.5}B_{14.5}Si_4$	58	
$Fe_{81.5}B_{14.5}Si_{3.9}Sb_{0.1}$	40	1.45
$Fe_{81.5}B_{14.5}Si_{3.9}Se_{0.1}$	≤ 20	≥ 2.90
$Fe_{81.5}B_{14.5}Si_{3.9}Te_{0.1}$	≤ 20	≥ 2.90
$Fe_{40}Ni_{40}B_{20}$	42	
$Fe_{40}Ni_{40}B_{19.99}Sb_{0.01}$	42	1.00
$Fe_{40}Ni_{40}B_{19.9}Sb_{0.10}$	40	1.05
$Fe_{40}Ni_{40}B_{19.8}Sb_{0.20}$	18	2.33
$Fe_{40}Ni_{40}B_{19.99}Se_{0.01}$	42	1.00
$Fe_{40}Ni_{40}B_{19.9}Se_{0.10}$	28	1.50
$Fe_{40}Ni_{40}B_{19.99}Te_{0.01}$	42	1.00
$Fe_{40}Ni_{40}B_{19.9}Te_{0.10}$	< 25	> 1.68
$Ni_{81.5}B_{14.5}Si_4$	40	
$Ni_{81.5}B_{14.5}Si_{3.9}Sb_{0.1}$	40	1.00
$Ni_{81.5}B_{14.5}Si_{3.9}Se_{0.1}$	40	1.00
$Ni_{81.5}B_{14.5}Si_{3.9}Te_{0.1}$	40	1.00

Relative maximum strain to fracture of ribbons as a function of 1 h isochronal annealing temperature is exemplified by the data for the $Ni_{81.5}B_{14.5}Si_4$ base metallic glass shown in Fig. 2. The 1 h embrittlement temperature is defined as that at which the relative maximum strain to fracture drops below unity and the sample begins to show loss of bend ductility. Fracture strain data scatter is more obvious in the less steep portions of the curves drawn. As in Fig. 1, the shape of the data curves has been drawn to comply with that typically found for glassy alloys [7]. Note that for the $\sim 25\,\mu$m thick ribbon samples annealed and tested, an embrittlement of the $Ni_{81.5}B_{14.5}Si_4$ base composition samples is only found for samples containing 0.1 at.% Se or Te. It is interesting that a 0.1 at.% Sb addition causes no detectable embrittlement beyond that of $Ni_{81.5}B_{14.5}Si_4$. The embrittling power of the three agents used follows the same sequence in each of the three base alloys: Te > Se $\gg$ Sb. A summary of 1 h embrittlement temperatures and the ratio of one hour embrittlement temperature for the base alloy to that of the embrittler-containing alloy (T_b/T_c) for the three base compositions appears in Table 2. An illustration of the embrittlement data in Table 2 is shown in Fig. 3 for the three base alloy compositions. The dashed curves are extrapolations. The T_b/T_c trends

Table 2. One hour annealing temperature above which ~25 μm thick glassy ribbons show a loss in ductility on bending and ratio of one hour embrittlement temperature for the base alloy to that of the embrittler-containing alloy T_b/T_e.

Composition	1 h T_{emb}, (K)	T_b/T_e
$Fe_{81.5}B_{14.5}Si_4$	600	—
$Fe_{81.5}B_{14.5}Si_{3.9}Sb_{0.1}$	510	1.18
$Fe_{81.5}B_{14.5}Si_{3.9}Se_{0.1}$	<RT	>2.01
$Fe_{81.5}B_{14.5}Si_{3.9}Te_{0.1}$	<RT	>2.01
$Fe_{40}Ni_{40}B_{20}$	600	—
$Fe_{40}Ni_{40}B_{19.9}Sb_{0.1}$	550	1.09
$Fe_{40}Ni_{40}B_{19.9}Se_{0.1}$	400	1.50
$Fe_{40}Ni_{40}B_{19.9}Te_{0.1}$	<RT	>2.01
$Ni_{81.5}B_{14.5}Si_4$	500	—
$Ni_{81.5}B_{14.5}Si_{3.9}Sb_{0.1}$	500	1.00
$Ni_{81.5}B_{14.5}Si_{3.9}Se_{0.1}$	340	1.47
$Ni_{81.5}B_{14.5}Si_{3.9}Te_{0.1}$	300	1.67

shown are not believed to be very much affected by the slight variations in transition metal: metalloid ratio or Si:B ratio in the three base alloy compositions and show apparently increased embrittlement as Ni is replaced by Fe.

Stress relaxation

Stress relaxation of ribbon samples was conducted as described by Luborsky *et al.* [15]. The results are an indication of the extent to which atomic rearrangement occurs during a given annealing treatment. A stress relief fraction of 1.0 corresponds to complete relaxation of the ribbon. As an example, the data taken for the $Ni_{81.5}B_{14.5}Si_4$ alloy series as a function of average ribbon thickness is shown in Fig. 4. The decrease in stress relief with increased ribbon thickness is presumably the result of self-annealing of the ribbon during casting, as discussed earlier. By determining the stress relaxations for a given sample thickness on the data curves shown in Fig. 4, the dependence of ribbon stress relaxation on embrittler concentration for various ribbon thicknesses may be plotted, as shown in Fig. 5. Note that these plots are linear because only two data points are available per ribbon composition and thickness. Table 3 lists the

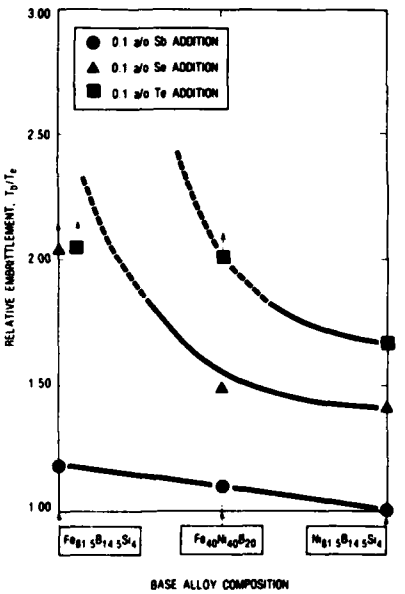

Fig. 3. Relative embrittlement (T_b/T_e) as a function of base alloy composition and 0.1 at.% embrittler species.

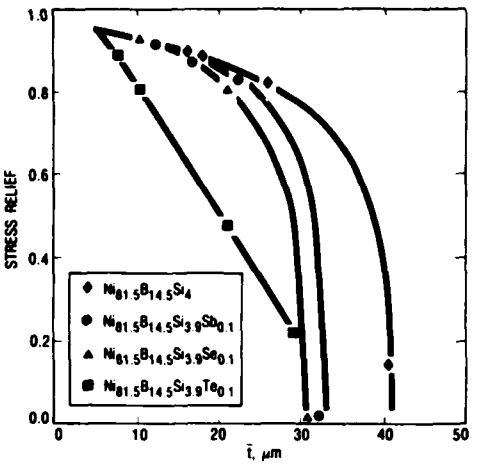

Fig. 4. Stress relaxation data for the $Ni_{81.5}B_{14.5}Si_4$ glassy alloy series is a function of average ribbon thickness. Samples were annealed 2 h at 498 K for relaxation.

Table 3. Linearized dependence of stress relaxation on embrittler content as a function of embrittler species and average sample thickness.

Base alloy	Embrittler	$\bar{t}$, μm	$-d(\sigma R)/dC$
$Fe_{81.5}B_{14.5}Si_4$	Sb	20	0.0
	Se	20	0.0
	Te	20	0.0
	Sb	30	1.5
	Se	30	1.5
	Te	30	2.5
	Sb	35	2.7
	Se	35	2.1
	Te	35	>5
$Fe_{40}Ni_{40}B_{20}$	Sb	20	0.8
	Se	20	0.8
	Te	20	3.4
	Sb	30	3.1
	Se	30	1.9
	Te	30	>5
	Sb	35	>5
	Se	35	3.5
	Te	35	>5
$Ni_{81.5}B_{14.5}Si_4$	Sb	10	0.0
	Se	10	0.0
	Te	10	0.8
	Sb	20	0.0
	Se	20	0.0
	Te	20	3.3
	Sb	30	1.5
	Se	30	3.2
	Te	30	5.7

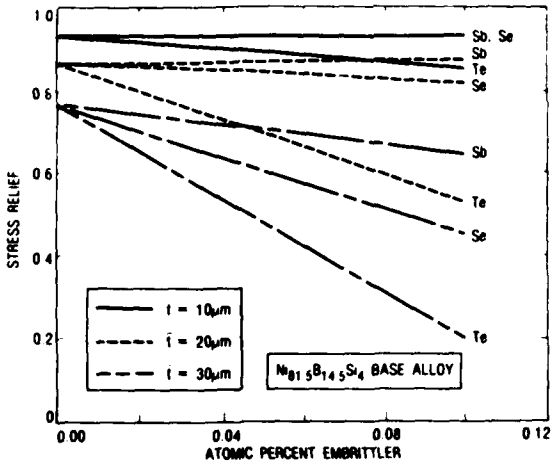

Fig. 5. Stress relaxation as a function of glassy alloy embrittler content and average ribbon thickness for the $Ni_{81.5}B_{14.5}Si_4$ alloy series.

slopes of the lines generated in such a fashion and thereby gives the extent to which atomic rearrangements occur on annealing with the addition of the three embrittlers to the base alloys. For a given ribbon thickness, a large negative value of $d\sigma/dC$ indicates a system for which the stress relaxation depends greatly on embrittler content.

Thermal and magnetic measurements

Differential scanning calorimetry (DSC) has been used to obtain start-of-crystallization temperatures, T_x^s, and crystallization peak temperatures, T_x^p, for sample compositions as listed in Table 4. The results show a slight decrease in crystallization temperature of the $Fe_{81.5}B_{14.5}Si_4$ alloy when replacing 0.1 at.% Si with Te. The scatter in the $Fe_{40}Ni_{40}B_{20}$ base alloy data shows no systematic trend. The $Ni_{81.5}B_{14.5}Si_4$ metallic glass temperatures are given for comparison with those of the other two base alloys.

As-cast ductile glassy alloy ribbons having nominal compositions $Fe_{40}Ni_{40}B_{20}$, $Fe_{40}Ni_{40}B_{19.8}Sb_{0.2}$, and $Fe_{40}Ni_{19.9}Se_{0.1}$ with similar cross-sections ($\sim 12\,\mu m \times 0.9$ mm) all were measured to have a magnetic coercivity of $\sim 1.3\,Am^{-1}$ (160 mOe) in a longitudinal drive field of $800\,Am^{-1}$ (10 Oe). A subsequent 1.5 hour anneal of these samples at 623 K reduced the magnetic coercivity to $\sim 0.6\,Am^{-1}$ (70 mOe). After this annealing treatment, only the Sb and Se-bearing samples showed embrittlement. Longer annealing times resulted in substantial embrittlement due to crystallization and a corresponding coercive field increase.

Table 4. Crystallization start, T_x^s and peak temperatures, T_x^p, as obtained by DSC at 40 K min.

Composition	T_{x1}^s (K)	T_{x1}^p (K)	T_{x2}^s (K)	T_{x2}^p (K)
$Fe_{81.5}B_{14.5}Si_4$	784	799	820	833
$Fe_{81.5}B_{14.5}Si_{3.9}Te_{0.1}$	777	793	813	827
$Fe_{40}Ni_{40}B_{20}$	699	727		
$Fe_{40}Ni_{40}B_{19.9}Sb_{0.1}$	708	734		
$Fe_{40}Ni_{40}B_{19.9}Se_{0.1}$	700	732		
$Ni_{81.5}B_{14.5}Si_4$	703	720		

CONCLUDING REMARKS

Enhanced temper embrittlement in Fe and/or Ni-based metallic glasses by small additions of Sb, Se and Te has been found in the present investigation. The precise embrittlement mechanism remains to be defined. From the present work, it appears that the embrittling strength of the elements investigated scales as Te > Se ≫ Sb, which is the same sequence found in steels [1]. Furthermore, the embrittling strength of P is feeble by comparison. For all of these embrittling elements, loss of metallic glass ductility is accelerated with increased embrittler content, as is exemplified in Table 1 for the case of Sb in $Fe_{40}Ni_{40}B_{20}$ base metallic glass. Walter *et al.* [6] have proposed an embrittlement model based on fast diffusion of the smaller metalloid atoms to form highly localized clusters which embrittle the sample. While such a concept perhaps seems feasible for explaining the temper embrittlement of metallic glasses containing P and smaller metalloids, it seems unlikely that atoms as large as the embrittlers studied in the present investigation would be capable of extensive diffusion at the annealing temperatures and times used. Furthermore, it is remarkable that the embrittling strength of these elements is as strong as has been shown in view of the relatively low atomic mobility anticipated.

Unlike the contention by Chen [16] that glassy alloy embrittlement comes about through incomplete filling of transition metal *3d* electron shells, and the

Walter *et al.* concept of long range metalloid diffusion, it seems that embrittlement by an individual species of atom in a metallic glass depends on a combination of aspects such as embrittler electronegativity and ionic size. The embrittler strength scales with neither electronegativity nor size alone. Figure 1 shows that similar embrittlement behaviors may be exhibited by Sb-bearing and Se and Te-bearing glassy alloys by simply increasing the content of the weaker embrittling element. Thus, embrittlement in metallic glasses most likely is based on the ability of embrittler atoms to localize electrons from the matrix.

Embrittlement of metallic glasses occurs as the result of annealing, whether intentionally by heat treatment or unintentionally by fabricating ribbon samples which are very thick and/or departing prematurely from the substrate surface on which they are cast. Nevertheless, the ribbons used in the present investigation may be viewed as having undergone varied degrees of heat treatment during casting, depending on the particular process conditions and sample composition used. Evidence for this appears in Table 1, in which the t_d^m of only the $Ni_{81.5}B_{14.5}Si_4$ metallic glasses are independent of embrittler additions. Both the $Fe_{81.5}B_{14.5}Si_4$ and the $Fe_{40}Ni_{40}B_{20}$ base glassy alloys show a variation in maximum as-cast ductile ribbon thickness which depends on the embrittler and its concentration. Thus, the anneal to which the ribbon is subjected during casting is sufficient to cause some ductility loss in $Fe_{40}Ni_{40}B_{20}$ and $Fe_{81.5}B_{14.5}Si_4$ ribbons having thickness $> t_d^m$. The ribbons selected for the 1 h annealing embrittlement treatments have therefore intentionally been selected to have a maximum thickness of less than t_d^m in order to have a fully ductile starting sample. However, the varying susceptibility of the various metallic glasses to embrittlement during casting should be considered in the interpretation of the results.

The trends in the stress relaxation data mirror those of the embrittlement data, although fractional change in stress relaxation is not as great as fractional change in bend ductility after a given anneal. This correspondence between stress relaxation and embrittlement data exists because the reduced stress relaxation observed during embrittlement indicates reduced atomic motion and presumably results from reduced atomic mobility caused by the embrittler atoms. A concurrent atomic mechanism resulting in reduced stress relaxation is the densification (reduction in free volume) found when metallic glasses are annealed. Thus, the contribution to stress relaxation due to embrittler atoms is rather small when the prominent contribution due to densification is subtracted out.

The DSC and magnetic measurements show that although glassy alloy embrittlement may occur as a result of low temperature annealing, the crystallization characteristics and structure-sensitive magnetic coercivity are relatively unaffected by small additions of embrittling elements. Finally, since the samples annealed to embrittlement show no detectable coercivity changes, the embrittler-induced atom localization is probably on a very fine scale.

Acknowledgements The authors are grateful to N. A Marotta for the DSC runs, S. J. Kelly for the magnetic measurements, and to C. L. Briant for helpful discussions and critical reading of the manuscript.

REFERENCES

1. C. J. McMahon, *Grain Boundaries in Engineering Materials* (Edited by J. L. Walter *et al*) p. 525, Claitor's Publishing (1975).
2. C. L. Briant and S. K. Banerji, *Int. Metall. Rev.* **23**, 164 (1978).
3. D. G. Ast and D. Krenitsky, *Mater. Sci. Engng.* **23**, 246 (1976).
4. F. E. Luborsky and J. L. Walter, *J. appl. Phys.* **47**, 3648 (1976).
5. R. S. Williams and T. Egami, *IEEE Trans. Mag.* **MAG-12**, 927 (1976).
6. J. L. Walter, F Bacon and F. E. Luborsky, *Mater. Sci. Engng.* **24**, 239 (1976).
7. J. L. Walter and F. E. Luborsky, *Mater. Sci. Engng.* **33**, 91 (1978).
8. R. S. Williams and T. Egami, *Rapidly Quenched Metals III* Vol. I, p. 214, The Metals Society, London (1978).
9. M. Guttmann and D. McLean, *Interfacial Segregation* (Edited by W. C. Johnson and J. M. Blakely) p. 261 ASM (1979).
10. G. C. Chi, H. S. Chen and C. E. Miller, *J. appl. Phys.* **49**, 1715 (1978).
11. H. H. Liebermann, *J. Mater. Sci.* **15**, 2771 (1980).
12. F. E. Luborsky, H. H. Liebermann and J. L. Walter, *Proc. Conf. Metallic Glasses*, Budapest (1980).
13. H. H. Liebermann, *Mater. Sci. Engng* **43**, 203 (1980).
14. P. Kozakevitch, *Surface Phenomena of Metals*, p. 223, S.C.I. Monograph No. 28, Society of Chemical Industry, London (1968).
15. F. E. Luborsky, J. J. Becker and R. O. McCary, *IEEE Trans. Mag.* **MAG-11**, 1644 (1975).
16. H. S. Chen, *Mater. Sci. Engng.* **26**, 79 (1976).

GENERAL ELECTRIC

General Electric Company
Corporate Research and Development
Schenectady, New York

TECHNICAL INFORMATION SERIES

AUTHOR
Luborsky, FE
Liebermann, HH

SUBJECT
amorphous alloy preparation

NO
81CRD060

DATE
March 1981

TITLE
Effect of Melt Temperature on Some Properties of $Fe_{80.5}B_{15}Si_4C_{0.5}$ and $Fe_{40}Ni_{40}B_{20}$ Amorphous Alloys

GE CLASS
1

NO PAGES
4

ORIGINATING COMPONENT
Metallurgy Laboratory

CORPORATE RESEARCH AND DEVELOPMENT
SCHENECTADY, N.Y.

SUMMARY

Increasing the melt temperature T_m of $Fe_{80.5}B_{15}Si_4C_{0.5}$ and $Fe_{40}Ni_{40}B_{20}$ liquid alloys increases the width and decreases the thickness of melt-spun ribbons as predicted by a solidification model based on the propagation of a thermal boundary layer. Increasing T_m is shown to decrease the as-cast ribbon coercivity, increase relative induction, and not affect Curie temperature. After annealing, these magnetic properties are independent of T_m. It is concluded that the dependence of the as-cast ribbon properties on T_m is due to decreasing residual stress in the ribbon with increasing T_m. As T_m increases, ribbon stress relaxation decreases as does the temperature required to embrittle the amorphous alloy. These trends in properties of amorphous ribbons suggest that there is a unique atomic structure in the amorphous ribbon corresponding to a given liquid alloy T_m.

KEY WORDS

amorphous alloys, preparation of amorphous alloys, stress relaxation, embrittlement

INFORMATION PREPARED FOR _____

Additional Hard or Microfiche Copies Available From

Technical Information Exchange
Bldg. 81 Room A133, Schenectady, N.Y., 12345

EFFECT OF MELT TEMPERATURE ON SOME PROPERTIES OF $Fe_{80.5}B_{15}Si_4C_{0.5}$ AND $Fe_{40}Ni_{40}B_{20}$ AMORPHOUS ALLOYS

F.E. Luborsky and H.H. Liebermann

INTRODUCTION

Several reports describing the effects of temperature on the properties of melt-spun amorphous ribbons have recently been published. The first of these[1] showed that the Curie temperature T_c, saturation magnetization M_s, crystallization temperature T_x, and microhardness H_v, for $Fe_{40}Ni_{40}B_{20}$ amorphous alloy were all independent of the melt temperature T_m. However the coercivity H_c was reported to have increased, the remnant induction B_r to have decreased slightly, and the maximum permeability μ_{max} to have decreased substantially as T_m increased. These results were discussed in terms of additional annealing during casting due to the increase in ribbon temperature caused by the increase in T_m. This ad nal annealing presumably resulted in a less di ed atomic structure.

In another report[2] crohardness, brittleness, and coercivity of Fe oys were studied. It was claimed that T_m affected H_v. Changes in H_v of up to 3 kN/mm^2 were reported over the melt temperature range of 1500 to 1700 K, while changes of 8 kN/mm^2 were reported for boron concentration range of $11.72 \leqslant B \leqslant 23.5$ at.%. It was further reported that the T_m-dependence of ribbon ductility changed in a sense opposite to that of H_v. The report shows further that H_c of as-quenched ribbons increases and then decreases with increasing T_m when using a constant linear substrate surface velocity during casting. The authors report the reverse property trend for casting on a wheel rotating with twice the linear substrate velocity. No trend in H_c was observable after stress relief annealing. Finally, it was concluded that the decrease in H_c on annealing was a consequence of the accompanying reduction in stresses and the change in H_v is a consequence of atomic short range ordering. No explanation was given for the subsequent increase in H_c. The same authors[3] studied the $Fe_{83.4}B_{16.6}$ glassy alloy in detail finding that H_c decreased with increased T_m.

In view of the varied behaviors reported for the effect of the melt temperature on amorphous ribbon properties, we have studied the T_m-dependence of the properties for two alloy compositions. $Fe_{80.5}B_{15}Si_4C_{0.5}$ was chosen as an example of a technologically useful alloy having high saturation magnetization and high magnetostriction; $Fe_{40}Ni_{40}B_{20}$, having about one-third the magnetostriction of the Fe-B-Si-C alloy, was chosen because of its potential for application in electronic devices where high permeability may be most important.

EXPERIMENTAL

Ribbon samples were prepared by chill block melt-spinning in vacuum using a 12.5-cm diameter OFHC copper wheel, quartz crucible with 0.51-mm orifice diameter, 0.7 kg/cm^2 Ar ejection pressure, 3-mm orifice-substrate spacing, perpendicular melt jet impingement, and a linear substrate velocity of 40 m/s for $Fe_{80.5}B_{15}Si_4C_{0.5}$ (analyzed) and 33 m/s for $Fe_{40}Ni_{40}B_{20}$ (nominal). Melt temperature was monitored with a thermocouple. Ribbon thicknesses t were determined both with a micrometer (maximum thickness) and by calculation from $t = m/(\rho \cdot l \cdot w)$; m = mass, ρ = density, l = length, and w = width of the ribbon. The intrinsic coercivity H_c and induction in 1 Oe field B_1 were measured using an integrating fluxmeter system[4] on 15-cm long samples. Annealing was carried out in a longitudinal field of 25 Oe for 2 h and the sample cooled in the field at about 0.5 °C/min. Stress relaxation was measured after annealing for 2 h at 225 and 300 °C by measuring the radius of curvature of a relaxed length of ribbon after annealing it constrained to a small diameter.[5] Sample brittleness was measured after various 2 h anneals by determining the radius of curvature required to fracture the ribbon.[6]

RESULTS AND DISCUSSION

The width and thickness of $Fe_{40}Ni_{40}B_{20}$ and $Fe_{80.5}B_{15}Si_4C_{0.5}$ amorphous alloy ribbons cast using various superheats are plotted against melt temperature in Figure 1. The slope of 0.73 μm/K for the average ribbon width data shown is in fair accord with the 1.00 μm/K slope predicted by a ribbon formation model based on the propagation of a thermal boundary layer, as proposed by Kavesh[7,8] under the experimental conditions we used. Similarly, the −9.6 nm/K slope for the ribbon thick-

Manuscript received March 11, 1981

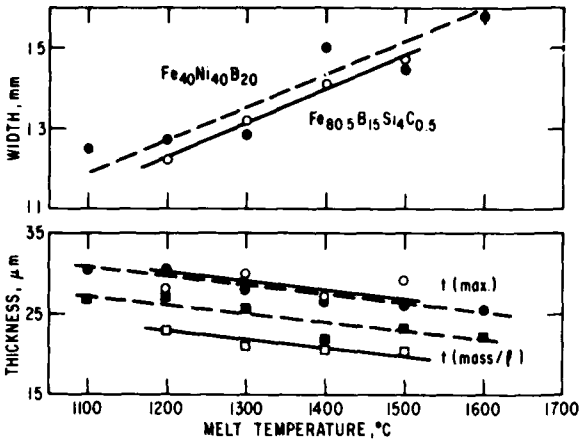

Figure 1. Effect of melt temperature on melt-spun amorphous ribbon width and thickness.

ness data is in compliance with the −8.3 nm/K figure predicted by the thermal boundary layer model. In spite of this agreement, absolute values of amorphous alloy ribbon width and thickness were greater and less, respectively, than the experimental figures when calculated using the thermal boundary layer model. This may be due to differences in solidification caused by differences in melt puddle shape between the vacuum melt-spinning results of the present investigation and the results of Kavesh obtained by casting in air. The fact that the data of maximum (micrometer) and average ribbon thickness vs. melt superheat are parallel (Figure 1) indicates that the average amorphous alloy ribbon surface roughness is independent of superheats, although the topography of this surface roughness may vary.

H_c and B_1/B_{100} vs T_m are shown in Figure 2 for Fe-B-Si-C and in Figure 3 for Fe-Ni-B amorphous ribbon, both in the as-cast state and after various 2 h anneals. In the as-cast state, both alloys exhibit a decrease in H_c and an increase in B_1/B_{100} with increased T_m. After annealing, this T_m-dependence disappears at ~335±10 °C for both alloys, indicating that the original dependence is most likely caused by quenched-in residual stresses in the ribbons. In fact, the 2 h anneal at 335 °C resulting in the disappearance of the T_m-dependence of ribbon properties is that required for complete stress relaxation.[5]

The Curie temperature measured by thermogravimetric analysis at 20 °C/min showed no trend with T_m: 379±1 °C for Fe-B-Si-C and 403±2 °C for Fe-Ni-B. Differential scanning calorimetry at 80 °C/min revealed no systematic trend in Curie temperature with T_m: 376±2 °C for Fe-B-Si-C and 399±2 °C for Fe-Ni-B. The same scans showed an

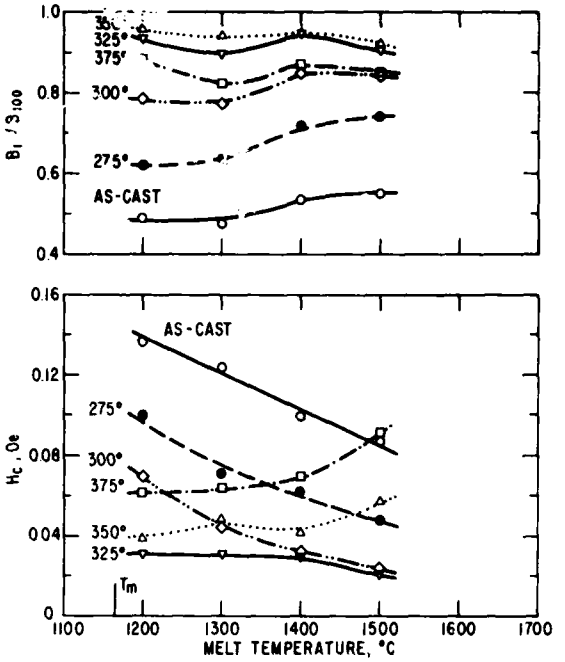

Figure 2. Effect of $Fe_{80.5}B_{15}Si_4C_{0.5}$ melt temperature on amorphous ribbon induction in 1 Oe field and on coercivity as a function of annealing for 2 h at various temperatures. The melt temperature T_m is indicated.

invariant start-of-crystallization temperature with T_m: 782±4 °C for Fe-B-Si-C and 711±4 °C for Fe-Ni-B. The glass transition endotherm was not clearly discernible in any of the scans. There was no evidence in the thermogravimetric or DSC scans for the existence of crystallites in the as-cast samples.

Stress relaxation for both alloys decreases with increased T_m, as shown in Figure 4. It is further shown that stress relaxation decreases with increased ribbon thickness, as previously reported.[9,10] This increase in relaxation rate with increasing T_m and ribbon thickness is probably the result of the lower average quench rate due to the greater amount of heat that must be removed during melt-spinning. Thus, a more relaxed atomic structure results when amorphous ribbon is cast when using a higher T_m or making a thicker ribbon. It should be noted that the increase in melt temperature, which causes the melt to become more disordered, could lead to an atomically more disordered ribbon, contrary to the results observed. Thus, the effect of the lower average ribbon quench rate due to the greater amount of heat which must be removed as T_m increases is dominant over the possible competing mechanism of the effect of

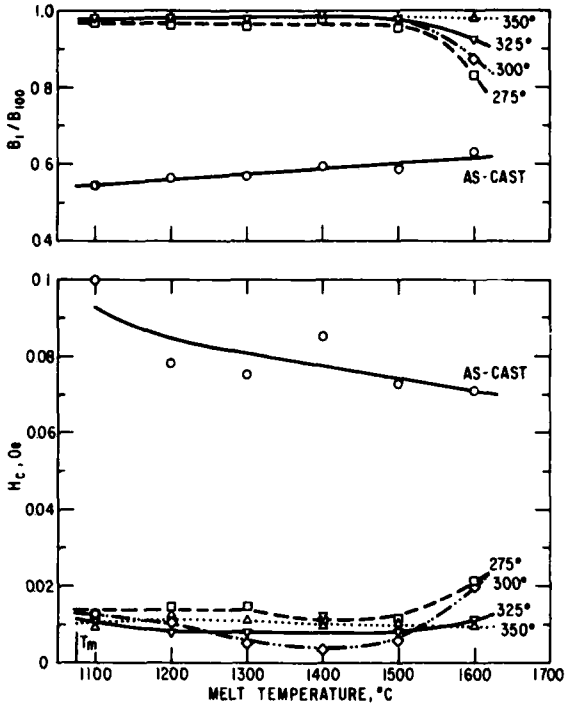

Figure 3. Effect of $Fe_{40}Ni_{40}B_{20}$ melt temperature on amorphous ribbon induction in 1 Oe field and on coercivity as a function of annealing for 2 h at various temperatures. The melt temperature T_m is indicated.

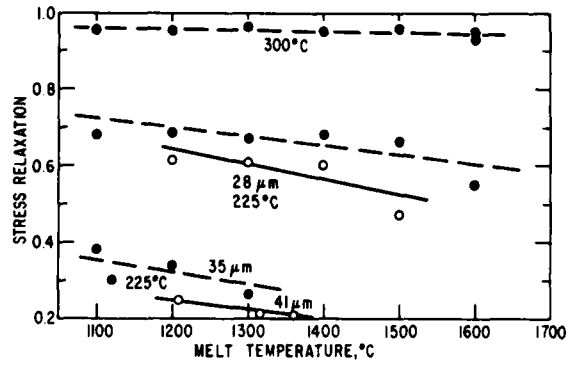

Figure 4. Effect of melt temperature on amorphous ribbon stress relaxation after annealing 2 h at 225 and 300 °C. Solid lines for $Fe_{80.5}B_{15}Si_4C_{0.5}$, dashed lines for $Fe_{40}Ni_{40}B_{20}$.

increased atomic disorder in the melt as T_m increases.

The brittleness, as measured by the strain-to-fracture ratio, is shown in Figure 5 for Fe-B-Si-C and in Figure 6 for the Fe-Ni-B as a function of T_m. These changes on annealing also suggest a

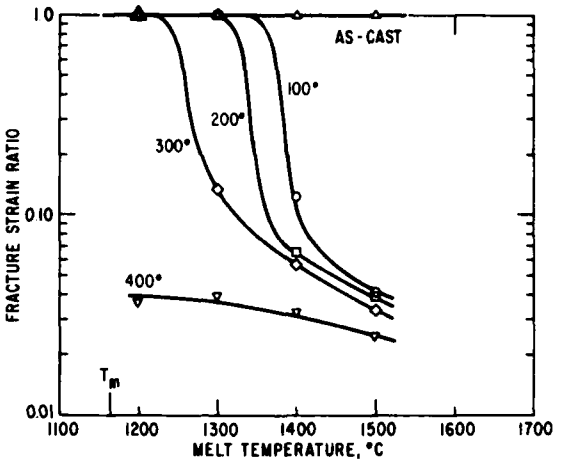

Figure 5. Effect of $Fe_{80.5}B_{15}Si_4C_{0.5}$ melt temperature on amorphous ribbon fracture strain ratio after annealing for 2 h at various temperatures. The melt temperature T_m is indicated.

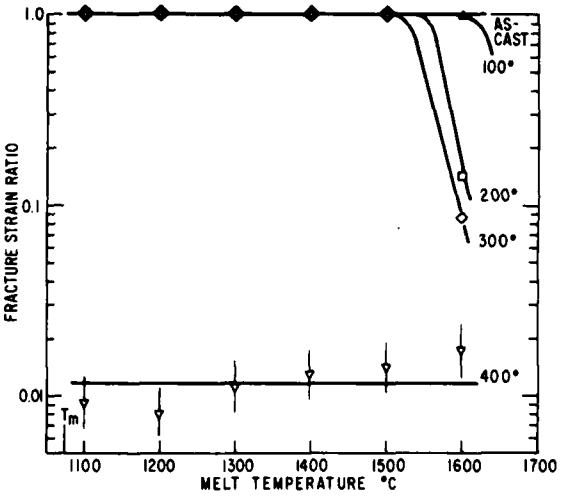

Figure 6. Effect of $Fe_{40}Ni_{40}B_{20}$ melt temperature on amorphous ribbon fracture strain ratio after annealing for 2 h at various temperatures. The melt temperature T_m is indicated.

different atomic structure for samples made at various T_m. The correlation between stress-relaxation and fracture strain is the same here as previously observed on changing ribbon thickness by changing wheel speed,[10] i.e., the stress-relaxation rate and embrittlement temperature increase with decreasing thickness (increasng substrate velocity). In the present work, stress relaxation and embrittlement temperature increase with decreasing T_m. We assume, as before,[10] that the atomic processes

associated with stress relaxation and with embrittlement respond differently to the average quench rate.

CONCLUSIONS AND SUMMARY

The variation of ribbon width and thickness with liquid alloy T_m follows the predictions of a solidification model based on the propagation of a thermal boundary layer, although absolute values of ribbon width and thickness are not well described by this model. The magnetic properties of the ribbon in the as-cast condition are most likely dominated by the internal stresses which are affected by T_m. The magnetic properties are independent of T_m after stress relief annealing. The stress relaxation rate varies inversely with T_m due to the lower average quench rate resulting from the increase in T_m. The temperature required to embrittle the ribbons increases as T_m decreases, in agreement with previous results on the change in quench rate brought about by the changes in ribbon thickness.

ACKNOWLEDGMENT

The authors wish to thank J. Gillespie for the magnetic measurements.

REFERENCES

1. S. Takayama and T. Oi, *J. Appl. Phys. 50,* 1595 (1979).
2. A. Lovas, C. Hargitai, E. Kisdi-Koszo, J. Takacs, J. Kiraly, and G. Sos, *J. Magnetism and Mag. Mat. 19,* 168 (1980).
3. L. Novak, L. Potocky, A. Lovas, E. Kisdi-Koszo, and J. Takacs, *J. Magnetism and Magn. Mat. 19,* 149 (1980).
4. F.E. Luborsky, J.J. Becker, and R.O. McCary, *IEEE Trans. Magnetics MAG-11,* 1644 (1975).
5. F.E. Luborsky and J.L. Walter, *Materials Science Eng. 35,* 255 (1978).
6. J.L. Walter and F.E. Luborsky, *Materials Science and Eng. 33,* 91 (1978).
7. S. Kavesh, *Metallic Glasses,* edited by H.J. Leamy and J.J. Gilman, Amer. Soc. Metals, Menlo Park, Ohio, 1977, p. 76.
8. S. Kavesh, Conf. on Melting and Solidification of Metals: Theory and Practice, General Electric Corporate Research and Development, Schenectady, N.Y., May 1978.
9. F.E. Luborsky and H.H. Liebermann, *J. Appl. Phys. 51,* 796 (1980).
10. F.E. Luborsky, H.H. Liebermann, and J.L. Walter, *Proc. Conf. Metallic Glasses,* Budapest 1980. Published by Kultura Foreign Trade Co., P.O. Box 149, Hungary, H-1389.

GENERAL ELECTRIC

General Electric Company
Corporate Research and Development
Schenectady, New York

TECHNICAL INFORMATION SERIES

AUTHOR
Luborsky, FE, Huang, SC,
Fiedler, HC

NO 81CRD062
DATE April 1981

TITLE
Effect of Surface Features of Amorphous Alloys on Magnetic Behavior

GE CLASS 1
NO. PAGES 4

ORIGINATING COMPONENT
Metallurgy Laboratory
CORPORATE RESEARCH AND DEVELOPMENT SCHENECTADY, N.Y.

SUMMARY

Air pockets were found on amorphous ribbons of Fe-B-Si and Fe-B-Si-C with different sizes, shapes, and orientations due to differences in processing conditions. The coercivity decreased and the magnetization in low fields increased as the size of the air pockets decreased. The coercivity was always higher, and the magnetization lower, for air pockets oriented parallel to the ribbon length. The same trends remained after stress relief annealing. Application of tensile stress produced changes correlated to differences in air pocket size and orientation. The 60 Hz coercivity, loss, and maximum drive field exhibited the same trends as the dc coercivity with changes in air pocket size and orientation. The difference between H_c (60 Hz) and H_c (dc) increased with decrease in air pocket size. It is concluded that the air pockets influence the magnetic properties of ribbon by providing wall pinning sites which control the number and motion of walls present during magnetization reversal.

SUBJECT
amorphous alloys, magnetic properties, surface features

KEY WORDS
amorphous alloys, magnetic properties, surfaces

INFORMATION PREPARED FOR _____

_____

Additional Hard or Microfiche Copies Available From

Technical Information Exchange
Bldg. 81 Room A133, Schenectady, N.Y., 12345

EFFECT OF SURFACE FEATURES OF AMORPHOUS ALLOYS ON MAGNETIC BEHAVIOR

F.E. Luborsky, S.C. Huang, and H.C. Fiedler

INTRODUCTION

It is well known that the magnetic properties of thin ribbons are influenced by pinning sites on the ribbon surfaces.[1-3] These pinning sites can be due to inclusions, strains, or surface irregularities, all of which impede wall motion. In the case of amorphous ribbons prepared by rapid quenching, air bubbles are trapped on the underside of the molten metal in contact with the quenching surface of the wheel.[4] This results in a pattern of "air pockets" on the underside of the ribbon and a corresponding depression on the top side of the ribbon. The size, shape, concentration, and orientation can be controlled by suitable adjustment of the processing parameters.[4] It was also shown that the atmosphere controls the uniformity of the surfaces and edges[5] as well as the magnetic quality[6] of the ribbon. These air pockets produce a strain distribution around them due to the different cooling rate. Thus, in the as-cast ribbons, both the physical geometry of the air pockets and their resulting strain distribution would be expected to influence the magnetic properties. After a stress relief anneal, only the geometry of the air pockets remains to influence the magnetic properties, although a stress induced anisotropy may be produced from the original strain pattern which will also influence the domain configuration and thus the properties.

The influence of an applied stress to ribbons should give us some information about the state of stress in as-cast ribbons. In particular, the stress required to orient the magnetization in the stress direction should be related to the magnitude and orientation distribution of the internal stress. Furthermore, the 60 Hz magnetic properties will depend on the number and structure of the walls developed during reversal. This in turn may depend on the size, shape, concentration, and orientation of the air pockets and the interaction of applied stresses with the internal stresses.

In this report, we will examine the relations between the air-pocket structure and the dc and 60 Hz magnetic properties and the influence of stress on these properties. These results will be discussed in terms of wall pinning.

EXPERIMENTAL

Samples were prepared with different surface features, as shown by some of the typical micrographs in Figure 1, by varying the wheel surface preparation.[4] Similar differences in features were observed on samples of ribbon from outside sources. All samples were 1.2 to 2.5 cm in width.

The effect of these different surface features on the dc and 60 Hz coercivity and magnetization in low fields for straight ribbons in the as-cast and annealed states was determined. In addition, the effect of tensile stress on these properties was determined.

RESULTS AND DISCUSSION

The coercivity H_c and magnetization ratio in 1 Oe to 100 Oe field, B_1/B_{100}, for samples as-cast and for samples annealed to their minimum coercivity are shown in Figures 2 and 3. The abscissa is an approximate scale for the size of the air pocketing ranging from very large air pockets in ribbons cast under certain conditions to very smooth surfaces displayed in vacuum-cast material. This decrease in H_c for vacuum-cast ribbons compared to air-cast ribbons has been reported previously[7] for ribbons in the Fe-B series. Although there is considerable scatter, particularly in the as-cast results, the decrease in H_c and increase in B_1/B_{100} with decreasing air-pocket size is clear. This effect

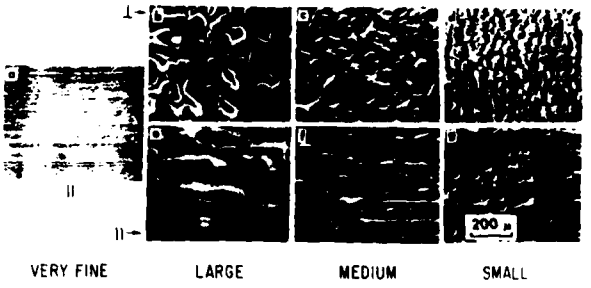

Figure 1. Air pockets observed in the scanning electron microscope on the underside of various samples. Casting direction is horizontal. Ribbon *a* cast in vacuum, remainder cast in air; *b*, *c* and *d* exhibit perpendicular air pockets; *e*, *f* and *g* exhibit parallel air pockets. All for $Fe_{81.5}B_{14.5}Si_4$ alloys.

Manuscript received March 11, 1981

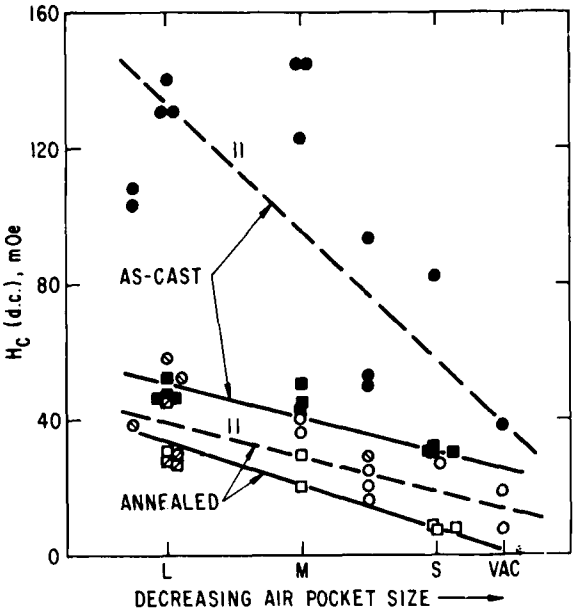

Figure 2. Coercive field as a function of air pocket size for parallel (○) and perpendicular (□) oriented air pockets in the as-cast (solid symbols) and annealed (open symbols) states for straight ribbons. Annealed for 2 h at 327±5 °C (○,□); at 350±5 °C (⊘,⊡); and at 367±3 °C (⊘,⊠).

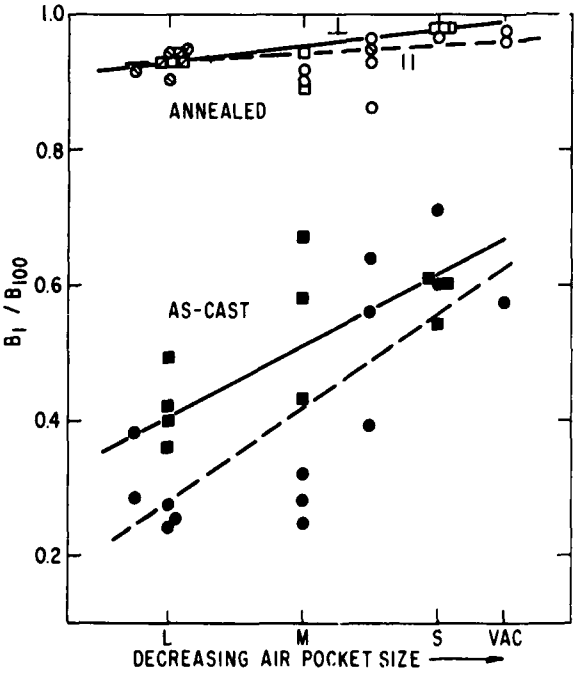

Figure 3. Magnetization ratio in 1 Oe field to 100 Oe field for the same samples as in Figure 3.

on the as-cast results is attributed to the interaction of domain walls with these surface defects and with the associated stresses around these defects; the larger the defect size the greater the pinning and thus the higher the H_c and the lower the B_1/B_{100}. The lower B_1/B_{100} may also be due to the rotation of the magnetization away from the easy axis due to these strains. Furthermore, the orientation of the surface defects would be expected to influence H_c and B_1/B_{100}; the parallel orientation would be expected to interact more strongly with the parallel orientation of the walls as is observed. The fact that the slopes of the curves in Figure 2 change on annealing suggests that stresses are also contributing to the observed H_c and B_1/B_{100}. The remaining dependence of H_c and B_1/B_{100} on air pocket size after annealing to remove the internal stresses is attributed to just the influence of the geometry and distribution of air pockets on wall pinning.

The effect of stresses on H_c and the stress to produce the minimum H_c for as-cast ribbons are shown in Figure 4. The remarkable feature of the effect of stress on these samples is the variability of the response. In most cases, increasing stress reduces H_c, but in the case of the large perpendicular air pockets, increasing stress increases H_c. Furthermore, in some cases, H_c first decreased to a minimum and then increased on application of stress, but in the case of large parallel air pockets,

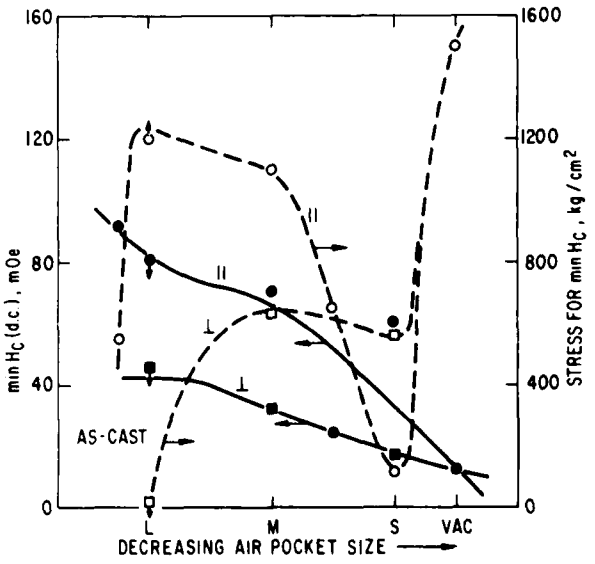

Figure 4. The minimum H_c achieved on applying tensile stress and the stress required to achieve the minimum H_c as a function of air pocket size for samples with air pockets oriented parallel and perpendicular to the casting direction. Samples all in as-cast state.

no minimum was achieved up to stresses of 1200 kg/cm^2. In all cases the minimum H_c achieved on application of stress is always greater for samples with parallel-oriented air pocketing as compared to perpendicular-oriented air pocketing (Figure 4). Further, the stress required to achieve the minimum H_c is typically greater for the parallel-oriented air pockets compared to the perpendicular-oriented air pockets; in fact, the larger the air pockets, in general, the greater the difference in stress between parallel and perpendicular air pockets required to achieve the minimum H_c (Figure 4). If we examine the curves in more detail, we find that the H_c drops very rapidly on application of stress to samples with parallel-oriented air pockets, while H_c decreases only very slowly on application of stress to samples with perpendicular air pockets. The samples with the large air pockets and the vacuum-cast ribbon with essentially no air pockets show no minimum. We attribute all of these effects qualitatively to the stresses developed around the air pockets during the casting of the ribbon and the interaction of these internal stresses with the applied stress.

The behavior of the magnetization B_s/B_{100} with applied stress helps to elucidate the changes in anisotropy with applied stress. As in the case of the changes in H_c with stress, the results of changes in B_s/B_{100} with stress also show a wide spectrum of behavior; some samples extrapolate to $B_s/B_{100} = 1$ as $\sigma \rightarrow \infty$ using a $1/\sigma$ plot; other samples extrapolate to values less than 1; still other samples become independent of σ at high values of σ. The following correlations appear to hold: the samples with parallel air pockets approach higher values of B_s/B_{100} on application of stress than samples with perpendicular air pockets. The smaller the air pockets, the higher the value of B_s/B_{100} and for the vacuum-cast sample $B_s/B_{100} \rightarrow 1$ as $1/\sigma \rightarrow 0$. These results can also be qualitatively attributed to the stresses developed around the air pockets during casting.

The ac characteristics measured at 60 Hz using sine flux drive conditions show the same correlations as for the dc results (Figure 5). The difference between ac and dc H_c [i.e., H_c(60 Hz) − H_c(dc) = ΔH_c] appeared to increase with decrease in air pocket size (Figure 6). This suggests that the number of walls is probably decreasing with decrease in air pocket size. It was further observed that ΔH_c decreased on annealing, reached a minimum value at the minimum H_c, and then increased again. Some typical results are shown in Table 1 for two different samples.

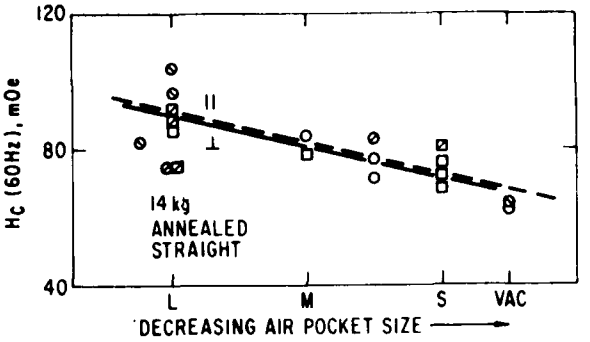

Figure 5. The 60 Hz coercivity measured at 14 kG as a function of air pocket size for straight ribbons annealed to their minimum coercivity with air pockets oriented parallel (○) and perpendicular (□) to the casting direction. Annealed for 2 h at 327±3 °C (○, □); at 350±5 °C (⊘, ⊡); and at 367±3 °C (⊙, ⊠).

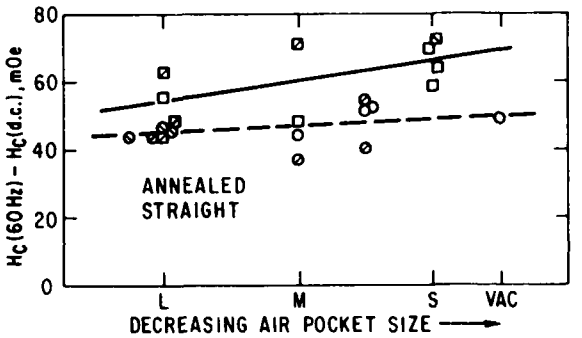

Figure 6. The difference between 60 Hz and dc coercive field for the same samples as in Figure 5.

Table 1
EFFECT OF ANNEALING ON H_c and ΔH_c

Sample	Anneal Temp. (°C)	H_c(ac) (Oe)	ΔH_c (Oe)	Sample Diameter (cm)
LMD521	325	0.12	0.080	4.3
	345	0.092	0.044	4.3
	365	0.092	0.027	4.3
	385	0.21	0.082	4.3
031380WW1	340	0.12	0.095	2.3
	350	0.11	0.079	4.3
	360	0.11	0.062	2.3
	365	0.10	0.054	4.3
	380	0.16	0.077	2.3

Even though the ΔH_c increased with decrease in air pocket size, the decrease in H_c (60 Hz) causes the loss, after stress relief annealing, to decrease slightly, as shown in Figure 7 for straight ribbons.

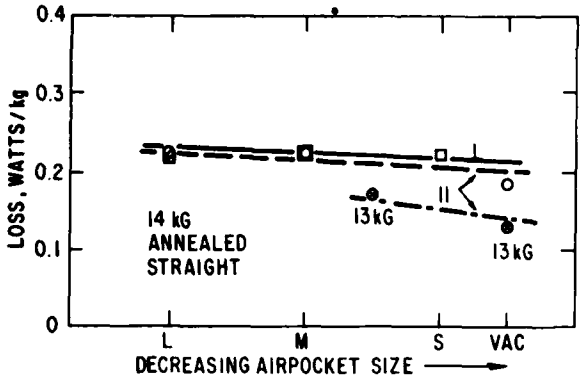

Figure 7. Magnetic loss at 60 Hz for the same samples as in Figure 5.

In addition, the increased squareness of the hysteresis loop with decrease in air pocket size (Figure 3) would be expected to decrease H_{max}. As shown in Figure 8, the large scatter in the results makes this conclusion very uncertain.

The effect of winding a toroid on H_c is shown in Figure 9. The difference between the H_c of the toroid and the H_c of the straight strip is shown to be independent of the air pocket size. However, it should be noted that the H_c of the toroid is up to 20 mOe higher, on average, than the H_c of a straight ribbon.

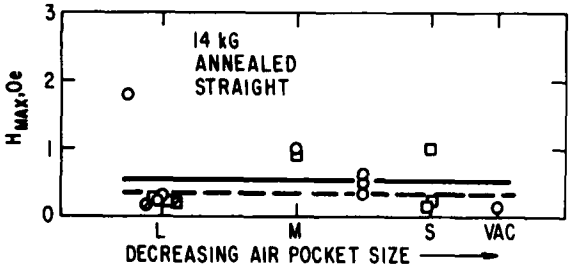

Figure 8. The field required to drive the sample to 14 kG for the same samples as in Figure 5.

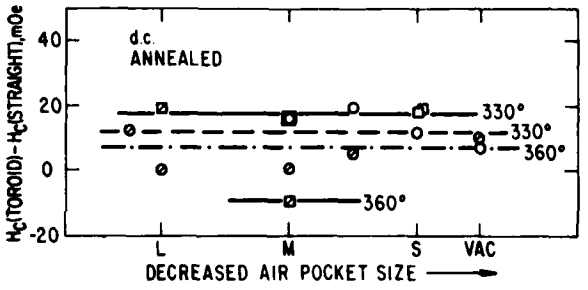

Figure 9. The difference in H_c between a toroid and a straight sample for the same samples as in Figure 5.

SUMMARY

The size and shape of air pockets on amorphous ribbons were found to greatly influence their magnetic properties. Decreasing air pocket size improved the properties both before and after the stress relief anneal. Application of tensile stress produced changes which were also a function of the air pocket size and orientation. It is concluded that the air pockets and the associated stress distribution around them provide pinning sites for the walls, thus influencing wall motion.

ACKNOWLEDGMENT

The authors greatly appreciate the work of S.J. Kelly on magnetic testing.

REFERENCES

1. E.M. Gyorgy, H.J. Leamy, R.C. Sherwood, and H.S. Chen, *AIP Conf. Proc.*, Vol. 29, 1976, p. 198.
2. F.E. Luborsky, *Ferromagnetic Materials*, Vol. 1, E.P. Wohlfarth (ed.), North Holland Publishing Co., N.Y. 1980, Chap. 6, p. 451.
3. H. Kronmuller, *J. de Physique 41*, p. 618, 1980.
4. S.C. Huang and H.C. Fiedler, *Met. Trans.*, submitted.
5. H.H. Liebermann, *Rapidly Quenched Metals III*, Vol. 1, B. Cantor (ed.), The Metals Soc., London, 1978, p. 34.
6. M. Matsura, M. Kikuchi, M. Yagi, and K. Suzuki, *Jap. J. Appl. Phys.*, Vol. 19, 1980, p. 1781.
7. F.E. Luborsky, H.H. Liebermann, J.J. Becker, and J.L. Walter, *Rapidly Quenched Metals III*, Vol. 2, B. Cantor (ed.), The Metals Soc., London, 1978, p. 188.

GENERAL ELECTRIC

General Electric Company
Corporate Research and Development
Schenectady, New York

TECHNICAL INFORMATION SERIES

AUTHOR: Luborsky, FE, Walter, JL, Liebermann, HH	NO. 81CRD123
	DATE July 1981
TITLE: Properties of Amorphous Alloys of Fe-B-Ga and Fe-B-Si-C-Al	GE CLASS 1
	NO. PAGES 5
ORIGINATING COMPONENT: Metallurgy Laboratory	CORPORATE RESEARCH AND DEVELOPMENT SCHENECTADY, N.Y.

SUMMARY

The crystallization temperature, Curie temperature, saturation magnetization, and coercivity of amorphous alloys in the ternary Fe-B-Ga system are reported. The range of composition containing Ga for which these alloys can be made amorphous by casting onto a rapidly rotating drum is much more restricted than for Fe-B-C, Fe-B-Si, or Fe-B-Ge alloys; only up to 5 a/o Ga could be substituted for B. On replacing B by Ga the crystallization temperature typically decreases, the Curie temperature increases, the saturation magnetization at low temperatures and at room temperature decreases, and the coercivity increases. Some alloys in the series Fe_{84}-B-Al, $Fe_{84}Si_2$-B-Al, $Fe_{80}Si_4$-B-Al, $FE_{82}B_9C_3$-Si-Al were also prepared. Al contents of only up to 3 a/o could be made as amorphous ribbons. In all of these alloys, with increasing Al the crystallization temperature decreased, the Curie temperature decreased, and the room temperature saturation magnetization decreased.

SUBJECT: amorphous alloys

KEY WORDS: amorphous alloys, magnetic properties, crystallization

INFORMATION PREPARED FOR _____

Additional Hard or Microfiche Copies Available From

Technical Information Exchange
Bldg. 81 Room A133, Schenectady, N.Y., 12345

PROPERTIES OF AMORPHOUS ALLOYS OF Fe-B-Ga AND Fe-B-Si-C-Al

F.E. Luborsky, J.L. Walter,
and H.H. Liebermann

INTRODUCTION

In previous work we reported the properties of amorphous alloys of Fe-B,[1] Fe-B-Si,[2] Fe-B-C,[3,4] Fe-B-Si-C,[5] and Fe-B-Ge.[6] The primary applied goal of this work was to maximize the room temperature saturation magnetization, M_s, without increasing the alloy cost. It was hoped that, although C, Si, and Ge all can contribute more electrons to the d-band than B and thus will decrease its moment, that with increasing atomic size the moment would increase. This was found to be true,[6] but in addition it was found that the temperature coefficient of M_s increased with atomic size[7] thus mitigating, at room temperature, the increase in M_s at low temperature. The highest value of M_s measured at room temperature was 17.6 kG for an Fe-B-Ge alloy after stress relief annealing. None of the other alloys had values of M_s less than 16.9 kG.

As part of this program we have now investigated the effect of adding Ga and Al on the properties of amorphous Fe-B alloys. These results will be reported here and compared to the properties of the previously reported alloys and to their predicted behavior.

EXPERIMENTAL

Amorphous ribbons were prepared[8,9] by melt quenching onto the surface of a rotating wheel. Curie temperatures T_c were determined using a thermogravimetric force recording balance fitted with a permament magnet to produce a field gradient in a field of 225 Oe. Samples were heated at 20 °C/min. The saturation magnetizations, σ_s in emu/g, were determined by using a vibrating sample magnetometer at fields up to 20 kOe on samples about 5 mm long. The results were extrapolated to infinite field using a $1/H^2$ function. The densities d were calculated as described previously,[3,10] by first calculating the packing fraction versus iron content for Fe-B alloys using the measured densities of Hasegawa and Ray.[11] Then the density of the alloy was calculated using these packing fractions for each iron content together with the tetrahedral covalent radii of B (0.88 A) and Ga (1.26 A). This technique gave excellent agreement with measured densities in the Fe-B-C[3] and Fe-B-Si[12] amorphous alloys. The density was used to convert σ_s to $4\pi M_s$ ($=4\pi\sigma_s d$).

RESULTS AND DISCUSSION

The crystallization temperatures are shown in Figure 1 for two different anneals. In Figure 1(a) the samples were annealed at a constant heating

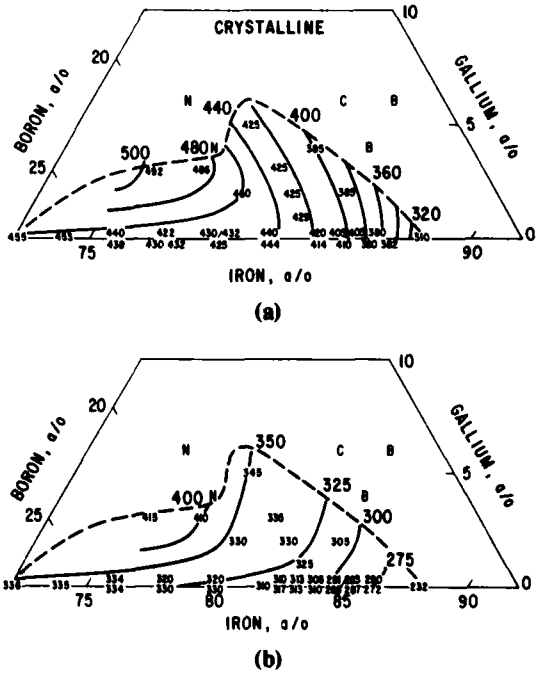

Figure 1. Crystallization temperatures for amorphous Fe-B-Ga alloys (a) on heating at 20 °C/min and (b) on heating for 2 hr. The dashed line indicates the boundary between the preparation of amorphous vs crystalline alloys. N indicates compositions which would not cast into ribbons; B indicates compositions which cast very blue, oxidized and brittle ribbons; C indicates compositions which contain some crystallites as identified by x-ray analysis.

Manuscript received May 4, 1981

rate of 20 °C/min and the magnetization was followed using the thermogravimetric force balance. The magnetization first decreased to zero when the Curie temperature T_c was reached and then suddenly increased as crystalline Fe and Fe compounds with high values of T_c started to nucleate and grow. The beginning of this increase in magnetization was taken as the beginning of crystallization. In Figure 1(b) the samples were heated for 2-hr periods at temperatures increasing in 30 °C steps. The coercivity H_c, typically, first dropped as the samples were stress relieved by the annealing and then rapidly increased. The beginning of this rapid increase in H_c was taken as the beginning of crystallization.[13] In general in both (a) and (b) the replacement of B by Ga decreases the stability of the amorphous alloy. However, at low Fe contents the stability increases, as shown in Table 1, but the increase for Ga is the smallest of those recorded. A somewhat greater decrease was observed for Fe-B-Al alloys shown in Figure 2 as recorded also in Table 1. The addition of $-Si_2$ to $Fe_{84}B_{16-y}Al_y$ increased the stability slightly, as expected, when comparing the quaternary alloy to the ternary alloy due to the greater alloy complexity.

It would appear, from the summary in Table 1 as graphed in part in Figure 3, that the stability of these amorphous alloys, on replacing B by another metalloid, is determined by the atom size, whether the added element is larger or smaller than B, i.e., whether it is an interstitial alloy or a substitutional alloy and on the iron content. Thus, with increasing atom size the stability of the substitutionally added elements, −Si, −Ge, −Ga and −Al, decreases, as seen in Figure 3 and Table 1. This appears to be

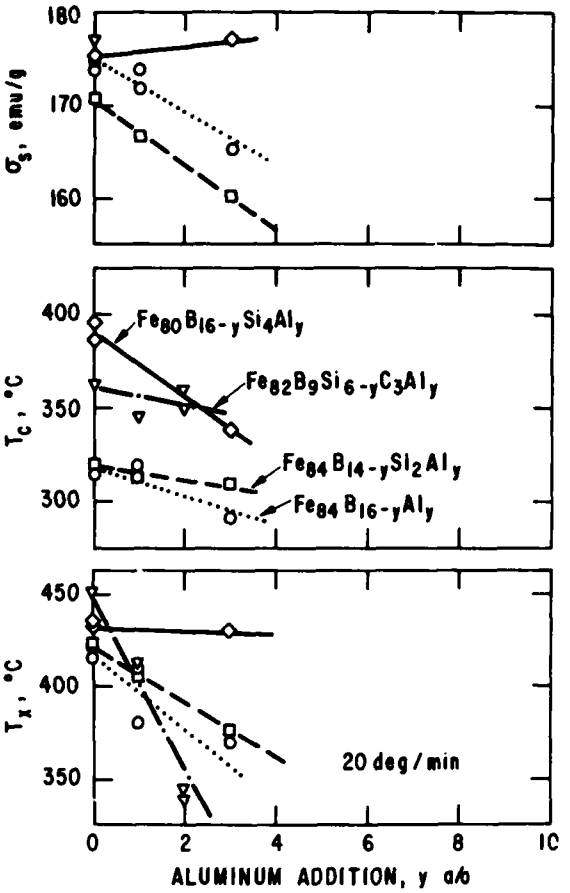

Figure 2. The saturation magnetization measured at room temperature, the Curie temperature, and the crystallization temperature for various amorphous alloys as a function of Al content.

Table 1

COMPARISON OF STABILITY OF VARIOUS ALLOYS*

Alloy Fe-B-X	r=Covalent radii of X (A)	$\Delta r = r_X - r_B$ (A)	X (a/o)	Crystallization Temperature, at 20 °/min.			Reference
				77.5 a/o Fe	80 a/o Fe	84 a/o Fe	
Fe-B	-	-	0	435	430	415	(1)
Fe-B-C	0.77	-0.11	5	470	461	395	(3)
Fe-B-Si	1.17	0.29	5	510	500	410	(2)
Fe-B-Ge	1.22	0.34	5	475	440	395	(6)
Fe-B-Si-C	-	-	5	507	483	390	(5)
Fe-B-Ga	1.26	0.38	3	485	445	370	this work
			5	450	410	-	this work
Fe-B-Al	1.26	0.38	3	-	-	360	this work

*From smoothed data. $r_B = 0.88$.

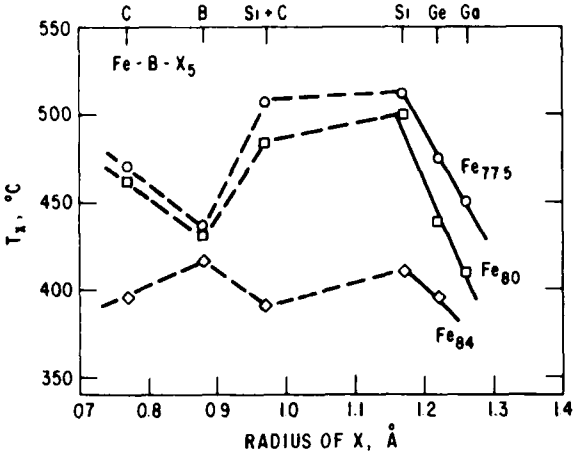

Figure 3. The beginning of crystallization, as determined from the beginning of the increase in coercivity, as a function of atom size of X for various Fe-B-X_5 amorphous alloys.

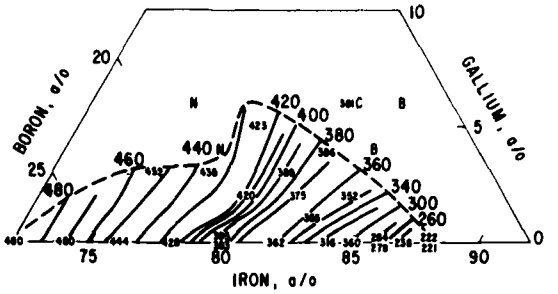

Figure 4. Curie temperatures for amorphous Fe-B-Ga alloys, as in Figure 1.

independent of the difference in electronic structure between Si and Ge and the Ga and Al atoms. Note that the stability of the equiatomic mixture of Si and C appears to have the stability representing roughly the average stability of the Fe-B-C and Fe-B-Si alloys. Addition of −C, Si-C, or Si to alloys of Fe_{80}− or $Fe_{77.5}$− increases the stability while addition of these same elements to Fe_{84}− decreases the stability. It is tempting to ascribe this difference in behavior to the difference in atomic structure which occurs around Fe_{81}−. That is, for boron-rich alloys containing less than Fe_{81}− all of the possible Bernal holes or free volume is filled. While for alloys containing more than Fe_{81}− there is a deficiency of boron and excess free volume exists and, as for the binary F-B alloys, the stability rapidly decreases as −B exceeds about 82 a/o Fe.

The Curie temperatures of the Fe-B-Ga alloys are shown in Figure 4. The increase in T_c on replacement of B by Ga is quite striking in contrast to the much smaller increases for Fe-B-C and Fe-B-Si alloys shown in Table 2. It is comparable to the increase observed for the Fe-B-Ge alloys. However, the very similar Fe-B-Al alloys show a decrease in T_c on replacement of B by Al, as shown in Figure 2 and summarized in Table 2. There is no explanation for this behavior.

The saturation magnetization measured at 77 K, room temperature, and 100 °C is shown in Figure 5. At the low temperature the replacement of B by Ga produces a decrease in σ_s at all iron contents. This follows the same trend as observed for the substitution of B by −C, −Si, and −Ge. As shown in Table 2, this substitution decreases the

Table 2

CURIE TEMPERATURES*

Alloy	T_c at $Fe_{80}B_{15}X_5$ (°C)	T_c at $Fe_{84}B_{11}X_5$ (°C)	Reference
Fe-B	389	318	(1)
Fe-B-C	396	325	(3)
Fe-B-Si	396	330	(2)
Fe-B-Ge	417	390	(6)
Fe-B-Si_x-C_x	404	325	(5)
Fe-B-Ga	410	-	this work
	$Fe_{80}B_{17}X_3$	$Fe_{84}B_{13}X_3$	
Fe-B-Ga	415	358	this work
Fe-B-Al	-	294	this work
Fe-B-Si_x-C_x- P_x	396	-	unpublished

*From smoothed data

saturation magnetization in the sequence given, presumably because of the increasing atom size since they all have the same outer electron configuration. It should be noted that the results for the −C, −Si, −Ge series forms the same sequence as calculated from the results reported by Kazama et al.[14] Furthermore, in going from −Ga to −Ge, where one *p* electron is added, with only a slight decrease in covalent or atomic radius, the σ_s decreases as expected. Thus, the decrease in σ_s on replacing B by the isoelectronic element Ga must be due to the increase in atomic size. At room temperature the contours resemble the contours for Fe-B-Ge and to a lesser extent those of Fe-B-C and Fe-B-Si. However, the ridge of constant σ_s which extends out into the −C- or −Si-rich regions in these alloys is just about absent in the −Ga alloys. Table 3 summarizes the maximum values observed

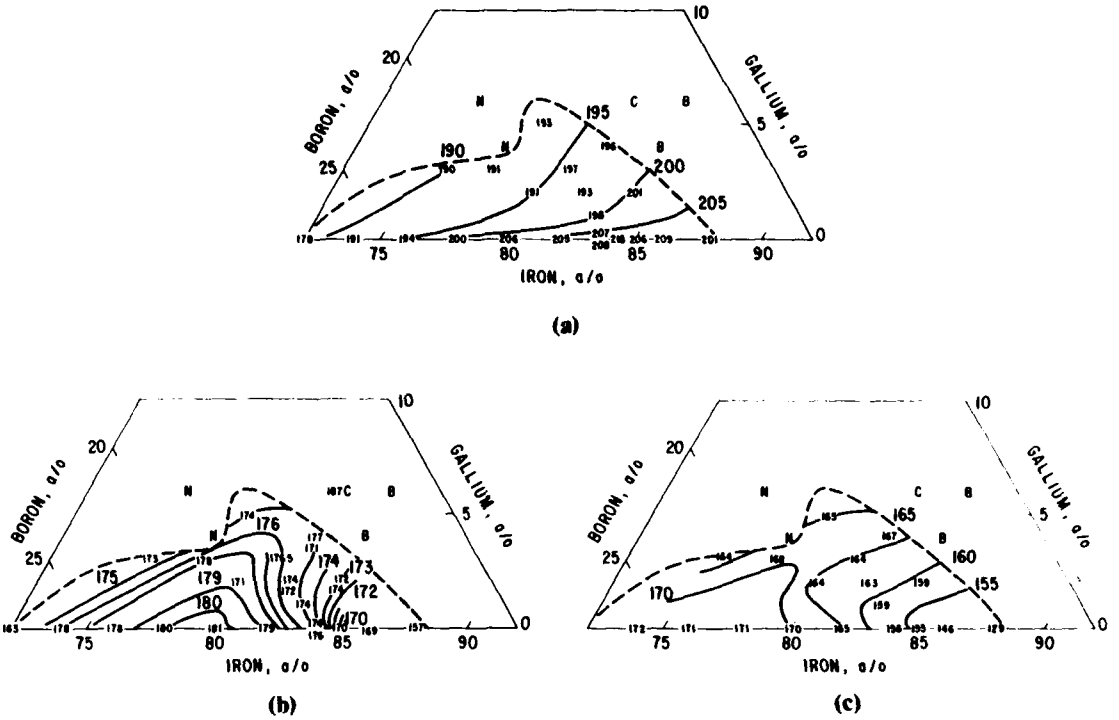

Figure 5. The saturation magnetization for amorphous Fe-B-Ga alloys, as in Figure 1, measured at (a) 77 K, (b) room temperature and (c) 100 °C.

Table 3

MAXIMUM SATURATION MAGNETIZATION OBTAINED IN VARIOUS AMORPHOUS ALLOY SYSTEMS*

Alloy System Fe-B-X	Maximum Saturation Magnetization at Room Temperature				Width of ridge at 5 % X for 175 emu/g	Composition at tip of the 178 emu/g contour	Reference
	As-Cast		Annealed				
	σ_s (emu/g)	$4\pi M_s$ (kG)	σ_s (emu/g)	$4\pi M_s$ (kG)	(percent)		
Fe-B	180	16.7	184	17.0	-	$Fe_{80}B_{20}$	(1)
Fe-B-C	180	16.9	184	17.3	8.0	$Fe_{82.5}B_6C_{11.5}$	(3)
Fe-B-Si	179	16.5	183	16.9	2.5	$Fe_{82}B_{12}Si_6$	(2)
Fe-B-Ge	179	17.2	183	17.6	4.5	$Fe_{82.5}B_{11}Ge_{6.5}$	(6)
Fe-B-Si_x-C_y	182	17.0	186	17.3	6.5	$Fe_{82}B_{12.4}Si_{2.8}C_{2.8}$	(5)
Fe-B-Ga	178	16.8	181	17.1	-	$Fe_{80}B_{17}Ga_3$	this work
Fe-B-Si_x-C_y-P_z	177	16.5	178	16.6	4.8	~ $Fe_{81}B_{13.6}Si_{1.8}C_{1.8}P_{1.8}$	unpublished

*From smoothed data.

in all of the alloy systems studied to this time. It further shows the much decreased length of the ridge of constant σ_s. The σ_s for the Al alloys measured at room temperature is also shown in Figure 2. It behaves as expected, i.e., at high iron contents σ_s decreases, while for Fe_{80} alloys σ_s is more nearly constant.

The coercivity of Fe-B-Ga alloys, after a stress relief anneal to achieve a minimum coercivity, is shown in Figure 6. The minimum coercivity occurs farthest in composition from the boundary between crystalline and amorphous alloy preparation, i.e., near the mid-point of the binary range. At and beyond the boundary the coercivity rises sharply as ferromagnetic precipitates develop.

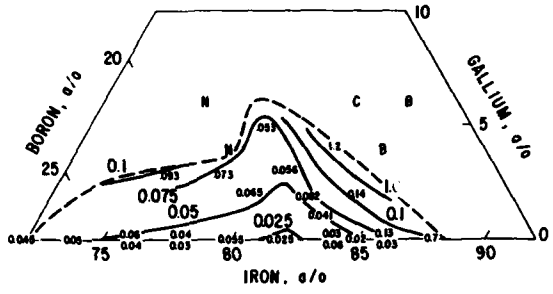

Figure 6. The coercivity of amorphous Fe-B-Ga alloys, as in Figure 1.

ACKNOWLEDGMENTS

We are grateful to W. Rollins for the preparation of the ribbons, to H. Patchen for the saturation magnetization measurements, and to N. Marotta for the Curie temperature measurements. The work reported here was supported in part by the Office of Naval Research.

REFERENCES

1. F.E. Luborsky, J.J. Becker, and J.L. Walter, in "Rapidly Quenched Metals III," B. Cantor, Ed., London: The Metals Soc., 1978, Vol. 2, p. 188.
2. F.E. Luborsky, J.J. Becker, J.L. Walter, and H.H. Liebermann, *IEEE Trans. Magn., Vol. MAG-15,* p. 1146, 1979.
3. F.E. Luborsky, J.J. Becker, J.L. Walter, and D.L. Martin, *IEEE Trans. Magn., Vol. MAG-16,* p. 521, 1980.
4. F.E. Luborsky, J.J. Becker, and H.H. Liebermann, in "Rapidly Quenched Metals III," B. Cantor, Ed., London: The Metals Soc., 1978, Vol. 2, p. 249.
5. F.E. Luborsky and J.L. Walter, *IEEE Trans. Magn., Vol. MAG-16,* p. 572, 1980.
6. F.E. Luborsky and J.L. Walter, *IEEE Trans. Magn., Vol. MAG-17,* p. 1204, 1981.
7. F.E. Luborsky, J.L. Walter, H.H. Liebermann, and E.P. Wohlfarth, *J. Magn. Magn. Mat., Vol. 15-18,* p. 1351 (1980).
8. J.L. Walter, in "Rapidly Quenched Metals III," B. Cantor, Ed., London: The Metals Soc. 1978, Vol. 1, p. 30.
9. H.H. Liebermann and C.D. Graham, Jr., *IEEE Trans. Magn., Vol. MAG-12,* p. 921, 1976.
10. G.S. Cargill III, *Solid State Phys., Vol. 30,* p. 227, 1975.
11. R. Hasegawa and R. Ray, *J. Appl. Phys., Vol. 49,* p. 4174, 1978.
12. F.E. Luborsky, P.G. Frischmann, and L.A. Johnson, *J. Magn. Magn. Mat., Vol. 19,* p. 130, 1980.
13. F.E. Luborsky, *Mater. Sci. Eng., Vol. 28,* p. 139, 1977.

Acta Metallurgica Vol. 29, pp. 1939 to 1948, 1981
Printed in Great Britain

0001-6160/81/121939-10$02.00/0

CREEP, STRESS RELAXATION AND STRUCTURAL CHANGE OF AMORPHOUS ALLOYS

A. I. TAUB and F. E. LUBORSKY

General Electric Corporate Research and Development, P.O. Box 8, Schenectady, New York, U.S.A.

(*Received* 30 *March* 1981)

Abstract—The time, temperature and stress dependence of the homogeneous flow of amorphous FeNiPB and PdCuSi has been examined in tensile creep, tensile stress relaxation and bend stress relaxation tests. The results are shown to be entirely self-consistent, and are used to reconcile the discrepancies found in the literature data. In all cases, the viscosity increases linearly with time, the rate of increase being both temperature and composition dependent. The stress dependence of the strain rate follows a hyperbolic sine relation. The volume strain element appears to be a function of temperature and composition. A general empirical flow law for amorphous alloys is presented based on these observations. It is shown to be in agreement with all the available data.

Résumé—Nous avons étudié au moyen d'essais de fluage en traction et de relaxation de la contrainte de traction ou de flexion, la variation de l'écoulement homogène de FeNiPb et PdCuSi amorphes en fonction du temps, de la température et de la contrainte. Nos résultats sont entièrement auto-cohérents et ils réconcilient les différences que l'on trouve dans la littérature. Dans tous les cas, la viscosité augmente linéairement en fonction du temps, sa vitesse d'augmentation dépendant de la température et de la composition. Cette vitesse de déformation varie en fonction de la contrainte selon une loi en sinus hyperbolique. L'élément de déformation en volume est fonction de la température et de la composition. Nous présentons une loi empirique générale pour l'écoulement des alliages amorphes, que repose sur ces observations. Elle est en accord avec tous les résultats dont on dispose.

Zusammenfassung—Zeit-, Temperatur- und Spannungsabhängigkeit des homogenen Fließens von amorphem FeNiPB und PdCuSi wurde im Kriechund im Spannungsrelaxationsversuch gemessen. Die erhaltenen Ergebnisse sind selbstkonsistent und werden benutzt, die in den Literaturdaten gefundenen Widersprüche aufzulösen. In sämtlichen Fällen nimmt die Viskosität linear mit der Zeit zu, wobei die Geschwindigkeit von Temperatur und Zusammensetzung abhängt. Die Abhängigkeit von Spannung und Dehngeschwindigkeit folgt einem hyperbolischen Sinus. Das Volumendehnungselement scheint von Temperatur und Zusammensetzung abzuhängen. Aufbauend auf diesen Beobachtungen wird ein allgemeines empirisches Fließgesetz für amorphe Legierungen vorgelegt, welches -wie gezeigt wird- mit den vorliegenden Ergebnissen übereinstimmt.

INTRODUCTION

There have been numerous investigations of homogeneous flow in metallic glasses using stress relaxation and creep measurements. When comparisons of some of the early work of different investigators are made, large discrepancies in the reported measurements are found. Of particular concern has been the differences in the reported values of the activation energy for isoconfigurational flow [1–5] and for the stress dependence of the strain rate [2, 3, 6–11]. The origin of many of these discrepancies has recently been clarified by taking into account the strong dependence of homogeneous flow on preannealing [2, 12–14] and by applying transition state theory to the flow process [13, 15–17].

Some questions still persist, however, concerning the details of the stress–strain rate relation. Transition state theory predicts that the strain rate sensitivity

$$m = \frac{\mathrm{d}(\ln \dot{\gamma})}{\mathrm{d}(\ln \tau)}$$

should be unity at low stresses, and increase rapidly at higher stresses. When the reported values of m measured during creep tests were tabulated against the testing stress, this trend was indeed observed [17]. Furthermore, one set of tensile tests conducted over a large stress range (330–750 MPa) also showed that m increases dramatically with stress [9]. However, for the one set of stress relaxation tests performed over a relatively large stress range (365–925 MPa), a constant

value of $m = 4$ has been reported [10, 18]. In an attempt to resolve this discrepancy, we performed tensile creep, tensile stress relaxation and bending stress relaxation tests on an amorphous FeNiPB alloy and on an amorphous PdCuSi alloy. These alloys were chosen because they are common to the work of many of the previous investigations. The tests were also used to examine the kinetics of structural change as they affect homogeneous flow. Several investigations have shown that structural relaxation is manifested as a decrease in the homogeneous flow rate [2, 12-14]. However, different values for the exponent

$$n = \frac{-\mathrm{d}(\ln \dot{\gamma})}{\mathrm{d}(\ln t)}$$

have been reported ($n = 0.5$ [13]; $n = 1.0$ [12]). In this paper we will present the results of our new tests, and show that they are entirely self-consistent and that they resolve the above questions concerning the stress-strain rate relation and the kinetics of structural change. The available literature data is also analyzed in relation to our observations.

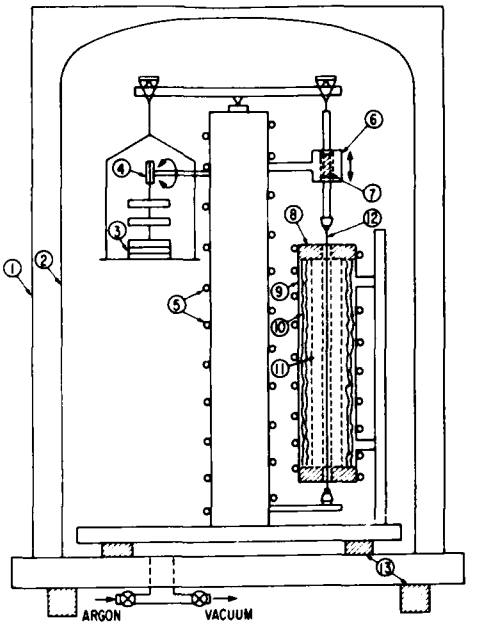

Fig. 1. Schematic of creep apparatus: (1) temperature controlled cage; (2) bell jar; (3) weights; (4) motor-driven weight pulley; (5) water coils; (6) motor-driven LVDT; (7) iron core; (8) Zircar board insulating caps; (9) heater housing; (10) Fiberfrax insulation; (11) aluminum heating block; (12) specimen; (13) rubber shock mounts.

EXPERIMENTAL

The specimens tested were amorphous $Fe_{40}Ni_{40}P_{14}B_6$ and $Pd_{77.5}Cu_6Si_{16.5}$. The FeNiPB was obtained from Allied Chemical Corporation (Metglas 2826) in the form of ribbons 1.4 mm wide × 48 microns thick. The PdCuSi was produced by single roller quenching as ribbons 1.4 mm wide × 33 microns thick.

The creep tests were performed with the apparatus shown in Fig. 1. The specimen is gripped on the bottom with a stationary pin vise and on the top by a pin vise that extends down from one arm of the balance beam. The load is transmitted across the balance beam from a weight pan suspended from the other arm of the beam. All the tests reported here were conducted at constant equivalent shear stress $\tau = \sigma/\sqrt{3} = 104 \pm 3$ MPa, where σ is the uniaxial tensile stress. Elongation of the specimen is measured by monitoring the displacement of an iron core in the grip support rod using a Schaevitz Corporation linear voltage displacement transformer (LVDT). The heating chamber can keep the specimen temperature to within ±1 C over a hot zone length of 10 inches. At both ends of the hot zone, the temperature drops rapidly to ambient temperature (approx. 50 C in the first 1/2 inch with the furnace at 250 C). Since the flow rate of these materials is so strongly temperature dependent and the temperature drops so rapidly out of the hot zone, we assume that only that part of the specimen in the 10-inch hot zone contributes to the flow. This allows us to define a specimen gage length without having to thin down and possibly change the state of the material. The entire apparatus is placed inside a bell jar that can be evacuated to 0.5 micron. During the tests, the system is backfilled with argon to provide a dynamic pressure of 200 microns. To minimize thermal expansion, the apparatus was constructed out of Invar and the temperature of the bell jar cage and the circulating water controlled at 36 C. Tensile strain rates as low as $1 \times 10^{-10}\,\mathrm{s}^{-1}$ can be detected.

The tensile stress relaxation tests were performed on an Instron Static Tensile Testing Machine. The lower end of the specimen was held by a friction grip which was attached to the bottom of a 1-inch dia. 12-inch-long quartz tube that was bolted to the underside of the crosshead. The top of the specimen was held by a friction grip that was attached to the bottom of a second quartz tube 5/8 inch in diameter, that was suspended from the load cell. The support rods were constructed from quartz to insure negligible thermal expansion of the grips. The upper quartz tube was inserted through the crosshead and into the lower tube, providing a gage length of 8 inches. At the start of the test, the sample was elastically loaded to the desired initial stress at a tensile strain rate of $2 \times 10^{-4}\,\mathrm{s}^{-1}$. Then a uniform temperature silicone oil bath was raised over the specimen. For testing at high stresses, it was necessary to add load during the heat-up stage to counteract the specimen thermal expansion. Holes in the lower quartz tube allowed the oil to reach the specimen to provide rapid temperature equilibration. It took 30 s to raise the oil over the

entire specimen length. To reduce oxidation of the specimen, nitrogen was bubbled through and blown over the oil. The elastic response of the machine was found to be less than 5% of the specimen response and was therefore ignored in the data analysis.

The bend stress relaxation tests were performed by spring back measurements as described elsewhere [19, 20]. The restraining ring was made of molybdenum with a diameter of 1.46 cm. The anneals were performed by submerging the coiled specimens into a silicone oil temperature bath held to ±0.5°C. To reduce oxidation, nitrogen was bubbled through the oil.

DATA ANALYSIS

Creep

The analog voltage signal from the LVDT was converted to a digital signal, averaged, transformed to a strain measure and periodically stored automatically during the test. Figure 2 shows a typical strain–time plot following a temperature increase. The equivalent shear strain $\gamma = \sqrt{3}\epsilon$ is shown, where ϵ is the uniaxial tensile strain [21]. The flow during the first 10 min after the initiation of a temperature change is ignored to allow for the decay of all the thermal transients. The dots are the actual data. The solid line is the least squares fit of an eighth order polynomial to the data.

The equivalent shear strain rate $\dot{\gamma} = \sqrt{3}\dot{\epsilon}$ is computed analytically from the derivative of the fit function. Similarly for the viscosity

$$\eta = \frac{\tau}{\dot{\gamma}} = \frac{1}{3}\frac{\sigma}{\dot{\epsilon}}.$$

Tensile stress relaxation

The voltage signal from the load cell was converted to a stress measure and handled in the same manner as the creep data. Figure 3 shows a typical stress–time plot following the raising of the oil bath. Shown is the equivalent shear stress $\tau = \sigma/\sqrt{3}$, where σ is the uniaxial tensile stress. The symbols are the actual data. The solid line is the fitted curve.

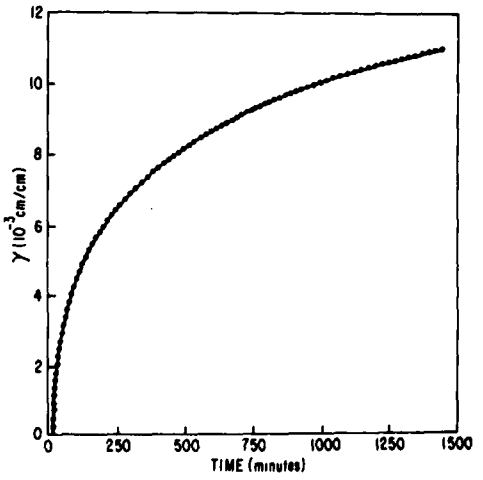

Fig. 2. Equivalent shear strain $\gamma = \sqrt{3}\epsilon$ as a function of time, for $Pd_{77.5}Cu_6Si_{16.5}$ tensile creep tested at 505 K. The symbols are the experimental data. The solid line is a least squares fitted polynomial.

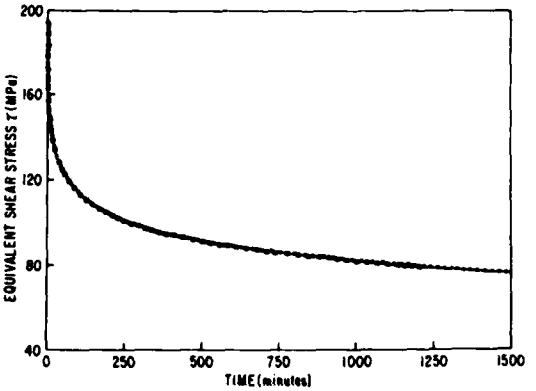

Fig. 3. Equivalent shear stress $\tau = \sigma/\sqrt{3}$ as a function of time, for two as-cast samples of $Fe_{40}Ni_{40}P_{14}B_6$ tensile stress relaxation tested at 500 K. The two different symbols are the actual data for two independent runs. Note the excellent reproducibility. The solid line is a least squares fitted polynomial.

The slope $d\tau/dt$ is computed analytically from the derivative of the fit function. Since we are assuming an infinitely stiff machine, we can write

$$\frac{d\sigma}{dt} = -E\dot{\epsilon} \quad \text{or} \quad \frac{d\tau}{dt} = \frac{-E\dot{\gamma}}{3}$$

where E is Young's modulus. Then for any time t, we can find corresponding values for τ and $\dot{\gamma}$.

Bend stress relaxation

At the start of the test, the initial radius of curvature of the ribbon r_i, is measured. The ribbon is then stressed by coiling it to a radius r_0, annealed, and allowed to spring back. The new radius of curvature r_a, is measured and the ribbon is coiled and annealed once again. This process continues, providing a radius–time history.

The maximum stress is computed from the thin-walled, pure bending solution $\sigma = Et/2r$ where t is the thickness of the ribbon. The quantity of interest σ/σ_0, where σ_0 is the initial coiled stress, is then:

$$\frac{\sigma}{\sigma_0} = 1 - \frac{\left(\frac{r_0}{r_a}\right) - \left(\frac{r_0}{r_i}\right)}{1 - \left(\frac{r_0}{r_i}\right)}.$$

RESULTS

$Fe_{40}Ni_{40}P_{14}B_6$

Figure 4 shows the strain rate history of samples creep tested from the as-cast condition at different

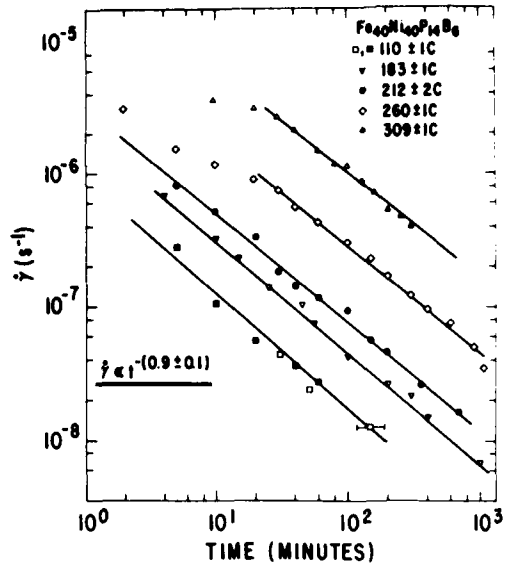

Fig. 4. Equivalent strain rate as a function of test time for samples creep tested from the as-cast condition at the indicated temperatures. The symbols are the experimental data. The solid lines indicate the linear portion of the data.

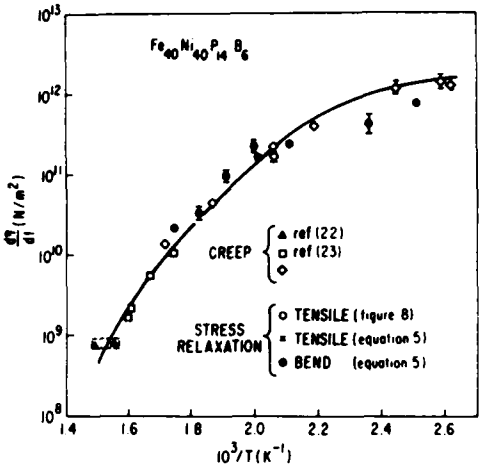

Fig. 6. Rate of change of viscosity with time as measured in tensile creep, tensile stress relaxation and bend stress relaxation tests.

temperatures. At the lower temperatures, the strain rate varies inversely with time from the start of the tests: $\dot{\gamma} \propto t^{-(0.9 \pm 0.1)}$. At the higher temperatures a similar decrease is observed, but only after an initial transient period of approx. 30 min.

It is sometimes more convenient to examine the viscosity $\eta = \tau/\dot{\gamma}$ rather than the strain rate. Figure 5 shows that the viscosity increases linearly with time at all the temperatures tested. Similar behavior has previously been reported by Anderson and Lord for this system at temperatures near the glass transition temperature [22]. We have re-examined recent measurements by Takamori, *et al.* and found that in the portion of their data where crystallization has not yet occurred, a linear increase in viscosity is also observed [23]. In Fig. 6, the rate of change of viscosity with time $\dot{\eta}$, is plotted against inverse temperature for both our new measurements and the above literature data. Although Arrhenius-type behavior is not exhibited, all the data lie on one smooth curve.

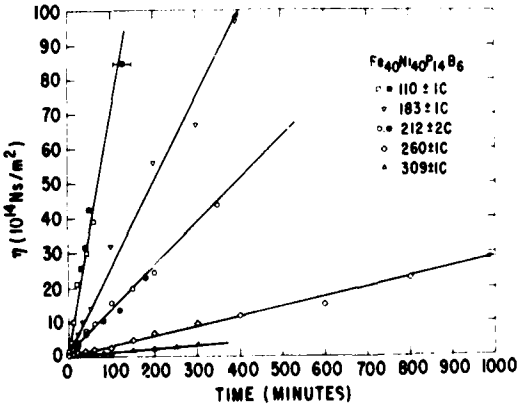

Fig. 5. Viscosity as a function of test time at the indicated temperatures.

Figure 7 is a plot of the tensile stress relaxation data for as-cast specimens tested at 500 K at different initial stresses. For each curve the strain rate

$$\dot{\gamma} = -\frac{3}{E}\frac{d\tau}{dt}$$

was computed at t = 0.255, 0.5, 1, 2, 5, 10, 15, 20, 50, 100, 150, 200, 500, 1000, 1500 and 2000 min. In Fig. 8, this strain rate is crossplotted against the corresponding stress value. For times greater than five minutes, we find a linear stress–strain rate relation, $\dot{\gamma} = \tau^{(1.08 \pm 0.06)}$. For times less than 5 min, however, the linearity appears to break down at the higher stresses. Previous creep investigations of $Pd_{82}Si_{18}$ [17] showed a similar transition from linear to non-linear stress-dependent flow at high stresses. This was explained by applying transition state theory to the flow process, which predicts a stress–strain rate relation of the form:

$$\dot{\gamma} = \dot{\gamma}_0 \sinh \frac{\tau \gamma_0 \Omega_f}{kT}. \qquad (1)$$

γ_0 is the local strain produced by shear site of volume Ω_f [15, 16]. Table 1 shows the least squares fit values of the free parameters of this relation for the data of times less than 5 min. In Fig. 9 the fitted curves are

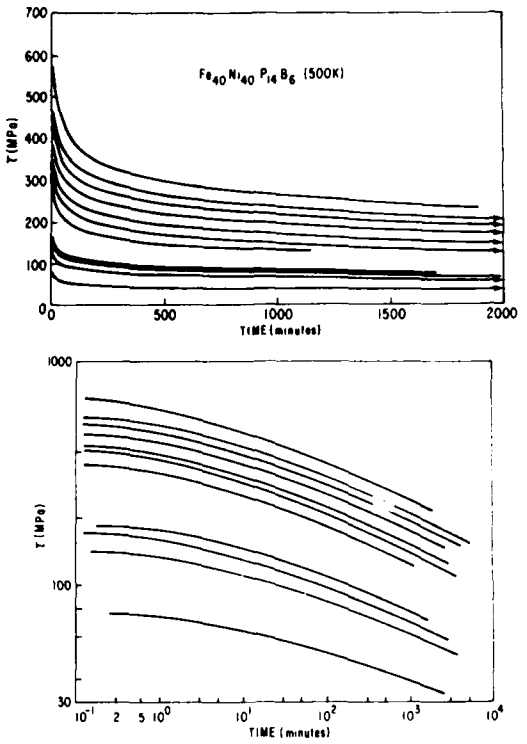

Fig. 7. Equivalent shear stress as a function of time for as-cast samples tensile stress relaxation tested at 500 K, starting at different initial stresses.

plotted with the experimental data. Note that at small stresses

$$(\tau < kT/\gamma_0\Omega_f = 411\ \text{MPa})$$

$$\sinh(\tau\gamma_0\Omega_f/kT) \simeq \tau\gamma_0\Omega_f/kT$$

and linear behavior should be observed. In fact, for times greater than 5 min where no linearity breakdown was found, the maximum stress had decayed to below 400 MPa.

The stress relaxation data can also be used to calculate an effective viscosity, to be compared with the creep results. From equation (1) we have at low stresses:

$$\eta = \frac{\tau}{\dot{\gamma}} \simeq \frac{kT}{\dot{\gamma}_0\gamma_0\Omega_f}. \tag{2}$$

The viscosities computed with this relation are listed in Table 1. For times greater than 5 min (i.e., those data sets with $\tau_{max} < 400$ MPa, for which a sinh fit is not practical), one can calculate the effective viscosity directly from Fig. 8. We construct a line on the figure at the same stress used in the creep tests ($\tau = 104$ MPa), then read off corresponding values of $\dot{\gamma}$ for each time and calculate $\eta = \tau/\dot{\gamma}$ directly. This effective viscosity calculation is compared with the results from equation (2) in Table 1. Figure 10 shows that the viscosity computed in this direct manner also increases linearly with time. In addition, the rate of change of the effective viscosity is in excellent agreement with the creep measurements (see Fig. 6).

Figure 11 is a plot of the ring coiling, bend stress relaxation data for as-cast $Fe_{40}Ni_{40}P_{14}B_6$ reported by Graham, *et al.* [24] and by Luborsky and Walter [20]. Note that although the work was performed at two different laboratories, the two data sets are in excellent agreement. We can compute an effective viscosity from these measurements using the same relations found for the tensile stress relaxation data. For the bend tests, the maximum stress

$$\tau = \frac{\sigma}{\sqrt{3}} = \frac{Et}{2\sqrt{3}r} = 330\ \text{MPa},$$

so linear stress strain rate applies. For high stress bend tests where non-linear effects become important,

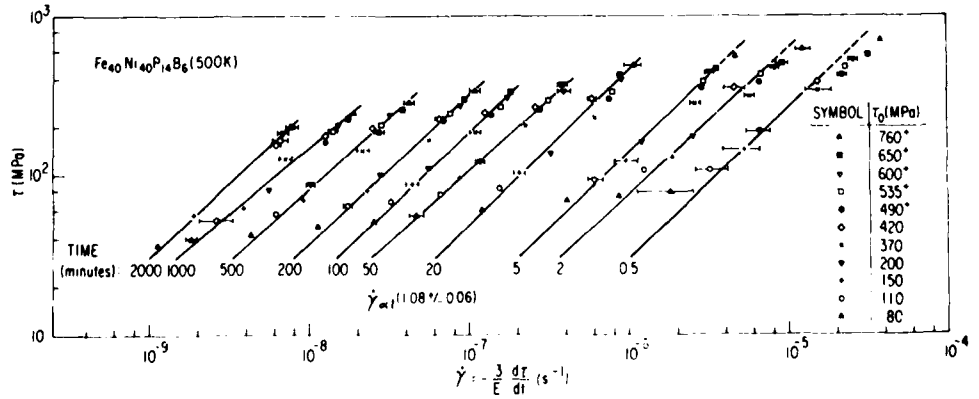

Fig. 8. Slopes at indicated times, of the tensile stress relaxation curves in Fig. 7(at, crossplotted with equivalent shear stress. Data for 0.225, 1, 10, 15, 150 and 1500 min has been deleted to simplify the plot. Solid lines show the stress strain rate dependence at each time. Dashed lines indicate where the data begin to deviate from a linear stress strain rate relation. τ_0 is the stress after the oil bath was raised. For those tests marked with a '+', the stress was increased during the raising of the oil.

AD-A111 436 GENERAL ELECTRIC CORPORATE RESEARCH AND DEVELOPMENT --ETC F/G 11/6
INVESTIGATION INTO THE ORIGIN OF MAGNETIC PROPERTIES OF AMORPHO--ETC(U)
OCT 81 F E LUBORSKY, J J BECKER N00014-76-C-0807
UNCLASSIFIED SRD-80-006 NL

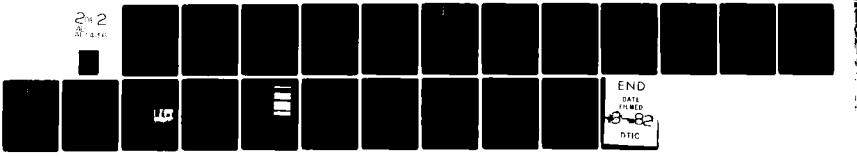

END
DATE FILMED
8-82
DTIC

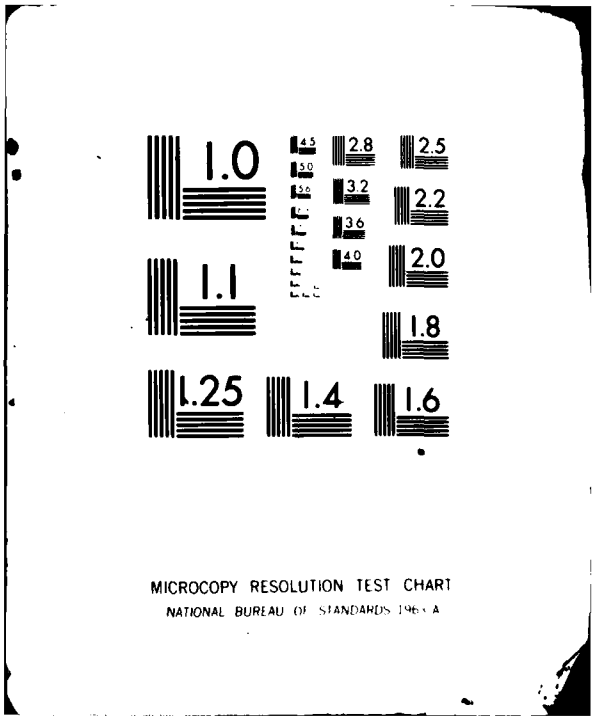
1.0
1.1
1.25
1.4
1.6
1.8
2.0
2.2
2.5
2.8
3.2
3.6
4.0
MICROCOPY RESOLUTION TEST CHART
NATIONAL BUREAU OF STANDARDS 1963 A

Table 1. Least squares fit parameters for equation (1) and computed viscosities for tensile stress relaxation data of $Fe_{40}Ni_{40}P_{14}B_6$ at 500 K

Time (min)	$\dot{\gamma}_0$ (10^{-6} s^{-1})	$\gamma_0\Omega_f/kT$ (10^{-9} Pa^{-1})	η (10^{13} Ns/m^2) [from equation (2)]	η (10^{13} Ns/m^2) (from Fig. 8)
0.225	35.3	2.13	1.32	1.8
0.5	19.3	2.13	2.43	3.6
1	7.93	2.84	4.44	5.1
2	5.71	2.50	7.01	7.3

$\gamma_0\Omega_f = (16.5 \pm 2.5)$ Å^3

the analysis is more complex. For a discussion of the analysis for a fully relaxed specimen (i.e. the effective viscosity is constant during the test), see Ref. [18]. For the low stress tests considered here, we can define an effective viscosity which should increase linearly with time. Then:

$$\frac{d\tau}{dt} = -\frac{E}{3}\dot{\gamma} = -\frac{E}{3}\frac{\tau}{\eta_0 + \dot{\eta}t}. \tag{3}$$

Integrating from $t = 0$ with initial stress τ_0:

$$\ln\frac{\tau}{\tau_0} = -\frac{E}{3\dot{\eta}}\ln\left|\frac{\eta_0 + \dot{\eta}t}{\eta_0}\right|. \tag{4}$$

At long times $\dot{\eta}t \gg \eta_0$ yielding:

$$\ln\frac{\tau}{\tau_0} \simeq B\ln\frac{\dot{\eta}t}{\eta_0} = B\ln\frac{\dot{\eta}}{\eta_0} + B\ln t \tag{5}$$

where

$$B = -\frac{E}{3\dot{\eta}}.$$

After an initial transient,

$$\ln\frac{\tau}{\tau_0} = \ln\frac{\sigma}{\sigma_0}$$

should decrease linearly with $\ln t$, as is observed (see Fig. 11). Note that the transient lasts approximately 30 min, in agreement with the decay time of the creep transient (see Fig. 4). The rate of effective viscosity increase, $\dot{\eta}$, can now be computed from equation (5), using the slope of linear region. We use the modulus measured during the loading stage of both the creep and tensile stress relaxation tests, $E = 120 \pm 3$ GPa. This is in good agreement with the reported value of 125 GPa [25]. In Figure 6 the values of $\dot{\eta}$ computed from equation (5) are shown together with the creep results. Also shown is the rate of change of the effective viscosity computed from the linear portion of the tensile relaxation data using equation 5. There is, as expected, no difference in the values of $\dot{\eta}$ computed for the tensile stress relaxation data by the linear slope method and the more rigorous analysis of the previous section. We find good agreement for the values of $\dot{\eta}$ computed from all three tests.

$Pd_{77.5}Cu_6Si_{16.5}$

Figure 12 shows the strain rate history of samples creep tested from the as-cast condition. As was the case for the FeNiPB, an inverse relation for the strain rate with time is observed $\dot{\gamma} \propto t^{-(1.0+-0.1)}$. In Fig. 13 the data is plotted as viscosity versus time at various anneal temperatures. In Fig. 14 the rate of change of viscosity, computed from the slopes of the data in Fig. 13, is plotted against inverse temperature. Also shown are the available literature data for this composition. Even though the literature tests were on specimens cast by a different technique than the one

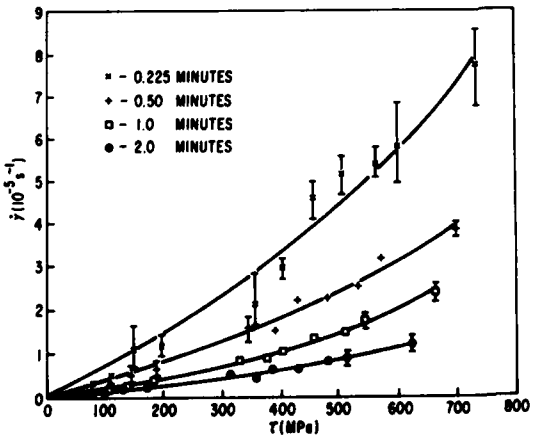

Fig. 9. Fit of Equation 1 to the data of Fig. 8, for times less than 5 min.

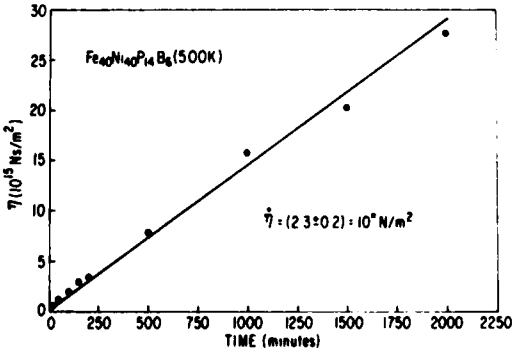

Fig. 10. Effective viscosity computed from the tensile stress relaxation data in Fig. 8.

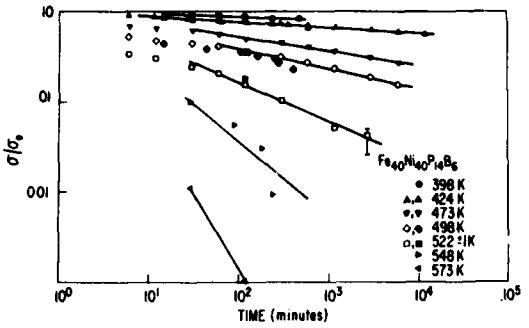

Fig. 11. Bond stress relaxation data for as-cast $Fe_{40}Ni_{40}P_{14}B_6$ at the indicated temperatures. Open symbols are from Ref. [24]. Closed symbols are from Ref. [20]. The solid lines indicate the slope of the linear region.

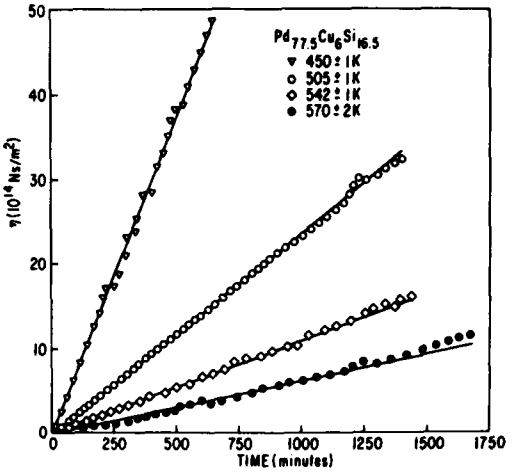

Fig. 13. Viscosity as a function of test time at the indicated temperatures.

used here (pendant drop melt extraction [2, 26] vs single roller quenching), all the creep data are in good agreement.

Figure 15 is a plot of the bend stress relaxation data obtained for as-cast specimens using the spring-back measurements on coiled rings. A linear decrease is observed at all temperatures. Using equation (5), the rate of change of the effective viscosity was computed. The modulus measured during the loading stage of the creep tests was used in the calculation, $E = 108 \pm 10$ GPa. This value is approx. 25% greater than the reported value of 88 GPa [25] for this composition. The computed values of $\dot{\eta}$ are shown in Fig. 14. Generally good agreement with the creep data is observed.

DISCUSSION

Amorphous metallic alloys appear to exhibit very similar flow properties whether tested in uniaxial creep, tensile stress relaxation, or bending stress relaxation. A linear increase in viscosity with time is common to both $Fe_{40}Ni_{40}P_{14}B_6$ and $Pd_{77.5}Cu_6Si_{16.5}$, as well as to $Pd_{82}Si_{18}$ [12]. Moreover, this linear relation seems to be valid over the entire temperature range examined T_g-250 < T < T_g. In addition, the results of a previous investigation of PdSi show that the rate of linear increase is not greatly affected by prior thermal treatment or by the application of stress [14, 29]. The latter point is verified by the data in Fig. 8, where the stress–strain rate relation generated by testing at different stresses is seen to shift

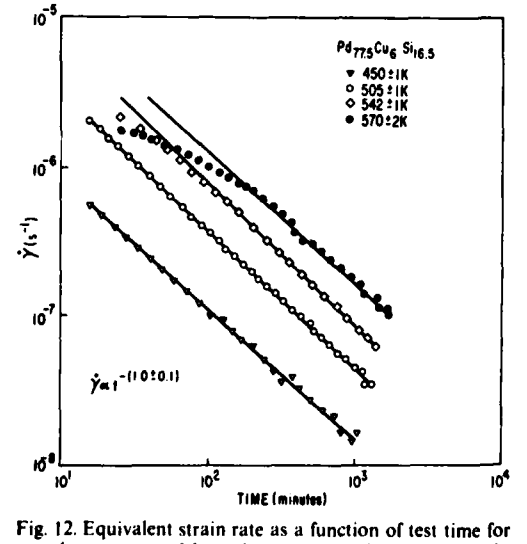

Fig. 12. Equivalent strain rate as a function of test time for samples creep tested from the as-cast condition at the indicated temperatures. The symbols are the experimental data. The solid lines indicate the linear portion of the data.

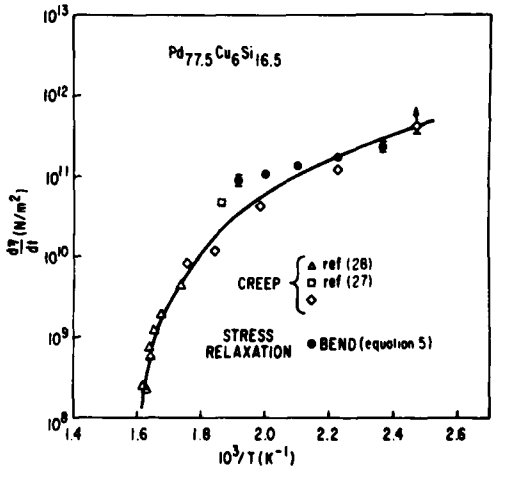

Fig. 14. Rate of change of viscosity with time as measured in tensile creep and bend stress relaxation tests.

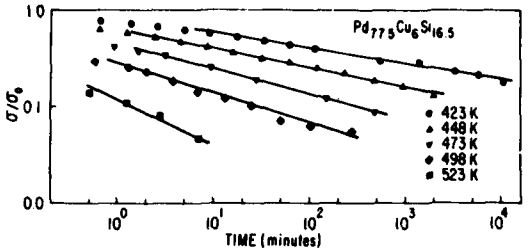

Fig. 15. Bend stress relaxation data for as-cast $Pd_{77.5}Cu_6Si_{16.5}$ at the indicated temperatures. The solid lines indicate the slope of the linear region.

uniformly with time. If the rate of viscosity increase was stress dependent, then the slopes of the curves would change as time increased. These observations indicate that the time dependence of the flow rate is only a function of temperature and composition:

$$\dot{\gamma}(t, T, \mathrm{M}) \propto [\eta_0(T, \mathrm{M}) + \dot{\eta}(T, \mathrm{M})t]^{-1} \qquad (6)$$
$$\mathrm{M} = \text{material}.$$

It is important to note that the transient period observed in the $\dot{\gamma}$–t plot (Fig. 4), is the time required for the increase in viscosity $\dot{\eta}t$, to become much larger than the initial viscosity η_0. During this transient, the exponent

$$n = -\frac{\mathrm{d}(\ln \dot{\gamma})}{\mathrm{d}(\ln t)}$$

is not a constant and is considerably less than unity. This has led to some confusion, particularly at high temperatures where exponents less than unity ($n = 0.5$) have been reported [13].

A structural relaxation model based on an extension of the free volume concept has been proposed to explain the observed increase in viscosity with annealing [12, 30–32]. The model attributes the viscosity increase to a decrease in the free volume of the material as the structural order of the system increases. The model predicts an Arrhenius-type temperature dependence for $\dot{\eta}$, where the activation energy $Q_{\dot{\eta}}$ consists of two terms:

$$Q_{\dot{\eta}} = Q_{\text{isoconfigurational}} + Q_{\text{free volume annihilation}}. \qquad (7)$$

$Q_{\text{isoconfigurational}}$ is the activation energy for constant configuration, constant free volume (i.e. isostructural) flow. $Q_{\text{free volume annihilation}}$ is the activation energy for free volume reduction or potential flow site annihilation. For PdSi, $Q_{\text{isoconfigurational}}$ was a constant, 192 ± 17 kJ/mole, over the entire temperature range tested $423\ \mathrm{K} \le T \le 553\ \mathrm{K}$ [12]. For that same temperature range, $\dot{\eta}$ had an Arrhenius-type temperature dependence with a constant activation energy, $Q_{\dot{\eta}} = 31 \pm 2$ kJ/mole. However, for FeNiPB and PdCuSi, the activation energy for viscosity increase $Q_{\dot{\eta}}$, is clearly not constant (see Figs 6 and 14). It remains to be seen whether the activation energy for isoconfigurational flow for these two alloys increases in a manner corresponding to the increase observed in $Q_{\dot{\eta}}$. In fact, an increase in $Q_{\text{isoconfigurational}}$, toward the higher activation energy that has been observed for equilibrium flow [7], is expected at temperatures near the glass transition temperature T_g.

The stress dependence of the strain rate has been shown to obey a hyperbolic sine relation [equation (1)]. For PdSi, $\gamma_0\Omega_f = 48\ \mathrm{A}^3$ at 500 K [17]. This quantity is approximately three times greater than that of a flow site with volume equal to one Pd atom undergoing a unit shear jump $\gamma_0 = 1$. Extrapolating the reported data for $Fe_{82}B_{15}Si_3$ [33] to 500 K, a large value of $\gamma_0\Omega_f \simeq 150\ \mathrm{A}^3$ is also observed. A strong temperature dependence of $\gamma_0\Omega_f$ is also indicated. For FeNiPB, we found $\gamma_0\Omega_f = 16.5\ \mathrm{A}^3$ at 500 K. In this case, the value is roughly equal to a unit strain of 1.5 times a single atomic volume ($\Omega_{\mathrm{Fe}} = 11.8\ \mathrm{A}^3$, $\Omega_{\mathrm{Ni}} = 10.9\ \mathrm{A}^3$ [34]). The large value of $\gamma_0\Omega_f$ can be explained in terms of a multiple shear jump of a single atomic unit, or a fractional shear strain of a larger atomic volume [15, 16]. Recent bubble raft experiments indicate that the local shear transformations involve regions approximately five atomic diameters wide [35]. Further work must be done in this area to clarify the atomic mechanism. However, the results indicate that at least empirically, the stress dependence can be incorporated into equation (6) as follows:

$$\dot{\gamma}(t, \sigma, T, \mathrm{M}) \propto \frac{\sinh\left[\dfrac{\tau\gamma_0\Omega_f(T, \mathrm{M})}{kT}\right]}{[\eta_0(T, \mathrm{M}) + \dot{\eta}(T, \mathrm{M})t]}. \qquad (8)$$

Finally, we can consider previous observations of isoconfigurational flow. In all cases, an Arrhenius-type temperature dependence has been reported [1, 36]. For PdCuSi structurally stabilized by an anneal at 534 K,

$$Q_{\text{isoconfigurational}} = 240 \pm 25\ \text{kJ/mole [27].}$$

The reported value for $Ni_{36}Fe_{32}C_{14}P_{12}B_6$ (Metglas 2826A), stabilized at 548 K, is

$$Q_{\text{isoconfig.}} \quad 250 \pm 15\ \text{kJ/mole [37].}$$

For PdSi,

$$Q_{\text{isoconfigurational}} = 192 \pm 17\ \text{kJ/mole}$$

for specimens stabilized by annealing over a wide temperature range [2, 12, 14]. In addition, it has been shown that for PdSi, the activation energy is unaffected by stress history. It remains to be shown whether or not $Q_{\text{isoconfigurational}}$ remains a constant for temperatures up to the glass transition temperature. As discussed previously, for PdCuSi and FeNiPB, the

activation energy probably increases near T_g. Incorporating these observations into equation (8), we obtain:

$$\dot{\eta}(t, \sigma, T, \mathrm{M}) \propto \frac{\exp\left[\frac{Q_{\mathrm{rso}}(T_a, t_a)}{kT}\right] \sinh\left[\frac{\tau\gamma_0\Omega_f(T, \mathrm{M})}{kT}\right]}{\eta_0(T, \mathrm{M}) + \dot{\eta}(T, \mathrm{M})t}. \quad (9)$$

T_a and t_a are the structure stabilizing preanneal temperature and time, respectively.

Equation (9) is a general law describing homogeneous flow for several Fe- and Pd-based amorphous alloys. It successfully describes flow under both uniaxial and bending stress conditions, as measured by creep or stress relaxation tests.

CONCLUSIONS

We have examined several Pd- and Fe-based amorphous alloys in tensile creep, tensile stress relaxation and bend stress relaxation tests. In all cases, including the available literature studies, the materials exhibited similar flow properties as summarized below:

1. During creep, the observed flow is characterized by a linear increase in viscosity throughout the test at all temperatures. The rate of viscosity increase is both temperature and composition dependent.
2. The creep strain rate varies inversely with time, but only after an initial transient. During this transient, the exponent

$$n = \frac{-\mathrm{d}(\ln \dot{\gamma})}{\mathrm{d}(\ln t)}$$

is not a constant and is less than unity. This has previously led to some confusion, particularly at high temperatures where the transient decay time is large (>30 min).
3. Stress relaxation data is characterized by a linear decrease in $\log \sigma\ \sigma_0$ with $\log t$, after the decay of a transient whose origin is the same as that observed in the creep tests. The rate of change of the effective viscosity computed from the slopes of the linear regions, is in agreement with the creep results.
4. Tensile stress relaxation tests were performed on $Fe_{40}Ni_{40}P_{14}B_6$ at 500 K, for different initial stresses. The data was analyzed to provide the stress strain rate relations at different test times. A hyperbolic sine relation was obeyed [equation (1)], with a volume strain element $\gamma_0\Omega_f = 16.5\ \mathrm{A}^3$. This value is greater than a unit shear of a single atomic volume, in agreement with the trend observed in other alloys.
5. Compiling the data of this study with previous investigations, a general empirical law describing homogeneous flow for several amorphous alloys under both uniaxial tension and pure bending has been developed [equation (9)].

Acknowledgements--The authors gratefully acknowledge the assistance of W. Mowrey and J. Wilson in designing and building the test apparatus, and W. Rollins for helping to run the tensile stress relaxation tests. The PdCuSi ribbon was vacuum cast by H. H. Liebermann.

REFERENCES

1. F. Spaepen and D. Turnbull, in *Metallic Glasses* (edited by J. J. Gilman and H. J. Leamy), p. 114. ASM, Cleveland, Ohio (1978).
2. A. I. Taub and F. Spaepen, *Scripta metall.* **13**, 195 (1979).
3. J. Logan and M. F. Ashby, *Acta. metall.* **22**, 1047 (1974).
4. R. Maddin and T. Masumoto, *Mater. Sci. Engng* **9**, 153 (1972).
5. F. Spaepen, *J. Non-Cryst. Solids* **31**, 207 (1978).
6. H. S. Chen and D. Turnbull, *J. chem. Phys.* **48**, 2560 (1968).
7. H. S. Chen and M. Goldstein, *J. appl. Phys.* **43**, 1642 (1971).
8. T. Murata, H. Kimura and T. Masumoto, *Scripta metall.* **10**, 705 (1976).
9. J. Megusar, A. S. Argon and N. J. Grant, *Proceeding of Third International Conference on Rapidly Quenched Metals*, Metals Society, Brighton, England, Vol. 2, p. 392 (1978).
10. T. D. Hadnagy, D. J. Krenitsky, D. G. Ast and Che-Yu Li, *Scripta metall.* **12**, 45 (1978).
11. J. C. Gibeling and W. D. Nix, *Scripta metall.* **12**, 919 (1978).
12. A. I. Taub and F. Spaepen, *Acta metall.* **28**, 1781 (1980).
13. J. P. Patterson and D. R. H. Jones, *Acta. metall.* **28**, 675 (1980).
14. A. I. Taub and F. Spaepen, submitted to *J. Mater. Sci.*
15. F. Spaepen, *Acta metall.* **25**, 407 (1977).
16. A. S. Argon, *Acta metall.* **27**, 47 (1979).
17. A. I. Taub, *Acta metall.* **28**, 633 (1980).
18. D. G. Ast and D. J Krenitsky, *J. Mater. Sci.* **14**, 287 (1979).
19. F. E. Luborsky, J. J. Becker and R. O. McCary, *IEEE Trans. Magn.*, **MAG-11**, 1644 (1975).
20. F. E. Luborsky and J. L. Walter, *Mater. Sci. Engng* **35**, 255 (1978).
21. F. A. McClintock and A. S. Argon, *Mechanical Behavior of Materials*, Ch. 7, Addison-Wesley, Reading, Mass (1966).
22. P. M. Anderson III and A. E. Lord, *Mater. Sci. Engng* **44**, 279 (1980).
23. T. Takamori, T. Mizoguchi and T. R. McGuire, *Mater. Res. Bull.* **15**, 81 (1980).
24. C. D. Graham, T. Egami, R. S. Williams and Y. Takei, *AIP Conf. Proc.* **29**, 218 (1976).

25. L. A. Davis, in *Metallic Glasses* (edited by J. J. Gilman and H. J. Leamy), ASM, Cleveland, Ohio (1978), p. 190.
26. R. E. Maringer and C. E. Mobley, *J. Vac. Sci. Tech.* **11**, 1067 (1974).
27. A. I. Taub and F. Spaepen, *Scripta metall.* **14**, 1197 (1980).
28. Private communication with Sylvia S. Tsao and F. Spaepen.
29. A. I. Taub and F. Spaepen, *Scripta metall.* **13**, 983 (1979).
30. M. H. Cohen and D. Turnbull, *J. chem. Phys.* **31**, 1164 (1959).
31. D. Turnbull and M. H. Cohen, *J. chem. Phys.* **34**, 120 (1961).
32. D. Turnbull and M. H. Cohen, *J. chem. Phys.* **52**, 3088 (1970).
33. D. Lee, *Metall. Trans.* **12**, 419 (1981).
34. R. W. Cahn, *Physical Metallurgy*, p. 60. Wiley, New York (1965).
35. A. S. Argon and H. Y. Kuo, *Proceedings of Third International Conference on Rapidly Quenched Metals*, Vol. 2, p. 269. Metals Society, Brighton, England (1978).
36. H. S. Chen, *Rep. Prog. Phys.* **43**, 353 (1980).
37. A. L. Mulder, J. W. Drijver and S. Radelaar, *J. Phys. Paris* **41**, C8-843 (1980).

GENERAL ELECTRIC

General Electric Company
Corporate Research and Development
Schenectady, New York 12345

TECHNICAL INFORMATION SERIES

AUTHOR	SUBJECT	NO.
Luborsky, FE Bacon, F*	diffusion in amorphous alloys	81CRD193
		DATE August 1981
TITLE		GE CLASS
Diffusion of Silicon Into Amorphous Fe-B and Fe-B-Si		1
		NO. PAGES 6
ORIGINATING COMPONENT		CORPORATE
Metallurgy Laboratory		RESEARCH AND DEVELOPMENT SCHENECTADY, N.Y.

SUMMARY

The diffusion constants for the diffusion of Si into amorphous $Fe_{82}B_{12}Si_6$ were determined from about 300 to 420 °C from composition-depth profiles obtained from Auger analysis during ion milling of a Si/Fe-B-Si couple. Various surface preparation techniques for the amorphous alloy had no effect on the diffusion profile. A single diffusion constant was obtained at each temperature, as indicated by the linearity of the graph of the concentration plotted as an error function vs. depth. A linear Arrhenius graph was obtained with $\Delta E = 2.2 \pm 0.4$ eV and $A = 0.029$ m^2/s. Preannealing the amorphous alloy before preparing the Si/Fe-B-Si couple did not significantly alter the values of D. These results for D are very similar to previously reported results for the diffusion of B into Fe-Ni-B and into Ni-Nb, and are about two orders of magnitude greater than results for crystalline α-Fe and six orders of magnitude larger than for fcc Ni, both obtained by extrapolation from much higher temperatures. It is concluded that an interstitial diffusion mechanism is taking place.

*Inorganic Materials and Structures Laboratory

KEY WORDS

amorphous alloys, diffusion, Auger analysis

INFORMATION PREPARED FOR _____

DIFFUSION OF SILICON INTO AMORPHOUS Fe-B-Si

F.E. Luborsky and F. Bacon*

INTRODUCTION

The results of studies in amorphous alloys of kinetics of crystallization[1,2] stress relaxation[3,4] induced anisotropy,[5,6] and embrittlement[7] all depend on atomic motions controlled by diffusivity of the various species present in the alloy. Until the past year or so, there have been very few direct measurements of diffusion of atoms in amorphous alloys. Thus, it has been difficult to interpret these kinetics on an atomistic basis.

In this report we present diffusion constants for silicon diffusing into Fe-B-Si. We discuss these results and compare them to previous results of diffusion of atoms into amorphous alloys.

EXPERIMENTAL

The amorphous alloy was obtained from the Allied Chemical Company as Metglas 2605S, an alloy with the nominal composition $Fe_{82}B_{12}Si_6$. To determine the effect of surface roughness on the analytical breadth of the silicon-amorphous metal interface during elemental profile analyses, the amorphous metal surfaces were prepared by four different procedures: (1) mechanically polishing the surface down to 0.05 μm Al_2O_3 powder, (2) mechanically polishing as in (1) followed by electrolytic polishing, (3) only electrolytic polishing of the shiny side of the ribbon, and (4) no surface treatment for deposition on the shiny side of the ribbon. The electrolyte used for the polishing contained 15 ml perchloric acid, 800 ml ethanol, and 100 ml propanol. It operated at 28 V and was used to remove $\sim$ 7 μm of material. The samples were then placed in a sputtering chamber, the silicon target sputter etched for 30 min, the amorphous ribbon sputter etched for 3 min at 1650 V and then immediately 600 to 4000 Å of Si deposited at 1700 V and 300 W RF, all in 18 μm of argon. Under these conditions the Si deposit is amorphous. This was confirmed by X-ray diffraction from the surface. The sputter etching removed about 100 Å of the ribbon which had previously been shown to be more than sufficient to remove any oxide, surface films, and inhomogeneity in composition.[8] The samples were then annealed in N_2, under Ti chips as a getter, at various temperatures. The Auger spectrometer used for the analyses was a Physical Electronic SAM-545. To obtain the elemental depth profiles, an in situ Ar^+-ion gun operating at a beam voltage of 2 kV was used. This gun, operating in a defocused mode, produces an etched crater of $\sim$5 mm in diameter which is substantially larger than the primary electron beam diameter of $\sim$25 μm used in the analysis. Thus only the central flat portion of the etched spot was analyzed. Elemental depth distributions were obtained simultaneously for boron (179 eV Auger transition), iron (703 eV), silicon (1619 eV), and oxygen (503 eV). Typical results are shown in Figure 1. The rate of ion gun etching was determined from the time required to etch through the deposited silicon layer to the midpoint in the Si profile. The thickness of Si deposited was determined from calibration runs using the weight increase of a glass slide. It was assumed that the rate of etching through the Si was the same as the rate through the amorphous alloy since there was no change in slope of the concentration vs sputter time curves at the interface when plotted on probability paper in any of the samples. An example is shown in Figure 2.

Annealing was carried out at temperatures both below and above the start of crystallization as previously determined from the beginning of the increase in coercivity.[9] We believe the results obtained above the start of crystallization are still representative of diffusion of Si through predominately the amorphous phase since DSC scans have shown that only a small fraction of the samples are crystallized at the highest temperature used for the diffusion (Table 1).

DATA ANALYSIS AND RESULTS

At the highest temperature used for the diffusion, the plateau in the depth profile representing the existence of a pure Si layer in Figure 1, is still in evidence. Thus, we are considering the diffusion of an atom from an infinite source into an infinite sink; i.e., one in which the diffusion distance $4(DT)^{1/2}$ is small relative to the length of the system. Accordingly, the concentration at any

* Inorganic Materials and Structures Laboratory

Manuscript received July 20, 1981

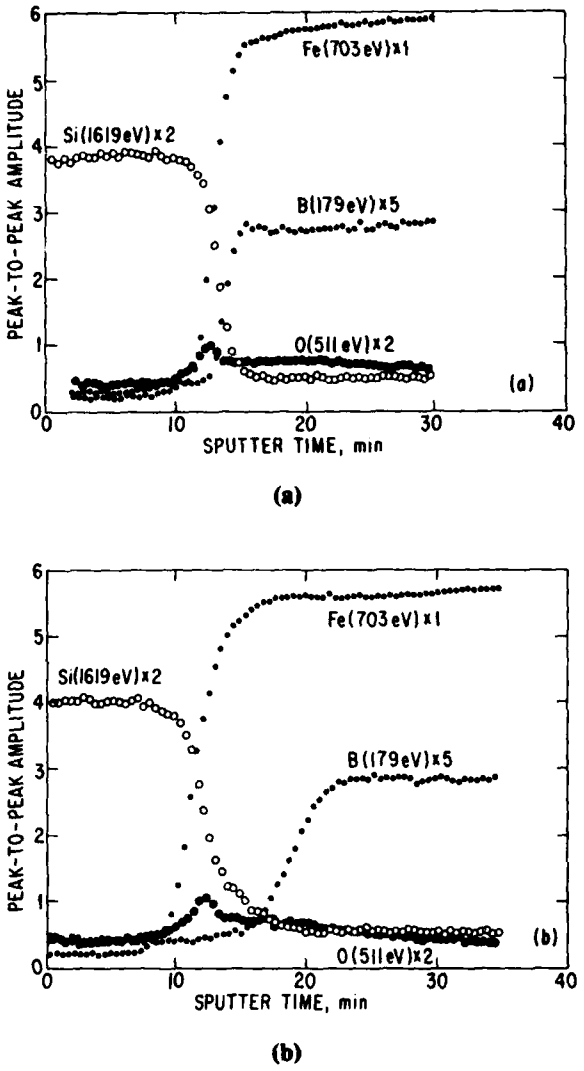

Figure 1. Typical Auger output on sputter etching and analysis of a 2500 Å layer of Si deposited on $Fe_{82}B_{12}Si_6$ (a) as prepared and (b) after annealing for 2 h at 377.5 °C.

given distance x from the center of the interface after time t will be

$$c(x,t) = \left[c'(4\pi Dt)^{-1/2}\right] \int_o^\infty \exp\left[-(x-\alpha)^2(4Dt)^{-1}\right] d\alpha \qquad (1)$$

where c' is the initial concentration of the diffusing species. In this case for Si $c' = 1$, D is the diffusion constant, t is the time, and α is the distance from

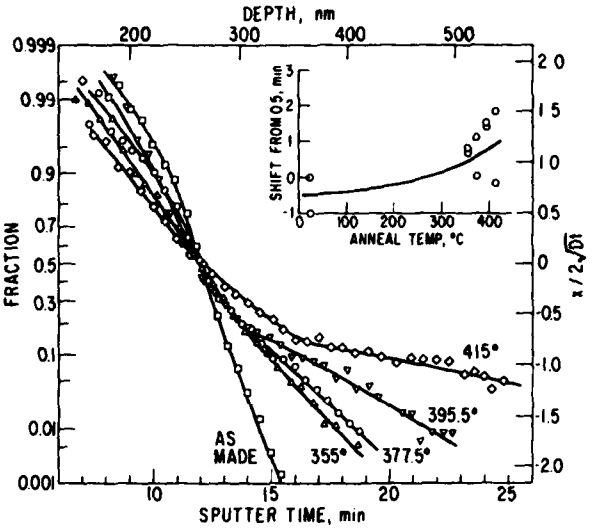

Figure 2. Probability and $x/(4Dt)^{1/2}$ graph of silicon concentration vs sputter time and sputter depth for a typical series of silicon/-amorphous $Fe_{82}B_{12}Si_6$ couples annealed for 2 h at various temperatures. The curves were normalized to the same sputter etching time at the 50% concentration point. Shown on the inset are the normalization times for the samples.

TABLE 1

FRACTION OF $Fe_{82}B_{12}Si_6$ CRYSTALLIZED VS ANNEAL TEMPERATURE (from area of first DSC peak at 40 °/min)

2 h at Anneal Temperature (°C)	Fraction Crystallized
as-cast	0.05
360	+0.04[a]
380	-0.03
400	-0.07
415	+0.02
436	+0.95
452	1.00
480	1.00

[a]beginning of crystallization as detected by the first increase in coercivity.

the diffusing slab to $x = 0$. If we define the error function

$$\mathrm{erf}(z) = 2\pi^{-1/2}\int_0^{\infty} \exp\left[-(x-\alpha)^2(4DT)^{-1}\right] d\left[(x-\alpha)(4Dt)^{-1/2}\right] \quad (2)$$

then

$$c(x,t) = 0.5 + 0.5\ \mathrm{erf}\left[x(4Dt)^{-1/2}\right] \quad (3)$$

where $z = x(4Dt)^{-1/2}$. The values for this error function cannot be evaluated in any simple manner but are available in tabular form in many mathematical tables. A graph of relative concentration vs depth on probability paper will be a straight line. Differentiating to obtain the slope $G = -(4\pi Dt)^{-1/2}\exp(-x^2/4Dt)$ which becomes $-(4\pi Dt)^{-1/2}$ at the interface $x = 0$. In the case where various contributions to the initial broadening become significant, the observed broadening must be corrected for this initial broadening, as has been described.[10] When a Gaussian diffusion process is observed with an instrument whose response is also Gaussian, then the uncorrected profile is also Gaussian. Then the observed broadening is given by the concentration gradient G as $G_{obs}^{-2} = G_{diff}^{-2} + G_{instr}^{-2}$. In addition, in a multistage diffusion process, since diffusion times add linearly, diffusion distances add as the square root of the sum of the squares. Thus a similar relation applies if some diffusion occurs before the initial profile is measured or if other broadening effects such as roughness and nonuniformity of thickness or composition occurs, provided they are Gaussian. Thus, we have $G_{obs}^{-2} = G_{diff}^{-2} + G_{init\ diff}^{-2} + G_{instr}^{-2} + G_{rough}^{-2} + \ldots$ and the deconvolution is a simple subtraction to give

$$G_{init\ diff}^{-2} = \left[G_{obs}^{-2}\right]_{t=t} - \left[G_{obs}^{-2}\right]_{t=0} = 4Dt. \quad (4)$$

Typical results of the Si data, as a function of annealing, are shown in Figure 2 on probability paper. The curves were shifted, for clarity in presentation, by the amount shown on the inset in the figure. The unannealed Si/amorphous alloy couple is always a straight line from ~5 to 95% of the profile with $\sigma = 20 \pm 5$ nm. This analytical broadening may be due to instrumental factors, insufficiently flat substrate surface, uneven etching across the pit, the "knock-in" effect, preferential sputtering, or penetration or atom transport during the Si deposition. These effects were discussed recently.[11] The change to be examined in the profiles on annealing is the result of Si diffusing into the amorphous alloy represented by the decrease in the slope of the deeper layers. These tails of the curves appear to be straight lines and thus represent a single value of D. The values of D were calculated from these straight line tails in the amorphous alloy. However, since the slope of the unannealed samples $(4Dt)_u^{-1/2}$ is comparable to the slope after annealing $(4Dt)_a^{-1/2}$, the slopes representing the Si diffusion were obtained by simply subtracting the squares of the inverse slopes as described above, where $(4Dt)_u^{-1/2}$ was obtained from the initial portion of each curve; i.e., from the Si-rich film. The value of D was then calculated from eq. (4). There appeared to be a small trend towards a decreasing initial slope as well as a small shift in the midpoint of the profile with increase in anneal temperature (Figure 2). These effects were ignored in the analysis.

The results of all of our measurements and calculations for D for two different alloys are shown in Figure 3, on an inverse temperature scale. The composition profile of two samples, prepared under identical conditions, was determined. One sample in the entire work was discarded because the value of D was two orders of magnitude above the trend shown. This sample had the highest oxygen content at the interface and this may presumably have been the cause for the high value. The ratio of the oxygen peak to the pure silicon peak was 1.3 for this sample; the average ratio for all other samples was 0.29. The different polishing procedures and the different Si layer thicknesses showed no significant effect on the half-width of the Si profile or on D. We also found no significant effect of preannealing on D as shown in Figure 3. The results in Figure 3 appear to be a straight line giving an activation energy of 2.2 ± 0.4 eV and a preexponential constant of 0.029 m^2/s.

Preliminary analysis by secondary ion mass spectrometry (SIMS) have been performed on a few $Si-Fe_{82}B_{12}Si_6$ couples. The results have not been analyzed quantitatively but they show the same trends as obtained from the Auger result.

DISCUSSION

There are now a number of measurements of diffusion of metals and metalloids in various amorphous alloys. These are summarized in Figure 4, plotted against the inverse temperature normalized to T_g, and include the results from the present

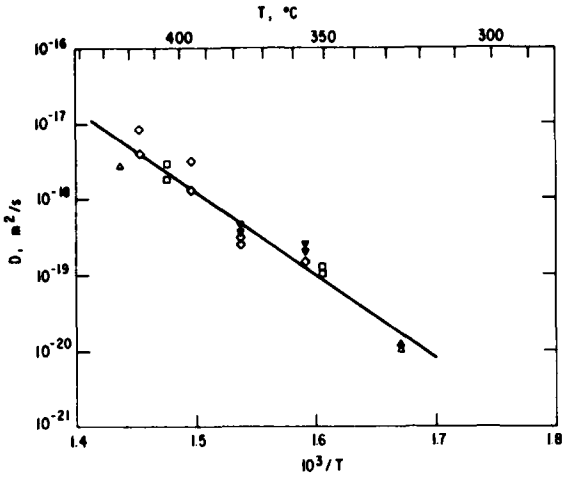

Figure 3. Diffusion constants as a function of inverse temperature. Solid points for preannealing for 2 h at 300 °C after electropolishing: ◇, □ electropolished; Δ no polishing before Si deposition; □ 1500 Å Si; ◇ and ▼ 2500 Å Si; Δ 3920 Å Si.

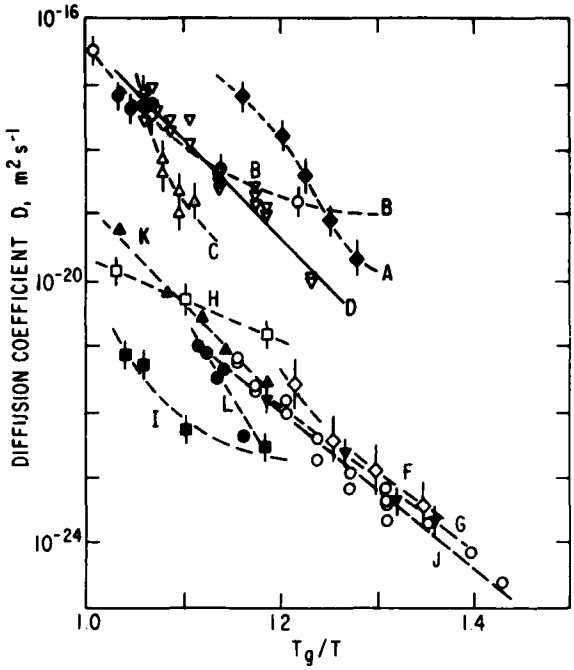

Figure 4. Direct measurements of diffusion coefficients in amorphous alloys vs normalized inverse temperature

A) Li in $Pd_{80}Si_{20}$ [12]
B) B in as-quenched (open circles) and relaxed (filled circles) $Ni_{59.5}Nb_{40.5}$ [13]
C) B in $Fe_{40}Ni_{40}B_{20}$ [14]
D) Si in as-quenched and relaxed $Fe_{82}B_{12}Si_6$ (this work)
F) P in $Fe_{85}B_{15}$ [15]
G) Ag in $Pd_{81}Si_{19}$ [16]
H) Au in as-quenched $Pd_{77.5}Cu_6Si_{16.5}$ [17]
I) Au in relaxed $Pd_{77.5}Cu_6Si_{16.5}$ [17]
J) P in relaxed $Fe_{32}Ni_{36}Cr_{14}P_{12}B_6$ [18]
K) Fe in $Fe_{40}Ni_{40}P_{14}B_6$ [19]
L) P in $Fe_{40}Ni_{40}P_{14}B_6$ [20].

study. It should be noted that values of T_g all at the same heating rate were not available, and, in fact, where T_g values were not obtainable the values of the start of crystallization $T_{x,0}$ were used (Table 2). Differences of 10 to 20° would make no difference in Figure 4. Note that the results tend to fall into two groups. The upper group comprises the diffusion of small atoms; Li in PdSi,[12] B in NiNb,[13] B in FeNiB,[14] and Si in as-quenched and relaxed FeBSi (this work). The lower group of curves comprises the diffusion of larger atoms: P in FeB,[15] Ag in PdSi,[16] Au in as-quenched PdCuSi,[17] Au in annealed PdCuSi,[17] P in annealed FeNiCrPB,[18] Fe in FeNiPB,[19] and P in FeNiPB.[20] Our new results confirm the previous observations.[21] First, the diffusion of small atoms is several orders of magnitude larger than the diffusion of large atoms at an equivalent fraction of T_g. Thus, the natural interpretation is that there are two different mechanisms. Secondly, annealing of the amorphous alloy before diffusing produces little or no change on the diffusion of a small atom into the amorphous alloy.

Kijek et al.[21] have summarized the possible diffusion processes in amorphous metals. There are three possibilities: vacancy, cooperative, and interstitial diffusion. They conclude from computer modeling studies that individual vacancies are not stable so that vacancy diffusion in amorphous alloys is not possible. As in crystals there is a high energy barrier to prevent a large atom from locating in an interstitial site so that the only possible diffusion mechanism is a cooperative process. This will be a slow process because of the low probability of correlated atom motions. The correlated jump mechanism has been proposed for the diffusion of Li in PdCuSi.[17] For small atoms, such as Li and B, interstitial diffusion occurs in crystalline metals and the same is likely in amorphous metals. An interstitial mechanism has been proposed for Li in PdSi.[12] If we extrapolate results from the literature for the diffusion of Si in crystalline α-Fe or in fcc Ni from the high temperature where the measurements were made down to our measurement temperatures, then the values of D are at least several orders of magnitude slower than obtained for our results on diffusion of Si in amorphous FeBSi (Table 3). The slower diffusion of the larger atoms is

TABLE 2

VALUES OF THE GLASS TEMPERATURE AND THE TEMPERATURE FOR THE START OF CRYSTALLIZATION USED IN FIGURE 4.

Alloy	T_g (K)	$T_{x,0}$ (K)	Heating rate (deg/min)	Reference
$Fe_{40}Ni_{40}B_{20}$	683	-	10	14
$Pd_{77.5}Cu_6Si_{16.5}$	632	-	10	17
$Ni_{59.5}Nb_{40.5}$	881	-	10	25
$Pd_{80}Si_{20}$	655	-	20	26
$Pd_{81}Si_{19}$	650	-	20	26
$Fe_{85}B_{15}$	-	660	10	27
$Fe_{40}Ni_{40}P_{14}B_6$	643		20	28
$Fe_{82}B_{12}Si_6$	-	740	20	this work
$Fe_{32}Ni_{36}Cr_{14}P_{12}B_6$	725	-	10	this work

TABLE 3

DIFFUSIVITY OF SI INTO CRYSTALLINE α-Fe, fcc Ni, AND AMORPHOUS Fe-B-Si

Temp. (°C)	D, m^2/s αFe^a	Ni[b]	$Fe_{82}B_{12}Si_6$[c]
300	1.5×10^{-23}	3.3×10^{-28}	7.1×10^{-22}
350	4.5×10^{-22}	2.6×10^{-26}	2.7×10^{-20}
405	1.1×10^{-20}	1.5×10^{-24}	7.7×10^{-19}

[a] calc. from ref. 22; $A = 4.4 \times 10^{-5}$ m^2/s, $Q = 2.10$ eV.
[b] calc. from ref. 24; $A = 1.5 \times 10^{-4}$ m^2/s, $Q = 2.69$ eV.
[c] from this work; $A = 0.0292$ m^2/s, $Q = 2.23$ eV.

assumed to be by a cooperative process from substitutional sites. All of these considerations mean that Si is diffusing rapidly by an interstitial mechanism.

There is expected to be a distribution of activation energies for individual interstitial jumps because of the distribution of sizes of interstitial sites in an amorphous alloy. Thus, interstitial diffusion is not a true random walk process and the diffusivity of a given atom should be smaller than in an fcc crystal because diffusing atoms can be trapped at the larger interstitial sites.[23] This result is not observed on comparing the diffusion of Si into fcc Ni[24] as calculated from higher temperature measurements to the diffusion of Si into amorphous FeBSi (Table 3). It was also argued that because interstitial diffusion is not a true random walk process in amorphous alloys, it may not follow the Arrhenius law. As seen in Figure 4, this appears to be true for some cases, namely for B in NiNb,[13] Li in PdSi,[12] and B in FeNiB.[14] However, the results from the literature presented in Figure 4 are

quite limited in the number of data points and in the temperature range covered. Thus, these conclusions should be regarded as tentative, especially in view of our new results on Si in FeBSi which do follow an Arrhenius law.

CONCLUSIONS AND SUMMARY

1. The diffusion constants for the diffusion of Si into amorphous $Fe_{82}B_{12}Si_6$ were determined from about 300 to 420 °C from composition-depth profiles obtained from Auger analysis during ion milling of a Si/Fe-B-Si couple.

2. Various surface preparation techniques for the amorphous alloy had no effect on the diffusion profile.

3. A single diffusion constant was obtained at each temperature, as indicated by the linearity of the graph of the concentration plotted as an error function vs. depth.

4. A linear Arrhenius graph was obtained with $\Delta E = 2.2 \pm 0.4$eV and $A = 0.029$ m^2/s.

5. Preannealing the amorphous alloy before preparing the Si/Fe-B-Si couple did not significantly alter the values of D.

6. These results for D are very similar to previously reported results for the diffusion of B into Fe-Ni-B and into Ni-Nb, and are about two orders of magnitude greater than results for crystalline α-Fe and six orders of magnitude larger than for fcc Ni, both obtained by extrapolation from much higher temperatures.

7. It is concluded that an interstitial diffusion mechanism is taking place.

ACKNOWLEDGMENTS

The authors thank the Office of Naval Research for partial support during the course of this work. They are especially grateful to the University of Sussex, School of Engineering and Applied Science, Professor R.W. Cahn and Dr. A.W. Simpson, for their stimulation and for the preliminary work with Dr. J. Venables while visiting there on a Senior Visiting Fellowship from the British Science Research Council in 1977. We also wish to thank Dr. S.C. Huang for his help in reviewing the analysis of our original data, Dr. G. Slack for several illuminating discussions concerned with diffusion in crystalline systems and Prof. R.W. Cahn for a critical review of the draft of this work.

REFERENCES

1. F.E. Luborsky, *Materials Sci. Eng. 28* (1977) 139.
2. F.E. Luborsky and H.H. Liebermann, *Appl. Phys. Lett. 33* (1978) 233.
3. F.E. Luborsky and J.L. Walter, *Materials Sci. Eng. 35* (1978) 255.
4. F.E. Luborsky and H.H. Liebermann, *J. Appl. Phys. 51* (1980) 796.
5. F.E. Luborsky, *AIP Conf. Proc. 29* (1976) 209.
6. F.E. Luborsky and J.L. Walter, *Materials Sci. Eng. 28* (1977) 77.
7. J.L. Walter and F.E. Luborsky, *Materials Sci. Eng. 33* (1978) 91.
8. J.L. Walter, F. Bacon, and F.E. Luborsky, *Materials Sci. Eng. 24* (1976) 239.
9. F.E. Luborsky, J.J. Becker, J.L. Walter, and H.H. Liebermann, *IEEE Trans. Magnetics, MAG-15* (1979) 1146.
10. P.M. Hall and J.M. Morabito, *Surface Science 54* (1976) 79.
11. S. Hofmann, *Surface and Interface Anal. 2* (1980) 148.
12. C. Birac and D. Lesueur, *Phys. Stat. Sol. A36* (1976) 247.
13. M. Kijek, B. Cantor, and D.W. Palmer, to be published.
14. R.W. Cahn, J.E. Evetts, J. Patterson, R.E. Somekh, and C. Kenway Jackson, *J. Mat. Sci. 15* (1980) 702.
15. G. Edelin and C. Tete, *Scripta Met.*, in press.
16. D. Gupta, K.N. Tu and K.W. Asai, *Phys. Rev. Lett. 35* (1975) 796.
17. H.S. Chen, L.C. Kimerling, J.M. Poate, and W.L. Brown, *Appl. Phys. Lett. 32* (1978) 461.
18. D.R. Baer, L.R. Pederson, and M.T. Thomas, *Materials Sci. Eng. 48* (1981) 283.
19. P. Valenta, K. Maier, H. Kronmuller, and K. Freitag, *Phys. Stat. Sol.*, in press.
20. P. Valenta, K. Maier, H. Kronmuller, and K. Freitag, *Phys. Stat. Sol., B 105* (1981) 537.
21. M. Kijek, M. Ahmadzadeh, B. Cantor, and R.W. Cahn, *Scripta Met. 14* (1980) 1337.
22. W. Balz, H.W. Mead, and C.E. Birchenall, *J. Metals, Trans. AIME 194* (1952) 1070.
23. M. Ahmadzadeh and B. Cantor, *J. Non-Cryst. Sol. 43* (1981) 189.
24. R.A. Swalin, A. Martin and R. Olson, *J. Metals, Trans. AIME 209* (1957) 936.
25. C. Clay, M.Sc. thesis, MIT (1978).
26. H.S. Chen and D. Turnbull, *Acta Met 17* (1969) 1021.
27. T. Kemeny, I. Vincze, B. Fogarassy, and S. Arajs, *Rapidly Quenched Metals III*, edited by B. Cantor, Vol. 1, p. 291, The Metals Soc., London (1978).
28. D.G. Ast and D. Krenitsky, *Materials Sci. Eng. 23* (1976) 241.

GENERAL ELECTRIC

General Electric Company
Corporate Research and Development
Schenectady, New York 12345

TECHNICAL INFORMATION SERIES

AUTHOR
S.C. Huang, P.G. Frishmann, F.E. Luborsky,
J.D. Livingston, A. Mogro-Campero*

NO. 81CRD213
DATE September 1981

TITLE
Effects of Ribbon Thickness and Annealing Temperature on the AC Magnetic Properties of the $Fe_{81.5}B_{14.5}Si_3C_1$ Alloy

GE CLASS 1
NO. PAGES 5

ORIGINATING COMPONENT
Metallurgy Laboratory

CORPORATE RESEARCH AND DEVELOPMENT SCHENECTADY, N.Y.

SUMMARY

The ac magnetic properties measured at 60 Hz are found to be strongly affected by ribbon thickness and annealing temperature. These magnetic results are further characterized by observations on magnetic domain structure, crystallization, stress relaxation, and ribbon surface finish. It is concluded that, under the optimum annealing condition of 2 hr at 345 °C, most of the cast-in stress (up to 90%) is relieved without significant crystallization (<4%). The optimum ribbon thickness found for ac properties is ~30 μm, which is consistent with that found previously for dc properties. A ribbon of optimum thickness, after the optimum anneal, has a core loss of 0.18 W/kg and an excitation of 0.2 VA/kg at the induction of 1.4 Tesla. It is determined that for thicker ribbons, properties are deteriorated by cast-in crystallites and remnant stress after annealing, both of which introduce transverse magnetic domains. On the other hand, for thinner ribbons, properties are degraded due to the large air pockets, which form as an inherent result of the casting conditions necessary for thin ribbons. The air pockets in thin ribbons result in local ribbon thickness variations and complicated stress fields and, therefore, tend to pin the magnetic domain walls.

*Physical Chemistry Laboratory

SUBJECT
amorphous metals

KEY WORDS
amorphous metals, amorphous ribbon,
soft magnetic properties, ribbon thickness,
air pocketing, annealing effect

INFORMATION PREPARED FOR _____

Additional Hard or Microfiche Copies Available from

Technical Information Exchange
Bldg. 81 Room A133, Schenectady, N.Y. 12345

EFFECTS OF RIBBON THICKNESS AND ANNEALING TEMPERATURE ON THE AC MAGNETIC PROPERTIES OF THE $Fe_{81.5}B_{14.5}Si_3C_1$ ALLOY

S.C. Huang, P.G. Frischmann, F.E. Luborsky, J.D. Livingston, and A. Mogro-Campero

INTRODUCTION

The effect of some process variables on the properties of melt-spun amorphous metal ribbons has been reported recently (see Reference 1 for a brief review). Of most interest is the finding that the soft magnetic properties are very sensitive to ribbon thickness as controlled by the casting speed.[1-3] More specifically, it has been demonstrated that a ribbon should be cast at an optimum thickness in order to obtain the best dc magnetic properties.[1,3] The degraded magnetic properties of thick ribbons were generally attributed to the reduced quench rate, but those of thin ribbons were not well understood. This work reports on the ac magnetic properties as influenced by ribbon thickness as well as annealing temperature. The ribbon thickness was controlled by the melt delivery conditions (e.g., ejection pressure, nozzle slot size, and the crucible-wheel gap), while the casting wheel speed was kept constant.[4] A number of ribbon characteristics relating to structure, stress, ribbon surface smoothness, and magnetic domain configuration were studied in order to obtain insights into the observed ribbon-thickness effect.

EXPERIMENTAL

Steady-state casting of $Fe_{81.5}B_{14.5}Si_3C_1$ ribbons was carried out in air on a copper-1% chromium wheel with internal water cooling. The casting wheel was rotated at a surface speed of 15 m/s and the wheel surface was maintained with wire brush at a "matte" finish during casting.[5] Variations in nozzle slot breadth (0.4 to 0.9 mm), ejection pressure (10^4 to 4×10^4 pascal), and crucible-wheel gap (0.35 to 0.7 mm) were made to change the ribbon thickness.[4] The resultant ribbon thickness was determined by calculation from ribbon weight divided by length, width, and density. The ribbon surface smoothness was studied by SEM and the ribbon cross-section profile by metallography. The ac core loss and excitation were measured with sinusoidal flux at 60 Hz for straight ribbons (40 cm long) and toroids (20 turns on 7.5 cm diameter cores). The magnetic domain configuration was observed by the SEM technique.[6] Also, the stress relaxation was studied by annealing a ring,[7] and the electrical resistivity by a four-probe dc technique.[8] Finally, the magnitude and direction of the magnetic anisotropy were determined by a torque magnetometer using disk specimens etched out of the ribbon.

RESULTS AND DISCUSSION

The excitation of a straight ribbon (33 μm thick) near saturation induction is compared for three annealing temperatures (Figure 1). Annealing 2 hr at 345 °C results in low excitation. Isochronal annealing at 305 or 385 °C yields high excitation, being characterized by a slow approach to saturation. Among the three temperatures studied here, 345 °C was selected as the optimum anneal temperature, although more thorough studies reveal that the best 2 hr anneal for minimum exciting power at useful flux densities occurs at 360 °C. The effect of varying ribbon thickness and annealing at 345 °C/2 hr is shown in Figure 2. For a thin ribbon, excitation is low at low inductions, but is high at high inductions due to a slow approach to saturation; and, for a thick ribbon, excitation is high at all levels of induction. The intermediate thickness gives the best ribbon property. The annealing condition and ribbon thickness influence the core loss of ribbons in a similar manner. Figure 3 summarizes the ribbon thickness effects on excitation and core loss at 1.4 Tesla after the optimum anneal. Clearly, an optimum ribbon thickness exists at $S \simeq 30$ μm, which achieves a low core loss of $\sim$0.18 W/kg and a low excitation of $\sim$0.2 VA/kg at 1.4 Tesla. The optimum thickness found here for the ac magnetic properties is in agreement with that reported for the dc properties.[1]

The excitations for straight samples and toroids at various ribbon thickness are also compared in Figure 3. They are similar in magnitude for thin ribbons, but the toroid excitation is significantly higher for ribbons thicker than 30 μm. Study of the excitation versus induction shows a slower approach to saturation when a thick ribbon is wound into a toroid. Compared with straight samples, the core loss of toroidally wound thin ribbons is unchanged and that of thick ribbons increases slightly.

Manuscript received August 11, 1981

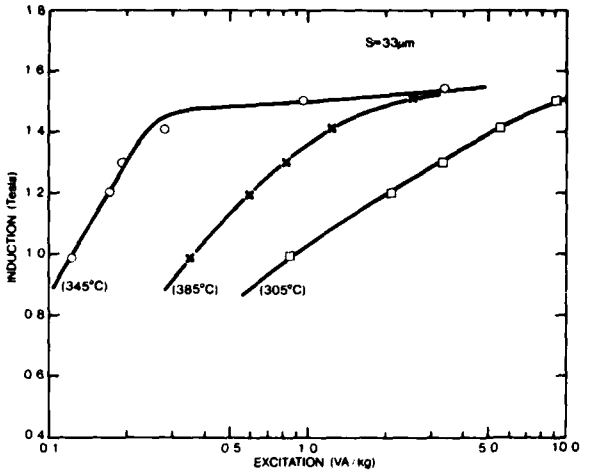

Figure 1. Excitation near the saturation induction for 2 hr annealing at 305, 345, and 385 °C. Ribbon thickness S = 33 μm.

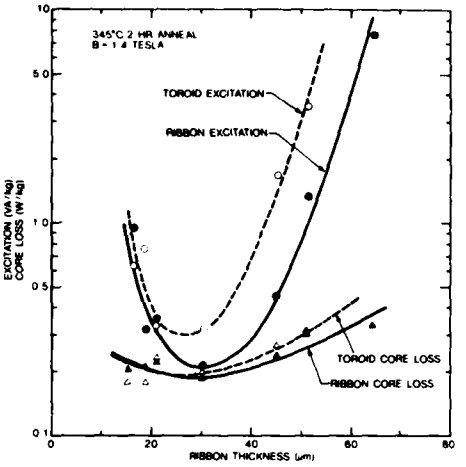

Figure 3. The ribbon thickness dependence of the core loss and excitation for straight ribbons and 7.5 cm toroids, annealed 2 hr at 345 °C. B = 1.4 Tesla.

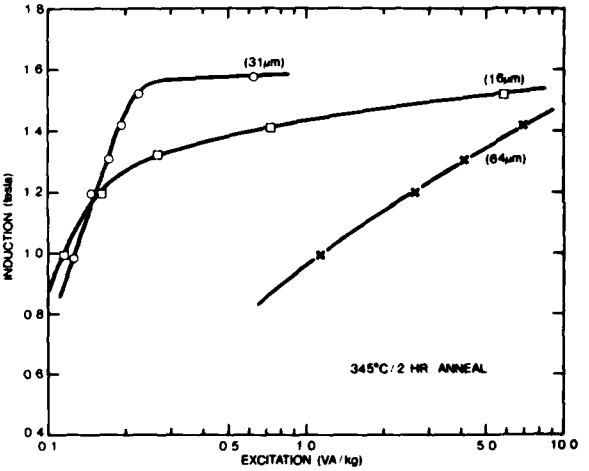

Figure 2. Excitation near the saturation induction for ribbons of the thickness of 16, 31, and 64 μm, annealed 2 hr at 345 °C.

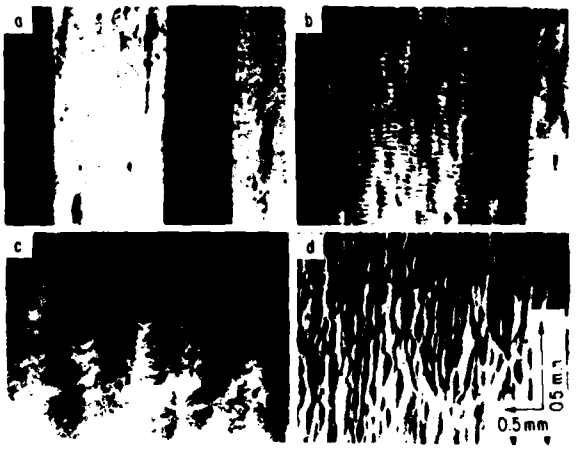

Figure 4. SEM magnetic domain configurations observed on the air-side surfaces of ribbons of (a) thickness S = 31 μm, annealed 2 hr at T = 345 °C; (b) S = 31 μm, T = 385 °C; (c) S = 64 μm, T = 345 °C; and (d) S = 16 μm, T = 305 °C. The ribbon axis is in the vertical direction. Difference in magnification in the horizontal and vertical direction is due to specimen tilt.

The magnetic domain structure observed in a ribbon of optimum thickness and after annealing at the optimum condition of 345 °C/2 hr is shown in Figure 4a. As shown, the wide domains separated by 180° domain walls are generally parallel to the ribbon length and are quite evenly spaced across the ribbon width. When an optimum thickness ribbon is annealed 2 hr at 385 °C, transverse fine domains can be found in a few areas superimposed on the longitudinal wide domains (Figure 4b). In a thick ribbon annealed at the optimum conditions, the domains are exclusively transverse (Figure 4c). The transverse closure domains in Figure 4b and 4c are indications of compressive stress fields and out-of-plane anisotropy. Thin ribbons annealed 2 hr at 305 °C show fine longitudinal domains, which are complicated by the internal stresses associated with the ribbon surface irregularities (Figure 4d). After the optimum anneal, the thin

ribbons show an increase in domain width and domain alignment, but the domain walls are still curved slightly at the vicinity of the surface irregularities. Application of tensile stresses on the order of 10-20 MPa removes the transverse domains of Figure 4b and 4c in favor of longitudinal domains, and tends to straighten the curved walls of Figure 4d.[6] The transverse or wavy longitudinal domains observed in ribbons of suboptimal thickness or annealing should give rise to the slow approach to saturation observed in Figures 1 and 2.

The fraction of crystallinity in the ribbon is estimated from resistivity measurements (Figure 5). It has been demonstrated previously that a nearly linear correlation exists between the resistivity and the fractional crystallinity of a ribbon.[8] Here, the normalized resistivity $\rho_{77}/\rho_{295} = 0.962$ is measured for completely amorphous $Fe_{81.5}B_{14.5}Si_3C_1$, and $\rho_{77}/\rho_{295} = 0.650$ for a ribbon fully crystallized (by annealing 2 hr at 465 °C). As shown in Figure 5, there is a tendency for an increase in crystallinity with ribbon thickness, for both as-cast or annealed specimens. In the 20 and 30 μm ribbons, crystallization occurs only after high-temperature annealing; and, in the 64 μm ribbon, there are cast-in crystals which grow in size upon annealing. The above results on crystallinity fraction have been confirmed qualitatively with TEM studies, and should explain, at least partially, the observed effects of ribbon thickness and annealing temperature on the magnetic properties. An interesting note from Figure 5 is the generally small fraction of crystallinity (<4%), even in the thick, annealed ribbon which has very high core loss and excitation.

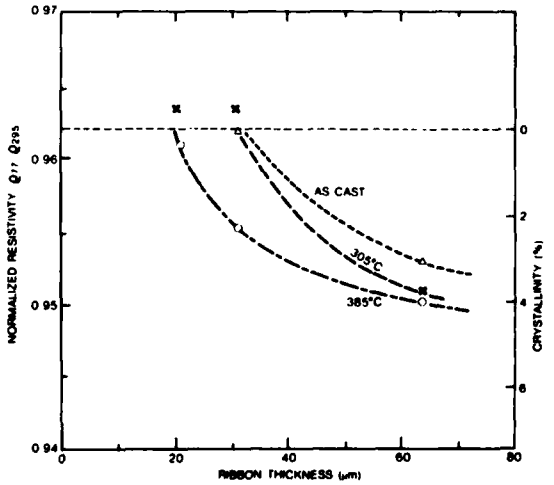

Figure 5. Crystallinity fraction determined by resistivity measurements as a function of ribbon thickness for as-cast, 304 °C/2 hr anneal, and 385 °C/2 hr anneal.

The stress relaxation results in Figure 6 show that the relieved fraction F of stress increases with annealing temperature. As derived from the slope of the log (F) versus $1/T$ relation, the apparent kinetic activation energy involved in the low-temperature relaxation (T < 250 °C) is 29 kJ/mole. This apparent energetic barrier for the stress relaxation is independent of the ribbon thickness. The relieved fraction F, however, decreases with increasing ribbon thickness at a given annealing temperature. The relatively slow stress relaxation in a thick ribbon can be attributed to the small free volume due to a low average quench rate,[9] and to partial crystallization.[10] After the 345 °C/2 hr anneal, therefore, the remnant stress (1-F) is 30% in the 64 μm ribbon, compared with 8% in the 31 μm ribbon. Because of the interaction of this high remnant stress and the magnetostriction (the magnetostriction coefficient $\lambda = 30 \times 10^{-6}$ cm/cm), the thick ribbon has degraded magnetic properties. Thus, both the remnant stress discussed here and the crystallization discussed in the preceding paragraph contribute to the poor properties of thick straight ribbons, but the former has a further deleterious effect on the properties of toroids. When a ribbon is wound into a toroid, the winding stress increases with ribbon thickness. This high initial stress plus the ineffectiveness of stress relaxation in a thick ribbon further deteriorates the properties of the thick-ribbon toroids (Figure 3).

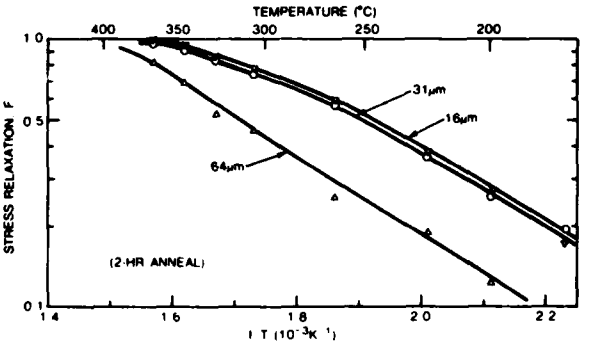

Figure 6. Stress relaxation as a function of temperature of the 2 hr anneal, for various ribbon thicknesses.

The peak torque measuring the magnetic anisotropy is shown in Figure 7 as a function of ribbon thickness. In general, the peak torque occurs in a direction within ±10 degrees of the casting direction. The peak torque remains ~10^4 erg/cm^3 for as-cast ribbons as thin as 20 μm, but increases drastically to 10^5 erg/cm^3 with thickness decreasing to 16 μm. Annealing at 345 °C does not change

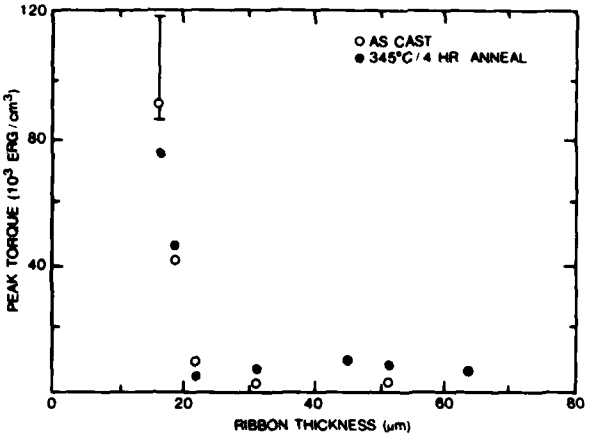

Figure 7. Peak torque vs. ribbon thickness, for as-cast and 345 °C/4 hr anneal. Each data point represents the average of a deck of 5 ribbon disks; the error bar shows the scatter of individual disk measurements.

the magnitude of the as-cast peak torque. This excess anisotropy is believed to result from the large quenched-in stresses due to the local variations in cooling rate in thin ribbons. In addition, the variations in cooling rate also result in ribbon thickness variations (see Figure 8), which may also increase the magnetic anisotropy like the quenched-in stresses. The cooling rate variations in thin ribbons can be attributed to the presence of large air pockets, which reduce the local thermal conductance at the metal-wheel interface.[5] The large air pockets on thin ribbon are formed by extensive air entrapment at the ribbon-wheel interface due to the low ejection pressure used for thin-ribbon casting.[4] They are, in general, elongated in the casting direction, which is the measured peak torque orientation. Even though this magnetic anisotropy in the ribbon length direction is favorable, the air pockets, being associated with stress fields and thickness variations, tend to curve and pin the magnetic domain walls (Figure 4d), resulting in the poor magnetic properties of thin ribbons.

CONCLUSIONS

Ribbon thickness as well as the annealing condition strongly influence ac magnetic properties. The optimum annealing is 2 hr at 345 °C, which removes most of the cast-in stress before crystallization starts. The optimum ribbon thickness occurs at $\sim 30\,\mu$m for the $Fe_{81.5}B_{14.5}Si_3C_1$ alloy. This result is consistent with Reference 1, regardless of whether the ribbon thickness is controlled by the melt delivery conditions (e.g., ejection pressure and

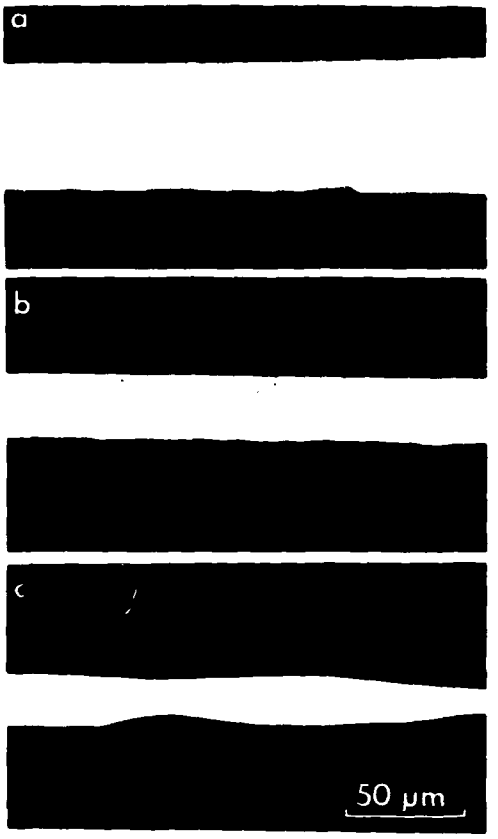

Figure 8. Metallography of the cross sections of ribbons of various thicknesses: (a) 64 μm, (b) 31 μm, and (c) 18.6 μm.

nozzle slot breadth) or by the melt extraction conditions (e.g., casting wheel speed). For thin ribbons, the properties degenerate because of the quenched-in stresses and the ribbon thickness variations associated with the air pockets, which tend to retard the magnetic domain wall motion. The air pockets are large and elongated in the casting direction, due to the low ejection pressure necessary for thin ribbon casting. For thick ribbons, the cast-in crystallites and the remnant stress not removed by annealing give rise to transverse domains, resist the approach to saturation, and yield high core loss and excitation. The ineffectiveness of stress relief in thick ribbons further impairs their toroid properties.

ACKNOWLEDGMENTS

The authors are grateful to R.P. Laforce, L.C. Perocchi, A.C. Rockwood, and L.A. Wojcik for ribbon fabrication, to S.J. Kelly and B.I. Gaechter for magnetic property measurements, to W.G.

Morris for magnetic domain observations, and to L.G. Turner for assistance in resistivity measurements. They also thank L.A. Johnson, H.C. Fiedler, and A.I. Taub for helpful suggestions.

REFERENCES

1. F.E. Luborsky, H.H. Liebermann, and J.L. Walter, *Proc. Conf. Metallic Glasses,* June 3-4, 1980, published by org. comm., Central Res. Inst. Phys., Budapest, Hungary, p. 203.
2. S. Takayama and T. Oi, *J. Appl. Phys. 50* (1979), p. 1595.
3. L. Novak, L. Potocky, A. Lovas, E. Kisdi-Koszo, and J. Takacs, *J. Magn. and Magn. Mat. 19* (1980), p. 149.
4. S.C. Huang, to be presented at the 4th International Conf. on Rapidly Quenched Metals, Sendai, Japan, August 1981.
5. S.C. Huang and H.C. Fiedler, *Met. Trans. 12A* (1981), p. 1107.
6. J.D. Livingston and W.G. Morris, *IEEE Trans. Magn. MAG-17* (1981), to appear.
7. F.E. Luborsky and J.L. Walter, *Mat. Sci. Eng. 35* (1978), p. 255.
8. A. Mogro-Campero and J.L. Walter, *J. Phys. 41* (1980), p. C8-497.
9. A.I. Taub and F. Spaepen, *Acta Met. 28* (1980), p. 1781.
10. J.P. Patterson and D.R.H. Jones, *Acta Met. 28* (1980), p. 675.

DISTRIBUTION LIST

ORGANIZATION	COPIES
Defense Documentation Center Cameron Station Alexandria, VA 22314	12
Office of Naval Research Department of the Navy 800 N. Quincy Street Arlington, VA 22217 ATTN: Code 471 Code 470	1 1
Commanding Officer Office of Naval Research Branch Office Building 114, Section D 666 Summer Street Boston, MA 02210	1
Commanding Officer Office of Naval Research Branch Office 536 South Clark Street Chicago, IL 60605	1
Office of Naval Research Western Regional Office 1030 East Green St Pasadena, CA 91106	1
Naval Research Laboratory Washington, DC 20375 ATTN: Codes 6000 6100 6300 2627	1 1 1 1
Naval Air Development Center Code 606 Warminster, PA 18974 ATTN: Dr. J. DeLuccia	1
Naval Air Propulsion Test Center Trenton, NJ 08628 ATTN: Library	1
Naval Construction Battallion Civil Engineering Laboratory Port Hueneme, CA 93043 ATTN: Materials Division	1
Naval Electronics Laboratory San Diego, CA 92152 ATTN: Electron Materials Sciences Division	1
Naval Missile Center Materials Consultant Code 3312-1 Point Mugu, CA 92041	1
Commanding Officer Naval Surface Weapons Center White Oak Laboratory Silver Spring, MD 20910 ATTN: Library	1
Commander David W. Taylor Naval Ship Research and Development Center Bethesda, MD 20084	1
Naval Oceans Systems Center San Diego, CA 92132 ATTN: Library	1
Naval Underwater System Center Newport, RI 02840 ATTN: Library	1
Naval Postgraduate School Monterey, CA 93940 ATTN: Mechanical Engineering Department	1
Naval Weapons Center China Lake, CA 93555 ATTN: Library	1

ORGANIZATION	COPIES
Naval Air Systems Command Washington, DC 20360 ATTN: Codes 52031 52032	1 1
Naval Sea System Command Washington, DC 20362 ATTN: Code 05R	1
Naval Facilities Engineering Command Alexandria, VA 22331 ATTN: Code 03	1
Scientific Advisor Commandant of the Marine Corps Washington, DC 20380 ATTN: Code AX	1
Army Research Office P.O. Box 12211 Triangle Park, NC 27709 ATTN: Metallurgy & Ceramics Program	1
Army Materials and Mechanics Research Center Watertown, MA 02172 ATTN: Research Programs Office	
Air Force Office of Scientific Research/NE Building 410 Bolling Air Force Base Washington, DC 20332 ATTN: Chemical Science Directorate Electronics & Materials Science Directorate	1 1
Air Force Materials Laboratory Wright-Patterson AFB Dayton, OH 45433	1
Library Building 50, Room 134 Lawrence Radiation Laboratory Berkely, CA	1
NASA Headquarters Washington, DC 20546 ATTN: Code RRM	1

ORGANIZATION	COPIES
NASA Lewis Research Center 21000 Brookpark Road Cleveland, OH 44135 ATTN: Library	1
National Bureau of Standards Washington, DC 20234 ATTN: Metals Science and Standards Division Ceramics Glass and Solid State Science Division Fracture and Deformation Division	1 1 1
Director Applied Physics Laboratory University of Washington 1013 Northeast Forthieth Street Seattle, WA 98105	1
Defense Metals and Ceramics Information Center Battelle Memorial Institute 505 King Avenue Columbus, OH 43201	1
Metals and Ceramics Division Oak Ridge National Laboratory P.O. Box X Oak Ridge, TN 37380	1
Los Alamos Scientific Laboratory P.O. Box 1663 Los Alamos, NM 87544 ATTN: Report Librarian	1
Argonne National Laboratory Metallurgy Division P.O. Box 229 Lemont, IL 60439	1
Brookhaven National Laboratory Technical Information Division Upton, Long Island New York 11973 ATTN: Research Library	1

Professor G.A. Ansell
Rensselaer Polytechnic Institute
Department of Metallurgical Engineering
Troy, NY 02181

Dr. C. Adam
Pratt & Whitney Aircraft Group
Government Products Division
P.O. Box 2691
West Palm Beach, FL 33402

Dr. E.M. Breinan
United Technology Corporation
United Technology Research Laboratories
East Hartford, CT 06108

Professor H.D. Brody
University of Pittsburgh
School of Engineering
Pittsburgh, PA 15213

Professor J.B. Cohen
Northwestern University
Department of Material Sciences
Evanston, IL 60201

Professor M. Cohen
Massachusetts Institute of Technology
Department of Metallurgy
Cambridge, MA 02139

Professor B.C. Giessen
Northeastern University
Department of Chemistry
Boston, MA 02115

Professor D. Turnbull
Harvard University
Division of Engineering and
Applied Physics
Cambridge, MA 02138

Dr. B.B. Rath
Naval Research Laboratory Code 6320
Material Science and Technology Division
Washington, DC 20375

Dr. N.C. Koon
Code 6632
Naval Research Lab
Washington, DC 20375

Professor N.S. Stoloff
Rensselaer Polytechnic Institute
School of Engineering
Troy, NY 12181

Professor A. Lawley
Drexal University
Department of Metallurgical Engineering
Philadelphia, PA 19104

Dr. F.E. Luborsky
Corporate Research and Development
General Electric Company
Schenectady, NY 12301

Professor C.D. Graham, Jr.
University of Pennsylvania
3451 Walnut Street
Philadelphia, PA 19104

Dr. J.J. Becker
Corporate Research and Development
General Electric Company
Schenectady, NY 12301

Professor D.G. Ast
Cornell University
Department of Materials Science and
Engineering
Ithaca, NY 14853

Professor O.D. Sherby
Stanford University
Materials Sciences Division
Stanford, CA 94300

Dr. K.S. Narasumhan
Crucible Research Center
P.O. Box 88
Pittsburgh, PA 15230

Dr. E.J. Yadlowsky
Kollmorgen Industrial Drives
801 First St.
Radford, VA 24141

D.L. Martin
759 Waite Road
Clifton Park, NY 12065

Dr. J.C. Williams
Carnegie-Mellon University
Department of Metallurgy and Materials Sciences
Schenley Park
Pittsburgh, PA 15213

Professor H.G.F. Wilsdorf
University of Virginia
School of Engineering and Applied Sciences
Charlottesville, VA 22903

R. Mehrabian
National Bureau of Standards
Metallurgy Division
Washington, DC 20234

Professor P.R. Strutt
University of Connecticut
School of Engineering
Department of Metallurgy
Storrs, CT 06268

Prof. R.W. Cahn
Laboratoire de Metallurgie Physique
Universite de Paris-Sud
91406 Orsay Cedex, FRANCE

Dr. H. Stadelmaier
North Carolina State Univ.
Dept. of Materials Engineering
Raleigh, North Carolina 27650

Dr. T.J. Dougherty
Columbia University
Chemical Engineering Research Labs
New York, NY 10027

Manfred Doser
Senior Development Engineer
Hitachi Magnetics Corp.
Edmore, MI 48829


FILMED
8